THE FORM-FINDING OF STRUCTURES POSSESSING A CONSTANT SURFACE STRESS

by

Trevor Stephen Lewis

University of Warwick

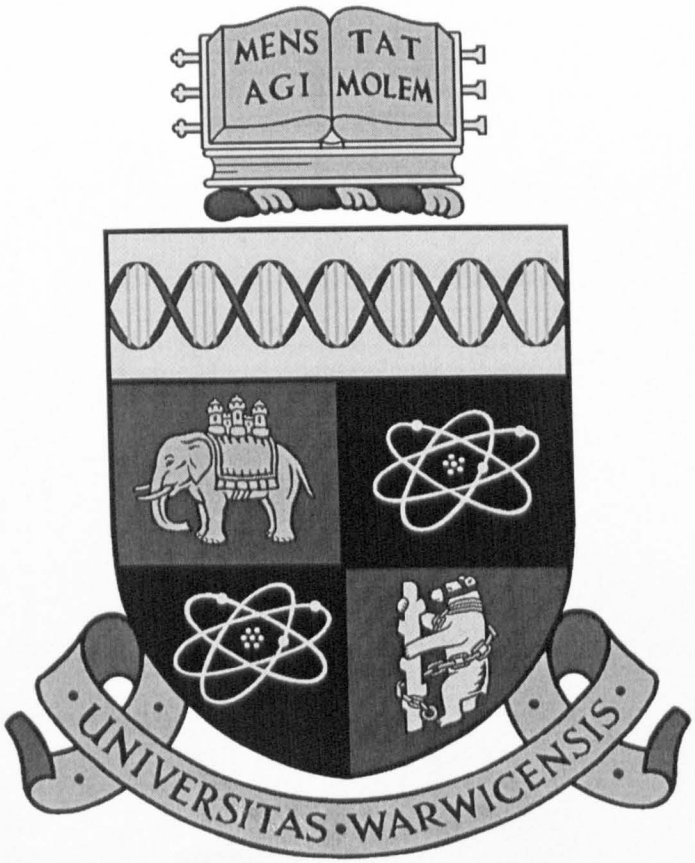

Department of Engineering

A Thesis Submitted for the Higher Degree of Doctor of Philosophy.

January 1997.

This thesis is dedicated to the memory of Avril Lewis ("Granma"), Daniel Nicholson ("Dan") and the grandparents I had the misfortune to never know.

"Libraries gave us power,
then work came and made us free....."
(N. Wire - "A Design for Life".)

CONTENTS.

LIST OF TABLES

LIST OF FIGURES

SYNOPSIS

A method for the generation of structures of a constant surface stress is presented; the prime application being the form-finding of light-weight tension structures. However, rigid forms generated from the principle are also discussed. The numerical approach adopted for the solution to the geometrically non-linear problem of form-finding is that of the Dynamic Relaxation method, incorporating kinetic damping. The numerical solutions produced describe surfaces of a minimum surface area and a zero mean curvature. These exist naturally in Nature as soap films - the mathematical term for such surfaces is a 'stable minimal surface'.

An approach utilising formex algebra for the generation of the geometry of the initial approximation to the numerical solution to a stable minimal surface is documented. The method is shown to be an efficient and powerful means for the creation of the data required for form-finding. Further, it is shown by the author, how Formex algebra can be used to manipulate the data relating to a numerical solution such that new forms may be created. As a consequence, an original means for the construction of an accurate small scale rigid model of a surface of constant stress is developed - the process involving the use of an advanced manufacturing technique called rapid prototyping. The integration of formex algebra with the form-finding algorithm is a novel approach, and it has led the author to define the process as "The Integrated Form-Finding Approach."

A detailed account of the problems and limitations of the methods of form-finding presently available for the generation of structures of a constant surface stress is included within the thesis. A comprehensive explanation of formex algebra follows - particular emphasis is placed on the generation of the data relevant for form-finding and the construction of rigid models. From observations relating to comparisons of the geometry of various numerical models with those produced from mathematical and experimental solutions, together with numerical solutions generated from alternative computational programmes, the "Integrated Form-Finding Approach" is shown to be an accurate and efficient means of form-finding. Further, the observations are linked to an assessment of the suitability of various convergence criteria, the aim being the selection of those criteria that will uniquely define the accuracy of a numerical solution. Using the selected criteria, further numerical models are generated whose geometry provide suitable configurations for light-weight tension structures. Finally, the possible advantages in adopting the geometry of a stable minimal surface when defining the configuration of a light-weight tension structure is addressed, together with some of the practical difficulties that need to be overcome for such surfaces to be reproduced in reality.

ACKNOWLEDGEMENTS.

Firstly, the author would like to thank Dr. W. J. Lewis for her considerable help and understanding; many thanks for the lengthy and stimulating discussions that provided much of the impetus for the writing of the work contained within this thesis.

Thanks to Prof. H. Nooshin, Dr. P. Disney and everyone at the Space Structures Research Centre, University of Surrey, UK; you provided invaluable assistance in explaining the concepts of Formex algebra, without which, much of this work would not have been completed.

The author is indebted to the management at IL (Institute of Light-weight Structures), University of Stuttgart, for giving the author the opportunity to study at such an inspirational place; thanks to everyone at IL for making my stay such an enjoyable and rewarding time.

The author would like to acknowledge the contribution from the staff of the Department of Engineering, University of Warwick, UK; thanks for your financial assistance, and the provision of facilities essential for the completion of my work.

And of course, special thanks to Mum, Dad and Caroline; without a doubt, your patience and support during my time of study is warmly appreciated.

Finally, the author would like to thank the social and intellectual wit afforded to me by my fellow 'Scholars' of Coventry and Swansea:

Jan, Lee, J, Alex, Steve D., Jem, General, Ian and Nina, Tracy, Barbara, Helena, Hele, Jon, Vicki, Helen, Peter, Steve H., Andy D, Richie D., Nick, Toni, Ollie, Lee S., Rob, Lyndon, Adam, Marv, Ceri, Andy T., Marion, Darren, Nigel, Richie E., Travis B., Perry, Jim, Lou, Noel, Andy M., Phil, Walter and Barbara, Alwyn and Josie, Windsor and Olive, Uncle John.

Declaration.

The author declares that the work presented in this thesis is a product of his own individual effort, except in those areas where an applicable reference has been made. This thesis has not been submitted for a higher degree at any institution other than the University of Warwick.

CHAPTER 1

Introduction.

It could be argued, that humankind's historical progress in the structural engineering domain pales into insignificance, when one considers those structures produced by Nature. Nature contains a vast culture of plants and animals that, by the process of evolution, have been highly optimised in terms of their weight, strength, and surface area, to ensure their prosperity in a highly competitive environment. The most important, or dangerous, load case governs the process of optimisation in a natural structure[1.1]. Consider the simple example of a tree, its trunk is optimised to resist the most important load case of wind acting perpendicular to its length. If the trunk of the tree were considered to be a simple cantilever fixed at one end, it can be observed that the thickness of the trunk increases in accordance with the magnitude of the internal bending moment induced by the loading i.e. the trunk is tapered from its base, where the bending moment and thickness of the trunk is the greatest, to its top where the thickness and bending moment tends to zero. The aim of this optimisation is the reduction in mass of the tree. Further, the circular shape of the trunk allows for a reduction in the magnitude of the imposed loading from wind through the ability of the wind to flow around the trunk. It is interesting to note, that a conic shape was adopted for precisely the same optimal properties of a tree trunk by the architect Sir. Norman Foster and the engineer Keizo Shimizu in the design of what will be the world's tallest sky scraper, the one kilometre high Millennium Tower[1.2].

Heinz Isler is a primary advocate of the use of Nature as a means of solving many practical engineering problems; his work having led to the construction of more than 1200 highly structurally efficient concrete shells from the geometry of physical models obtained from

natural processes[1.3]. Prior to the work of Isler, shells were designed according to mathematical formulae to produce "geometric" shapes e.g. hyperbolic paraboloids and barrel vaults[1.4]. Isler's method was revolutionary; the shapes he generated were obtained directly from models and were "non-geometric", due to the inability to define their surfaces mathematically. The models included plaster casts of the surfaces of inflated rubber membranes together with hanging membranes, constructed from a cloth saturated with a thermo-setting resin, that were inverted when cured. The accurate measurement of the surface of the physical model was the basis for the initial geometry of the shell, the geometry being checked, or altered, in accordance with the results of small scale model tests and the measurement of the final full scale structure. Although Isler has now recently employed computers in the assessment of the initial surface, he continues to stress the need not to deviate from the process of using natural processes in the selection of the initial geometry of the shell[1.5]. Isler's shells are considered to be optimised due to the minimal thickness of the material used, and the adoption of a surface geometry that ensures that the forces, arising from the prevalent loading of gravity and self weight, are purely in compression. These qualities result in a structure that is aesthetically pleasing and extremely structurally efficient due to: a reduction in the self-weight of the concrete, a reduction in the displacement of the structure, thereby reducing the possibility of the cracking and leaking of the roof, and an optimisation of the construction materials through the assurance that the concrete will experience a negligible tensile force. Figure 1-1 depicts a triangular shell, designed by Isler, of dimensions 25m × 32m, used to provide cover for a petrol station in Switzerland. Isler's methods of obtaining 'non-geometric' forms through a natural process are examples of 'form-finding'; a phrase also used when describing the process of generating structures of a constant surface stress.

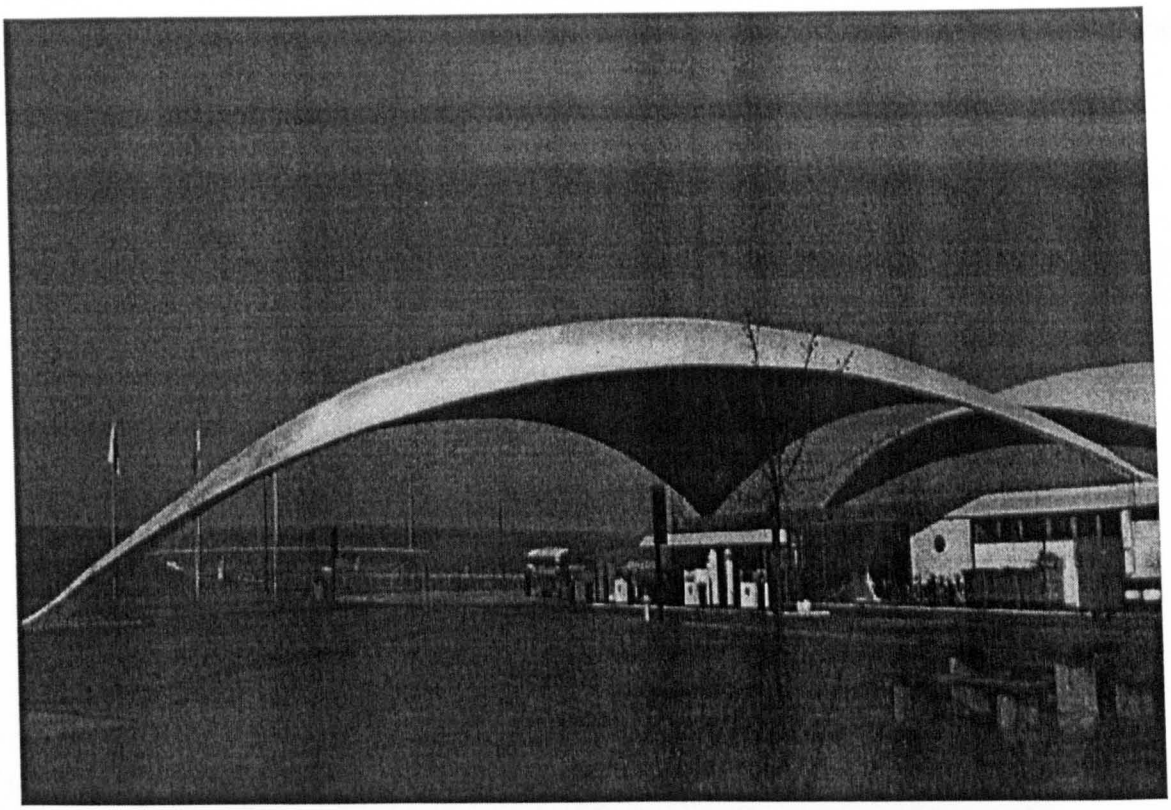

Figure 1-1 Isler's Concrete Shell. (Photo: "Structural Art", Concrete Quarterly, Winter 1992).

The author's realm of investigation concerns structures of a constant surface stress; the practical application being in the design of light-weight tension structures . A soap film is an optimised natural object representing a uniformly stressed surface. In addition, a soap film possesses a minimum surface area. The mathematical term for soap laminae is "stable minimal surface"; a term that will be used throughout this thesis when referring to a surface of minimum area and a uniform surface stress. For much of the 18th, 19th and early 20th centuries, mathematicians and physicists endeavoured to explain the geometrical and physical properties of a soap film (Chapter 2, Section 2.2). Their aim was to obtain analytical solutions to the problem of how to describe the geometry of a surface of minimum area. Although the Belgian physicist Plateau is credited as deriving many experimental soap laminae solutions to stable minimal surfaces (Chapter 2, Section 2.2), the modern day work of the German architect Frei Otto (Chapter 2, Section 2.2) is considered

to be revelatory, in that it shows how soap films can be used as design tools for the determination of the geometry of a uniformly stressed membrane structure.

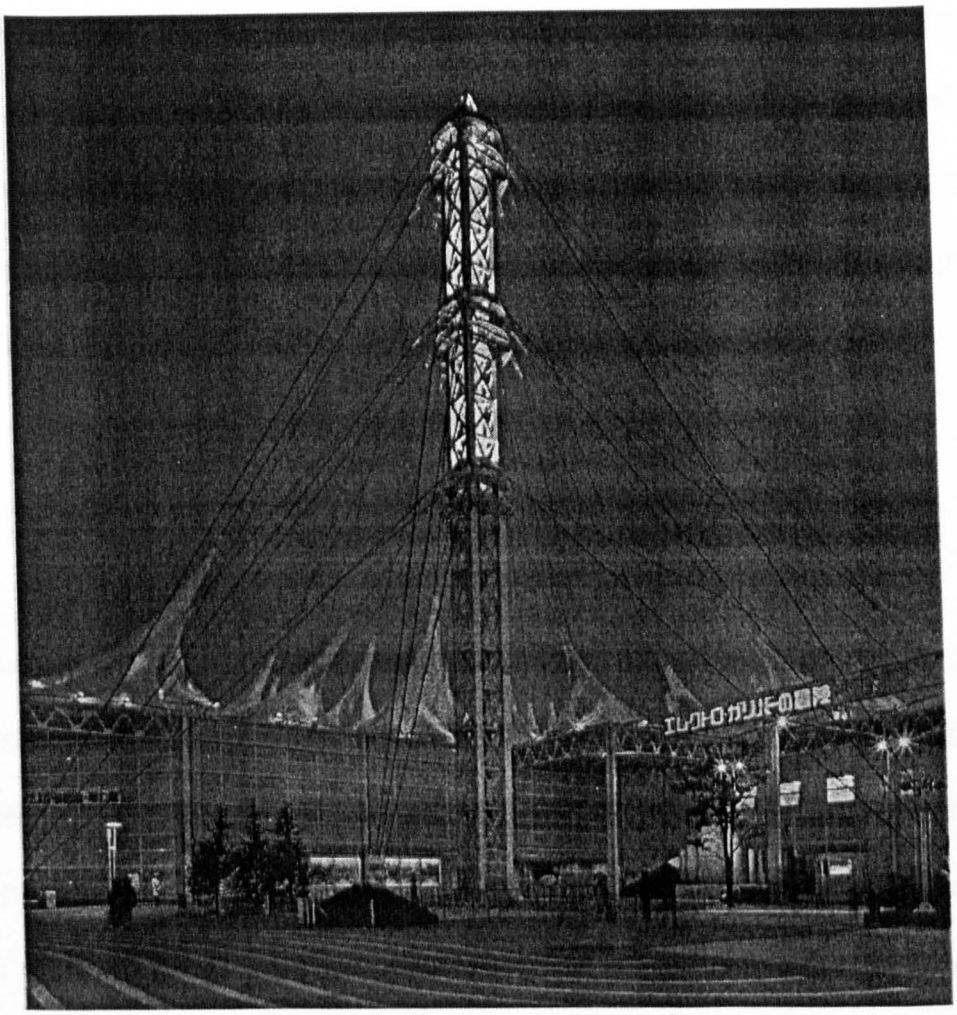

Figure 1-2 "Electric Power Pavilion" World Expo.' 85 (Photo: "Membrane Design in Japan 1967-1990.", Shinkenchiku-sha Co., Ltd., 1990.)

The term light-weight tension structure refers to either a pre-stressed cable network or a stressed woven fabric membrane; the latter being the subject of the work presented within this thesis. Light-weight tension structures are ideally suited to the covering of large spans where the presence of internal columns is undesirable. The surface of a light-weight tension structure is doubly curved, or saddle shaped, and possesses purely tensile forces; compression forces are only induced in the supporting columns or masts. Hence, the amount of material needed to resist the bending moments and buckling forces in covering a

given span is kept to a minimum. As a result, unlike traditional structures, tension structures have a significantly high span/weight ratio. An example of a light-weight membrane structure is illustrated in Figure 1-2. The illustration depicts a series of fabric conic structures, composed of a PVC coated fabric material that have been pre-stressed through the use of pre-tensioned cables that connect the apex of each cone to a central mast. The roofing covers an area of 3,500 m^2, and was constructed for the 1985 World Exposition in Tsukuba, Japan[1.6].

1.1 Light-weight Tension Structure Design.

A traditional tent consists of fabric suspended from a series of poles. The structure is only able to resist loads from gravity; wind loading causes the fabric to deflect significantly. In comparison, a pre-stressed light-weight membrane is able to resist loading due to wind, snow, or rain. A doubly curved, or saddle shaped, surface is the preferred geometry. This is because it improves the structural stability of the membrane structure; the internal tension forces are ideally aligned to resist both the forces arising from the wind, and those from the depression of the surface due to snow or ponding of rain water. The pre-stressing of a membrane surface refers to the process of inducing a surface stress, pre-stress, that recreates the desired form of the structure. The pre-stress is the level of stress that exists within the membrane surface due to the edge pre-stressing of the membrane, and before the application of an external imposed load such as wind, or dead weight. After the process of weaving, the fibres of a fabric are aligned orthogonal to each other in the warp and weft directions (Chapter 6, Section 6.2.1). The warp and weft directions in turn follow the direction of the principal curvatures of the fabric membrane structure. Hence, the fibres in these principal curvature directions extend and contract in accordance with an imposed

loading. When a load such as snow acts downwards on the surface, there will be an increase in the tensional force of the fibres aligned in the "sagging" direction; the forces in the "hogging" direction will decrease. In contrast, imposed forces created from wind uplift will cause the tensional forces to increase in the "hogging" direction and decrease in the "sagging" direction. The design of a light-weight tension structure is a unique area in structural engineering because of: i) the geometrically non-linear nature of the problem (Section 1.3) and ii) the shape of the structure playing an important part in the design process; the shape cannot be dictated. The shape of a membrane is dependent on the surface stresses applied to the membrane, in addition to the geometry of the membrane boundary. Adopting a shape that has been designed from methods, or tools, that do not take account of the geometrically non-linear nature of the problem is undesirable. This will result in an ill-defined geometry, causing the constructed structure to deform as it adopts its equilibrated configuration under an applied pre-stress, leading to the introduction of unwanted stress deviations which impair the structural performance and the life-span of the structure (Chapter 6, Section 6.2.3). Further, the level of pre-stress should be adequate to ensure the surface is purely in tension, as the introduction of any compression forces will result in the wrinkling of the surface. Wrinkling is detrimental as it produces an aesthetically displeasing appearance, and reduces the stiffness, while increasing the displacement, of the structure when resisting imposed loads.

The first stage of design concerns the derivation, or "form-finding", of the geometry of the equilibrated structure for a known boundary configuration and an applied pre-stress. No externally applied loads are considered at this stage; the equilibrium concerning solely that of the internal forces arising within the surface due to the pre-stress. The following stage involves the determination of the cutting pattern of the un-stressed membrane fabric.

Finally, the performance of the structure is analysed when it is subjected to various imposed load cases. The work recorded within this thesis concerns primarily "form-finding", although Chapter 6 includes a brief discussion concerning the merits of adopting the geometry of a stable minimal surface when contemplating the cutting pattern, and static analysis stages of design.

1.2 Approaches to Form-Finding.

Chapter 2 includes a comprehensive discussion of the merits of the various possible solutions to the problem of form-finding. The major methods can be summarised in the format given below.

1.2.1 Analytical Modelling.

The problem of describing mathematically the shape of a soap film has puzzled mathematicians since 1744, when Euler formulated an equation to describe a surface of minimal area. Further, Euler applied his equation to find a minimum area surface spanning the distance between two parallel circular rings positioned perpendicular to the axis passing through their centres. Such a surface is called a catenoid. Euler's work intrigued Lagrange; he reformulated Euler's equation to derive what is now known as the Euler-Lagrange equation (Chapter 2, Section 2.2). The non-linear nature of the equation means that it is extremely difficult to solve, and to this date, there are very few minimal surfaces that can be described by an exact analytical solution. Meusnier derived a geometrical interpretation of Euler's equation. He discovered that the mean of the principal curvatures at every point within the surface is zero (Chapter 2, Section 2.2). Surfaces possessing such a property are called "minimal surfaces". The physicists Laplace and Young endeavoured to explain the

physical behaviour of the rise of fluid in a capillary tube through the action of surface tension (Chapter 2, Section 2.2). Their theory was later derived by Gauss using the principle of virtual work (Chapter 2, Section 2.2). Gauss's derivation was significant, in that it showed that a soap film was in a state of stable equilibrium and always possessed a surface of minimum area (Chapter 3, Section 3.3.2). Mesunier's condition was hence a necessary condition for both stable and unstable minimal surfaces; it did not uniquely define a surface of minimum area. Consequently, soap laminae are referred to as "stable minimal surfaces". Plateau conducted many soap film experiments looking at experimental solutions to minimum area surfaces spanning a variety of different geometrical boundaries (Chapter 2, Section 2.2). Plateau realised that any contour, composed of a single closed wire, could be made to contain at least one soap film irrespective of the geometry of the contour. His work motivated many mathematicians to try and prove that any given closed curve in space could be spanned by a minimal surface. To some extent, the question has been answered by Douglas and Rado who described mathematically some of the surfaces obtained by Plateau (Chapter 2, Section 2.2). In addition, Goldschmidt showed that, for the particular boundary case of a minimal surface bounded by two rings (Chapter 4, Section 4.3), there is a maximum attainable height, after which, a stable minimal surface cannot be formed.

1.2.2 Physical Modelling

During the period 1950-1970, the pioneering work of the architect Frei Otto, and his team at the Institute of Light-weight Structures in Stuttgart (IL), led to the generation of many striking and ethereal natural shapes from models that had no conceivable mathematical description for their geometry i.e. as in the case with Isler's shells, they were 'non-geometric' forms. Architects encountered a frustrating period, the inability to define the

shapes mathematically meant that engineers had no theoretical design tools to construct life sized replicas of these miniature models[1.7]. Consequently, a radically new design approach was initiated that relied entirely on physical models. The design process had a major limitation; the models had to be representative of both the material and the geometry of the full scale structure.

Physical models were made from rigid materials such as chains, wire nets and fabrics (in this instance the models were used to assess only the static behaviour of the structure and not for form-finding[1.7]), elastic sheets and fabric such as lycra, and soap films bounded by rigid wires, or flexible cotton threads (Chapter 2, Section 2.2). Often, none of these materials on their own were the sole solution in the design process, all the various types of models were used in tandem to generate different information[1.7]. Soap films were recognised as being the ideal means for the initial determination of the shape of a pre-stressed membrane. This was because shapes could be defined that were independent of the size of the model and the stretching of the model material. (A soap film has a constant surface stress (Chapter 3, 3.3.2) irrespective of the dimensions of a model i.e. the surface geometry of the model only depends on the geometrical configuration of the boundaries enclosing the soap film[1.7]). Clearly, the major limitation of the method was the temporary existence of the model and the difficulty of getting a soap film to span lengths of up to 1m[1.7]. Hence, a specialist machine ("soap machine") and soap film solutions were devised to improve the stability and prolong the existence of the soap laminae.

The next problem requiring addressing was that of accurately scaling up the physical model (sometimes by up to hundred times) to recreate the geometry of the life size structure, and thereby provide the structural fabricator with essential manufacturing information. Little

difficulty was encountered in obtaining information from those models composed of inelastic nets and chains. For the other models, it was necessary to project, or draw, a regular grid onto the doubly curved surface of the model. In the case of a soap laminae, the "soap machine" was modified, so that it was possible to take accurate photographs of various profiles of the model against a luminous glass plate inscribed with an orthogonal grid.

The next stage of the design process concerned the manufacture of a fabric, elastic sheet, or wire, model from the photographs of the soap film; thus a more permanent 'secondary' model of the life size structure was created. (Fabric and elastic sheets can be extremely inaccurate. This is due to the elastic stretching of the material which makes it difficult to ensure that the curvature of the surface matches that of the soap film[1.8]). The cutting pattern[i] of the actual full scale structure was then determined from the careful measurement of a rigid model constructed from either a plaster cast of the fabric/elastic model, or the laying of a heat shrinkable PVC foil onto the surface of the secondary model[1.9]. The rigid model allowed for the curvature of the surface to be measured and checked, together with an assessment made of the accuracy of the cutting pattern through the unfolding of the fabric onto the surface of the rigid model. Equations were derived which related the stresses in the fabric of the life scale structure to the radii of curvature of the surface of the rigid model. Thus, by measuring the curvature of the surface with specialist tools, the forces and stresses anticipated in the final structure could be calculated and modifications to the cutting pattern, or the surface geometry, made; the latter amendment can be seen to be undesirable as it requires the whole design process to be repeated. Finally, to test the suitability of the

[i] As explained in Chapter 6, the cutting pattern is a two-dimensional representation of a three dimensional surface, usually produced from strips of fabric two to three metres in width.

design solution, a series of trial structures spanning a few metres were constructed and tested.

Otto's model experiments were a primary influence in the design of many early light-weight tension structures; his most notable work being that of the pavilion for the Federal Republic of Germany at the 1967 Montreal world exposition (Figure 1-3). The structure was constructed solely from a design process that used physical models. The pavilion consisted of a pre-stressed cable net, supported by masts and underlined with a polyester membrane cladding. The total surface area covered by the structure was 10,000 m^2. The structure was innovative as there appeared to be no noticeable boundary between the structural form and the surrounding landscape; the products of man and Nature had merged, the building had effectively become the landcsape[1.10].

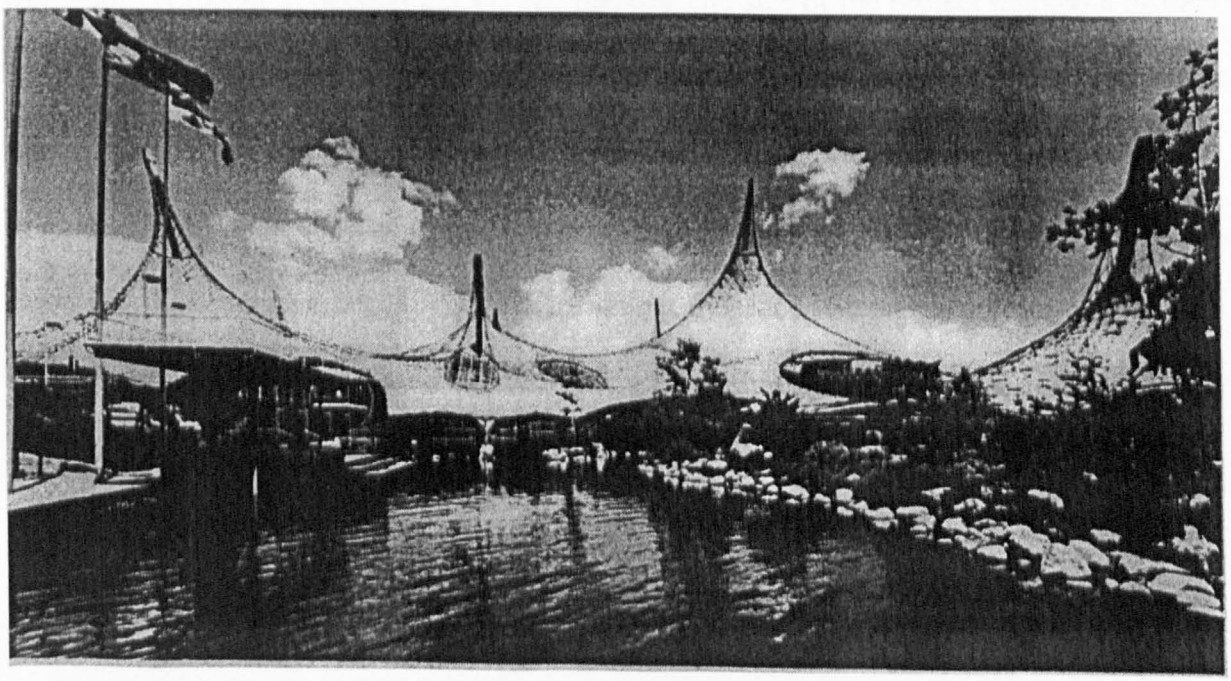

Figure 1-3 Pavilion of the Federal Republic of Germany, World Exposition, Montreal, 1967.(Photo: The Arup Journal - October 1980, IL Archive).

To summarise, nowadays, the lengthy process of manufacture required in the creation of an accurate physical model has led to physical models being used only in the initial stages of design, where it is necessary to convey an architectural vision of a structure. (However, in Chapter 3, the author describes an alternative process-of manufacturing physical models directly from the data supplied from a computational form-finding analysis. The approach is highly accurate, and requires a considerably shorter time for the manufacture of a model).

1.2.3 Computational Modelling.

It was not until the arrival of computers, and the development of mathematical models, that engineers had the power to assess the feasibility of structures constructed according to small scale physical models, and soap laminae experiments. The Munich Olympic complex was the first example of a tension structure designed with some assistance from computational techniques (Chapter 2, Section 2.5.1). The prestige and size of the project marked a distinct shift away from physical model testing to computational methods to justify the structural behaviour and capacity of the building[1.10]. However, ultimately, the computations were only used for the determination of the roof cutting pattern, and not for the form-finding of the roof geometry (Section 2.3.2). The responsibility for form-finding lay once more with Otto who, together with the architect Rolf Gutbord, used physical models in the generation of the overall form of the structure[1.10].

Computational, or numerical modelling, requires the surface membrane to be replaced by a series of small elements of the same material properties as that of the overall membrane; this process is called surface discretisation. The geometrically non-linear nature of the problem (Section 1.3) requires an iterative process to determine the internal residual forces, arising from the applied surface stress, at the nodes that join each element. Equilibrium occurs

when the residual forces are less than a pre-scribed maximum admissible value. (A detailed description of the various computational methods developed for form-finding are documented in Chapter 2, Section 2.3).

1.3 Geometric Non-Linearity.

The structural analysis of a light-weight tension structure is considered to be a geometrically non-linear problem. In traditional static analysis, an external load is applied to an initially "static" rigid structure. Equations are derived to relate the displacement δ and the stiffness K of the structure to the internal forces required to resist the external loading P. Equilibrium is attained once the external imposed load (P) and the internal resistive force ($K\delta$) are equal, i.e.

$$P - K\delta = 0 \qquad (1.1)$$

Such structures are said to be "linear", that is the calculation of the resistive internal forces and the associated displacement of the structure at equilibrium may be determined in one step due to the linear relationship between force and displacement. In linear structural design, the magnitude of the internal resistive force tends to be highly dependent on the strength and stiffness of the material used. Conversely, a geometrically non- linear structure possesses resistive forces whose magnitude is inherently linked to the geometry of the structure; any movement of the structure can radically alter the size of the resistive force as the stiffness K is constantly changing with the surface geometry i.e. K is transient. The force-displacement relationship is hence non-linear and equation (1.1) cannot be solved in one step for a geometrically non-linear structure. Instead, the changing geometry and resulting internal forces imply that the right hand side of equation 1.1 is unlikely to be ever

exactly equal to zero, and, instead, it is equal to an out-of-balance, or residual force. Equilibrium can only be attained by an iterative solution, whereby the geometry of the structure is altered according to the magnitude of the residual forces at a given time step, until such forces are acceptably small.

1.4 The Application of Stable Minimal Surfaces in Light-weight Tension Structure Design.

Light-weight tension structures are invariably not designed according to a soap lamina analogy; this may be explained through the contrasting roles of the engineer and the architect. Firstly, the engineer is usually only concerned with the effects of external loading on a pre-defined shape. It is often argued by the engineer that stable minimal surfaces provide the possibility of onerous imposed load cases. However, it is sometimes forgotten that the load case that also needs addressing is that which is there during the whole life-span of the structure; the surface pre-stress (Chapter 6, Section 6.2.2). Secondly, architects may not comprehend the dependency of the shape on the equilibrium of the structure, and may be unwilling to compromise their aesthetic ideals for the benefit of structural efficiency. Owing to the fact that the geometry of a soap film is heavily dependent on its boundaries, the objections of both parties to an undesirable surface shape may be satisfied by the alteration of the boundary configuration. Unfortunately, again, concessions to the 'ideal' shape might be made, due to the need to achieve a suitable cutting pattern, and this leads to the dictation of the shape during form-finding (Chapter 6, Section 6.2.3). Lastly, a structure may be designed according to an analysis that assumes a non-uniform pre-stress field. This will result in a membrane that cannot be realised in practice, due to the impossibility of introducing the same pre-stress pattern in the real life structure as found in the computational model (Chapter 6, Section 6.2.3).

A light-weight tension structure, which adopts the shape of a stable minimal surface, is beneficial in terms of an economic use of material, an equilibrated form for an even distribution of surface stress and a more aesthetically pleasing geometry (Chapter 6).

1.5 The Aim.

As stated earlier, the work contained within this thesis concerns the form-finding of structures of a constant surface stress; the practical application being in the form-finding of light-weight tension structures. The aim of the work is to develop an efficient and effective method of calculating the geometry of a stable minimal surface, based on a given closed boundary configuration, with an emphasis on achieving a satisfactory means for the pre and post-processing of the data associated with a given surface.

The author recognises that there are many world-wide examples of light-weight tension structures designed according to a wide range of alternative computational methods. However, as discussed in Chapter 2, Section 2.3, the validity of the methods in problems concerning the form-finding of a stable minimal surface is suspect due to the assumptions of one, or more, of the following:

- The creation of a non-uniform stress field leading to the violation of the principle of a stable minimal surface.

- Form-dictation through the restriction of nodal displacements during the process of obtaining static equilibrium.

- Incorrectly formulated numerical models producing surfaces that are not stable minimal forms.

- A pre-requisite of an initial surface that closely approximates the form-found shape closely.

- Inefficient algorithms that require considerable computational effort for the manipulation of complex element formulations during form-finding .

These limitations have led the author to develop an original piece of work concerning an "integrated" approach to form-finding, whereby a mesh generating programme, Formian, has been coupled with a form-finding "equation solver". (The reader may be interested to note that a simplified account of the major points concerning the authors form-finding method is documented in ref. 1.11). Formian is not a commercial package dedicated to a particular means of computational analysis, it is, instead, the programming language of formex algebra. The importance of Formian to form-finding lies in its ability to create, modify, and store large volumes of data relating to a discretised surface, quickly and efficiently. This is an essential requirement, in cases where convergence cannot be attained, due to an ill-defined initial surface causing the discretised surface elements to undergo large scale deformations. By changing parameters, it is possible to make a modification to either the surface geometry, element orientation or the boundary dimensions quickly. An original method of using Formian for the post-processing of stable minimal surfaces has been developed, leading to the construction of a series of solid models using Rapid Prototyping and Manufacturing (R.P.&M.) technology. The Dynamic Relaxation method, incorporating kinetic damping, is utilised for the "equation solver" in the form-finding algorithm together

with a 'simplex' triangular element formulation (as suggested in research by Barnes[1.12] (Chapter 2 Section 2.3.3)).

1.6 Scope.

Documented within Chapter 2 is a literature review concerning various methods and ideologies that have been employed for the solution to the problem of calculating the geometry of a minimal surface. Also included is a survey of literature relating to the application of formex algebra in structural analysis (Section 2.4) and examples of structures constructed according to a minimal surface geometry (Section 2.5).

The components of the "integrated" form-finding technique are described in detail in Chapter 3. The chapter is divided into three sections, Section 3.2 includes a discussion of formex algebra and its application to the generation of the relevant form-finding data required by the equation solver. Section 3.3 presents the iterative technique utilised in the form-finding analysis, together with the derivation of the simplex triangle element used in the surface discretisation. Also documented within Section 3.3 is an investigation of the behaviour of a surface undergoing a form-finding analysis. Finally, Section 3.4 concerns the post-processing of surfaces using Formian and the construction of physical models.

The validity of the form-finding method is discussed in Chapter 4. A selection of numerical models is assessed in accordance with expected theoretical and experimental results. In addition, comparisons between similar surfaces generated from alternative computational techniques are discussed. The findings are further analysed in the investigation of the acceptability of various convergence criteria; the aim being the selection of a criteria that is

a universal measurement of the convergence of any given numerical solution to a stable minimal surface.

To illustrate the potential application of the author's 'integrated' form-finding method in the creation of structural configurations suitable for use in light-weight tension structure design, further numerical examples are generated, and the results recorded in Chapter 5.

Chapter 6 concerns the discussion of the possible structural benefits offered by adopting the geometry of a stable minimal surface, and the problems to be overcome in the manufacture of such forms; the main focus being that of the generation of a suitable cutting pattern. From this discussion, suggestions are put forward concerning possible future areas of research.

Chapter 7 contains a summary and a discussion of the main conclusions reached by the author during the writing of the work presented.

REFERENCES.

1.1 C. Mattheck,
"Engineering Components Grow Like Trees."
Mat. -wiss. u. Werkstofftech. 21, pages 143-168, 1990.

1.2 "The Limit-Tall Tower."
Broadcast 12.0 a.m., 6/9/1996 BBC 2.

1.3 Heinz Isler,
"Indications by Nature."
SFB 230 1992.

1.4 T. Copeland,
"Structural Art."
Concrete Quarterly, Winter 1992, pages. 12-15.

1.5 D. P. Billington,
"The Tower and the Bridge. The New Art of Structural Engineering."
Princeton University Press, New Jersey, pages 222-229, 1983.

1.6 "Membrane Design in Japan 1967-1990."
Shinkenchiku-sha Co., Ltd., 1990.

1.7 W. Addis,
"Design Revolutions in the History of Tension Structures."
Structural Engineering Review, vol. 6, no. 1, Elsevier Science Ltd., pages 1-10, February 1994.

1.8 P. Rice,
"Lightweight Structures: Introduction."
The Arup Journal, October 1980, pages 2-5.

1.9 I. Liddel
"Tension Structures II: Membranes."
Buro Happold Tehcnical Manual.

1.10 B. Forster,
"Cable and Membrane Roofs - A Historical Survey."
Structural Engineering Review, vol. 6, no. 3-4, Elsevier Science Ltd., pages 145-174, 1994.

1.11 W. J. Lewis and T. S. Lewis,
"Application of Form-Finding of Minimal Surfaces."
Journal of the International Association for Shell and Spatial Structures, Vol. 37, no 3, December 1996, pages 165-187.

1.12 M. R. Barnes,
"Form-Finding of Minimum Surface Membranes."
ASS World Congress on Space Enclosures Building Research Centre, Concordia University, Montreal, July 1976.

CHAPTER 2.

Critical Appraisal of Literature Relating to Minimal Surfaces and Form-Finding.

2.1 Introduction.

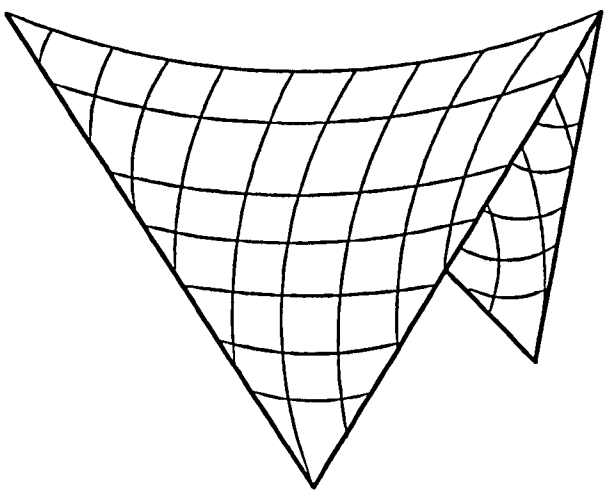

Figure 2-1 Minimal Surface Bounded by a Skew Quadrilateral (ref. 2.8).

The mathematicians of the 17th Century tried to find an all encompassing mathematical solution for the determination of a surface of minimal area[2.1]. The term "minimal surface" refers to surfaces of a zero mean curvature. (The relationship between minimal surfaces and surfaces of a minimum area is described in detail in Section 2.2). Regrettably, mathematicians are only able to provide complete mathematical solutions for a very few minimal surfaces which are defined by boundary configurations of a certain kind. One example being the analytical solution for a saddle shaped minimal surface spanning a skew quadrilateral, as derived by Schwarz in 1890[2.2] (Figure 2-1). Many of the mathematical theories can be used for the explanation of the unique properties of a minimal surface. Of particular interest is the application of Bernoulli's principle of virtual work to the topology of a minimal surface derived from the shape of a soap film. It can be shown that for any

given boundary, there are at least two minimal surfaces of which one is in a state of stable equilibrium, while the other is in a state of unstable equilibrium. Only the stable minimal surface possesses a minimum surface area. Literature regarding the experimental work of Plateau, and more recently Frei Otto, has shown that soap films are a competent means for the resolution of stable minimal surfaces, based on a given closed boundary.

Cable nets were the first structural configurations to be subjected to a non-linear method of computational analysis. Many of the numerical approaches used for the form-finding of tensile membrane structures can be said to be directly descended from studies relating to cable networks. Advances made in the area of finite elements led engineers, such as Argysis[2.3] & Scharpf and Haug[2.4] & Powell, to apply the method to cable net structures and soap films respectively. In 1965, A. S. Day introduced a new approach called Dynamic Relaxation; it was originally developed for use in the computational analysis of portal frames[2.5]. Later, it was demonstrated how the method was particularly suited to the structural analysis of cable net and membrane structures[2.6]. Most non-linear methods of solution may be roughly divided into two groups, those that are ***vector*** based and those that are ***matrix*** based. Matrix based methods rely on the construction of a global stiffness matrix; the matrix is transient as it is only valid for small incremental displacements used in the updating of a structure's geometry. The stress, strain, displacement and residual force of a discretised element are coupled together within the global stiffness matrix of a structure. Thus, the calculation of the incremental nodal displacements are calculated all at once, by the multiplication of the inverted global stiffness matrix. In contrast, the nodal displacements of a surface undergoing analysis using a vector method, are due solely to the vectors of the nodal residual forces calculated locally, from elements sharing the same node [2.7]. All forms of computational modelling require some means of generating the data relating to the surface geometry of the initial approximate solution. A discussion of the applicability,

and use, of formex algebra in generating such information is included in Section 2.4. In order to provide a full and balanced review of the major developments and applications of minimal surface ideology, the following topics of interest have been reviewed in a chronological order:

- Mathematical and Experimental Investigations of Minimal Surfaces.
- Computational Investigations of Minimal Surfaces.
- The Application of Formex Algebra in Structural Analysis.
- Examples of 'Form-Found' Structures.

2.2 Mathematical and Experimental Investigations of Minimal Surfaces.

A new mathematical technique called 'the calculus of variations' was introduced in the 17th Century by the mathematicians Johann and Jakob Bernoulli, Leonhard Euler and Joseph Louis Lagrange[2.8]. The aim of the technique was to assist the mathematicians in their quest to acquire mathematical descriptions for optimal objects. Initially, the Bernoulli brothers addressed the problem of describing mathematically the optimum shape, or the equilibrium shape, of a freely hanging chain subjected to a gravitational force. It was concluded that such a shape was obtained when it was not possible to lower any link of the chain without having to raise another link. Johann Bernoulli formulated the exact equation of this optimum shape in 1690 and called the curved shape a catenary, or a hyperbolic cosine as it is known today[2.8]. Architects realised that the inverse shape of a catenary gave the optimum shape for the natural transference path of the compression forces of a supporting member, subjected to gravitational forces or imposed loads. "Hanging models", composed of a series of chains, were used by the famous architect Antoni Gaudi. Using the geometry of the

inverted models, Gaudi was able to derive the shapes of spectacular towers and vaulted ceilings. Gaudi used these models for the design of many remarkable cathedrals; his most notable being the still unfinished Church of the "Sagrada Familia" [2.9]. More recently, a catenary was adopted in the design of the supporting structure enclosing a conic fabric tensioned structure in Riyadh[2.10].

Johann Bernoulli proposed his principle of virtual work in 1717 in which he concluded that in equilibrium, no work is required to achieve an infinitesimal displacement of a mechanical system[2.11]. Both stable and unstable equilibrated systems are governed by this rule. Hildebrandt & Tromba explains the principle of virtual work in a simplified geometric manner[2.8]:

Each state of a physical system may be classified by a quantity called the total potential energy. The potential energy is considered to be a function of the various states of the system. Each state is thought of as being representative of a point in a plane, and the potential energy analogous to the height of a mountain over a plane. Hence, the potential energy of the system at all its various states is analogous to a 'mountain range.'

Using this simplification, Bernoulli's principle is further defined by the following two rules:

1. The stable state of rest, which represents the equilibrium of the physical system, is when the potential energy of the system is less than that for any other alternative system

The absolute minimum potential energy is obtained when the tangent plane is horizontal to the 'pit' of a 'mountain range'. This describes the stable equilibrium of a physical system. It is analogous to considering the displacement of a ball placed in a bowl (Figure 2-2). If the

ball is displaced slightly, the ball will return to its state of rest at the centre of the bowl, equilibrium position, irrespective of the direction of displacement[i]. Assuming the only force acting is that due to gravity and neglecting the effects of friction, no work is deemed to have occurred in moving the ball from its equilibrium position at the tangent plane to the bottom of the bowl; the gravitational force is completely balanced by the reaction acting perpendicularly from the tangent plane.

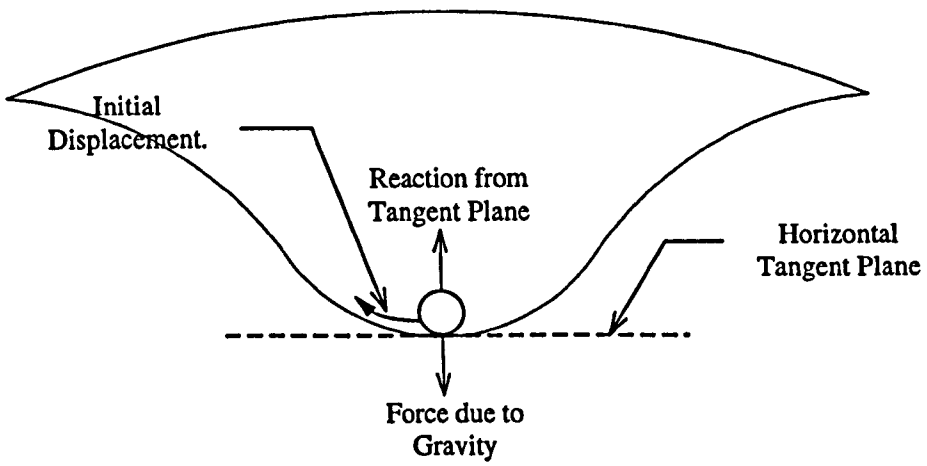

Figure 2-2 Stable Equilibrium Position of a Ball.

2. *The equilibrium states of a physical system are the stationary states of its potential energy.*

The stationary potential energy states are given by the horizontal tangent planes of a 'mountain range'. Unstable states of rest are characterised by tangent planes aligned horizontal to the peaks Figure 2-3 (a) and saddle points Figure 2-3 (b) of the range. Unstable systems are analogous to the behaviour of an initially stationary ball placed on the peak, or saddle point, of the mountain range. A stationary ball positioned on the peak of a mountain will irrecoverably lose its equilibrium when subjected to a slight displacement,

[i] In this analogy, the effects of friction are neglected and no energy is lost, hence, in accordance with the law of conservation of energy, the ball will continuously move up and down the sides of the bowl through its initial point of rest at the bottom of the bowl, either gaining potential energy at the expense of motion and kinetic energy, or vice versa

whereas the equilibrium of a ball positioned on the saddle point may be recoverable, depending on the direction of the displacement imparted on the ball. Rule 2 is a condition satisfied by physical systems of a stable or unstable state, whereas rule 1 is only satisfied for physical systems of a stable state.

(a)

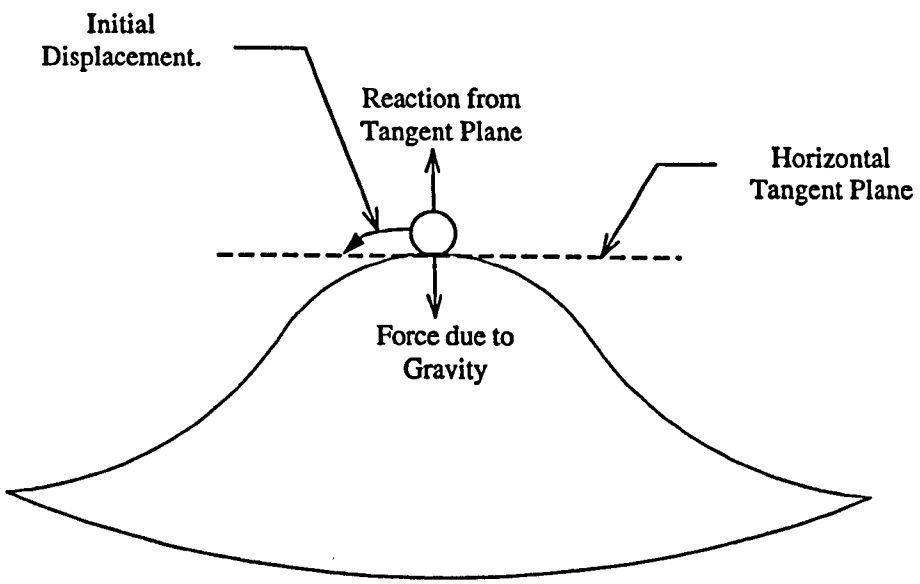

(b)

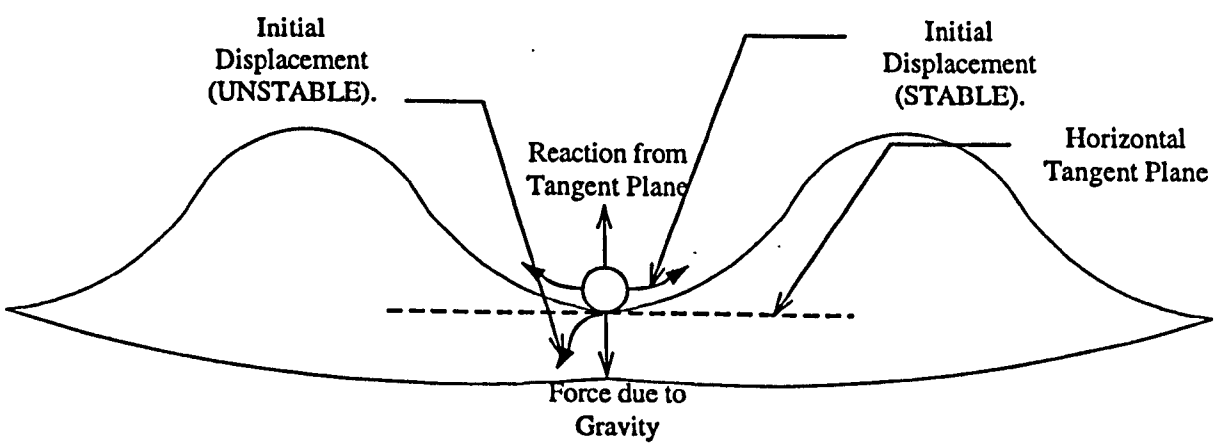

Figure 2-3 Unstable Equilibrium Positions of a Ball. (a) Peak (b) Saddle

In 1744, Euler derived an equation to describe a surface of minimum area; at the same time he produced the earliest example of a non-flat minimal surface[2.12]. Euler discovered that a minimal surface could be produced from the rotation of a catenary curve about an axis aligned horizontally with the curve, and positioned at a distance below the curve's point of

zero gradient. This surface was termed a catenoid, and is the only example of a curved minimal surface of revolution, (Chapter 4, Section 4.3). Further investigation led to the definition of another minimal surface called a helicoid. The surface is formed by pulling apart the circular boundaries of a catenoid, for the instance when the boundaries are cut such that the incision passes along the meridian of the catenoid. Notably, Euler managed to obtain an exact analytical solution to describe the topology of a catenoid based on the radius of the cross-section of the catenoid at its mid-point (The equation is described in Chapter 4 Section 4.3).

When Lagrange reformulated Euler's equation in 1760, it was hoped that this would enable a minimal surface, of any given boundary geometry, to be defined mathematically [2.13]. In its one dimensional form the equation is given by[ii]:

$$\frac{d}{dx}\left(\frac{\partial f}{\partial y_x}\right)-\frac{\partial f}{\partial y}=0 \qquad (2.1)$$

where $y=y(x)$, $y_x=\left(\frac{dy}{dx}\right)$, and $f=f(x,y,y_x)$.

Equation (2.1) can only be solved using a suitable iterative solution for certain kinds of boundary conditions. Ultimately, Lagrange did not manage to produce any exact analytical solutions to the minimal surface equation.

Meusnier produced a geometrical interpretation of Lagrange's formulae in 1785[2.14]. He realised that the helicoid minimal surface possessed a zero mean curvature. It was concluded that a minimal surface always satisfies the condition that the mean curvature of every point found within the surface is equal to zero. Equation 2.2 describes the mean

[ii] The equation is commonly known as the Euler-Lagrange equation.

curvature H of a surface S at an arbitrary point P. It describes the arithmetic mean of the two principal curvatures $\frac{1}{R_1}$ and $\frac{1}{R_2}$ that pass through point P.

$$H = \frac{1}{2}\left(\frac{1}{R_1} + \frac{1}{R_2}\right) \qquad (2.2)$$

where,

R_1 is the maximum radius of principal curvature and R_2 is the minimum radius of principal curvature. Hildebrandt[2.1] describes the process of obtaining the principal curvatures using the steps described below:

First define the vector V, of length v, aligned normal to the tangent plane N passing through the surface S at the point P. The surface S is then intersected by the plane M that contains the vector V. Plane M is perpendicular to S at point P. The curvature of the cross-section C of the surface is contained within plane M. Next, determine the radius R of the 'best fitting' circle that passes through point P. This circle lies in the same plane as the normal section C and has a radius R that is aligned in the direction of V. If the vector V points from P towards the centre of the best fit circle then the principal curvature is given by $\frac{1}{R}$. If V points away from the centre of the circle, the principal curvature is given by $-\frac{1}{R}$. By considering all the principal curvatures of the normal cross-sections C, it can be shown that there are two special sections, C_1 and C_2, that contain the largest and smallest principal curvatures, $\frac{1}{R_1}$ and $\frac{1}{R_2}$. Furthermore, the normal sections C_1 and C_2 intersect each other at right angles.

According to Meusnier, when viewing the normal sections C_1 and C_2 that contain the principal curvatures of a point on a minimal surface, it is apparent that these curvatures are

equal in magnitude, but curved in opposite directions to one another. Hence, the geometry of a non-flat minimal surface will always be of a' saddle' type shape.

Both Thomas Young[2.15] and the Marquis de Laplace[2.16] were able to explain the behaviour of soap films from work concerning the rise of liquid in a capillary tube. Young's work was later corroborated using mathematical techniques by Laplace. In 1806, both authors derived independently a solution to describe the pressure p acting across a curved fluid surface, at a point circumscribed by the maximum and minimum principal curvatures of radii R_1 and R_2. The equation is known as the Laplace-Young equation (equation 2.3),

$$p = \sigma\left(\frac{1}{R_1}+\frac{1}{R_2}\right) \qquad (2.3)$$

or,

$$p = FH \qquad (2.4)$$

where, σ is a constant and represents the surface tension of the liquid and $F = 2\sigma$. F is the film tension; the force per unit length of film[iii].

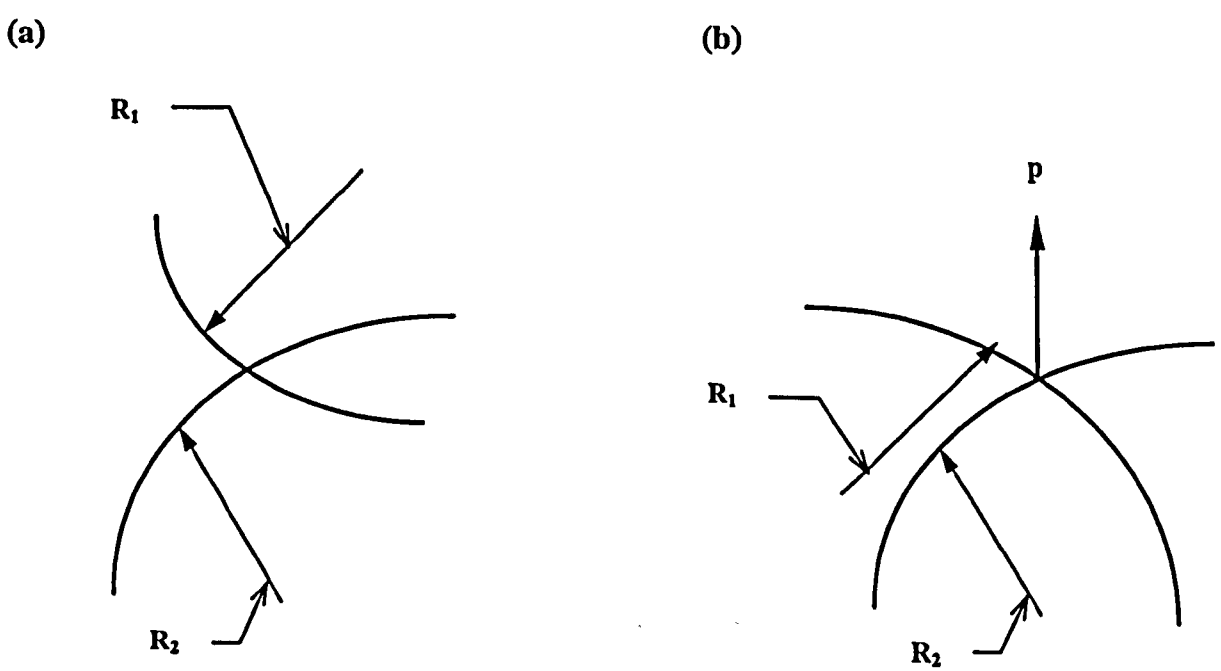

Figure 2-4 Principal Curvature for (a) Soap Film (b) Soap Bubble.

[iii] The characteristic behaviour of the surface tension of soap laminae is documented in Chapter 3, Section 3.3.2.

For the instance where there is a zero excess pressure acting on the surface of the soap film, it can be seen that the principal curvatures must be equal and opposite to each other, Figure 2-4 (a) (This property is described using a numerical example in Chapter 4, Section 4.3). Should pressure act on the surface of the liquid, then the equation describes the principal curvature of a soap bubble, Figure 2-4 (b). Equation 2.4 is significant, it is the earliest equation that relates the physical properties of a soap film to the mathematical properties of a minimal surface. The relationship between minimal surfaces, and surfaces of minimal area, was not adequately addressed until Carl Friedrich Gauss considered the soap film to be a mechanical system, and explained the physical property of the soap lamina through the use of Bernoulli's principle of Virtual Work[2.17]. He believed that because the soap lamina was in a state of stable equilibrium, the condition implied that the film also possessed a minimum area due to the potential energy being proportional to the surface area (Chapter 3, Section 3.3.2). The unstable minimal surface of a soap laminae could not be modelled, as the slightest infinitesimal perturbation would cause the loss of equilibrium, and the breaking, of the lamina. (This phenomenon is recorded in Chapter 4, Section 4.3) This statement was in accordance with Bernoulli's principle of virtual work for an unstable mechanical system and was subsequently corroborated in a paper by Trong Thi & Formenko in 1991[2.18]. The implication of this observation is again extremely significant; it showed that the condition of zero curvature was satisfied for both surfaces of minimal area and minimal curvature, indicating that the equations suggested by Lagrange and Euler were a necessary, but not a sufficient condition for the generation of a surface of minimal area. For example, by looking at a catenoid, Trong showed that depending on the value of the radius of the cross-section of the catenoid at its mid-point, there existed a stable and an unstable minimal surface (Chapter 4, Section 4.3). Furthermore, the absolute minimum area spanning between two coaxial, parallel rings was described, analytically, by Goldschmidt in 1831[2.2] as the area of a

catenoid of a height less than $1.056 \times a$, where a is the boundary ring radius. (Hence a non planar stable minimal surface could span from both rings at this height) For a height between $1.056 \times a$ and $1.325 \times a$, the area of the catenoid was shown to be a relative minimum, and for heights greater than $1.325 \times a$, the surface area of the catenoid was greater than that of the two rings. (A non-planar stable minimal surface spanning from ring to ring (i.e. a catenoid) could not be formed and, instead, the solution to the minimum surface area was given by the two planar stable minimal surfaces enclosed by each ring).

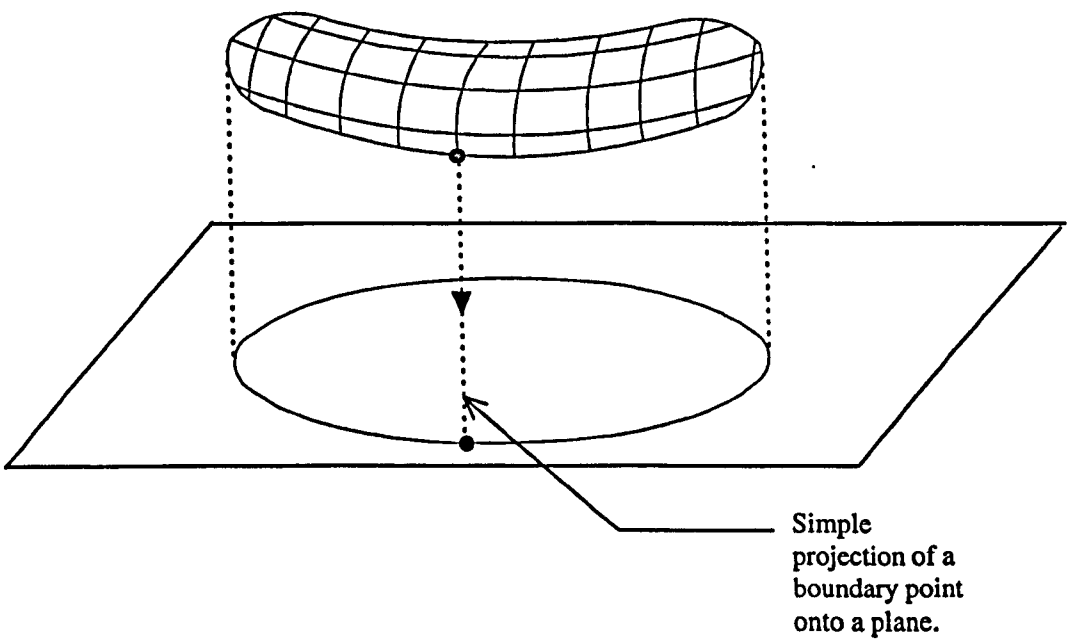

Figure 2-5 Minimal Surface Bounded by a Convex Simple Projection onto a Flat Plane (ref. 2.8).

Experiments with soap films undertaken by the physicist Plateau, during the 19th century, led him to an intriguing problem. In his publication of 1873, he asked whether it was true that for every closed boundary, there lied at least one minimal surface[2.19]. Another mathematical interpretation of this rule was to find all surfaces that satisfied the condition $H = 0$ for equation (2.2). Plateau's problem was not solved analytically until the work of the mathematicians Douglas[2.20] and Rado[2.21] appeared independently in 1931. They produced some general analytical solutions that described minimal surfaces spanning contours of a

specific geometry. The Plateau problem is easily solved for a planar boundary; the minimal surface must also be planar, and hence there is only one minimal surface[2.8]. Furthermore, in 1932, Rado stated that for convex boundaries formed from the simple projection[iv] of a series of points lying on a plane (Figure 2-5), only one minimal surface may bound the curve[2.8]. The last unique boundary condition for which the Plateau problem can be solved concerns the total curvature of the boundary[2.8]. A boundary composed of a spatial curve will contain only one minimal surface, if the total curvature of the boundary is less than 4π. For boundaries not satisfying the aforementioned criteria; it is not known how many minimal surfaces may span a given closed boundary.

A century later, Frei Otto published many texts documenting soap film experiments. His work differed from that of Plateau's in that he was particularly innovative in the choosing of non- conventional boundary configurations. For example, Otto discovered that it was possible to create unusual tent-like surfaces by using boundaries made of cotton threads. The threads deformed in tandem with the soap laminae until taut, at which time, the stable minimal form would possess elegantly curved boundaries [2.8]. (The numerical solutions to such surfaces bounded by flexible boundaries are given in Chapter 5, Examples 5.2.6 and 5.2.7). In a book published jointly with Otto in 1967, Trostel showed that the stable minimal form of a catenoid lamina could only be produced if the distance separating the two circular boundaries was less than a maximum height given by $1.3 \times R$, R being the radius of the rings[2.22] The result reaffirmed Goldschmidt's hypothesis, that at this height, it was not possible to generate a surface of a minimum area spanning both ring boundaries.

[iv] A simple projection refers to the case where every point on the boundary curve corresponds to a single point on the plane of projection.

For a more detailed and graphic account of the development of the mathematical formulations of minimal surfaces, it is recommended that the reader consults references 2.1, 2.8 and 2.23.

2.3 Computational Investigations of Minimal Surfaces.

2.3.1 Linear Solutions to Geometrically Non-linear Problems.

The non-linear relationship between force and form of tension structures was linearised by Siev[2.24] & Eidelman in 1961. In order to do that, a cable network was considered to be composed of members that were aligned orthogonal to each other when viewed on plan. Provided a constant pre-tensional force was acting within the elements, and planar deformations were ignored; the orthogonal nature of the horizontal cables implied that the planar equilibrium was automatically satisfied. Thus, the assumption led to the derivation of a linear solution, which could be solved in a single step, for the determination of the vertical displacements necessary to achieve the equilibrium of the cable net.

Another linear solution which, unlike the approach of Siev &Eidelman, had no restriction on the degree of movement of a cable element was devised by Linkwitz & Schek[2.25] from work relating to the determination of the cutting pattern of the roofs of the Munich Olympic games[2.26]. The method of analysis used a mathematical deception whereby the value of the cable force divided by the cable length was assumed to be equal to a constant called the 'force density'. The assumption simplified the non-linear problem into a series of linear equations arranged in a matrix formulation. At the time, the approach was seen to be far superior to other methods of non-linear analysis. This was due to the fact that the method allowed the calculation of a network to be completed in a single step, irrespective of the

initial surface geometry, and without any numerical inaccuracies being introduced. In addition, a wide variety of surfaces could be generated by specifying different values for the force density for different branches of the network. It is now acknowledged that the approach is not suitable for the analysis of equilibrated cable networks possessing a constant pre-tensional force. Both the force density method, and the method of Siev &Eidelman, can be used in the shape finding of forms that are used as an initial approximation in the modelling of a surface by some other non-linear method of analysis [2.27].

2.3.2 Non-linear Matrix Analysis.

Haug & Powell presented two papers in 1971 that dealt separately with the form-finding of cable networks[2.28] and membrane structures[2.4]. In the first paper[2.28], a finite element package, together with the Newton-Rhapson iterative technique, was used for the analysis of a cable net. Excessive displacements and strains were found to reduce the speed of convergence and, in some cases, prevent the convergence of the solution. These problems could be alleviated through a judicious choice of the topology of the initial surface based on the geometry obtained from physical models[2.29]. Stability and convergence were also improved by restricting the size of the nodal displacements, or by the scaling of the size of the maximum out-of-balance forces. The method was limited, as not even the full implementation of the aforementioned restrictions was enough to ensure the convergence of networks that were of a strongly geometric non-linear nature.

In the second paper of Haug & Powell[2.4], the properties of a soap film were considered for the analysis of a pre-stressed membrane. A quadrilateral element was assumed to possess the unique soap lamina property of a constant isotropic stress with zero elastic straining.

These material properties were constantly maintained, irrespective of the degree of element deformation. In addition, the element was formulated according to an iso-parametric principle i.e. the displacements of the element were dependent on the assumed shape function of the element. The Newton-Rhapson technique was again used for the solution of the non-linear equations. Although it was claimed that the element was particularly suited and efficient in the modelling of minimal surfaces, no literature was published concerning the efficiency of the approach and its accuracy, when compared to physical models of soap film laminae of a corresponding boundary configuration. It is not clear whether the initial starting surfaces were obtained from some prior knowledge of the likely equilibrated geometry based on soap film experiments.

The need to model computationally, the tents of the sports hall of the 1972 Munich Olympic Stadium games led Argysis & Scharpf to develop a method where the roofs were considered to be assembled from a series of cables[2.3]. (Ultimately, the method was only used in the determination of the roof's cutting pattern, it was not used in any form-finding calculations). The general method involved the formulation of a global stiffness matrix that linearised the relationship between the force, and displacement, acting at each node positioned at the intersection of a series of a cables. The calculation of the stiffness matrix was obtained from expressions describing the elastic and geometric stiffnesses of a cable. (Previously these expressions had been derived for use in aeronautical applications by Turner et al in 1959[2.30]). The linearity of the stiffness matrix was valid only for very small displacements, hence the condition of equilibrium could not be satisfied immediately. Instead, the magnitude of the out-of-balance force was reduced to a suitably small value through iterations using the Newton Rhapson technique. The solution of Argysis & Scharpf tended not to converge in cases where the geometrical data of an initial surface was ill-

defined due to the misinterpretation of the geometry of a physical model or sketch. Such a problem was also encountered when using the method of Haug & Powell[2.28].

Argysis et al developed his work further and called his computational method the 'natural shape finding approach[2.31]. Once again, a cable net idealisation was used with elements assumed to behave in a linearly elastic manner. The initial surface was taken to be flat, with the final form found from the incremental displacement of those nodes that ultimately formed the fixed supports of the network. Once the support nodes had reached their pre-known 'target values', the geometry of the cable network was deemed to have been calculated. Each increment required the calculation of the displacements of the non-support nodes from the multiplication of the matrix representing the out of balance residual nodal forces with that of the inverted global stiffness matrix. If the cable net to be analysed was not subjected to an externally applied load, then the nodal residual force was purely a product of the internal pre-stress force i.e. the approach was a means of form-finding. Before lifting, the nets were initially in equilibrium as the orthogonal planar nature of the starting surface implied a residual force of zero. Both the residual force matrix and the global stiffness matrix were calculated from the configuration of the network at a previous incremental displacement and hence the equilibrated surface was only an approximate solution. As soon as the boundary supports had reached their target value, the approximate equilibrated form was refined through the application of the Newton Rhapson iterative technique. Further iterations were necessary, as large elastic forces tended to be present in the final form, due to the excessive straining undertaken by the cables in their displacement from an initially planar position. Consequently, the cable lengths required modification for the determination of their unstressed lengths to achieve an acceptable stress distribution.

2.3.3 Vector Approach.

The Dynamic Relaxation method forms the main topic of discussion within this section. Other vector methods include the scaled conjugate method[2.32] and the method of steepest descent[2.33]. In 1964, Hussey stated that the configuration of a deformed cable net could be obtained by minimising its potential energy[2.34]. This observation is used in the aforementioned vector methods. Dynamic Relaxation can be described as the process of reducing an initially static surface to a group of lumped fictitious masses, situated at the nodes, and causing these masses to oscillate about their positions of equilibrium, due to the application of a static force. The geometry of the structure is updated in accordance with the nodal displacements; the motion of the structure being gradually reduced by the effects of damping. Iterations continue until the residual forces are negligible, and the potential energy has been minimised at the static equilibrium state.

Dynamic Relaxation was originally used in cases where continuum differential equations needed to be solved for difficult boundary conditions. It was stated by Day[2.5] in his paper of 1965, that the applicability of Dynamic Relaxation to the solving of non-linear problems was limited by the need to determine the time interval used in the finite difference iterative step, and the value for the viscous damping factor used for the reduction in amplitude of the vibrating system.(The critical damping factor was found from the natural frequency of the system). Significantly, Day stated that the technique could be applied to problems requiring a finite element type of solution. The finite element form of Dynamic Relaxation was described as being the means by which a kinetically unstable discretised system may be brought to rest, through the application of viscous damping and a reduction in the magnitude of the out of balance forces responsible for the vibration of the system according

to Newton's second law of motion. A centred finite difference technique applied to the D'Alembert equation was utilised for the calculation of the incremental velocities and the corresponding displacements of the system. At each increment, the geometry of the system was updated together with the residual forces, iterations were continued until such forces were acceptably small. Rushton[2.35] extensively used Dynamic Relaxation in the analysis of elastic plates under a variety of load and boundary conditions. The first application of Dynamic Relaxation to the solution of a geometrically non-linear structure was completed by A. S. Day and Bunce in 1970[2.6]. A centrally placed load was applied to a cable net, and the resulting deformed shape obtained using the Dynamic Relaxation algorithm.

Between the period of 1971 to 1975, the Dynamic Relaxation method was comprehensively used by Barnes[2.36,2.37] in the analysis of a variety of cable nets. A paper written by Barnes[2.38] describing the form-finding of minimal surface membranes stated that both elastic and purely geometric forces could be used to define a form. A 'simplex' planar triangle element was introduced which used the planar geometry of an element for the quick and accurate determination of the forces acting along the sides of the element. The approach was significant, in that rigid body rotations did not have to be considered, and no complex matrix manipulations were required in the calculation of forces, or stiffnesses. Hence, both the force and the displacement were now decoupled from an element stiffness matrix, making the method a truly vector based approach. An assumption of zero elasticity produced a minimum surface form. The examples tended to be very crude planar forms whose geometry did not clearly exhibit the requirement of a zero mean curvature. Also, the paper did not include any comparisons with soap laminae of similar boundary dimensions. Barnes explained how the large deformations encountered during the analysis led to the gross deformation of some elements causing collapse. Consequently, he suggested that the

algorithm should allow for some automatic refinement of the element mesh in areas where collapse occurred, or alternatively, the lumped masses of the collapsed nodes should be increased. The latter method implied that the nodal stiffnesses at the vertices of a semi-collapsed node were very high, causing negligible nodal displacements and thereby preventing the element from collapsing further. Barnes stated that although the amendment produced a non-equilibrated surface, the approximation was acceptable as there was little discrepancy between the geometry of the equilibrated surface and the un-equilibrated surface. This statement could be considered to be in context for the simple planar models analysed by Barnes, but not for those of more complicated non-planar surfaces.

A major development in the Dynamic Relaxation solution was derived from research by Cundall[2.39] relating to unstable geo-mechanical problems. A revised procedure was implemented whereby viscous damping was neglected. Instead, the kinetic energy of the undamped vibrating system was monitored to ascertain whether the kinetic energy had peaked, at which point, the vibrating system was brought to rest by setting the nodal velocities to zero. The system was then permitted to vibrate about the new updated position, usually with decreasing kinetic energy peaks, until the residual forces were acceptably small and the energy was totally dissipated. The method was found to be very stable and rapidly convergent in cases where the system exhibited large local disturbances. Consequently, the approach was found to be well suited to problems of form-finding where very high forces, and displacements, were induced by grossly deformed members during the initial stages of form-finding due to an ill-defined initial surface.

Literature concerning the application of both viscous and kinetic damping to the form-finding of membranes and cable net structures using Dynamic Relaxation can be found in

work by Barnes[2.7,2.40] and Lewis & Jones[2.41]. To ensure stability, Barnes stated a maximum time increment that should not be exceeded (Chapter 3 Section 3.3.5.2). The limit also allowed the vibrating fictitious nodal masses to be simply determined from the sum of the principal stiffnesses of the cables meeting at a given node. Furthermore, Barnes considered the patterning of the membrane during form-finding; the displacement of nodes positioned along the seam line of a fabric strip was restricted during form-finding, thereby simplifying the process of determining a cutting pattern. (An explanation of Barnes's approach is included in a brief discussion concerning possible methods of determining a suitable cutting pattern, Chapter 6, Section 6.2.3). The surfaces generated from the dictation of the nodal displacements were not examples of stable minimal surfaces.

The efficiency of the Dynamic Relaxation algorithm, when compared with other non-linear means of solution, has been extensively documented by the aforementioned authors in references 2.42 and 2.43. It was concluded by Lewis, that the vector method of solution provided by the Dynamic Relaxation approach required more iterations than the global stiffness matrix method. However, the matrix method required a greater computational time for each iteration and was hence far less efficient when the overall time for convergence was considered. Results obtained using the matrix method indicated a sensitivity to ill conditioning when the global stiffness matrix of a large complicated structure was inverted, leading to a lack of convergence of the solution. Conversely, Dynamic Relaxation was shown to be extremely stable provided that the limit on the maximum time increment was obeyed. It was suggested that kinetic damping should be implemented in the Dynamic Relaxation algorithm as the method gave a saving in real time, when compared to a viscous damping means of solution, which required calculations to determine the optimum damping coefficient. In 1990 Shan[2.44] illustrated how the number of iterations necessary to achieve

convergence could be reduced, or increased, through the multiplication of the fictitious nodal masses by a weighting factor found by trial and error (Chapter 3, Section 3.3.5.2).

2.3.4 Alternative Non-linear Approaches.

A mathematical solution to the problem of generating a minimal surface through the assumption of a zero mean curvature was recorded in 1972 by Ishii and Suzuki[2.45]. A series of non-linear differential equations were solved using finite differences and the Gauss Siedel iterative method. The solution's major draw backs were: i) the need to have a system of equations that were diagonally dominant so that the Gauss-Siedel method would converge, and (ii) the non-uniqueness of the solution i.e. the production of stable and unstable minimal surfaces.

In 1974 Schek presented an amended force density approach to the form-finding of geodesic, or uniform mesh cable networks[2.46]. In the original method, the use of a pre-defined constant force density value meant that, in practice, a cable net subjected to a constant pre-stress would only conform to the equilibrated geometry, if the solution possessed cable elements of a constant length. This requirement could not be satisfied by the original approach. Consequently, the magnitude of the force, or the length of a cable, was constrained which resulted in variable force density values. At each node, the non-constant force densities were summed. Using a suitable iterative approach, the residual force density value was used to update the co-ordinates of the surface until the residual had been reduced to a minimum. More recently the approach has been further developed by Motro et al[2.47, 2.48]. A paper published by Motro in 1995[2.49] showed that the validity of the amended force density method was suspect due to the convergence of the solution being

highly dependent on the geometry of the initial starting surface, with the final equilibrated shape shown to vary by selecting different elemental mesh arrangements.

Kneen used a suite of programmes in assessing the equilibrium of a tensioned fabric structure[2.50]. Initial shapes were generated from a mesh generating programme, developed by Kneen, and subsequently analysed using a non-linear programme called LISA[v]. Displacements of the order of 1500 mm, in a direction normal to the membrane surface, were stated as being common during analysis. For each iteration, the displacements were restricted to a maximum admissible value of 200 mm, thereby ensuring convergence by controlling the in-plane strains. Up to three convergence criteria were given, of which at least one should be satisfied. The criteria were that the maximum nodal displacement in a given iteration should be small, the maximum nodal residual force should be small, and there should be a minimal change in the surface area for successive iterations. A programme for the post-processing of data was implemented by Kneen to allow the user to examine the 'history' of the displacements, forces and surface area for up to thirty previous iterations. (The influence of these criteria on convergence is recorded in Chapter 4). Kneen explained that the analysis of soap-film surfaces led to elements with nodes free to move around within the surface, implying that the maximum nodal displacement was not a satisfactory convergence condition.

Grundig[2.51] used the minimisation of the area of a surface, discretised by a series of triangle elements, as a means for form-finding. The surface area of each element was calculated according to Heron's formulae[vi]. A series of linear equations was formulated, so as to

[v] LISA is a non-linear analysis package developed from the work of Haug & Oelberman (ref. 2.29). Chapter 4, Section 4.5 includes a comparison between a numerical surface produced using LISA with that produced by the author's form-finding approach.

[vi] Heron's formulae is given in Appendix 4A.1.

enable the initial surface to be calculated in one step before the iterative minimisation of the surface area. Simple numerical examples included membranes subjected to an internal pressure. The work of Singer et al[2.52] adopted a similar vein, except his numerical examples were related to well-known minimal surfaces obtained from soap film experiments. The validity of the approach could not be assessed, because no record was made concerning a comparison between the geometry of the numerical models and those of soap laminas of a corresponding boundary configuration.

A numerical approach that implemented the classical minimal surface function as a means of solution was published in a paper by Suzuki & Hangai[2.53] in 1991. Their numerical approach was said to be more convergent than methods that used finite differences, or the finite element method. Differential equations with three unknown co-ordinate functions were derived from the function describing a minimal surface. The solution to the differential equations was formulated so as to require only one unknown variable representing the distance from the initial surface to the unknown minimal surface. Numerical analysis was accomplished through the use of finite elements. Results obtained from their method for a catenoid minimal surface compared favourably with the exact results based on Euler's equation for a catenoid. Both stable and unstable minimal surface were modelled (Chapter 4 includes a comparison between Suzuki & Hangai's results and those obtained from the form-finding approach adopted in this thesis).

A non-linear method of solution that was a hybrid of a vector and a matrix approach was recorded by Gosling & Lewis in a Research Report written in 1991[2.54]. The approach, suggested originally in an earlier paper by Barnes[2.40], utilised a planar triangle element that was represented as three equivalent 'pseudo' cables enclosing an area of the pre-stressed

surface. According to the formulae suggested by Barnes, in-plane stresses were determined from the application of Hook's law to the global elastic strains. The strains were found from a transformation matrix, which related the direct strains of the sides of the element to the global surface strains through the application of Mohr's circle of strain. Elastic straining of the element was considered. Contrary to comments made by Barnes[2.40], the triangle element formulation demanded that the straining, and hence the nodal displacements, were small. Using the global stresses and the volume of each element, the tensional pseudo-cable forces were found from a transformation matrix corresponding to the geometry of the surface. The residual forces were then obtained from the summation of the cable forces meeting at a given node. The Dynamic Relaxation algorithm was used for the determination of the resulting displacements. It was suggested that the amount of matrix manipulation could be reduced if elastic straining was neglected, and only geometric forces[vii] were considered during form-finding. The assumption required that the principal planar stresses were constant and equal, with the shear stress set to zero. This gave the same stress field as that exhibited by soap laminae, or stable minimal surfaces.

Gosling & Lewis showed that their algorithm produced numerical surfaces of a geometry consistent with those of soap laminae spanning similar boundary configurations, provided a maximum allowable percentage of 0.025% of the maximum nodal force component to the maximum pseudo-cable force was reached[2.55] This was the adopted criterion of equilibrium (Chapter 4 Section 4.2).

A comparison between line and triangular element surface discretisation during form-finding has been documented by Lewis & Gosling[2.56] . The paper explained that more line elements

[vii] Geometric forces refer to those internal forces induced in a member/membrane due to a constant force/stress whose line of action depends on the geometry of the member/membrane. The contribution of elastic forces/stresses to the magnitude of the force acting in a member/membrane is neglected.

were needed to model the surface, with the elements tending to follow geodesic lines[viii], causing a loss in surface definition. The triangular elements of Barnes/Gosling's approach were said to require a greater computational effort, but fewer elements were needed to model the surface, when compared to a similar surface modelled using line elements. Also, the triangular elements were generally more efficient, but were stiff, and hence less tolerant of an ill chosen initial surface, due to the inherent assumption of small straining. Line elements were not suited to describing minimal surfaces with high curvatures, unless an accurate description of the final surface was known.

Further research indicated that Gosling's force percentage (ref. 2.56) was not a sufficient criterion for equilibrium[2.57, 2.58]. Due to the transformation matrix being updated only at kinetic energy peaks, the assumption of small element straining and nodal displacements could be violated, causing the pseudo-cable-forces to be incorrectly calculated. Consequently, non-uniform pre-stressing was required to recreate the magnitude of the forces in the equilibrated numerical model. This violated the principle of a stable minimal surface. (A description of Gosling's numerical approach is included in Chapter 4, Section 4.5).

The adoption of the algorithm suggested by Gosling led Lewis to conclude that a judicious choice of an initial topology, that approximated the form found surface closely, would reduce errors inherent in the assumption of small straining[2.59]. Initial surfaces could be defined using Hermitian polynomials, which improved convergence and reduced the magnitude of the stress deviations. Also, the introduction of elastic straining during form-

[viii] Geodesic lines are described in Chapter 6.

finding was given as a means of improving surface definition by eliminating the problems of ill-conditioning of elements due to buckling and inversion.

An alternative iso-parametric element formulation was adopted by Gosling and later published in his thesis of 1993[2.58]. Dynamic Relaxation was used, together with a quadratic iso-parametric element that was warped in 3 dimensional space and possessed 8 nodes and 24 degrees of freedom. The complex element formulation required a significant computational effort in manipulating the stiffness matrices of the elements of a discretised surface. It was found that the element was highly sensitive to large changes in geometry, and hence numerical instabilities could arise during the early stages of form-finding. A loss in surface smoothness was exhibited in cases where the surface curvature changed rapidly. These factors, combined with the fact that the condition of uniform stress was violated at equilibrium, suggested that the element was not ideally suited to form-finding problems.

2.4 The Application of Formex Algebra in Structural Analysis.

Over the past two decades, the increased use of C.A.D. by engineers in the structural design process has led to a greater dependency on quick, convenient and simple means of data generation using configuration processing tools. Examples range from the obscure WDKM programme developed by Obrebski[2.60], to the well established Formian programme. Formian is the programming language of a mathematical system called formex algebra.

Formex algebra was initially developed by Prof. H. Nooshin for the automated generation of large volumes of data relating to the configuration of space structures. The early ideologies of formex algebra can be traced back to 1975 when Nooshin published a paper in the

International Journal of Computers and Space Structures[2.61]. During the next fifteen years there occurred major revisions of Nooshin's work[2.62,2.63,2.64] in particular, a definitive book documenting all the unique rules, syntax, algebraic manipulations and applications of Formex algebra was published in 1984[2.65]. (For a simple account of the fundamentals of formex algebra it is recommended that the reader consults ref. 2.62). Nooshin, Yamada and Disney have since published a comprehensive manual to be used by architects and engineers for use with the Formian package[2.66]. A full description and account of the concepts of formex algebra and Formian are covered in Chapter 3, Section 3.2.

It is common for most structural analysis, or finite element, programmes to have some form of sub-programmes, or 'mesh generators', responsible for data generation. In a paper by Cheah[2.67], it was stated that these programmes are restricted in their applicability to the problem of data generation for the following reason. Mesh generators tend to have a limited choice of commands as they are required to produce data for a particular purpose, usually as input to a given analysis package. As a consequence, Engineers have little freedom of expression, with the programmes tending to direct the user to a solution instead of allowing the user a degree of freedom and adaptability in solving problems of a non-traditional nature. He proposed that formex algebra was a more refined solution. Furthermore, it was noted that formex algebra was a convenient and elegant means for the storage and organisation of data. Often, only a few lines of formex algebraic expressions were all that was required to generate the data for a large and complicated structure.

Sanchez[2.68] illustrated how formex algebra could be used to generate easily a variety of intricate doubly curved surfaces possessing the same interconnection pattern, but a differing surface geometry. This was a major development, as the surfaces generated using

formex algebra in the past tended to be related to space structures, which possessed a regular linear geometry and a 'skeletal' cable assembly[2.63]. Many of the surfaces described by Sanchez were ideally suited as approximate solutions before the determination of minimal surfaces using appropriate computational techniques. Recent work undertaken in the area of doubly curved shapes has been completed by Moore[2.69] and Hadker[2.70]. Moore's dissertation centred on the surface configuration of space structures and shells based on a hyperbolic paraboloidal geometry, whereas Hadker's thesis concerned the classification of a new branch of formex algebraic functions (paragenic formex formulations) that were created from the repetitive application of standard formex algebra expressions. The surfaces produced by Hadker were again doubly curved (Paragenic formex formulations are discussed in Chapter 3 Section 3.2.2.5).

Very little literature has been published addressing the applicability of Formian in the form-finding of membrane structures. The most notable publications being the two papers published by Nooshin & Yamada in 1991 and 1993[2.71, 2.72]. Yamada's paper of 1993 described the analysis of three simple membrane structures that were bound, both internally and externally, by tensioned cables. A computational analysis package, used by Yamada in previous form-finding investigations, was used for the determination of the equilibrated membrane geometry from geometric data generated using Formian. Regrettably, no information was given concerning the degree of accuracy and efficiency of the algorithm. The method of solution adopted by the programme was again not recorded. It may be argued that the surfaces could not be examples of stable minimal forms due to the negligible distortion of the membrane elements from the initial configuration, the use of internal cable elements to restrain the in-plane surface displacements, and, significantly, the violation of the condition of a constant pre-stress due to the inclusion of non-equal stressing in the warp

and weft directions of the fabric. Consequently, the examples were likely to have been 'dictated' and not 'form-found' shapes.

2.5 Examples of 'Form-Found' Structures.

2.5.1 Light-weight Tension Structures.

Day documented the design of a papal canopy in Dublin[2.73]. A soap film analogy was initially assumed during the design process However, restrictions were placed on the lateral nodal movement of the surface during form-finding, so as to enable the development of fabric strips with smooth edges. (This procedure is described using a simple example in Chapter 6, Section 6.2.3). Static analysis showed that the conic nature of the canopy provided difficulties in the generation of a uniform surface tension within the fabric during pre-stressing. This was because the form-found equilibrated surface was unsuitable, due to the excessive height of the conic hoop giving a very high curvature at the neck of the cone, leading to radial tension forces that were three times larger than those in the hoop direction. For reasons of aesthetics, fabrication and stressing, the shape was altered through the introduction of tension cables that lifted the form-found shape, reducing the neck curvature. After modification to the height of the hoop and the extension to the boundaries, the form was found to contain a fairly uneven surface pre-stress.

The Institute of Light-weight Structures (IL), based in Stuttgart, has published text concerning a history of all the structures the architect Frei Otto was involved in between the period 1955 and 1976[2.74]. Included were descriptions of structural materials, detailing and architectural concepts based on soap film models. The institute was itself designed by Otto as a cable and mast supported roof, which housed his architectural team in an "open and

flexible space". At Munich, Otto, in collaboration with the architectural firm Behnisch & Partner and the engineers Leonhardt & Andra, was given a brief to design a single 'environmental entity'. Otto was responsible for the configuration of the Olympic stadium; the geometry being obtained from rigid models constructed from soap film experiments. His solution was the creation of a series of tents, that appeared to form a continuous roof that covered one half of the main stadium, the Olympic entrance and the athletic and swimming halls. Otto stated his aversion to the engineers demand of a rigid transparent covering of acrylic panels; he believed that the Olympic roofs no longer supported his concept of a 'membrane structure'.

The Japanese book "Membrane Design in Japan" includes examples of many light-weight membranes, pneumatic roofs and hybrid membrane space structures[2.75]. A notable example being the Tokyo Dome "Big Egg" baseball stadium; a pneumatic structure[ix] constructed in 1988 which covers a floor area of 116,463 m^2. Little detail is included concerning the analysis and design of the documented structures.

Addis charts the history and advancement of tension structures through developments in computational techniques and fabric materials[2.76]. He believes it is a minor task to create aesthetic and dynamic structures, it is far harder to justify the manufacture and building of the form for all the variations in the anticipated imposed load conditions.

One of the most striking membrane structures constructed in recent years have been the unfolding membrane umbrellas designed by the German architectural firm SL[2.77]. These structures cover variable spans, the largest umbrella possessing a span of 17m × 8m.

[ix] A pneumatic structure refers to a membrane that has been pre-stressed through pressurised air; the air is maintained at a constant pressure within the closed environment spanned by the membrane. (The shape of such a structure is analogous to that of a soap bubble (Figure 2-5)).

Essentially, the membranes are light-weight mechanisms, that unfold in accordance with the intensity of the solar light, thereby providing shade and a comfortable environment in the court-yard of the Prophet's Holy Mosque in Madinah. The initial geometry of the structures were obtained from soap film experiments; an assessment of the suitability of the shape being made from a computational analysis using a transient matrix approach. The importance of a working prototype of the structure was emphasised as being essential.

2.5.2 Rigid Structures

Other than the work of Heinz Isler, previously mentioned in Chapter 1, there is little documentation available relating to the optimisation of the shape, and stress, of a rigid structure. This is probably because the stiffness of the structure, and the strength of the material, usually give more than an adequate resistance to the combinations of dead and live load cases. Normally, the geometry is only paramount in satisfying the aesthetic demands of the architect. An exception to this rule was the construction of a rigid structure of a health spa in Germany[2.78]. A rigid spatial timber structure was designed according to a brief where only axial forces under dead loading were to be present, a feature unique to tension structure design. The shape was form-found using the modified force density approach (ref. 2.46).

Aesthetic considerations led Hudson & Topping to use Dynamic Relaxation in the design of the geometry of reinforced concrete tents in Saudi Arabia[2.79]. A necessary requirement was that the structures should represent a series of traditional Arab tents, with each structure having no apparent support from beams. It was noted that the dead weight of the concrete was more than adequate in resisting the design uplift due to wind loading, a problem often encountered with fabric structures.

2.6 Summary

The major points of interest raised by the review of literature carried out within this Chapter are summarised below:

- The term 'minimal surface' refers to those surfaces where the mean curvature is zero[2.14]. Stable minimal surfaces describe surfaces modelled in Nature as soap films. They are characterised by minimum potential energy of surface tension (Chapter 3, Section 3.3.2) and, as a consequence, they possess a zero mean curvature[2.15, 2.16], a minimum surface area[2.17], a constant surface stress[x], and a stable equilibrated state[2.17].

- Unstable minimal surfaces cannot be modelled by soap films, it is not known how many unstable minimal surfaces span a given closed boundary[2.8].

- Mathematics can provide analytical solutions to only a few minimal surfaces bounded by a particular geometry e.g. the catenoid[2.12] by Euler and the skew quadrilateral by Schwarz[2.2]. There is no universal mathematical solution for the derivation of a minimal surface bounded by any boundary configuration. Hence the need for computational and numerical methods.

- Matrix methods of form-finding are susceptible to ill-conditioning problems during analysis. Further, forces can be calculated incorrectly due to an assumption of small scale displacements and straining. To prevent ill conditioning, it is usual to reformulate the matrix after a specified incremental period i.e. the matrix is transient. Controls may also be placed on the maximum allowable incremental displacement[2.28, 2.50] or the magnitude of the surface stresses during form-finding[2.31, 2.57, 2.58]. Divergence and ill-conditioning

[x] The property of a constant surface stress is explained in accordance to the surface tension in Chapter 3, Section 3.2.

may also be prevented by a judicious choice of the initial starting geometry[2.28, 2.29, 2.59]. For highly discretised surfaces, complex element formulations can result in an inefficient algorithm due to the tedious manipulation of a large matrix[2.43, 2.58].

- In the Dynamic Relaxation method, the nodal movement in any iteration is not a direct function of the element stiffness matrix[2.7]. The displacements depend only on the values of the previous nodal residual forces and the deformation of the surface at a prior increment of displacement. The problems of ill-conditioning associated with large matrices are avoided, because the method does not require a global matrix solution; it relies on the relaxation of out-of-balance forces at each node in turn, rather than all the nodes simultaneously. Kinetic damping is the preferred option, due to its efficiency, and ability, in handling problems where there are high out-of-balance forces, or the problem is highly geometrically non-linear[2.39, 2.43].

- Using a simplex element suggested by Barnes[2.38], it is possible to calculate forces from the current updated surface configuration without the need to consider a stiffness matrix, or the rigid body rotations of the element. Also, the formulation ensures the condition of constant stress will not be violated; the equilibrated forces are correctly related to the current geometry of the surface.

- To ensure the generation of a suitable cutting pattern, the nodal displacements may be restricted during form-finding[2.7,2.40,2.73]. It is not possible to recreate the geometry of a stable minimal surface from such a technique.

REFERENCES

2.1 S. Hildebrandt,
"Minimal Surfaces- A Short History."
Forming Bubbles, IL no. 18, Publication of the Institut für Leichte Flächentragwerke, University of Stuttgart, 1987, pages 310-317.

2.2 H. A. Schwarz,
"Gesammelte Mathematische Abhandlungen."
2 Vols. (1890) (Springer).

2.3 J. H. Argysis and D. W. Scharpf,
"Large Deflection Analysis of Pre-stressed Networks."
Journal of the Structural Division ASCE, Vol. 98, number st3, march 1972, pages 633 -654.

2.4 E. Haug and G. H. Powell,
"Finite Element Analysis of Non-Linear Membrane Structures."
Proceedings IASS Symposium Pacific part 11 on Tension Structures and Space Frames, Tokyo and Kyoto, 1971, pages 165-175.

2.5 A. S. Day,
"An Introduction to Dynamic Relaxation."
The Engineer, January 29th, no. 219, 1965, pages 218-2121.

2.6 A. S. Day and J. W. Bunce,
"Analysis of Cable Networks by Dynamic Relaxation."
Civil Engineering Public Works Review, Number 4, 1970, pages 383-386.

2.7 M. Barnes,
"Form and Stress Engineering of Tension Structures."
Structural Engineering Review, Vol. 6, no. 3-4, Elsevier Science Ltd., pages 175-202 1994.

2.8 S. Hildebrandt and A. Tromba,
"Mathematical and Optimal Form."
Scientific American Library, 1985, pages 21-24.

2.9 J. Tomlow,
"Design and Construction with Bricks-the Contribution of Antoni Gaudi (1852-1926)."
Ziegel Industrie International, October 1993, pages 597 - 605.

2.10 E. Happold, T. Ealey, W. I. Liddel and J. Pugh,
"The Design and Construction of a Diplomatic Club in Riyadh."
The Structural Engineer, Vol. 65a no. 1, January, 1987.

2.11 P. Varignon,
"Nouvelle Mecanique."
Vol. 2, 1725.

2.12 L. Euler,
"Methodus Inveniendi Lineas Curvas Maximi Minimive Proprietate Gaudentes Sive Solutio Problematis Isoperimetrici Latissimo Sensu Accepti."
Bousquet, Lausanne & Genf (1744). (vgl. auch: opera Omina Ser.I, Band 24.)

2.13J. L. Lagrange
"Essai d'une nouvelle methode pour determiner les maxima et les minima des formules integrales indefinies."
Miscellanea Taurinensia 2, 1760-61, pages 173-195.

2.14 J. B. M. C. Meusnier,
"Memorie sur la courborne des surfaces."
Mem. Math.-Phys. Acad. Sci. Paris, pages 477-510 (1785), verlesen 1776.

2.15 T. Young,
An essay on the Cohesion of Fluids."
Presented to the Royal Society London in 1805. (Miscellaneous Works, Vol. 1, pages 418-453, John Murray, London (1855).

2.16 M. Laplace,
"Traité dé Mécanique céleste."
Tome 4, Courcier, Paris (1805).

2.17 C. F. Gauss,
"Principia Generalia theorie figurae fluidorum in statu aequilibrii."
Göttingen 1830.

2.18 D. Trong Thi, A. T. Fomenko,
"Minimal Surfaces, Stratified Multivarifolds and the Plateau Problem."
American Mathematical Society, 1991, pages 32-34.

2.19 J. Plateau
"Statique experimentale et theoretique des liquides soumis aux seules forces moleculaires".
Tomes 1&2, Paris, Gauthiers-Villars, (1873).

2.20 J. Douglas,
"Solution of the problem of Plateau".
Journal Math. Phys., MIT 10, (1930-1931), pages 106-130.

2.21 T. Rado ,
" On Plateau's Problem".
Ann. of Math. (2) 31, (1930), pages 457-469.

2.22 F. Otto, R. Trostel,
"Tensile structures."
The MIT Press, Cambridge, Volume 1, 1967, p 290-296.

2.23 C. Isenberg,
"The Science of Soap Films and Bubbles."
Teito Ltd., 1978.

2.24 A. Siev and J. Eidelman,
"Shapes of Suspended Roofs."
Proceedings IASS colloquium on Hanging Roofs, Paris, 1962, pages 42-47.

2.25 K. Linkwitz and H. J. Scheck,
"Einige Bemerkungen zur Berechung von vorgespannten Seilnetzkonstruktionen."
Ingenieur-Archiv 40, pages 145-158 1971.

2.26 K. Linkwitz
"Analogies as a Powerful Tool for the Analysis of Nets."
Natural Structures, Principles, Strategies and Models in Architecture and Nature, Part 111, pages 11- 20.

2.27 K. Y. Tan,
"The Computer Design of Tensile Membrane Structures."
PhD Thesis, Dept. of Civil Engineering, Queensland University, 1989.

2.28 E. Haug and G. H. Powell,
"Analytical Shape Finding of Cable Nets."
Proceedings IASS Symposium Pacific part 11 on Tension Structures and Space Frames, Tokyo and Kyoto, 1971 pages 83-92.

2.29E. Haug and J. Oelberman,
"Numerical Calculation of Minimal Surfaces."
IL no. 18, Publication of the Institut für Leichte Flächentragwerke, University of Stuttgart, 1987, pages 370-380.

2.30M. J. Turner, E. H. Martin and R. J. Melosh,
"Large Deflections of Structures Subjected to Heating and External Loads."
Journal of Aero-Space Sciences, Volume 27, February, 1960, pages 97-106.

2.31 J. Argysis T. Angelopoulos and B. Bichat,
"A General Method for the Shape Finding of Light Weight Tension Structures."
Computer Methods in Applied Mechanics and Engineering, Vol. 3, 1974, pages 135-149.

2.32 O. A. Bussinger,
"Matrices which can be Scaled Optimally Scaled."
Num. Maths. 12, pages 346-348, 1968.

2.33 H. A. Bucholdt,
"Introduction to Cable Roof Structures."
Cambridge Uni. Press, 1985.

2.34 M. Hussey,
"Skeletal Assemblies Subject to Geometrically Significant Displacements."
2nd Pan-American Conference on Structures, Lima, 1964.

2.35 K. R. Rushton,
"The Dynamic Relaxation Method Used for Stress Analysis"
Proceedings of the Conference on Recent Advances in Stress Analysis,
Royal Aeronautical Society, 26-29 March 1968, London, pages 3.41-4.46.

2.36 M. R. Barnes,
"Pre-stressed Cable Networks."
Construction Research and Development Journal, Vol. 3, 1971.

2.37 M. R. Barnes,
"Applications of Dynamic Relaxation to the Design and Analysis of Tension Structures by Dynamic Relaxation."
2nd International Conference on Space Structures, Guildford, 1975.

2.38 M. R. Barnes,
"Form-Finding of Minimum Surface Membranes",
ASS World Congress on Space Enclosures Building Research Centre, Concordia University, Montreal, July 1976.

2.39 P.A. Cundall,
"Explicit Finite Difference Methods in Geo-mechanics."
Proceedings of E. F. Conference on the numerical methods in Geo-mechanics, Blacksburg, V.A., 1976.

2.40 M. R. Barnes,
"Form-Finding and Analysis of Pre-stressed Nets and Membranes."
Proceedings of the International Conference on Non-Conventional Structures, Volume 1, 1987, pages 327-338.

2.41 W. J. Lewis and M. S. Jones,
"Dynamic Relaxation Analysis of the Non-Linear Static Response of Pre-Tensioned Cable Roofs."
Computers and Structures, Vol. 18, no. 6, 1984, Pergamon Press Ltd., p 989-997.

2.42 M. R. Barnes,
"Non-Linear Numerical Solution Methods for Static and Dynamic analysis."
IL no. 15, Publication of the Institut für Leichte Flächentragwerke, University of Stuttgart, 1982, pages 150-166.

2.43 W. J. Lewis,
"The Efficiency of Numerical Methods for the Analysis of Pre-Stressed Nets and Pin Jointed Frame Structures."
Computers and Structures, Vol. 33, no. 3, pages 791-800.

2.44 J. Shan,
"Application of the Sub-Region Mixed Energy Principle to Numerical Modelling of Pre-Stressed Clad Cable Nets."
PhD, University of Warwick, Department of Engineering, 1990.

2.45 K. Ishii and T. Suzuki,
"Shape of Membrane Structures."
Proceedings of IASS Symposium, part 2 on Tension Structures and Space Frames, Tokyo and Kyoto, 1972, pages 127-136.

2.46 H. J. Schek,
"The Force Density Method for Form Finding and Computation of General Networks."
Computer Methods in Applied Mechanics and Engineering, Vol. 3, 1974, pages 115-134.

2.47 N. Pauli, A. Marty, D. Pierre and R. Motro,
"Two Cad Systems for Architectural Membranes."
Proceedings of the First International Seminar on Structural Morphology,
7-11 September 1992, pages 239-250.

2.48 N. Pauli and R. Motro,
"Latest Developments of Archimedes - the CAD System for Architectural Membranes under MS-DOS Environment."
Proceedings of the Second International Seminar on the Application of Structural Morphology to Architecture, October 1995, pages 139-148.

2.49 R. Motro,
"Structure and Space Structures."
Proceedings of the Second International Seminar on the Application of Structural Morphology to Architecture, October 1995, pages 119-128.

2.50 P. Kneen,
"Computer Aided Design of Tensioned Fabric Structures."
LSA 86, 1st International Conference on Light Weight Structures in Architecture, Sydney, 1986, proceedings Vol. 2, pages 992-1009.

2.51 L. Grundig,
"Minimal Surfaces for Finding Forms of Structural Membranes."
Computers and Structures, Vol. 30, no. 3, pages 679-683 1988.

2.52 P. Singer, D. Strobel, R. Hordt and J. Bahndorf,
"A Method for Finding Minimal Surfaces."
2nd International Symposium SFB 230, Stuttgart, 1991, pages 137-142.

2.53 T. Suzuki and Y. Hangai,
"Shape Analysis of Minimal Surface by the Finite Element Method"
Proceedings of the International IASS Symposium, 2-6 September 1991, Copenhagen, Denmark, 1991, pages 103-110.

2.54 P. D. Gosling and W. J. Lewis,
"Application of Constant Strain Triangular Membrane Elements to the Investigation of Minimal Energy Forms."
Research Report CE 36, Department of Engineering, University of Warwick, 1991.

2.55 P. D. Gosling and W. J. Lewis,
"Computer Modelling of Stable Minimal Surfaces."
Research Report CE 32, Department of Engineering, University of Warwick, 1990.

2.56 W. J. Lewis and P. D. Gosling,
"Minimum Energy Forms of Light Weight Tension Structures."
Proceedings of the first International Seminar on Structural Morphology, Montpellier, 7/11 September, 1992, pages 227-237.

2.57 W. J. Lewis and P. D. Gosling,
"Stable Minimal Surfaces in Form-Finding of Light weight Tension Structures."
International Journal of Space Structures, Vol. 8, no. 3, 1993, pages 149-166.

2.58 P. D. Gosling,
"Numerical Modelling of Stable Minimal Surfaces."
PhD, Dept. of Engineering, University of Warwick, 1992.

2.59 W. J. Lewis,
"Mathematical Formulae as a Medium for Shaping Membrane Forms."
Space Structures 4, Thomas Telford, London, 1993, pages 907-915.

2.60 J. B. Obrebski,
"On the Morphology of Certain Class of Two-Curvature Structures."
Proceedings of the Second International Seminar on the Application of Structural Morphology to Architecture, October 1995, pages 129-138.

2.61 H. Nooshin,
"Algebraic Representation and Processing of Structural Configurations."
International Journal of Computers and Structures, Volume 5, 1975, pages 119-130.

2.62 H. Nooshin,
"Basic Concepts of Formex Configuration Processing."
International Symposium on Membrane Structures and Space Frames, Osaka, Japan, September 15-19, 1986.

2.63 H. Nooshin,
"Formex Data Generation."
International Symposium on "Innovative Applications of Shells and Spatial Forms", Bangalore, India, November 21-25, 1988.

2.64 H. Nooshin and P. Disney,
"Elements of Formian."
Computers and Structures, Pergamon Press, Vol. 41, No. 6, pages 1183-1215, 1991.

2.65 H. Nooshin,
"Formex Configuration Processing in Structural Engineering."
Elsevier Applied Science Publishers, 1984.

2.66 H. Nooshin, P. Disney and C. Yamamoto,
"Formian."
Multi-Science Publishing Co. Ltd., 1993.

2.67 I. N. A. Cheah,
"Plenix Structural Analysis."
LSA 86, 1st International Conference on Light Weight Structures in Architecture, Proceedings Vol. 2, Sydney, 1986, pages 783-790.

2.68 J. Sanchez,
"Formex Algebra: an Algebra of Forms."
IL no. 36, Publication of the Institut für Leichte Flächentragwerke, University of Stuttgart, 1984, pages 194-195.

2.69 J. Moore,
"Investigation of Hyperbolic Paraboloidal Roof Structures."
MEng, Department of Civil Engineering, University of Surrey, 1994.

2.70 D. Hadker,
"Formex Configuration Processing for Space Structures."
PhD, Department of Civil Engineering, University of Surrey, 1993.

2.71 H. Nooshin and N. Yamada,
"Formex Pre-Processing for Membrane Structures."
Proceedings First U.S. National Congress on Computational Mechanics, Chicago, Illinois, July 1991.

2.72 N. Yamada,
"Initial Shape Generation for Membrane Structures"
Space Structures 4, Thomas Telford, London, 1993, pages 1169-1175.

2.73 A. S. Day,
"Form-Finding Control and Modification for Tension Structures."
The Arup Journal, Ove Arup Partnership, 1980, pages 19-20.

2.74 "The Work Of Frei Otto and his Team 1955-1976."
IL no. 17, Publication of the Institut für Leichte Flächentragwerke, University of Stuttgart, 1986.

2.75 "Membrane Design in Japan 1967-1990."
Shinkenchiku-sha Co., Ltd., 1990.

2.76 Bill Addis,
"The Engineers' Contribution to Contemporary Architecture: Tension Structures."
Building Centre Trust, 1992.

2.77 Sonderkonstruktionen und Leichtbau (SL),
"SL - Company Brochure."
Rohrer Strasse 140 D-70771 Leinfelden-Oberaichen.

2.78 L. Grundig and J. Bahndorf,
"Form-Finding of a Roof Structure for a Health Spa."
LSA 86, 1st International Conference on Light Weight Structures in Architecture, Sydney, 1986.

2.79 P. Hudson and B. Topping,
"The Design and Construction of Reinforced Concrete Tents in the Middle East."
The Structural Engineer, Vol. 69, no. 22, 19 November, 1991, pages 379-385.

CHAPTER 3

The Integrated Form-Finding Approach

3.1 Introduction.

Every form of computational analysis used in the assessment of the deformations induced upon a structural body under the application of a force, or an assumed surface stress (as is the case in the deisgn of light-weight tension structures), will consist of three main design stages: pre-processing, structural analysis and post-processing. With regards to form-finding, pre-processing concerns the generation of the discretised surface, the "**initial surface**", from data representing: the nodal co-ordinates, the numbers of the nodes connecting the surface elements and the node numbers forming the boundaries of the surface. Evidently, the second stage involves the determination of the topology of a stable minimal surface, using a suitable numerical approach that accurately mimics the properties of a soap lamina. Post-processing refers to the manipulation of the results obtained from a form-finding analysis, such that the surface may be used in practice.

It is common for all of these tasks to be accomplished within a single computer package[3.1]. This is often an undesirable option, as the package will have been designed for particular applications and may prove inadequate in solving problems unforeseen at the time of programme development. It is also likely to limit the number of possible geometrical arrangements of the elements forming a discretised surface. Documented within this Chapter is an alternative and novel approach, whereby three individual programmes, or programme segments, have been used to create an "integrated" method of form-finding that can be viewed as being an unconstrained and adaptive means of analysis. (i.e. the possible

applications of the computational solution presented in this thesis is shown to be limited only by the users imagination in his/her choice of the boundary geometry (Chapter 5), in addition to the expedient choice of the boundary geometry and discretisation of the surface such that an accurate stable minimal surface can be produced - not all boundaries can be spanned by a stable minimal surface (Chapter 2, Section 2.2, Chapter 4, Section 4.3.3), while the density of elements (Chapter 4, Section 4.3.1) and "crudeness" of the "initial surface" may well affect the accuracy of the final numerical solution (Chapter 4, Section 4.3.1 and Section 4.4.2)). Using an example of a stable minimal surface, the form-finding process is illustrated from the conception of the initial surface, through to the actual construction of a solid prototype from the numerical model (Each of the aforementioned stages of analysis form a sub-section of Chapter 3).

The integrated approach consists of the following programme segments:

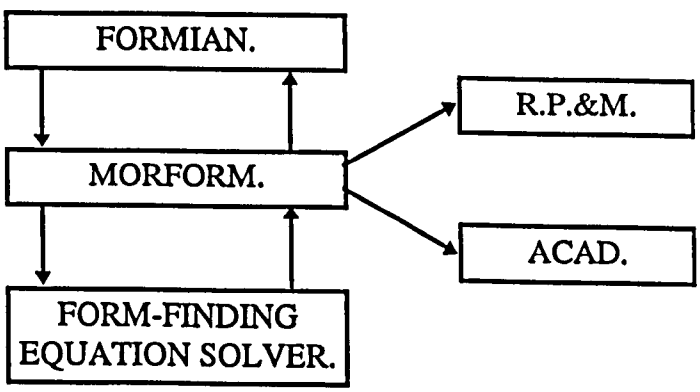

Figure 3-1 Components of the Integrated Form-Finding Approach.

Each segment has a particular purpose; the programme MORFORM is used as a medium for the transfer of data between the segments, leading to their integration into the form-finding process. (AutoCAD (ACAD) and FORMIAN are commercial programmes that were not written by the author. However, the 'form-finding equation solver' and the MORFORM programme were written by the author).

3.1.1 Pre-Processing.

As mentioned in Chapter 2 Section 2.2, there exist only a few analytical solutions that describe the topology of a stable minimal surface. Consequently, since it is impossible to predict the likely geometry of the form-found surface, the configuration must literally be 'found', and the approximate geometry of the initial surface becomes paramount in dictating the accuracy of the final solution. The use of formex algebra gives a significant degree of freedom and efficiency to the generation and alteration of the initial surface, in cases where convergence cannot be assured. The particular advantages of formex algebra will become apparent in subsequent chapters, but primarily they concern the ability to alter the boundary dimensions, element orientations and concentrations of elements efficiently and quickly. Pre-Processing (Section 3.2) is accomplished through the use of Formian, a computational configuration processing tool that is the programming language of formex algebra. Formex algebra is a mathematical system which has its own rules and syntax, in much the same manner as matrix algebra has its own.

3.1.2 Numerical Analysis.

The equation solver, discussed in Section 3.3, utilises the Dynamic Relaxation algorithm to find the solution of a stable minimal surface based on the initial surface created from Formian.

3.1.3 Post-Processing.

Post-processing involves the generation of solid models through the use of rapid prototyping manufacture (R.P.&M.). Soap film models can be used for the accurate 'ideal' representation of the geometry of a stable minimal surface[1]. However, although a soap film model adequately depicts the surface geometry and allows one to make a basic assessment

[1] Chapter 4 includes examples of soap film experiments.

of the surface's practicality, the model is not durable, and often breaks, leaving behind photographs as the only evidence of the form (Chapter 1, Section 1.2). The problem of constructing a physical model according to the exact configuration of a numerical form-found minimal surface has, until now, not been solved. Section 3.4 shows how the integration of Formian with the Dynamic Relaxation algorithm enables one to post-process form-found data. This is an original concept, which facilitates the process of obtaining computational models suitable for manufacture using R.P.&M. Solid models are important for the physical visualisation of a form, the determination of a fabric structures' cutting pattern, and for comparisons of the topology of the computationally derived surface with that of the 'ideal' soap film model, or any other model. Also, the question of the role aerodynamics plays in the efficiency and durability of a life-size rigid structure[ii], with a stable minimal surface geometry, could be addressed through wind tests carried out on a solid model. Rapid prototyping is a relatively new technology which has begun to take over from more traditional manufacturing methods such as computationally numerically controlled tooling (C.N.C.), owing to its far superior accuracy, and ability to construct models directly from CAD data. Much work has been published dedicated to the process of the translation of CAD data to the ".STL" format used by R.P.&M. (Section 3.4). The format requires the creation of an enclosed tessellated model, a process accomplished by the author through the use of formex algebra, and the subsequent translation of the data using an algorithm incorporated into the MORFORM programme. Post-processing can also entail the manipulation, by Formian, of those surfaces generated by the equation solver, in order to create totally new forms. A graphical visualisation of the form-found surface may be achieved through the use of ACAD, which includes options such as the addition of detailing to the numerical model, or the use of such graphical effects as rendering.

[ii] Examples of structures that are solid non-fabric minimal forms include the concrete tents constructed in Saudi Arabia at the Jandiryah complex, (ref. 2.79).

3.1 Pre-Processing Discretisation of the Initial Surface.

3.1.1 Introduction.

An explanation of some of the basic concepts of formex algebra are included in this Section. A more detailed account can be found in the significant volume of text published by Nooshin et al[3.2,3.3]. A simple example of a discretised surface is given in Section 3.2.3 as a means of illustrating the necessary formex algebra manipulations required for the calculation of form-finding data. It is described how such manipulations may be grouped together and used in a single step within Formian, by creating a Formian file called a 'scheme'.

3.1.2 Explanation of Formex Algebra.

Formex algebra simplifies the generation of geometric data by separating the creation of data relating to the interconnection pattern of the elements forming the discretised surface, **(compretic information)**, from that of the geometry of the surface, **(normic information)**. Instead, the geometric description of a surface is found from the application of a suitable geometrical transformation, a **'retronorm'**, to a formex depicting the compretic information; a formex being the mathematical entity of formex algebra.

3.1.2.1 Generation of Compretic Information.

Formex algebra uses the term **'compret'** to describe the arrangement of the entity, or entities, used in the discretisation of a surface. For example, the 'compret' of the mesh of Figure 3-2 (a) would be either a single triangle element, or the single square element composed of two triangles. Before describing the configuration pattern of a surface, it is

necessary to define a suitable reference system called a 'normat'. A **'normat'** is the array of points, or grid lines, used for the convenient graphical representation of a formex's configuration pattern. Figure 3-2 (b) illustrates a suitable normat arrangement. Formian has the ability to display graphically the output produced from a series of formex algebra expressions, thereby enabling the validity of the compretic information to be easily assessed.

(a)

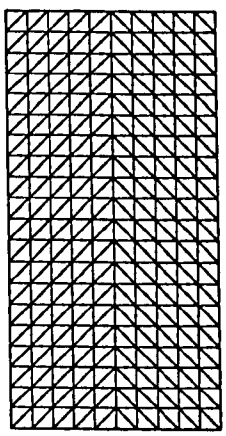

(b)

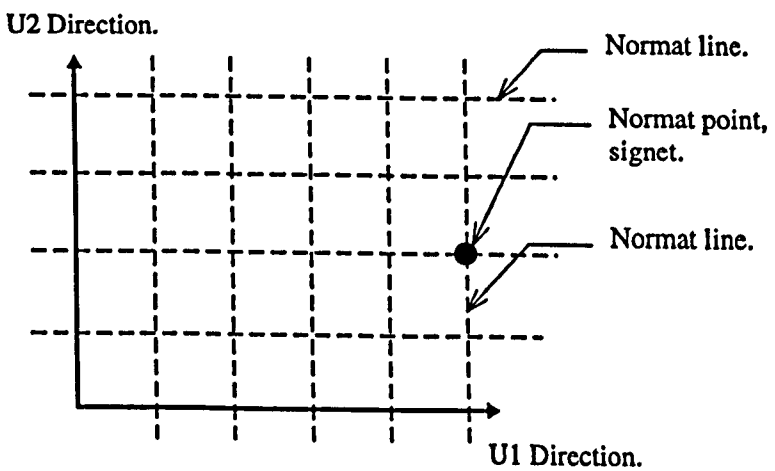

Figure 3-2 (a) Example of a Simple Discretised Surface. (b) Suitable Normat Arrangement for the Generation of the Formex 'mesh'.

(a)

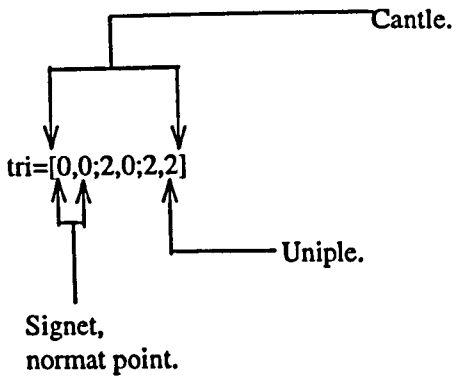

(b)

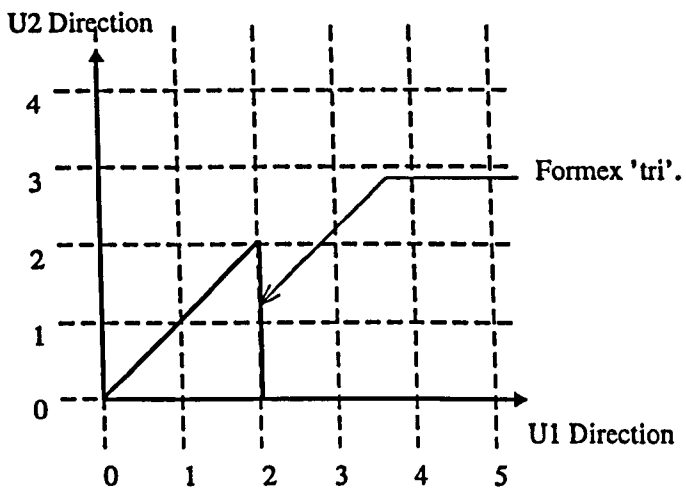

Figure 3-3 (a) Construct of Formex 'tri'. (b) Configuration Pattern of Formex 'tri'.

The square pair of brackets contained within the construct of a formex are called the **'cantles'** of a formex. A formex always contains at least one cantle. From Figure 3-3 (a) it can be seen that formex 'tri' possesses only one cantle, which represents the configuration of the compret in Figure 3-3(b). Each cantle of a formex contains a series of integers, or real numbers, called **'uniples'**. A uniple relates to one of the normat lines. Although real numbers may be used to describe the compretic information, it is more convenient to use integer 'uniples' and, instead, convert these values into real numbers after the application of a retronorm transformation. The position whereby two, or more normat lines intersect is called a **'normat point'**, Figure 3-2(b). Such points may be depicted by the values of the 'uniples' contained within a **'signet'**. 'Signets' are separated from each other by semi-colons, whereas 'uniples' are separated from each other by commas. According to the

normat arrangement of Figure 3-2 (b), the first uniple of a signet corresponds to the U1 direction, while the second uniple corresponds to the U2 direction. A series of 'signets' separated from one another by a semicolon indicates that there is a connection between the 'signets', or 'normat points'. For example, a formex that contains a series of cantles with only one signet being held within each cantle, may be thought of as giving the co-ordinates, or configuration pattern, of a series of nodes. Alternatively, a formex containing cantles that possess two or more signets separated from each other by a semi-colon, can be thought of as representing a series of lines joining the normat points of a cantle's signets, in the order in which the signets are found. The **'order'** of a formex is used to describe the number of cantles contained within a formex, while the term **'plexitude'** refers to the number of signets contained within a cantle. The phrase **'grade'** relates to the number of uniples contained within each signet. According to the formex construct of Figure 3-3 (a), formex 'tri' can be seen to have a value of 1 for the 'order', and values of 3 and 2 for the 'plexitude' and 'grade' respectively.

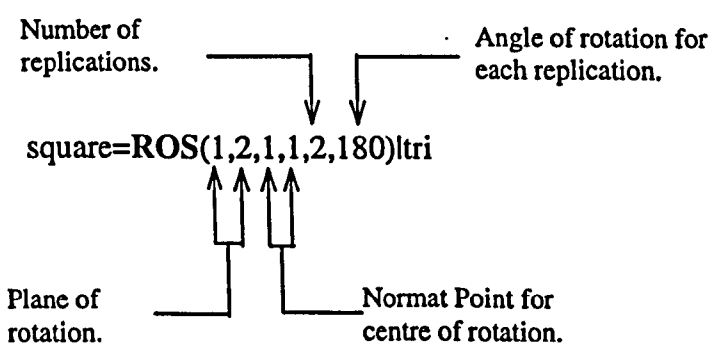

Figure 3-4 Construct of Formex 'square'.

To obtain the required 'square' compret, the formex algebra function rosette (**ROS**) function is used, as shown in Figure 3-4. **'Formex functions'** are used to change one formex into another formex according to the rule associated with the function. The **'argument'** of a formex function is used to refer to the formex that is to be changed by a function. The argument is separated from the function statement by the operator symbol '|'.

Like all functions in formex algebra, the ROS function requires a value/values for its 'canonic' parameters. The **'canonic parameters'** of a function are the parameters, contained within brackets, used for the definition of the action of the formex function on the formex argument. For instance, the ROS function has canonic parameters that define the plane of rotation used for the rotation of the 'tri' formex about a pre-defined centre point. It can be seen from the formex construct shown in Figure 3-4, that the generation of formex 'square' involves the rotation of the 'tri' argument in the U1, U2 plane about the centre point 1,1. The remaining canonic parameters are used to define the number of replications of the 'tri' argument and the angle of rotation for each replication. Figure 3-5(b) gives the configuration pattern for the 'square' formex, situated in the left hand corner of the mesh illustrated in Figure 3-2 (a). With respect to Figure 3-5 (a), it is apparent that formex 'square' has an 'order' of two, where each cantle represents the triangle elements of Figure 3-5 (b). Each cantle contains three signets, where each signet gives the U1, U2 normat points of the vertices of a triangle element. Consequently, 'square' possesses a 'plexitude' of three and a 'grade' of two.

(a)

square = [0,0;2,0;2,2], [2,2;0,2;0,0]

(b)

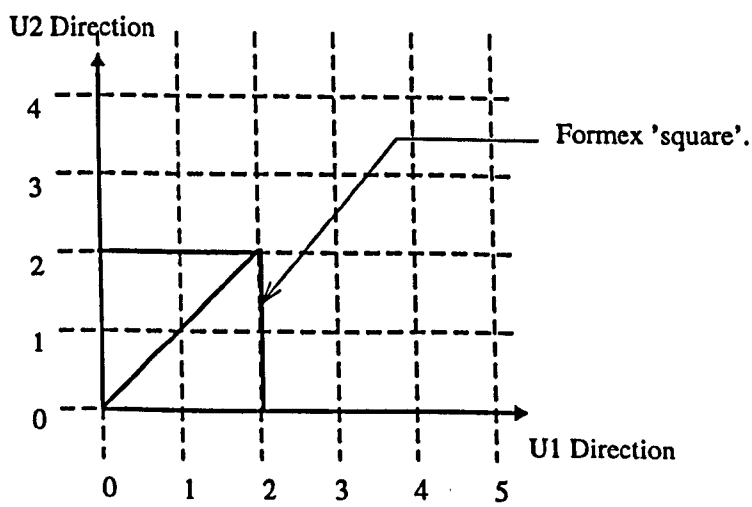

Figure 3-5 (a) Value of Formex 'square'. (b) Configuration Pattern of Formex 'square'.

Using the compret 'square', one half of the mesh of Figure 3-2 (a) can be created through the implementation of the 'rindle tendid' function (**RINID**); a function which allows for the replication of a formex in the U1 and U2 directions over a translational distance specified in its canonic parameters, as shown in Figure 3-6(a).

(a)

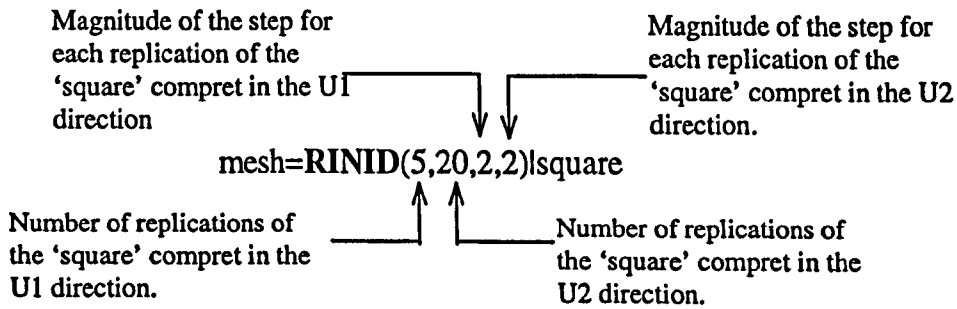

(b)

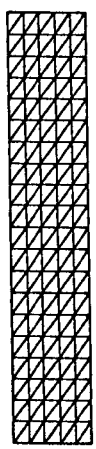

Figure 3-6 (a) Construct of Formex 'mesh'. (b) Configuration Pattern of Formex 'mesh'.

The mesh shown in Figure 3-7 (b), formex 'mesh2', is found by reflecting the 'mesh' formex, shown in Figure 3-6 (b), about a plane perpendicular to both the U1 normat direction and the U1, U2 plane, an action made possible through the use of the lambda function (**LAM**). The following statement reflects the 'mesh' formex about a plane intersecting the U1 normat at the point 10:

$$\text{mesh2} = \text{LAM}(1,10)|\text{mesh}$$

Figure 3-7 (a) gives the values for the first and last two cantles of the formex 'mesh2'. The first two cantles of 'mesh2' correspond to the cantles of formex 'square' as illustrated in

Figure 3-5 (b). As a result of the earlier transformations, the 'mesh2' formex contains four hundred elements i.e. each triangle element is represented by a cantle of the 'mesh2' formex and therefore the formex has an order of four hundred.

(a)

mesh2 =[0,0;2,0;2,2],[2,2;0,2;0,0],....cantles 3-398.....,[20,38;18,38;18,40],[20,38;20,40;18,40]

(b)

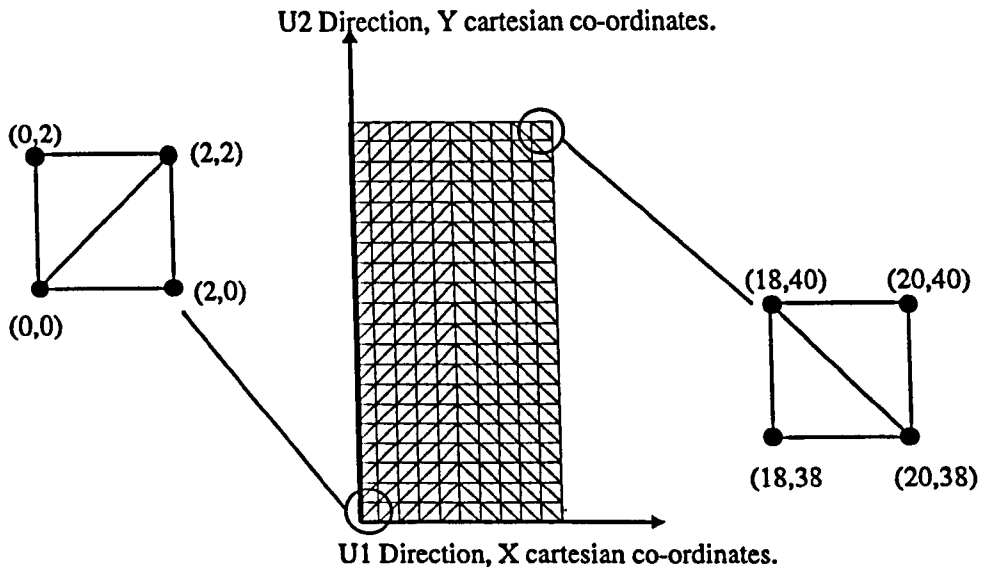

Figure 3-7 (a) Value of Formex 'mesh2'. (b) Configuration Pattern of Formex 'mesh2'.

The normat arrangement of the configuration pattern shown in Figure 3-7 (b) can be considered to conform to the Cartesian 'X' and 'Y' axes. Hence, the values of the signets, or normat points, of the formex 'mesh2' may be used to obtain the 'X', 'Y' co-ordinates of the nodes of the surface. Should it be necessary to define the position of the mesh contained in the 'X', 'Y' Cartesian plane relative to the Cartesian 'Z' axis, a third uniple would be required for the definition of the U3 normat direction aligned perpendicular to the U1, U2 plane. Such a requirement would increase the grade of the aforementioned formices to three.

The reader should be reminded that the formex functions described previously are not indicative of the actual capability of formex algebra in configuration processing.

3.1.2.2 Retronorms.

Once a formex has been defined according to a normat arrangement, formex retronorm functions are used to alter the surface geometrically. The compretic pattern of the elements and nodes remains the same, but the retronorms cause the transformed formex to be referenced according to a new Cartesian global system. The process is used to obtain the normic properties of a surface. Normic information refers to the actual dimensions of the surface. In the case of Figure 3-7 (b), the normat lines are aligned in the directions of the axes of a Cartesian co-ordinate system, and hence define both the compretic, and normic information of the formex 'mesh2'.

The compretic information of the 'mesh2' formex can be used for the creation of a new surface based on a different geometric arrangement, but a similar element configuration. A simple alteration would be to change the dimensions of the surface shown in Figure 3-7 (b) in the 'X', 'Y' Cartesian directions by the use of the basi-bifect retronorm (BB):

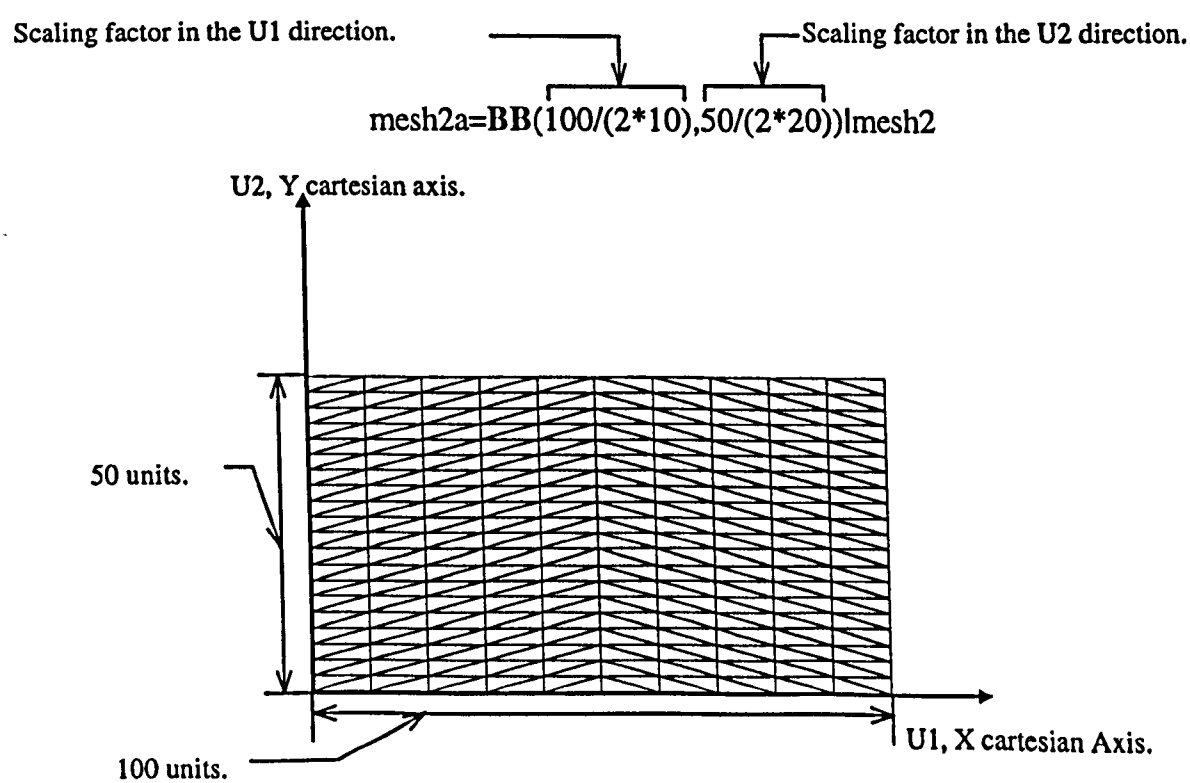

Figure 3-8 Configuration Pattern of Formex 'mesh2a'.

A more interesting barrel vault structure can be created by using the basi-cylindrical retronorm (BC). The basi-cylindrical normat may be thought of as representing the surfaces formed by concentric cylinders of an infinite length. Depending on the values of the scaling parameters of the BC function, it is possible to describe a cylinder of a given radius, length and circumferential distance. The normat used by the BC function is given in Figure 3-12. In this instance, the values of the second uniple of a signet determine the position of the normat points relative to the R2 normat direction i.e. along the circumference of the barrel, (angular co-ordinate). The R3 direction is parallel to the length of the barrel, while the R1 direction is parallel to the radius of curvature of the barrel vault (radial co-ordinate). With respect to the barrel vault shown in Figure 3-12, each angular division in the R2 direction is found from the calculation of 60/20 i.e. the barrel vault radius sweeps through an angle of 3 degrees, at each step in the R2 direction, as shown in Figure 3-11.

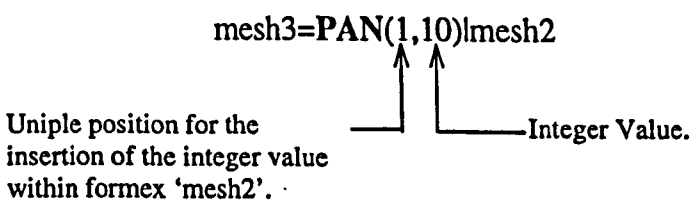

Figure 3-9 Construct of Formex 'mesh3'.

Because the BC retronorm requires a normat possessing lines in three directions, it is necessary to alter the signets of the 'mesh2' formex to take account of the direction of the third normat line, the radial co-ordinate R1. The statement in Figure 3-9 is used to create the 'mesh3' formex by the insertion of an integer value of 10, accomplished through the use of the pansion function (PAN), at the position of the first uniple in every signet contained within the cantles of the formex 'mesh2'.

mesh3 =[10,0,0;10,2,0;10,2,2],[10,2,2;10,0,2;10,0,0],....cantles 3-398.....,[10,20,38;10,20,40;10,18,40],[10,18,40;10,18,38;10,20,38]

Figure 3-10 Value of Formex 'mesh3'.

The effect of the pansion function may be observed by comparing the values of the two formices 'mesh2', Figure 3-7 (a), and 'mesh3', Figure 3-10. It is evident that the uniple values of formex 'mesh2' remain unchanged, they simply occupy a different position in the signets of formex 'mesh3'. The formex 'mesh3' has a grade of three due to the inclusion of the uniple integer ten.

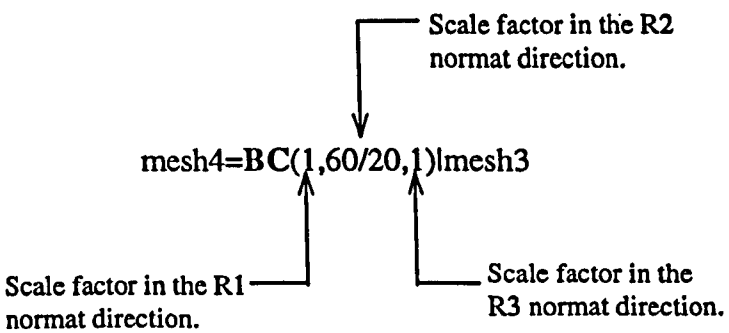

Figure 3-11 Construct of Formex 'mesh4'.

The formex construct given in Figure 3-11 creates the configuration pattern shown in Figure 3-12. It should be noted that the directions of the 'X', 'Y' and 'Z'[iii] axes are the reference directions of the global co-ordinates after application of the basi-cylindrical retronorm (BC)to the indicated R1, R2, R3 normat lines. Such global co-ordinates are represented by the values of the first, second and third uniples of a signet contained within a cantle of 'mesh4'.

[iii] The arrangement of the global X, Y, Z axes is relative to a right handed three dimensional co-ordinate system.

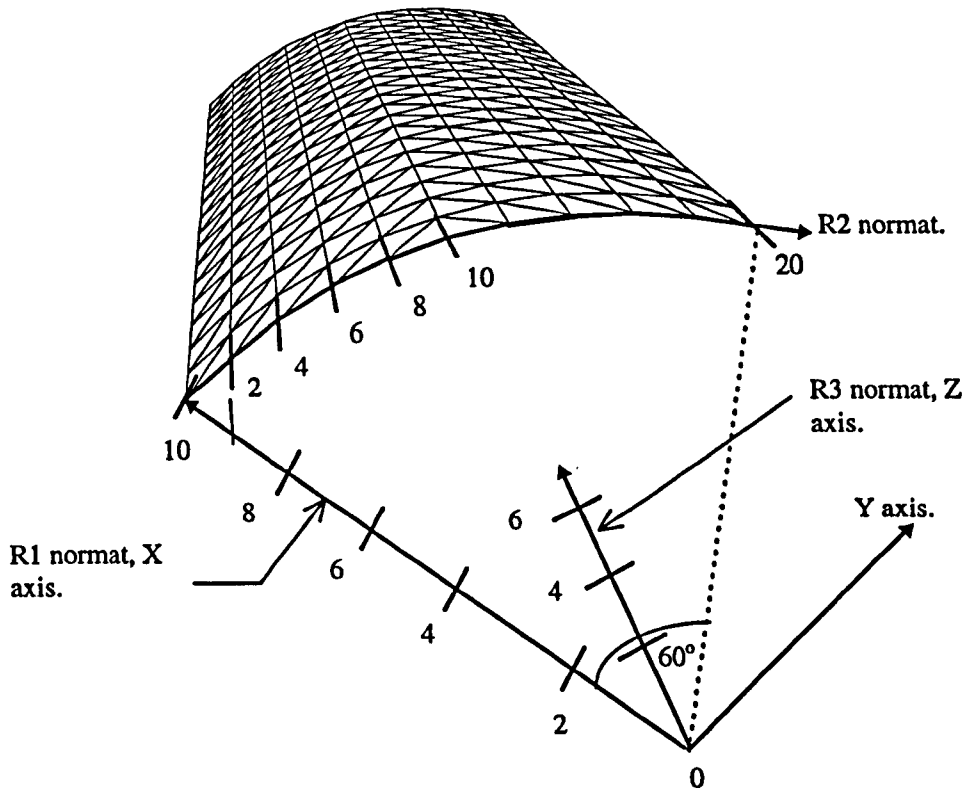

Figure 3-12 Configuration Pattern and Normat Directions of Formex 'Mesh4'.

Both formices 'mesh4' and 'mesh3' possess similar compretic properties. However, the normic properties of the formices are different. The separation of the compretic and normic information is a convenient option; it allows one to consider the configuration pattern of the surface, with respect to a normat, without having to consider the values of the actual co-ordinates of the surface at the same time.

3.1.2.3 Generic Formex Formulations.

Generic formex formulations refer to those formex algebra statements that have been defined according to a series of variable parameters. Such formulations allow a wide range of structural configurations to be constructed by the change of the parameters.

3.1.2.4 Formex Schemes.

A scheme is a means of grouping together all the Formian commands and formex algebra constructs necessary for the generation of a discretised surface and its associated geometric data. It removes the necessity of having to consider each aspect of the surface a step at a time.

The barrel vault structure of Figure 3-12 can be generated from the scheme below:

```
VAULT ='[::
tri =[0,0;2,0;2,2]
square = ROS(1,2,1,1,2,180)|tri
mesh = RINID(5,20,2,2)|square
mesh2 = LAM(1,10)|mesh
mesh3 = PAN(1,10)|mesh2
mesh4 = BC(1,60/20,1)|mesh3
USE VM(2),VT(2),VP(10,10,-40),VC(0,0,100),..
      VR(0,0,0,1,1,0)
SHOW mesh4]'
```

Table 3-1 Scheme 'VAULT'

It can be seen from Table 3-1 that it is necessary to assign a name to the scheme initially. Once completed, the formex statements contained within the scheme's 'body' may be written; such statements are enclosed by the symbol "[::]". The Formian command *SHOW* is used for the displaying of the formex 'mesh4' on a graphics terminal according to the co-ordinates of the view point, *VP*, the view centre, *VC* and the view rise, *VR*. *VM* is the viewing mode; *VM(2)* implying that the picture should be scaled to fit on the screen. *VT* states the view type; *VT(2)* specifying a perspective view.

By entering the Formian command:

KEEP VAULT

the scheme is stored as an ASCII text file and may be loaded into Formian by the command:

TAKE VAULT.

Typing the name of the scheme will invoke the series of formex algebra statements and Formian commands that form the 'body' of the scheme.

Assigning variable parameters to a scheme allows the formex statements contained within the scheme's 'body' to be of a generic formex formulation. Consider the scheme below:

```
VAULT2 ='[:m,n,angle,radius:
tri =[0,0;2,0;2,2]
square = ROS(1,2,1,1,2,180)|tri
mesh = RINID(m,n,2,2)|square
mesh2 = LAM(1,2*m)|mesh
mesh3 = PAN(1,radius)|mesh2
mesh4 = BC(1,angle/(4*m),1)|mesh3
USE VM(2),VT(2),VP(2*radius,2*radius,-4*radius),VC(0,0,5*radius),..
    VR(0,0,0,1,1,0)
SHOW mesh4]'
```

Table 3-2 Scheme 'VAULT2'.

The parameters 'm' and 'n' refer to the number of elements in the R2 and R3 normat directions, (Figure 3-12), while 'angle' and 'radius' refer to the length of the cylinder radius in the R1 normat direction, and the angle swept by the radius in the R2 normat direction. The parameters of a scheme are called the **'nominal parameters'**, and must be defined within the 'head' of the scheme; enclosed by the symbol '::'. In the case of the scheme 'VAULT2', the values of the parameters must also be supplied to the scheme when invoking it.

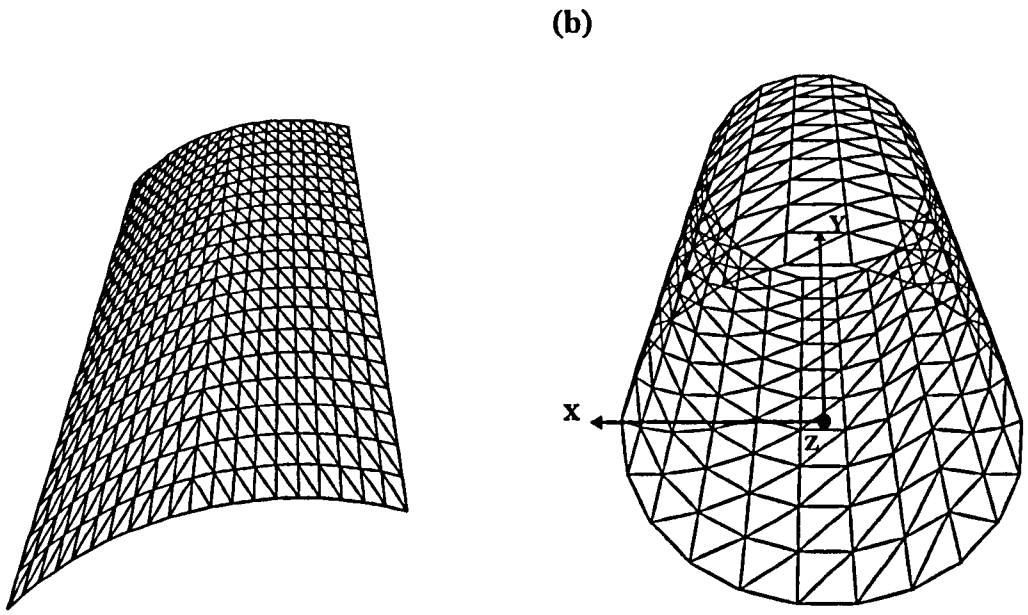

Figure 3-13 Surfaces Obtained from (a) 'VAULT2(10,20,60,10)'. (b) 'VAULT2(10,10,360,5)'.

The two formices created from the VAULT2 scheme (Table 3-2), and depicted in Figure 3-13, possess contrasting 'compretic' and 'normic' properties. Thus, it is possible to create a diverse range of surfaces by simply changing the parameters of a scheme. Furthermore, the parameters and the text used to form a scheme are the only data that needs to be saved. There is no need for the storage of vast amounts of numerical input data for every slight topographic adjustment of a discretised surface.

3.1.2.5 Paragenic Retronorm Formulations.

A non-standard geometric transformation may be created by combining a range of standard retronorm functions[3.4]. Such a transformation is called a paragenic formex formulation. Many of the numerical examples in Chapters 4 and 5 have been generated using such an approach. As a simple example, the generation of a doubly curved surface, created from the repeated application of the basi-cylindrical retronorm (**BC**), is documented. The surface is similar to the initial surface used in the form-finding of the numerical solution presented in Chapter 5, Section 5.2. It is recommended that the reader consults the author's research report[3.5] and ref.[3.4] should further details of paragenic formulations be required.

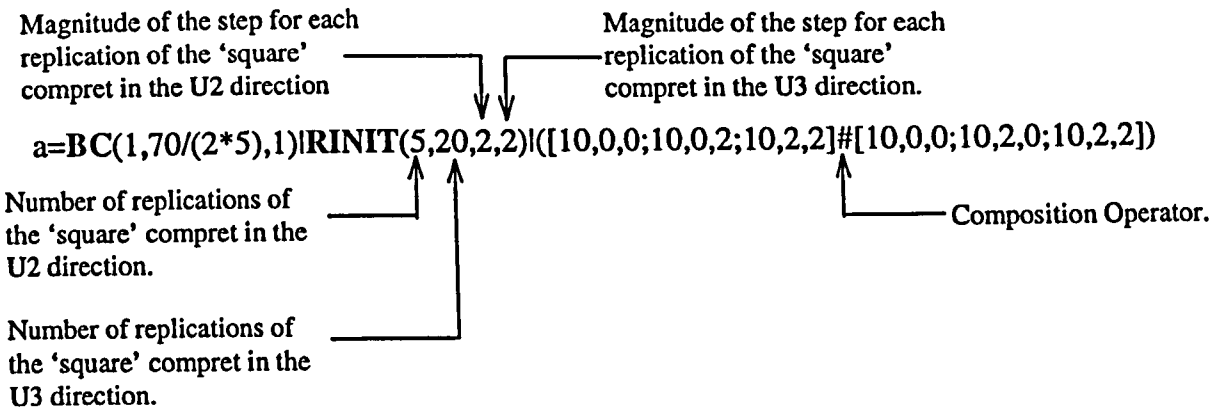

Figure 3-14 Construct of Formex 'a'.

The formex statement in Figure 3-14 generates a barrel vault structure of a similar configuration as that of 'mesh4'. In this instance, there are 5 elements along the circumference of the cylinder in the R2 normat direction, and 20 elements along the length of the vault, the R3 direction. The vault is formed from the compret consisting of a square containing two triangular elements. The compret is obtained from the composition[iv] of two formices, each representing a triangle, through the use of the '#' operator. The compret is then replicated in the R2 and R3 directions by the use of the 'rindle tendit' function. The front profile of the vault formex 'a' is given in Figure 3-15

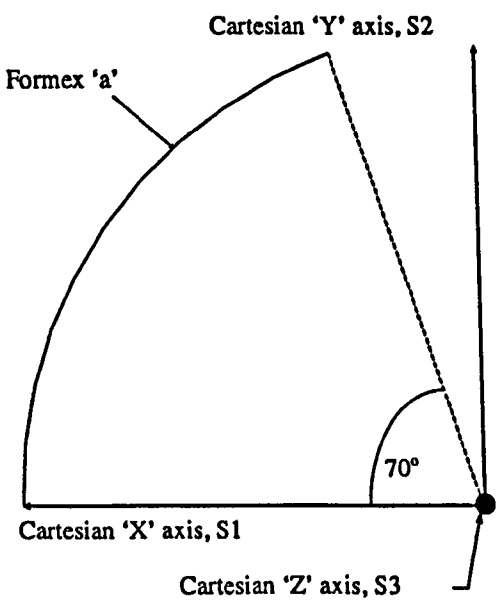

Figure 3-15 Front Elevation of Formex 'a'.

[iv] 'Composition' implies the joining together of two, or more, formices such that a new formex is created that contains all the properties of the formices to be united.

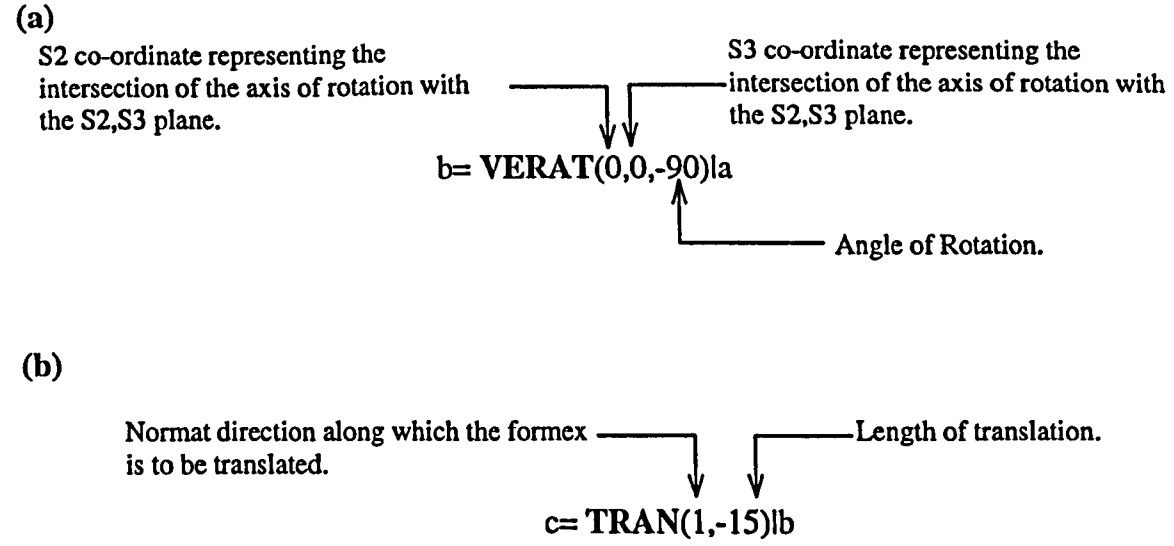

Figure 3-16 (a) Construct of Formex 'b'. (b) Construct of Formex 'c'.

Further manipulations of formex 'a' are now relative to the Cartesian X, Y, Z, axes, i.e., subsequent formex functions correspond to a new normat; in this instance the normat is given by S1, S2, S3. The surface is now rotated about an axis perpendicular to the S2, S3 normat lines, and through an angle of ninety degrees. This is accomplished by the 'vertitian proviat' function (VERAT). The canonic parameters of the function require the normat point that the perpendicular axis intersects with the S2, S3 plane, and also the angle of rotation about this axis. The positive angle of rotation is taken as the direction of rotation the positive S2 normat line makes, when rotating towards the positive S3 normat line. From Figure 3-17, it can be seen that the positive direction is given by the clock-wise rotation of the S2 axis towards the S3 axis, when the angle of rotation is viewed from a point behind the S2, S3 plane and in a direction looking along the S1 axis. Formex 'b' is created from the negative, or anti-clockwise rotation, of formex 'a'. Formex 'b' is now translated through 15 divisions in the negative S1 direction; an action accomplished through the use of the translation function (TRAN), (Figure 3-16 (b)). The effect of the aforementioned transformations is illustrated in Figure 3-17.

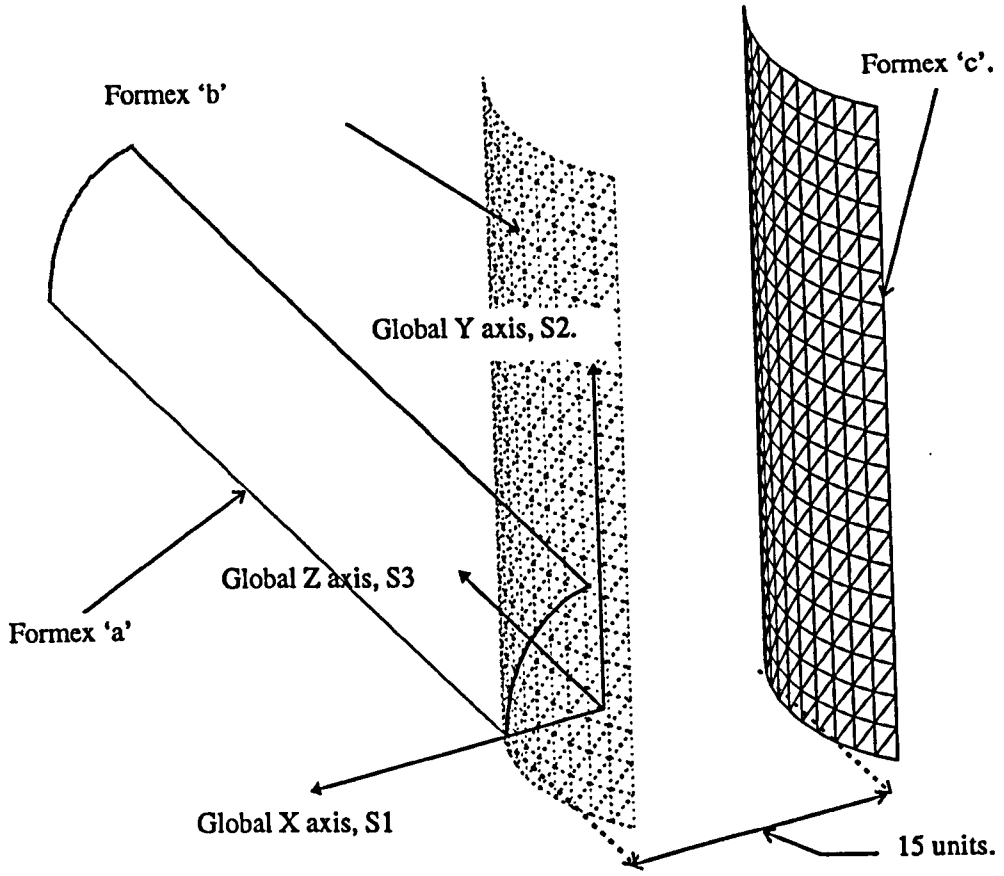

Figure 3-17 Rotation and Translation of Formex 'a'.

surf=BC(1,360/(2*20),1)lc

The final manipulation involves the implementation of the BC retronorm for the 'wrapping' of the formex 'c' through an angle of three hundred and sixty degrees, in an anticlockwise direction[v], about the S3 axis. This enables the top and bottom edges of the surface to form two closed circular rings.

v The BC retronorm assumes a direction of rotation according to the ascending values of the points in the R2 normat direction and about an axis defined by the centre-point of the radius, or R1 normat line.

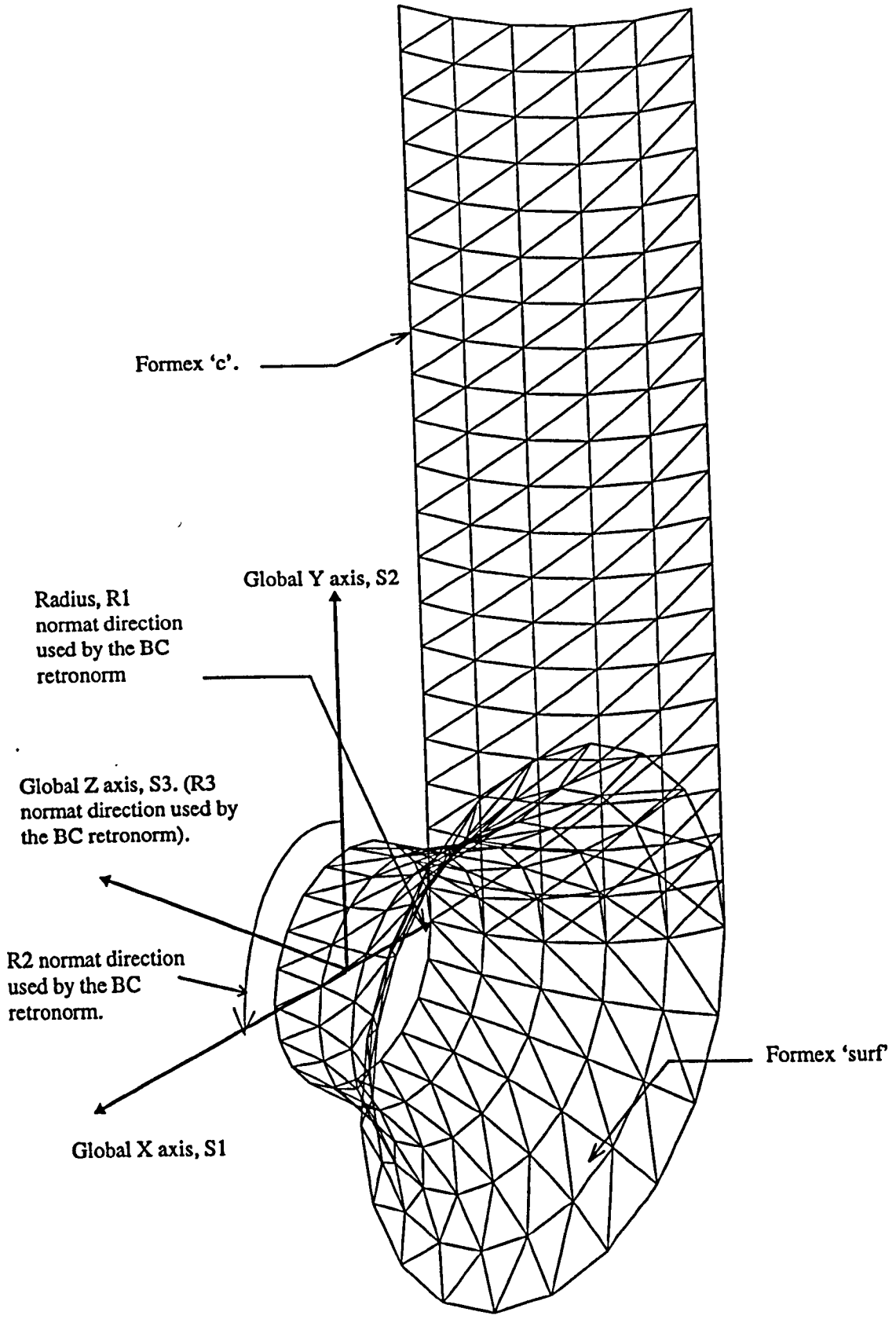

Figure 3-18 Generation of Formex 'surf'.

3.1.3 Procedure for the Generation of Form-Finding Data Using Formex Algebra.

The generation of form-finding data requires the derivation of a scheme, of a generic formex formulation, that creates a group of three formices containing information relating to:

- The global co-ordinates of each node, formex ***'totnod'*** (Table 3-3).
- The connectivity of the elements i.e. the numbers of the nodes forming the vertices of a triangle element, formex ***'mem'*** (Table 3-3).
- The connectivity of the nodes forming the fixed boundary of the surface, formex ***'memb'*** (Table 3-3).

On invoking the ***KEEP*** command, the data within a formex is saved by Formian as a binary file. Binary files differ from ASCII text files in that they consist of a series of unintelligible characters that cannot be interpreted for use by an external programme, unless the composition of the data and the format used for the writing of the information to the file is known beforehand[vi]. This requires the translation of the formex form-finding data into a format suitable for use by the form-finding equation solver using the MORFORM programme.

The method by which formices 'mem', 'totnod' and 'memb' are derived is best explained using an example. The scheme presented in Table 3-3 is used for the creation of the surface depicted in Figure 3-19.

[vi] Details of how Formian creates and stores formex files are given in "Formian", ref. 3.2.

BOX='[:m,n,width,length,height:	*A)* **Definition of the variables used within the body of the scheme.**
square =[0,0,0;0,2,0;2,0,0]#[2,0,0;0,2,0;2,2,0] rect = **LAM**(1,2)|square segment = **ROSAD**(2,2,2,180)|rect	*B)***Generation of the configuration pattern of the 'compret' of the surface.**

base = **RINID**(m,n,4,4)|segment
side = **VERAS**(ric|4*m,0,-90)|base
surf =(**TRAN**(1,-4*m)|side)#side#base
nod =(**RIN**(1,(2*m)+1,2)|([0,0,0]#[0,4*n,0]))
sidenod = **RIN**(2,(2*n)-1,2)|[0,2,0]
noda = **VERAS**(ric|4*m,0,-90)|(nod#sidenod)
nodb =(**TRAN**(1,-4*m)|noda)#noda#nod
nodb = **PEX**|nodb
	C) **Generation of the configuration pattern of the discretised surface and the boundary nodes.**

u1 = width/(4*m) u2 = length/(4*n) u3 = height/(4*m) surface = **BT**(u1,u2,u3)|surf bound = **BT**(u1,u2,u3)|nodb	*D)* **Geometrical transformation of the configuration pattern of the surface, and the boundary nodes using a retronorm.**
interior = **LUX**(bound)|surface interior = MED|interior bound = MED|bound totnod = bound#interior mem = **DIC**(totnod)|surface memb = **DIC**(totnod)|bound	*E)* **Determination of formices representing the form-finding data.**
KEEP mem,totnod,memb *CLEAR* *USE VM(2),VH(10,0,20,0,5,0,0,5,1)* *SHOW* surface]'	*F)* **Formian commands used for the graphical representation of the surface, and the saving of any formices containing form-finding data.**

Table 3-3 Scheme 'BOX'.

Figure 3-19 shows the discretised surface, depicted by the formex 'surface', after invoking the scheme **BOX(4,4,10,10,10).**

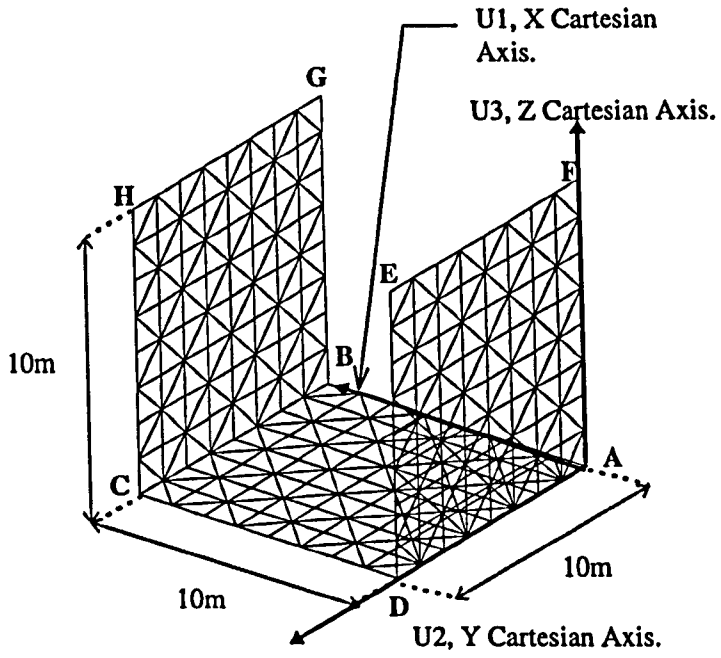

Figure 3-19 Initial Surface Obtained from the Scheme 'BOX' - Formex 'surface'.

The formex manipulations involved in stages A)-F), (Table 3-3), may be explained with reference to the 'BOX' scheme.

Stage *A)*

In this instance, it is convenient to consider the normat arrangement to be representative of both the compretic and normic properties of the initial surface. The nominal parameters refer to a surface containing 'm' elements in the U1 normat direction, 'n' elements in the U2 normat direction (compretic nominal parameters), and an overall dimension of 'width' 'length' and 'height' in the U1, U2 and U3 normat directions (normic nominal parameters).

Stage *B)*

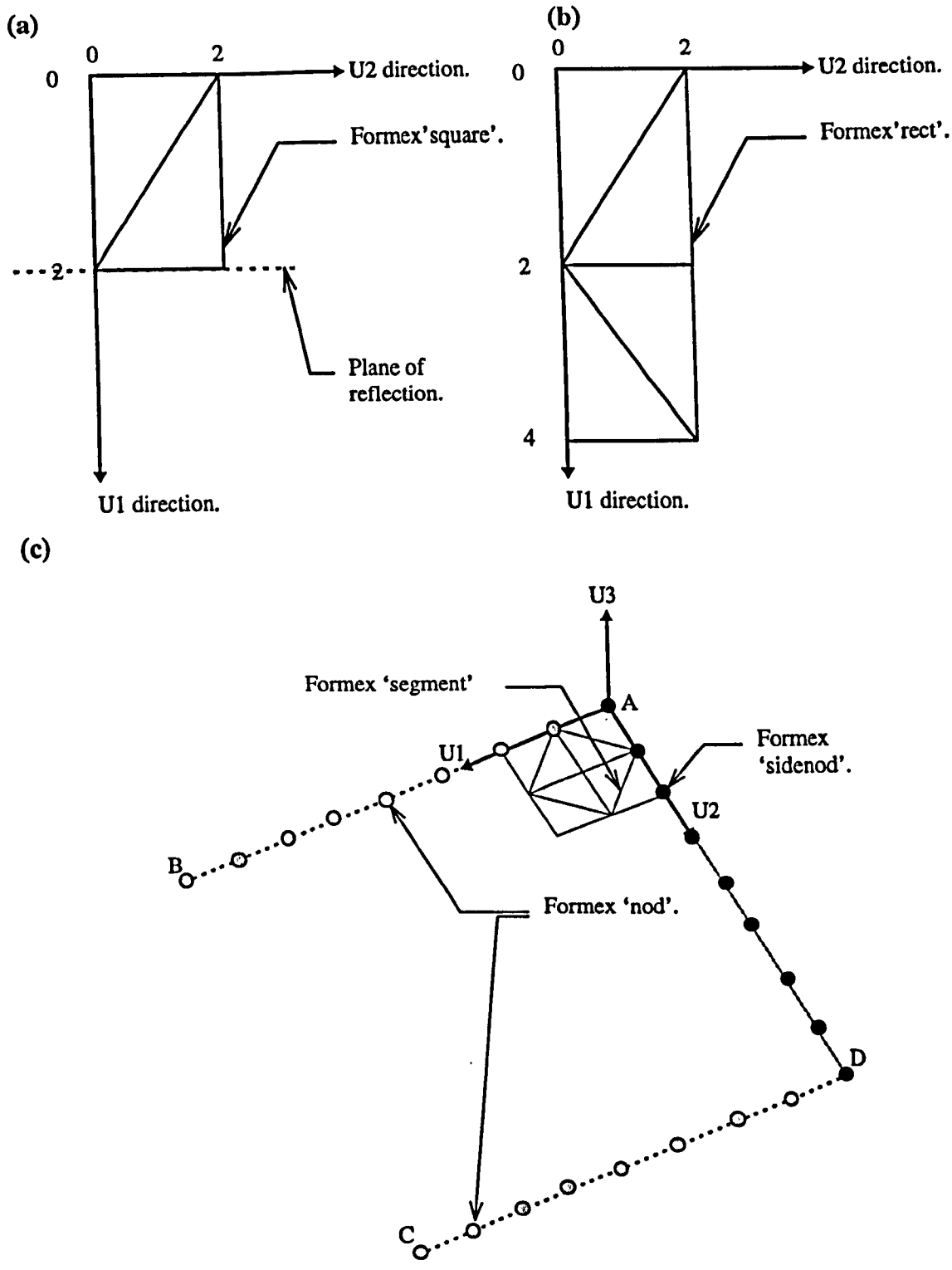

Figure 3-20 Configuration Pattern (a) Formex 'square' (b) Formex 'rect'. (c) Formex 'segment'.

'Square' is the formex formed by the composition of two formices (through the application of the '#' operator); each representing a triangular pattern, as shown in Figure 3-20 (a). By reflecting formex 'square' about a plane perpendicular to the U1, U2 plane and intersecting

the U2 normat line at the point 2, the formex 'rect' is formed, as shown in Figure 3-20 (b). The 'compret' of the initial surface is given by formex 'segment', and is found from the rotation of the 'rect' formex through one hundred and eighty degrees about the normat point 2,2 in the U1, U2 plane (Figure 3-20 (c)).

STAGE *C)*

This stage involves the creation of the formices 'nodb' and 'surf'. These formices represent respectively the compretic information of the boundary nodes aligned along the dashed lines of Figure 3-21, and the elements of the discretised surface of Figure 3-19.

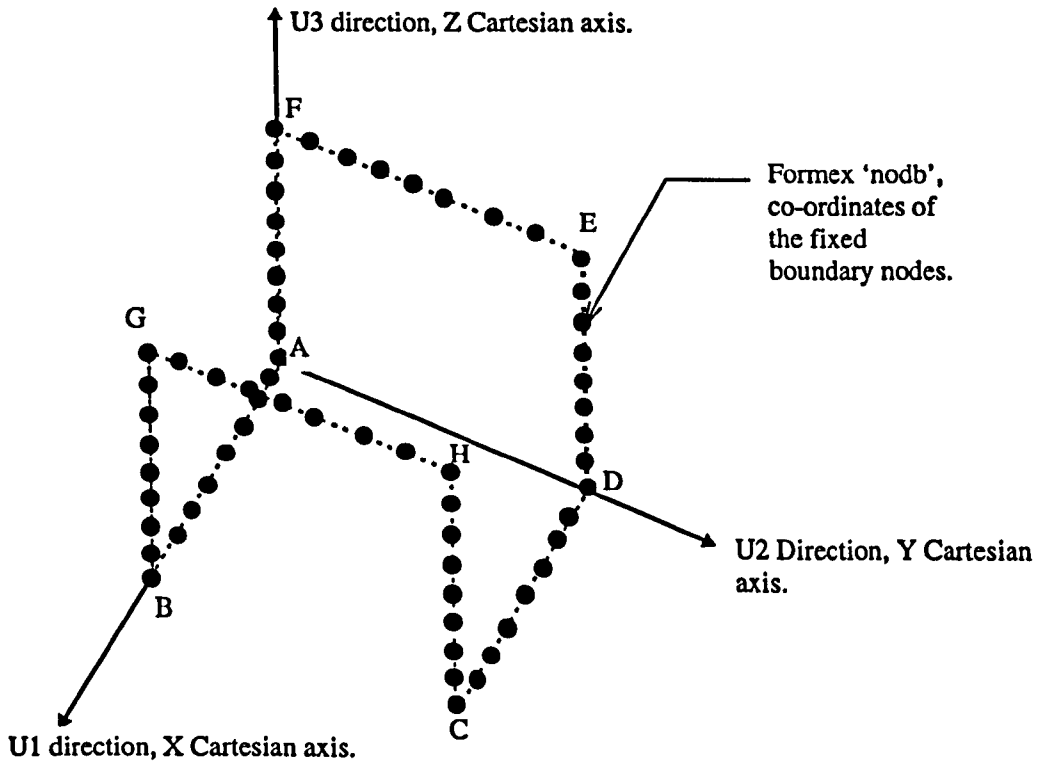

Figure 3-21 Configuration Pattern of the Formex 'nodb'.

Both formices are constructed by initially considering the base ABCD of the discretised surface. Formex 'base' represents the configuration pattern of the base, formex 'nod' gives the co-ordinates of the fixed boundary nodes aligned along sides AB and CD, while 'sidenod' depicts the unrestrained boundary nodes lying on length AD. Formex 'base' is depicted in Figure 3-22, formices 'nod' and 'sidenod' are described in Figure 3-20 (c).

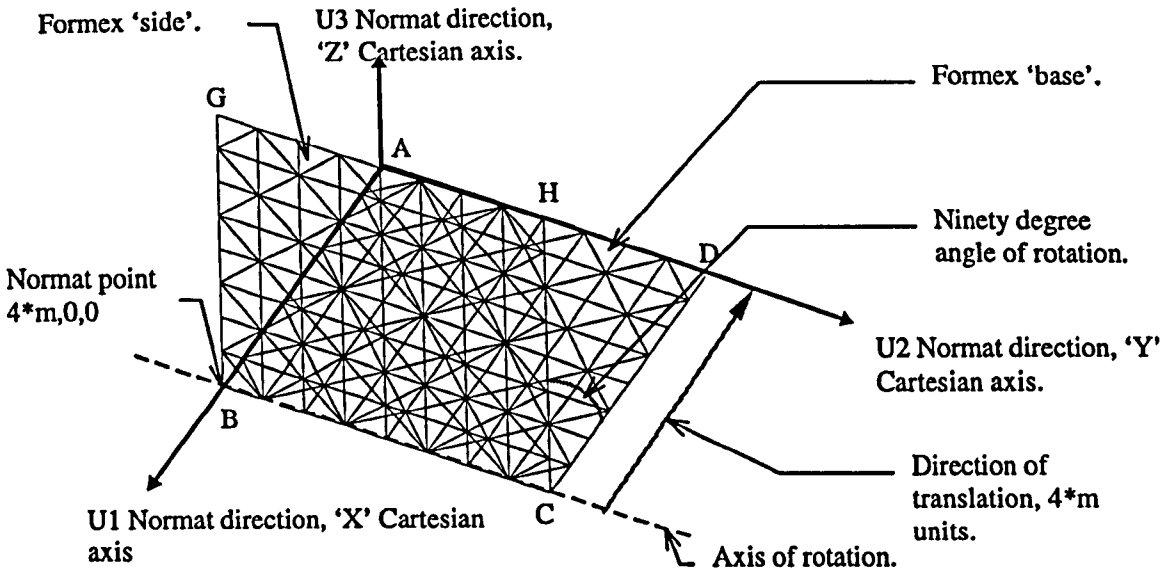

Figure 3-22 Configuration pattern of Formices 'side' and 'base'.

The process of generating formex 'surf' is as follows:

First, the base of the discretised surface, formex 'base', is found by simply replicating the compret 'segment' (Figure 3-20 (c)) 'm' times in the U1 direction and 'n' times in the U2 direction. Next, formex 'side', which depicts the plane BCGH (Figure 3-22), is created by rotating formex 'base' about an axis perpendicular to the U1 and U3 plane and passing through the normat point 4*m. (This action is accomplished by the implementation of the formex function vertition provias (VERAS)). Finally, formex 'surf' is constructed from the translation of formex 'side' (using the translation formex function (TRAN)) to give the configuration pattern of plane ADEF (Figure 3-19), which is then combined with formices 'base' and 'side'. (The direction of translation of formex 'side' is in the negative U1 direction and the distance is given by the value of 4*m units).

The process of generating formex 'nodb' is as follows:

Firstly, the co-ordinates of the fixed boundary nodes lying along the boundaries BG, GH and CH, (formex 'noda'), are generated. This involves the rotation of the composition of

formices 'nod' and 'sidenod' (Figure 3-20 (c)) in a manner identical to that used to find the configuration pattern of plane BCGH (formex 'side', (Figure 3-22)). Finally, formex 'nodb' is obtained from the composition of the co-ordinates of the nodes lying along the fixed boundaries of the plane opposite to plane BCGH with formices 'noda' and 'nod'.

The pexum function (**PEX**) creates a new formex from the removal of every cantle of the argument, that contains the same signets as a preceding cantle contained within the argument. With respect to the 'BOX' scheme, the action of the function is the removal, from formex 'nodb', of those boundary nodes that have normat points corresponding to another boundary node. The pexum function is required, as the aforementioned transformations used in generating formex 'nodb' will produce duplicate, or even triplicate, nodes, which, if not removed, will result in the connectivity data of the initial surface being incorrectly calculated for the boundary nodes.

STAGE D)

Values u1, u2 and u3 are the scale factors used by the basi-trefect retronorm (**BT**). The retronorm assumes the normat lines conform to those of a right handed Cartesian system. The configuration pattern of the initial surface that satisfies the dimensions specified by the nominal parameters of the scheme is given by formex 'surface'. Formex 'bound' represents the Cartesian co-ordinates of the boundary nodes.

STAGE E)

The medulla formex function (**MED**) enables the distinct and non-repeated normat points of a formex to be calculated. The global co-ordinates of the boundary nodes are given by formex 'bound', whereas those nodes not connected to the boundary are given by formex

'interior'[vii]. The composition of these formices give the global co-ordinates of the complete structure i.e. formex 'totnod'. The numbers of the nodes aligned with the boundaries and upon the element vertices of the discretised surface are obtained by the application of the dictum function, **(DIC)**, to the formices 'bound' and 'surface'.

[vii] Formex 'interior' is found from the application of the luxum function (LUX). This function removes those elements of a configuration pattern, given by the argument of the function i.e. formex 'surface', that are connected to the normat points of the formex contained within the canonic parameter of the LUX function i.e. formex 'bound'.

3.3 Numerical Analysis.

3.3.1 Introduction.

The method of solution adopted by the "equation solver" is that of Dynamic Relaxation. In form-finding, the initial surface of the assumed geometry of the membrane is divided into a series of triangular patches and the internal forces produced by a uniform tension field, as exhibited by a soap film, are resolved along the sides of the triangles. Static equilibrium is satisfied through an iterative process, involving the method of Dynamic Relaxation. During this process, out-of-balance forces, calculated at the nodes, are minimised.

3.3.2 Physical Characteristics of a Soap Film.

Before discussing the surface idealisation used by the numerical model, it is necessary to define some of the unique properties of a soap film first[3.6].

3.3.2.1 Surface Tension.

A soap lamina is composed of a mixture of soap and water molecules, and the forces of attraction and repulsion between these molecules cause the formation of the soap film. The negatively charged ions of the soap film solution are absorbed onto the surface due to an attractive force between the positive ions of the soap solution. This induces a macroscopic force that is localised within one atomic thickness of the surface. The force is called the surface tension and is represented by the symbol σ. The force is equivalent to the force per unit length of a 'membrane' of negligible thickness. A soap film consists of two such 'membranes'; each 'membrane' being separated from one another by a thin layer of fluid of a thickness ranging from 2×10^5 Å to 50 Å, where Å is the unit of atomic thickness (10 Å = 1 nm).

A soap film possesses a uniform tension field which implies that;

- σ is constant at every point
- σ is perpendicular to any line drawn within the surface, Figure 3-23.

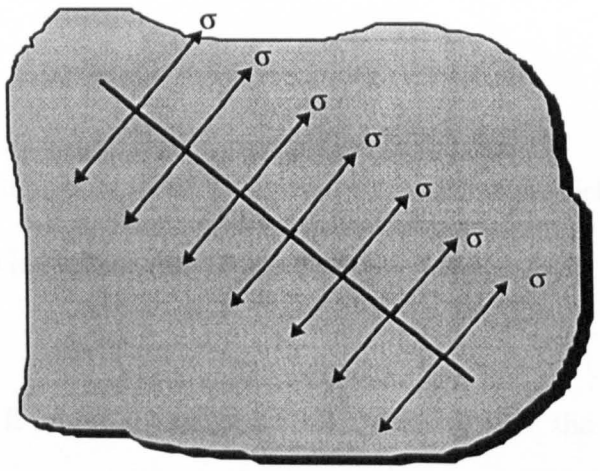

Figure 3-23 Alignment of Surface Tension (Top Layer of a Soap film).

3.3.2.2 Surface Area.

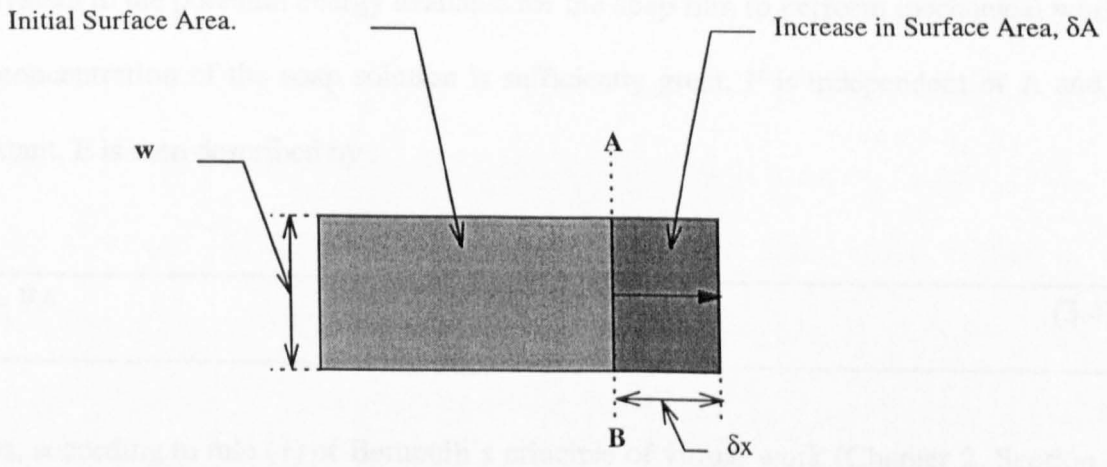

Figure 3-24 Free Energy of a Soap Film[3.6].

The ability of a soap film to model a surface of minimum area may be described by considering the energy of the film. Consider the soap film bounded by a rectangular wire of width w, as shown in Figure 3-24. Boundary AB is free to move in a direction perpendicular

to AB. The tension force, F, or force per unit length of film, acting along the top and bottom layers of the soap film is $F=2\sigma$. By moving the frame through a distance δx, the work done against the film tension force F is given by:

$$(Fw)\delta x \qquad (3.1)$$

In addition, the assumption of a value of unity for the constant thickness of the soap film implies that the increase in surface area of the film, δA, is given by:

$$\delta A = w\delta x \qquad (3.2)$$

Hence, the total energy E required to increase the surface area of the soap film from zero to A is given by:

$$E = \int_0^A F dA \qquad (3.3)$$

The free energy at constant temperature of the soap film is represented by E, and is equivalent to the potential energy available for the soap film to perform mechanical work. If the concentration of the soap solution is sufficiently great, F is independent of A and is a constant. E is then described by :

$$E = FA \qquad (3.4)$$

Thus, according to rule (1) of Bernoulli's principle of virtual work (Chapter 2, Section 2.2), a soap film in a state of stable equilibrium must have a minimum value of E, and hence, a corresponding minimum value of area A.

By adopting the same distribution of forces as given in Figure 3-23, it is subsequently described how the Dynamic Relaxation method may be used to minimise the potential energy of a soap film, thereby arriving at an equilibrated surface of minimum area.

3.3.3 Numerical Representation of a Soap Film.

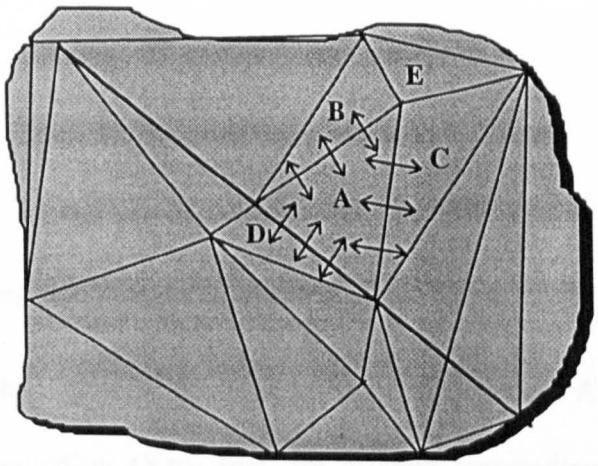

Figure 3-25 Alignment of the Forces of a Discretised Surface.

The numerical modelling of the soap film surface using triangular elements, and the assumption of a uniform tension field, gives rise to a set of forces aligned perpendicular to each triangle side. By way of illustration, consider the same patch of soap film depicted in Figure 3-23, whose surface has been divided into a series of triangles, (Figure 3-25). In the numerical model, the force per unit length F_k, acts along the whole thickness of the membrane and not just the top and bottom layers of the soap film. Furthermore, the surface tension σ is replaced by the surface stress σ_S. Consequently, for a membrane of thickness t, the force per unit length, F_k, acting along side k of a triangular element, is given by:

$$F_k = \sigma_S \times t \qquad \textbf{(3.5)}$$

where, k=1,2,3.

F_k is a measure of the surface stress; it remains constant for a constant membrane thickness t. In reality, the thickness of the soap film can vary depending on the soap solution used, the boundaries of the soap film, and the temperature of the environment. This would result in some variation of F_k, but for a thin soap film such variation would be small. The total force, F_k^T, acting along side k of a triangle is given by:

$$F_k^T = F_k \times L_k \tag{3.6}$$

where, L_k is the length of side k of a triangle.

Hence, with reference to Figure 3-25, it can be seen that element A will exert forces F_k^T, of magnitudes given by equation (3.6), that are aligned perpendicular to the sides of the element. By considering the static equilibrium of an element subjected to the forces arising from the surface tension of the elements surrounding it, it is possible to resolve the forces in the directions of three equivalent "pseudo cables" (Figure 3-26)

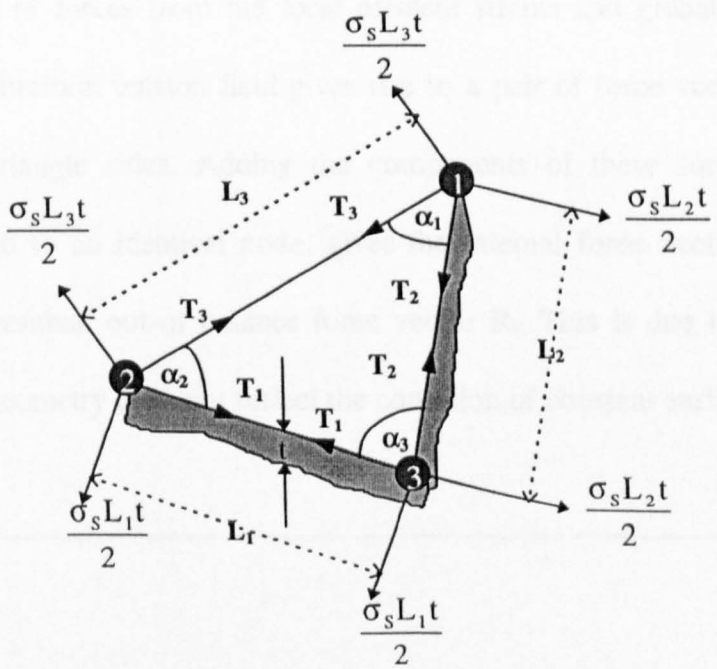

Figure 3-26 Discretised Surface Element.

Assuming F_K is constant, apportioning half of the force acting along an element side to the nodes common to that side and resolving in plane vertically and horizontally at each node, the following equation is derived[3.7],

$$T_k = \frac{F_k^T}{2\tan\alpha_k} \qquad (3.7)$$

where, T_k are the "pseudo-cable forces", (or element side forces), such that they maintain the static equilibrium of the element under a constant surface stress σ, and α_K are the internal angles of the triangle as shown in Figure 3-26. The proof of equation (3.7) is given in Appendix 3A.1

Equation (3.7) is a simple formulation that depends only on the planar geometry of a triangle; it negates the need to involve complex geometrical transformations relating to the rigid body rotation of the element, or the implementation of a transformation matrix used for the calculation of forces from the local element strains and global stresses. At each element node, the uniform tension field gives rise to a pair of force vectors aligned in the direction of the triangle sides. Adding the components of these forces with those of elements connected to an identical node, gives the internal force vector, which, in turn, gives rise to the residual out-of balance force vector R_{ij}. This is due to the fact that the assumed surface geometry does not reflect the condition of constant surface stress.

$$R_{ij} = \sum_{m=1}^{n_j} T_{mj} \qquad (3.8)$$

where, n is the number of pseudo cables meeting at node i, T_{mj} is the pseudo cable force of member m joined to node i and resolved in the global j direction, i.e. j=1,2,3, which denotes the global x, y, z directions.

Equation (3.8) has an advantage over other methods of solution in terms of improved accuracy. Summation of the residual components at each node individually reduces the problems of round off errors, as associated with other methods that consider the nodal forces globally through the formulation of a large global stiffness matrix.

For cases where the triangular element contains an internal angle of ninety degrees, equation (3.7) will cause the ill-conditioning of the algorithm. Hence, the equation is replaced by,

$$T_{90} = 0 \qquad (3.9)$$

$$T_a = \frac{\sigma_s \times L_b \times t}{2} \qquad (3.10)$$

$$T_b = \frac{\sigma_s \times L_a \times t}{2} \qquad (3.11)$$

where, T_{90} corresponds to a side adjacent to an interior angle of ninety degrees[viii], a and b are sides adjacent to interior angles less than ninety degrees. The derivations of equations (3.9), (3.10) and (3.11) are given in Appendix 3A.1.

[viii] An angle is defined as being ninety degrees for the instance; $89.99^{o} \leq a_k \leq 90.01^{o}$.

3.3.4 General Form of Dynamic Relaxation.

One of the assumptions used in the Dynamic Relaxation method is to replace a structural configuration with a series of lumped masses situated at the nodes of the discretised surface, which, in the absence of damping and under the influence of an external load, oscillate about their positions of equilibrium. Once damping is introduced, then, by applying the D'Alembert principle[ix], at a given time increment, the dynamic equilibrium of each node is given by:

$$P_{ij} - K_{ij}\delta_{ij} - C\dot{\delta}_{ij} = M_{ij}\ddot{\delta}_{ij} \qquad (3.12)$$

where, P_{ij} is the vector representing the external force applied at node i, $K_{ij}\delta_{ij}$ is the internal force given by the summation of the elastic and/or geometric forces of those elements joined to node i, K is the sum of the 'lumped' stiffness applied to node i, M is the lumped nodal mass, C is the viscous damping factor, and $\ddot{\delta}_{ij}$, $\dot{\delta}_{ij}$ are the acceleration and nodal velocity terms respectively.

Equation (3.12) describes the equilibrium state of a body in motion, in which the external force P_{ij} is balanced out by forces of inertia, stiffness and damping. The oscillations of the system are suppressed by the presence of viscous damping. By expressing the difference of the external and internal forces as a residual force R_{ij}, and rearranging, equation (3.13) is derived,

$$R_{ij} = M_{ij}\ddot{\delta}_{ij} + C\dot{\delta}_{ij} \qquad (3.13)$$

[ix] The D'Alembert principle is the means by which forces are related to nodal displacements via the equation of dynamic equilibrium (equation 3.12).

Through the application of the centred finite difference approximation of the first and second order derivatives (Chapter 3, Section 3.3.5.1), the nodal displacements resulting from the residual forces can be determined at a given finite time increment and the surface geometry updated, in an iterative manner, until the residual forces are acceptably small.

3.3.4.1 Viscous Damping.

Viscous damping requires a judicious choice of the value of the damping coefficient C, in order to reduce the number of iterations required for the convergence of the solution[3.8]. The optimum value of C is obtained from the lowest frequency of vibration of the structure. Adopting such an approach implies that, before form-finding can commence, it is necessary to complete a trial run for an undamped oscillating system, based on the topology of the initial surface, where the nodal displacements are plotted on a graph to obtain the number of iterations N necessary for one complete cycle, or oscillation. The fundamental frequency f is then found from,

$$f = \frac{1}{N\Delta t} \tag{3.14}$$

where, Δt is the time increment, or iterative step size, at which displacements are calculated according to the finite difference method.

The critical value for C is then calculated from,

$$C = 4\pi f_L \tag{3.15}$$

where, f_L is the lowest value of the frequency f obtained from equation (3.14).

The viscous damping approach is not widely used nowadays, instead, it has been replaced by kinetic damping. This is discussed in the following section.

3.3.4.2 Kinetic Damping.

A technique of damping called 'kinetic damping' is known as being more efficient in aiding the process of obtaining static equilibrium[3.9]. It is able to cope with large displacements, making it particularly suited to cases of form-finding where there are high initial out-of - balance forces due to a poorly defined initial surface. The approach involves monitoring the kinetic energy of a discretised system, which is moving with undamped oscillations, and bringing the system to rest, once a peak in kinetic energy (K.E.) has been detected. The geometry is then updated until it eventually conforms to the stable equilibrated state.

The effect of kinetic damping may be illustrated by equating the lumped masses to a series of oscillating pendulums[3.10]. A pendulum swinging under its own weight is stationary at the top of its swing, and has purely potential energy (P.E.). At this point, the pendulum is in its quasi stable, or unstable equilibrated, state. On its downward swing, the motion of the pendulum increases, along with the K.E. Neglecting the effects of friction and applying the law of conservation of energy, at the mid-point of the swing, the P.E. of the pendulum is at its minimum, while that of the K.E. is of a value equivalent to the P.E. at the top of the swing. According to the principle of virtual work, the pendulum is in its quasi stable state of static equilibrium at this point. Thus, the efficiency of the Dynamic Relaxation algorithm is enhanced by restarting iterations from an updated surface geometry that has an improved state of equilibrium through the minimisation of its P.E.

An ideal plot of the variation in magnitude of the K.E. of a vibrating system undergoing Dynamic Relaxation would show a gradual decrease in the size of the K.E. peaks. Once the kinetic energy peaks become negligible, the system possesses purely P.E. of a minimum value. The approach is in effect minimising the P.E. of the vibrating system such that it reaches static equilibrium according to Bernoulli's principle of virtual work. The implementation of Dynamic Relaxation with kinetic damping implies that C is equal to zero, reducing equation (3.13) to:

$$R_{ij} = M_{ij} \ddot{\delta}_{ij} \qquad (3.16)$$

3.3.5 Application of the Dynamic Relaxation Algorithm to Form-Finding.

The adoption of a soap film analogy implies that the form-finding of a membrane will be dependant on the deformations induced by the internal forces arising from an applied constant surface pre-stress. There are no external forces applied to the system. Consequently, R_{ij} of equation (3.16) is a purely geometric force obtained from equation (3.7); it does not rely on any contribution from the elastic straining of the membrane, which would violate the assumption of a constant surface stress. It is evident that the K.E. of the system depends on the degree of residual forces. Once Rij is equal to zero, or less than a prescribed limit, for every node of the discretised surface, the K.E. and hence the P.E. (or free energy E) will be at its absolute minimum. It is at this point that equation (3.4) informs us that the equilibrated surface should possess a minimum surface area.

In summary, Dynamic Relaxation is not a actually a dynamic analysis, it is the means whereby an initially un-equilibrated physical system is allowed to vibrate about its discretised nodes, using lumped masses, with accelerations proportional to the magnitude of

the residual force at each node. By monitoring the displacements, velocities and residual forces, the vibrating system may be brought to rest, at its static equilibrium, through the application of kinetic or viscous damping. Kinetic damping is the method of damping adopted in this thesis.

3.3.5.1 Governing Equations.

The governing equations of the Dynamic Relaxation method are well documented. A brief summary of them is given here.

At a given time t, the "current" time, the residual force is equal to the acceleration of the lumped masses[x],

$$R_{ij}^{t} = M_{ij}\ddot{\delta}^{t}. \tag{3.17}$$

The centred finite difference approximation may now be implemented for representing the acceleration in terms of the velocities of the nodal masses at a "previous" increment, time $t-\frac{\Delta t}{2}$, and a "subsequent" increment, time $t+\frac{\Delta t}{2}$, giving,

$$R_{ij}^{t} = M_{ij}\frac{\dot{\delta}_{ij}^{\,t+\frac{\Delta t}{2}} - \dot{\delta}_{ij}^{\,t-\frac{\Delta t}{2}}}{\Delta t} \tag{3.18}$$

Rearranging,

$$\dot{\delta}_{ij}^{\,t+\frac{\Delta t}{2}} = \dot{\delta}_{ij}^{\,t-\frac{\Delta t}{2}} + \frac{R_{ij}^{t}\Delta t}{M_{ij}} \tag{3.19}$$

[x] As noted earlier, kinetic damping is implemented and hence the viscous damping term C is zero.

Equation (3.19) gives the value of the velocity at a "subsequent" iterative step based on the values of the velocity at a prior increment and the "current" value for the residual force. The displacements can also be expressed in a finite difference form,

$$\delta_{ij}{}^{t+\Delta t} = \delta_{ij}{}^{t} + \dot{\delta}_{ij}{}^{t+\frac{\Delta t}{2}} \Delta t . \qquad (3.20)$$

Equations (3.19) and (3.20) are the governing recurrent equations used in the solution algorithm. As soon as the displacements have been calculated from equation (3.20), the configuration of the structure may be updated according to,

$$X_{ij}{}^{t+\Delta t} = X_{ij}{}^{t} + \delta_{ij}{}^{t+\Delta t} \qquad (3.21)$$

where, X_{ij} are the co-ordinates of node i in the jth global direction. The updated co-ordinates correspond to a new "current" surface geometry at time $t + \Delta t$, at which stage the residual forces are recalculated in accordance with equation (3.8).

Expressing the residual force in terms of the current co-ordinates has the advantage of a more accurate calculation of the nodal displacements. Methods of numerical analysis that rely on a stiffness matrix, tend to relate the displacements incorrectly due to the inherent assumption of a small value for the nodal displacements between successive iterations, and due to the fact that the stiffness matrix is transient, and is hence, 'lagging behind' one or more iterations.

At the start of iterations, "current" time t = 0, and after the topology has been updated after a peak in K.E., the velocity at a "subsequent" time $\frac{\Delta t}{2}$ is given by,

$$\dot{\delta}_{ij}^{\,t+\frac{\Delta t}{2}} = \frac{R_{ij}^{t=0}\Delta t}{2M_{ij}} \qquad (3.22)$$

3.3.5.2 Stability and Calculation of Fictitious Masses.

The stability of the solution is dependent upon the value of the iterative step size Δt. Barnes stated that in cases where Δt is too large, or the value of the lumped masses too small, instability was likely to occur[3.11]. Consequently, to ensure convergence, the following criterion should be observed,

$$\Delta t \leq \sqrt{\frac{2M_{ij}}{S_{ij}}} \qquad (3.23)$$

where, S_{ij} is the sum of the stiffness of the "pseudo" cable forces meeting at node i, and resolved in the jth global direction. Equation (3.23) is not an adequate criterion should the topology of the surface change significantly during form-finding. For numerical stability, it is recommended that the maximum possible stiffness S_i in each of the global directions should be used i.e. the sum of each of the ratios of the "pseudo cable force" divided by the length of the element for each cable meeting at a node[3.7]. By setting Δt to unity and rearranging (3.23), it is possible to arrive at a simplified expression for the lumped masses in terms of the lumped stiffness, such that stability is ensured,

$$M_{ij} = \sum_{m=1}^{n} \frac{T_m}{L_m} = \frac{S_i}{2} \qquad (3.24)$$

Convergence and stability is further improved by recalculating the values of the lumped masses after a peak in kinetic energy, rather than at every iteration[3.12]. Equation (3.24) is quite a conservative value and as a result, a weighting factor of λ has been suggested to improve the rate of convergence[3.12]

$$M_{ij} = \frac{1}{\lambda}\sum_{m=1}^{n}\frac{T_m}{L_m} = \frac{S_i}{\lambda} \qquad (3.25)$$

To determine the optimum value of λ, a series of trial runs using values of λ ranging from 0.6 to 1.1, have been used by the author to asses the number of iterations required for convergence in satisfying a value of the residual force higher than that expected in the final solution[3.12]. Within this thesis, all the numerical examples have been generated with λ set to unity.

3.3.5.3 Updating of Surface Geometry after a Kinetic Energy Peak.

During form-finding, the total kinetic energy of the structure at a "subsequent" time increment, $t+\frac{\Delta t}{2}$, is given by,

$$K.E.^{t+\frac{\Delta t}{2}} = \sum_{i=1}^{num} S_i \left(\dot{\delta}_{ij}^{\,t+\frac{\Delta t}{2}} \right)^2 \qquad (3.26)$$

where, num is the total number of nodes.

If the kinetic energy is less than that at a "previous" time interval, $t-\frac{\Delta t}{2}$, then a peak in kinetic energy has occurred. In order to derive the point at which this peak occurred, it is necessary to store values of the kinetic energy at any three successive iterations i.e. KE_1 at $t-\frac{3\Delta t}{2}$, KE_2 at $t-\frac{\Delta t}{2}$, and KE_3 at $t+\frac{\Delta t}{2}$.

If KE_3 is smaller than KE_2, a quadratic curve passing the rough the peaks KE_1, KE_2 and KE_3 can be fitted, as suggested by Barnes[3.7]. This will allow the displacement at time $t-t_{up}$ at which the peak in kinetic energy occurs to be found as[3.7],:

$$\delta^{t-t_{up}} = \delta^{t+\Delta t} - \dot{\delta}_{ij}^{\,t+\Delta t}(1+\beta) + \beta\Delta t^2 \frac{R^t}{M} \qquad (3.27)$$

where,

$$\beta = \frac{KE_2 - KE_3}{2KE_2 - KE_3 - KE_1} \qquad (3.28)$$

The surface geometry at time $t-t_{up}$ is then updated according to;

$$X^{t-t_{up}} = \delta^{t-t_{up}} + X^{t+\Delta t} \qquad (3.29)$$

3.3.5.4 Solution Procedure.

Before iterations commence, set KE_1, KE_2 and KE_3 to zero.

a) Calculate R_{ij} for each node from equation **(3.8)**.

b) If iterations are just commencing, or if the surface geometry has been updated, calculate the lumped nodal masses according to equation **(3.24)** or equation **(3.25)**.

c) Stop iterations if the maximum value of R_{ij} for each node is less than a pre-scribed limit (If a node is connected to a fixed boundary, set R_{ij} to zero).

d) If iterations are just commencing, or if the surface has been updated after a K.E. peak, use equation **(3.22)** to give the nodal velocities and begin step **f)**.

e) Use equation **(3.19)** to determine the velocities.

f) Calculate the nodal displacements from equation **(3.20)**.

g) Calculate the value of the kinetic energy KE_3 from equation **(3.26)** for the velocities of step **e)** or **d)**.

h) If KE_3 is less than the value for the previous iteration, use equations **(3.27)**, **(3.28)** and **(3.29)** for the updating of the surface. Set the values KE_1, KE_2, KE_3 and the nodal velocities and displacements to zero. Return to step **a)**. Otherwise, update the surface geometry according to equation **(3.21)**. Set KE_1 to the value of KE_2, set KE_2 to the value of KE_3 and reset the value of KE_3 to zero. Return to step **a)**.

3.3.6 Form-Finding Example ('BOX' Surface).

The initial discrete surface of the Box model is described in section 3.2 and Figure 4-18. The dimensions of the surface are in metres (m), the surface stress is equal to $5\times10^{6}\,kNm^{-2}$ and the thickness equal to 1 millimetre (1×10^{-3} m). The criterion of convergence is deemed to have been satisfied once the global components of the residual force at every node, except those restrained at the boundaries, are less than or equal to a maximum admissible value of 0.5 kN. The variables, NIT and ER refer respectively to the number of iterations and the value of error, or residual, used as the convergence criterion. A value of unity for the scaling factor λ has been used. Figure 3-27 shows the stable minimal surface produced after 850 iterations, it is an example of a soap lamina that has been the subject of a previous numerical analysis by Singer et al[3.13]. A discussion of the accuracy of the numerical result with that of the expected theoretical surface is recorded in Chapter 4.

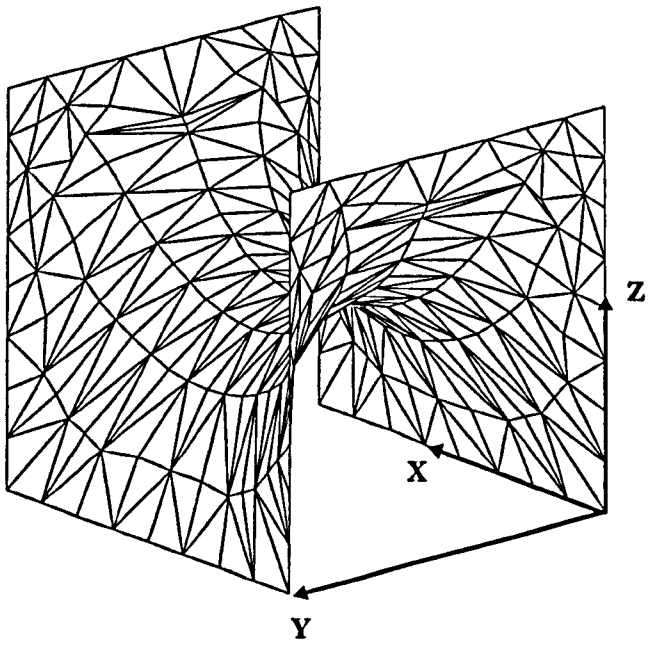

Figure 3-27 'BOX' Form-Found Surface (NIT = 850, ER = 0.5 kN).

3.3.7 Analysis of Results ('BOX' Surface).

The following set of graphs and illustrations, relating to the 'BOX' analysis, are intended to give the reader some knowledge of the likely manner of the surface deformations taking place during a form finding analysis. A detailed account of the implications of the 'BOX' surface results, together with those of other numerical examples, in terms of the efficiency and validity of the approach, are given in Chapter 4.

A form-finding analysis commonly consists of three distinct incremental intervals during which a surface will deform in a characteristic way. These are:

Stage (1) *A large scale deformation is expected in those elements positioned at the unrestrained boundaries, and the areas where a high degree of curvature is present. The residual forces are at their greatest in such areas, producing nodal displacements that tend to be aligned perpendicular to the patch of elements surrounding a node. During the interval, the peaks in K. E. are of high frequency and magnitude. Elements connected to a fixed boundary, or lying in a low curvature region, remain undeformed. (Stage (1) is commonly associated with cases where the "initial surface" is inaccurately defined and is, hence, a crude approximation of the final form-found surface.)*

Iterations 1-63

Stage (1) is defined with reference to the deformation of the 'BOX' surface for the incremental period 1-63 iterations. Figure 3-28 shows how the K.E. increases very rapidly to a maximum value of 1.3E+5 until 5 iterations, at which point the K.E. has peaked. Kinetic damping is very frequent up until 63 iterations, the peaks being spread over small

iterative periods and thus having a high frequency. This is due to the presence of large residual forces arising from the highly un-equilibrated geometry of the crude initial surface. After 63 iterations, the K.E. appears to have been significantly reduced.

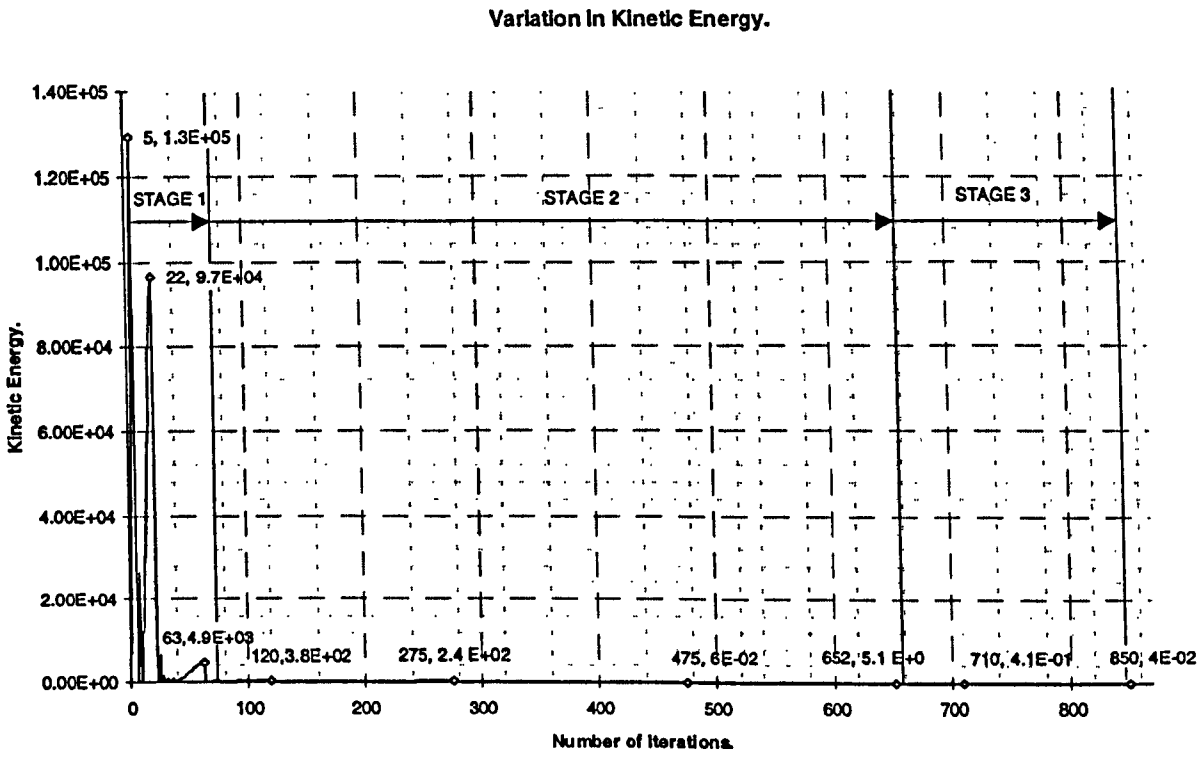

Figure 3-28 Variation In Kinetic Energy (Iterations 1-850).

Figure 3-29 (a) describes the variation of the maximum residual nodal force, calculated from equation 3.8, acting at a node at a "current" time. The magnitude of the residual force fluctuates from iteration to iteration, according to the continuously updated geometry of the surface. The graph shows that a maximum residual nodal force of 1.1E+3 kN is acting at node number 210 at increment number 63. Figure 3-29 (b) gives an account of the magnitude of the maximum displacement vector of a node, during a non-damped iterative period i.e. the incremental interval spread between successive peaks in K.E., (Figure 3-29 (b)) At 22 iterations, node number 198 has displaced 3.4 m from its initial stationary damped state at 6 iterations. The effect of the deformation on the geometry of the surface is depicted in Figure 3-30 (a). Between 1 and 63 iterations, the surface geometry is rapidly changing, as shown by the cluster of high peaks.

(a)

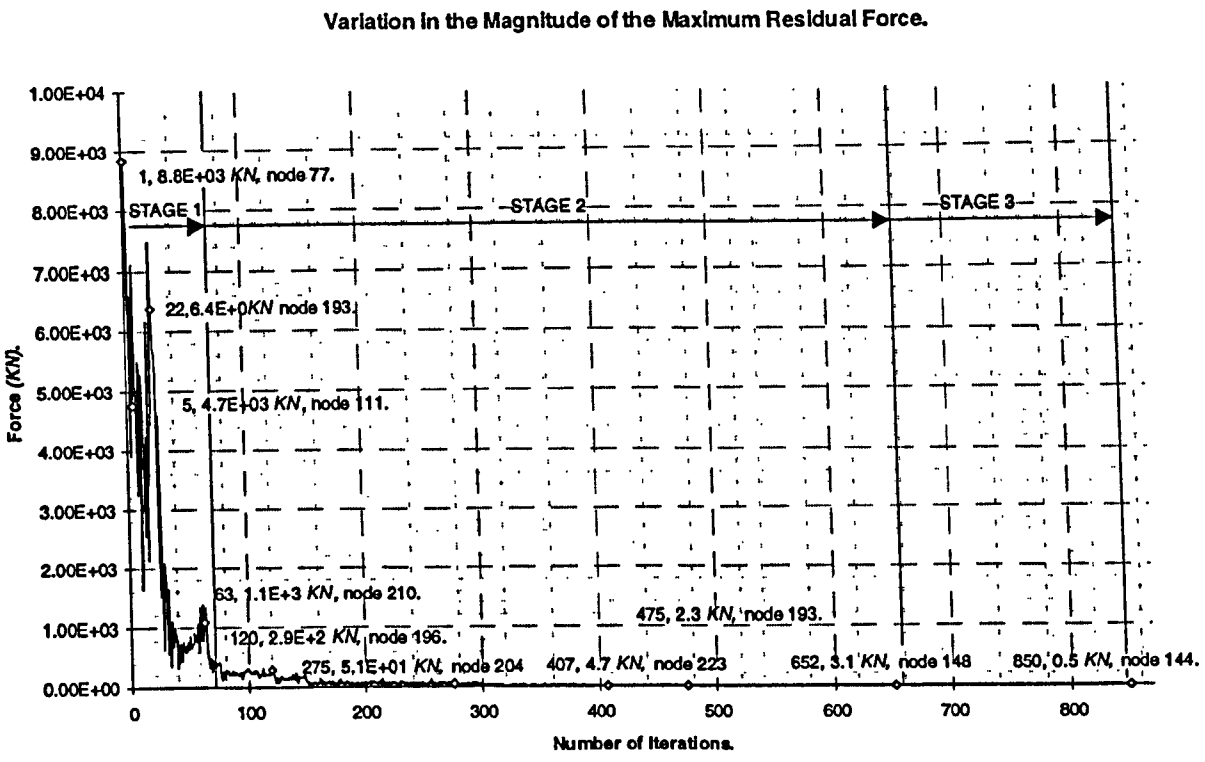

(b)

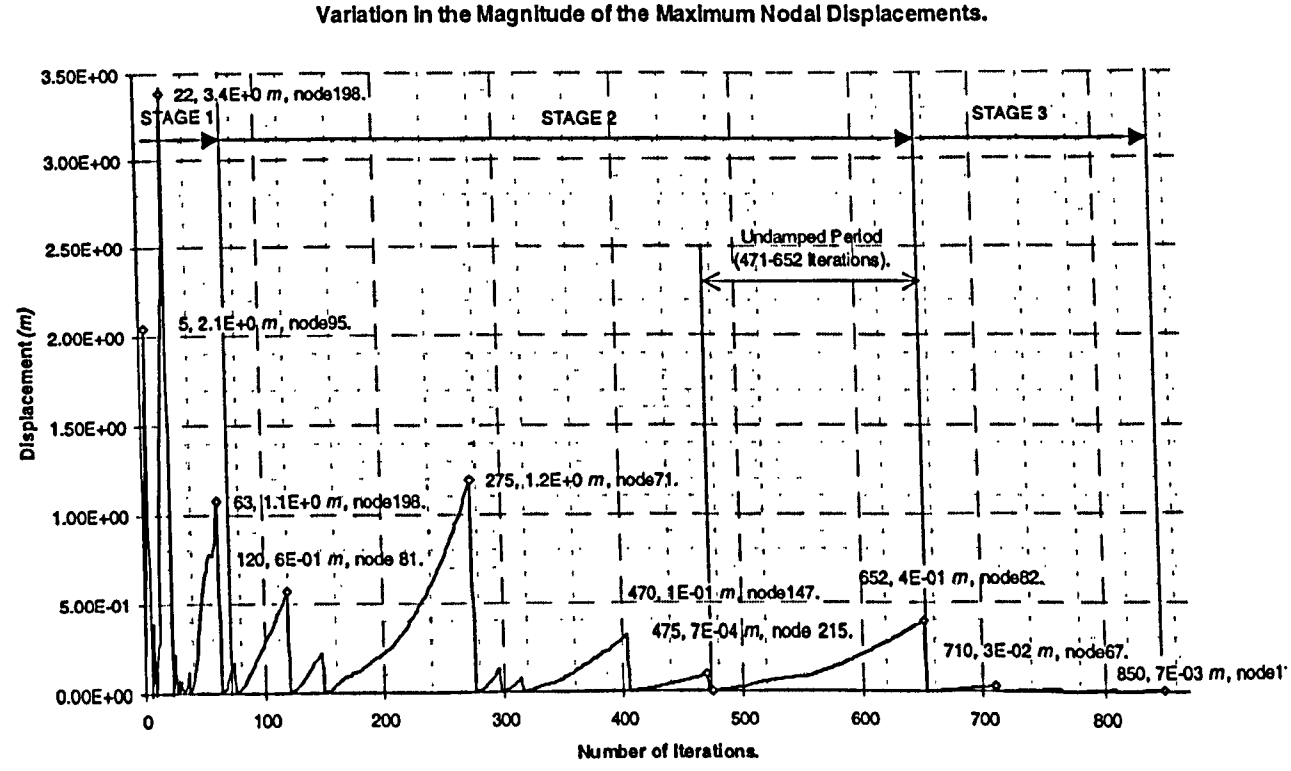

Figure 3-29 Variation of (a) Maximum Residual Force(Iterations 1-850)

(b) Maximum Nodal Displacement (Iterations 1-850).

Figure 3-30 and Figure 3-31 illustrate the changing geometry of the 'BOX' surface up to 63 iterations

(a)

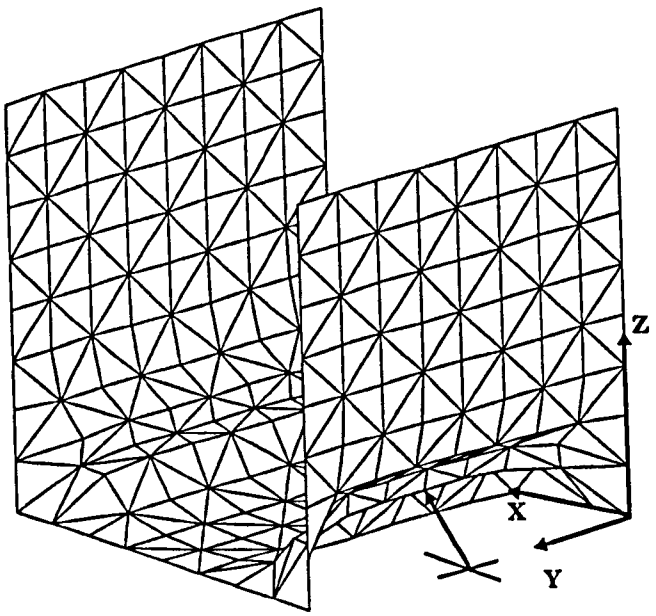

Displacement vector, $1.451i + 1.451k$.

Original Position of node 95, co-ordinates 0,5,0

(b)

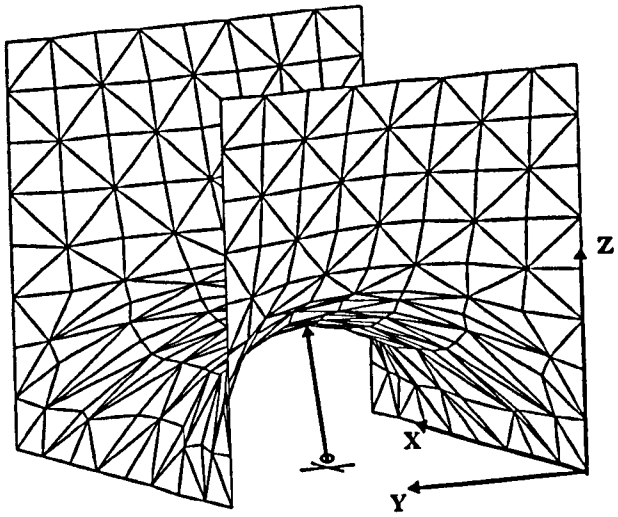

Displacement vector, $0.788i + 3.290k$.

Position of node 198 at updating of topology at iteration 6, co-ordinates 3.769, 5, 0.155.

Position of node 198 before iterations commence, co-ordinates 3.75,5,0.

Figure 3-30 Deformation of 'BOX' Surface (a) at 5 Iterations (b) at 22 Iterations.

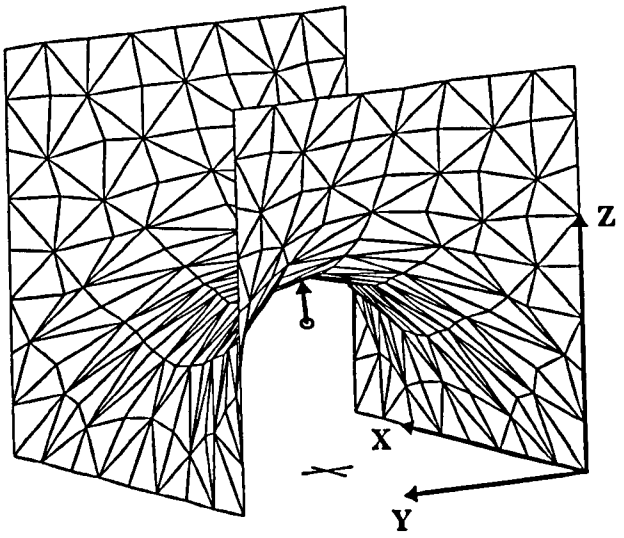

Displacement vector, 0.149*i* +1.065*k*.

Position of node **198** at updating of topology at iteration 36, co-ordinates 4.566, 5, 3.5.

Position of node **198** before iterations commence, co-ordinates 3.75,5,0.

Figure 3-31 Deformation of 'BOX' Surface - 63 Iterations.

Stage (2) *During the second phase of analysis, nodal displacements tend to be aligned in-plane, being of a lower magnitude than those of stage (1). The surface deformations during stage (1) cause the propagation of displacements from the elements positioned in the unrestrained boundary and high curvature regions to the remaining unaltered surface elements. The peaks in K.E. are of a significantly lower magnitude and frequency than at stage (1).*

Iterations 64-652.

On closer examination of the K.E. over the period 100 to 850 iterations (Figure 3-32) it is noticeable that after 275 iterations, the peaks decrease in magnitude from a maximum value of 2.4 E+02. After this point, there is no significant change in the magnitude of the K.E. and the peaks occur with less frequency, notably from iteration 470 to iteration 652. Although at 652 iterations, the displacements could be considered to be fairly significant, being of the order of 4E-01 m for node 82, the in-plane nature of the displacement does not produce a noticeable change in the surface geometry (Figure 3-34 (b) At this point, the surface has still not satisfied the convergence criterion; the residual nodal force being of a magnitude of 3.1 kN.

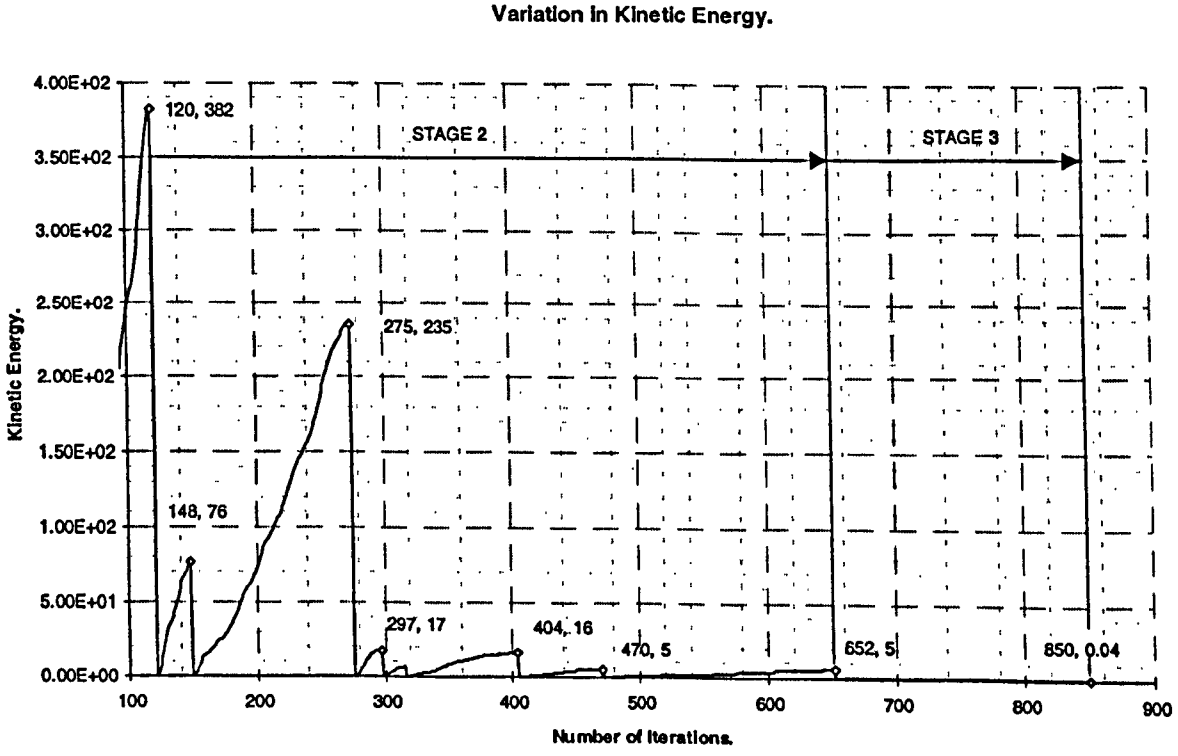

Figure 3-32 Variation in Kinetic Energy (Iterations 100-850).

(a)

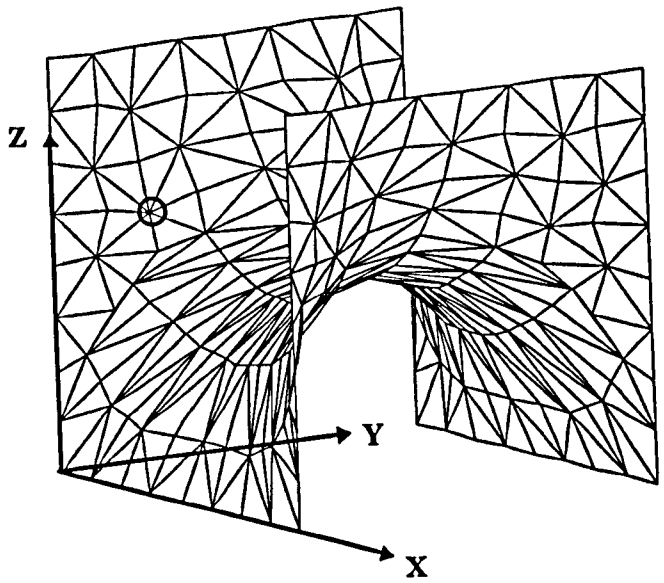

○ Node 71, co-ordinates 1.127, 1.984, 6.245

(b)

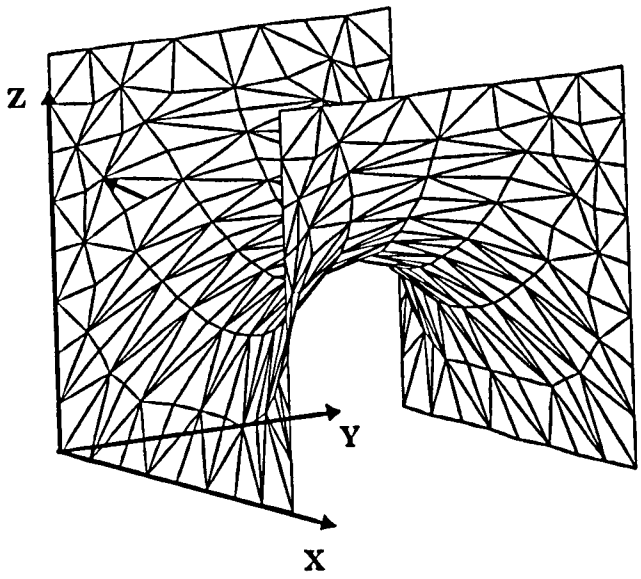

⟶ Displacement vector for node 71, -0.590*i*,-0.876*j*+0.549*k*.

Figure 3-33 Deformation of 'BOX' Surface (a) Updated Geometry at 149 Iterations. (b) Deformation at 275 Iterations.

(a)

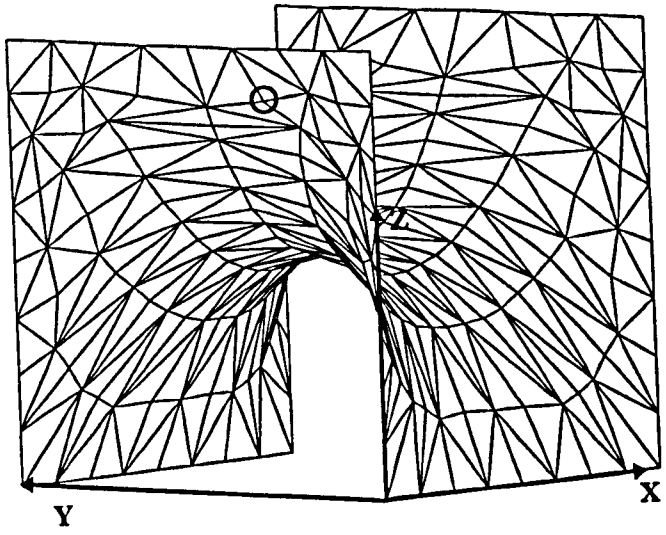

○ Node 82, co-ordinates 0.408, 3.232, 8.777.

(b)

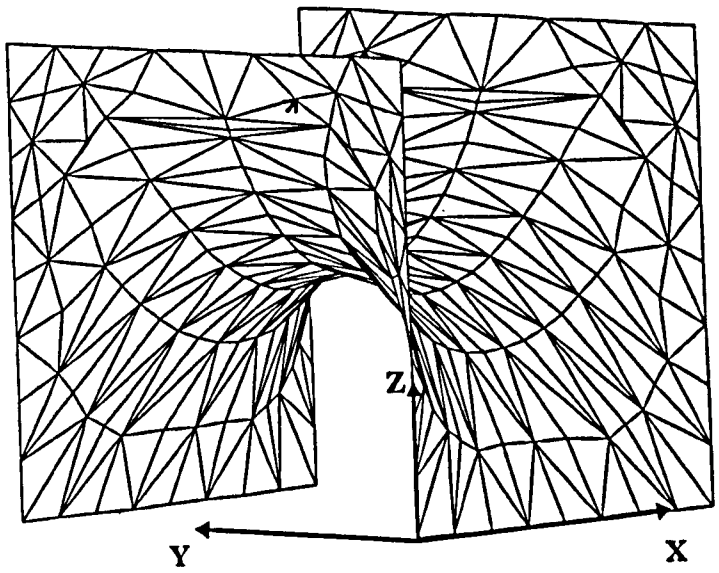

⟶ Displacement vector for node 82, -0.103*i*,-0.295*j*+0.233*k*.

Figure 3-34 Deformation of 'BOX' Surface (a) Updated Geometry at 471 Iterations. (b) Deformation at 652 Iterations.

Stage (3) *This stage of the analysis is distinguished by superficial in-plane deformations caused by the fine adjustment of the surface configuration as it approaches its equilibrated stable state. A negligible change in the overall surface geometry occurs between successive K.E. peaks. The peaks show a characteristic increase in frequency towards the onset of convergence, due to the fluctuation of the in-plane displacements.*

Iterations 650-850.

Between 650 to 850 iterations, four distinct kinetic energy peaks of a clearly curved quadratic nature can be observed (Figure 3-35) together with four maximum nodal displacement peaks (Figure 3-36 (a)). The maximum nodal displacement of the surface from 809 iterations, where the form is static due to kinetic damping, to when convergence is satisfied, is less than 7E-03 m for node 115.

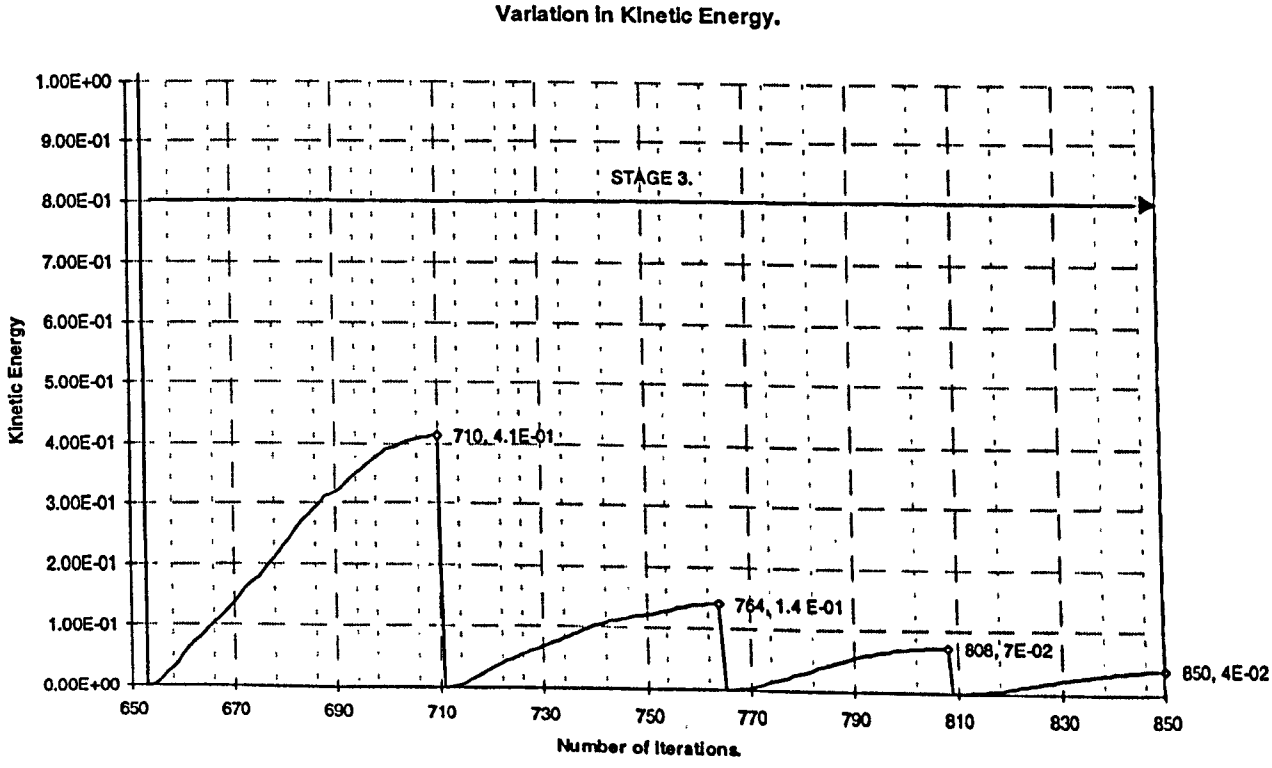

Figure 3-35 Variation in Kinetic Energy (Iterations 650-850).

(a)

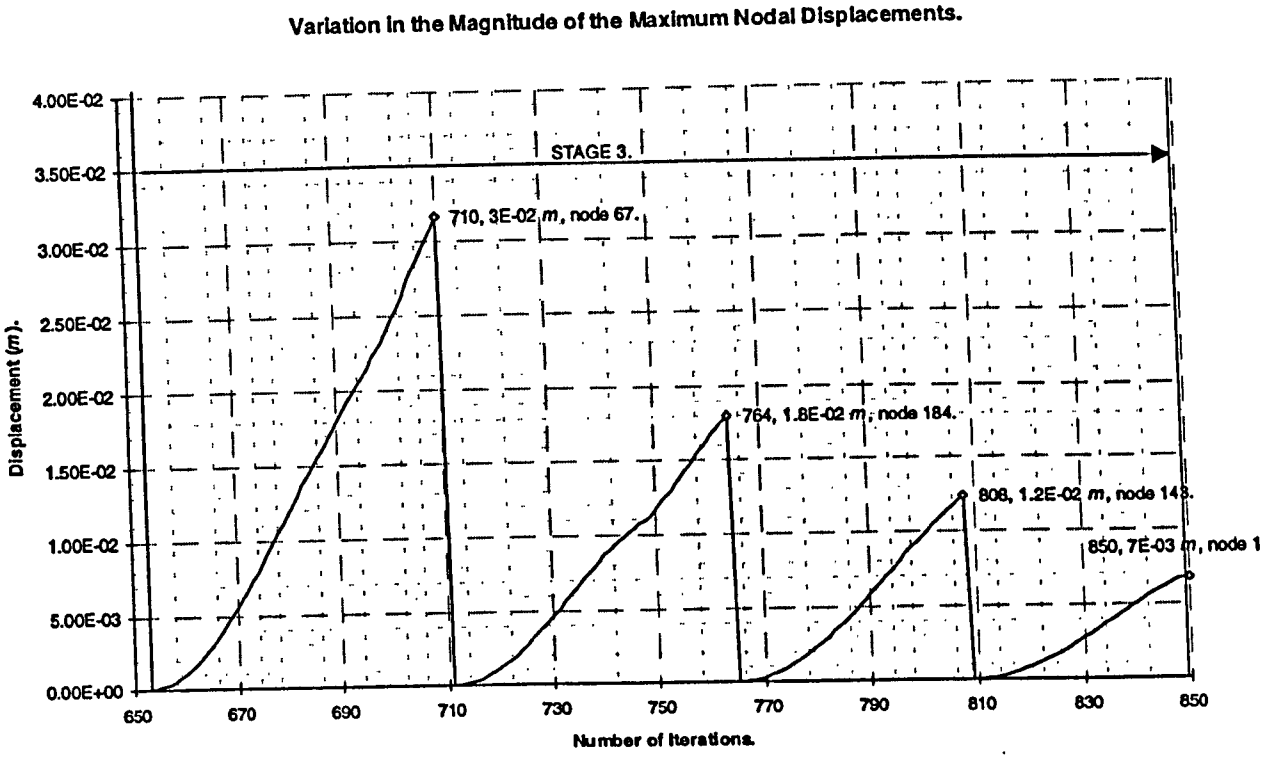

(b)

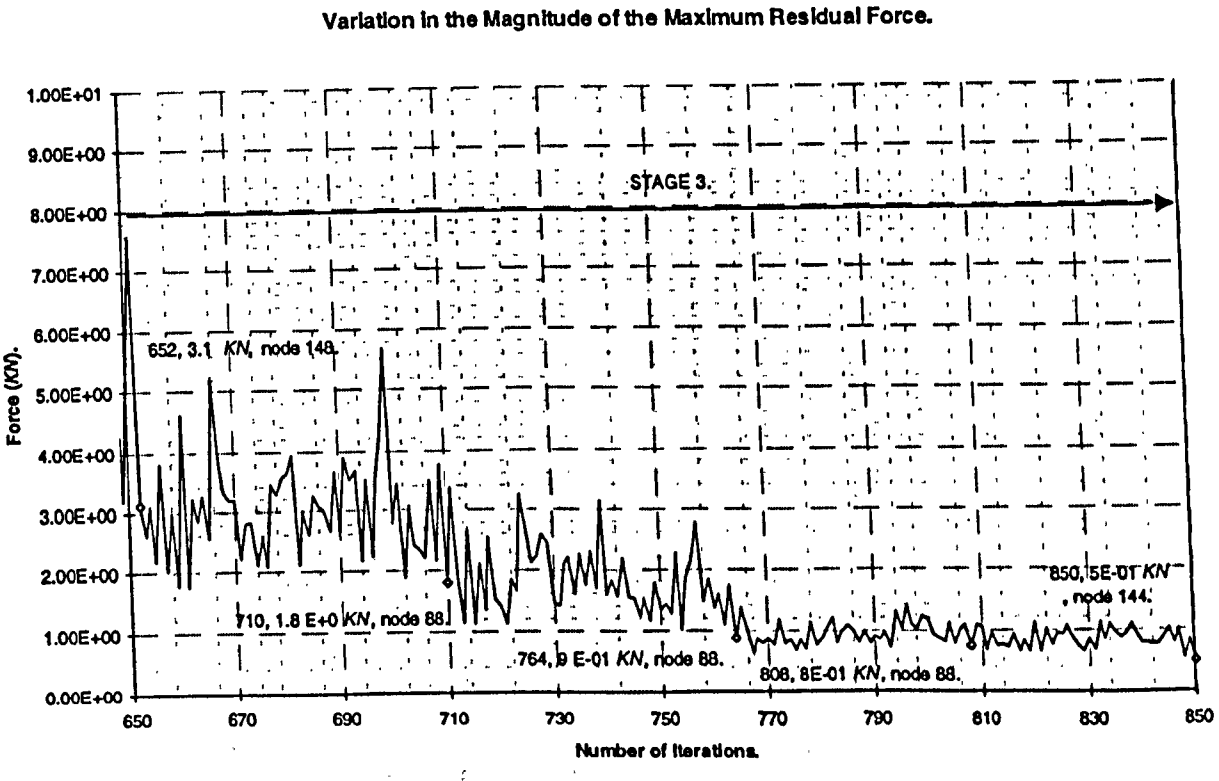

Figure 3-36 Variation of (a) Maximum Nodal Displacement (Iterations 650-850) (b) Maximum Residual Force (Iterations 650-850).

Figure 3-37 and Figure 3-38 depict how the overall surface geometry of the surface remains essentially unaltered during the third stage of analysis; the displacements are of an extremely small magnitude and are once more aligned in-plane.

(a)

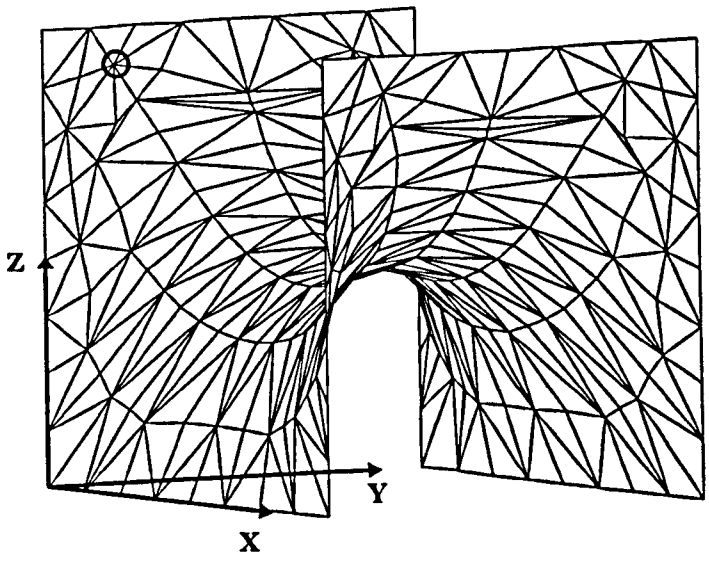

○ Node 67, co-ordinates 0.192, 1.78, 9.197.

(b)

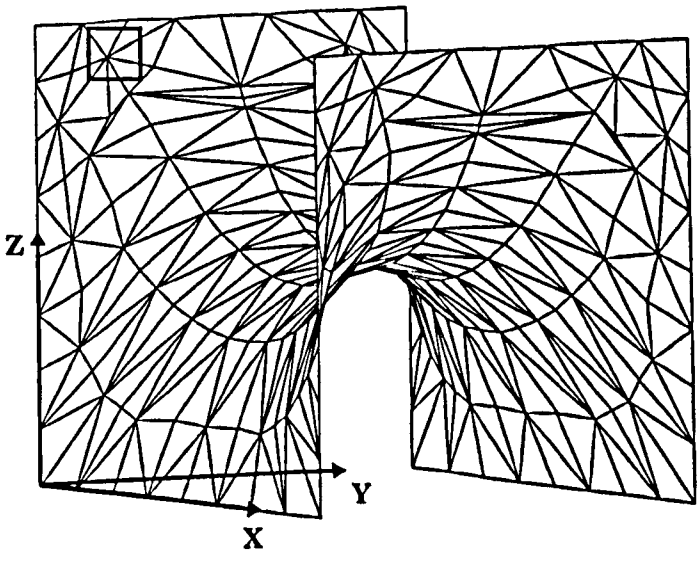

□ Location of the exploded view of node 67, (Figure 3-37).

Figure 3-37 Deformation of 'BOX' Surface (a) Updated Geometry at 653 Iterations. (b) Surface Deformation at 710 Iterations.

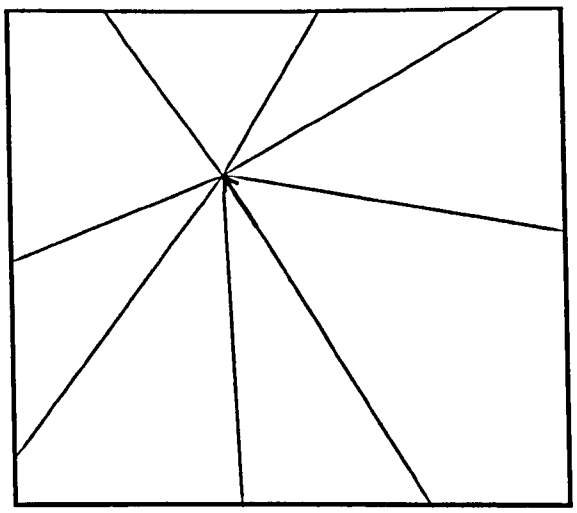

⟶ Displacement vector for node 67,
-0.007*i*,-0.015*j*+0.027*k*.

Figure 3-38 Deformation of 'BOX' Surface - Exploded View of the Displacement Vector of Node 67 at 710 Iterations (Figure 3-37 (b)).

3.4 Post-Processing

3.4.1 Introduction

Documented within this chapter is the method by which a solid model may be manufactured from the numerical model obtained from a form-finding analysis. The chosen process of manufacture is Rapid Prototyping, and entails the construction of a 3D model from the successive adhering of 2D planar sections. It is shown how formex algebra is ideally suited for the generation of the data required by the Rapid Prototyping process. The form-found surface discussed in Section 3.3 is used to illustrate this manufacturing technique.

3.4.2 Rapid Prototyping.

Rapid Prototyping and Manufacture (R.P.&M.) allows a physical model to be constructed directly from the data supplied by a three dimensional CAD model. The manufacturing process is so accurate, that medical science has used the technology for the construction of parts of the human anatomy. Examples include models of a human skull and a protein cell[3.14].

The first rapid prototype machines were developed in California by a company called 3D Systems; the machines were in operation from 1988 and used a process called Stereolithography[xi] (SLA). A few years later, the Laminated Object Manufacturing (L.O.M.) method of Rapid Prototyping appeared. This technique was pioneered by Helisys,

[xi] Stereolithography is the term used to describe the three dimensional printing of an object.

a company also based in California. Both methods apply similar theoretical concepts in the construction of a model, but use different materials and manufacturing processes.

3.4.2.1 SLA Method of Rapid Prototyping.

SLA involves the construction of a solid model within a bath which contains a photosensitive resin. The model is created from a series of planar sections; each section having been formed from a layer of resin that has been cured to a solid by a laser. Successive layers of the model are built upon a platform, which lowers solid cured resin sections into the bath, thereby enabling a new layer of uncured resin to be solidified. Initially, the platform lies just below the surface of the resin and, thus, at this point, the cured resin section forms the base of the model.

3.4.2.2 L.O.M Method of Rapid Prototyping.

L.O.M. utilises a laser for cutting a model's 2D section from a thin piece of material, normally paper, which is coated on one side with a thermoplastic resin. The process begins with paper being fed into the machine and aligned upon a moving platform. Once the paper is adequately tensioned, a laser is used to cut the required section outline from the material; the movement of the laser is controlled by a plotter. The platform is then lowered to allow a new sheet of paper to be positioned above the previously cut layer. Following this, the platform rises and a roller is used to apply heat and pressure to the new paper layer so that it bonds with the previous one.

3.4.2.3 Rapid Prototyping Process.

Rapid Prototyping manufacture consists of the following steps[3.15]

(a) CAD Model. A 3D graphical representation of the physical model must be assembled so that the object's surface topology and dimensions may be accurately determined and scrutinised.

(b) Translation of CAD data to STL data. Although there are different Rapid Prototyping methods available, all methods require a suitable data format for the correct representation of a prototype based on the geometry given by a 3D CAD model. The standard data format used by all Rapid Prototyping methods is the 'tessellated' **STL** format; originally developed by 3D systems. The STL format requires the alteration of the CAD model, such that the surface is composed entirely of triangular facets that satisfy the conditions stated in section 3.4.2.4.

(c) Formation of Supports. Supports are analogous to the work holding devices used in traditional machining processes. Rapid Prototyping involves an additive process whereby successive material layers are built upon each other, consequently, a base support is needed to prevent the model from sticking to the platform of the machine, and to allow the model to be safely removed from the platform. Supports are also necessary to ensure that there are no distortions in the model due to the overhanging of successive layers.

(d) Slicing. This process involves the slicing of a 2D section of the prototype and its supports. Each section is mathematically defined so that when successive planar material layers are stacked upon each other, the desired surface is formed from the base up. The work area in which the laser cuts, or cures, a 2D planar section is called the universe. The size of the universe is dependent on the class of Rapid Prototyping machine used, and dictates the maximum allowable size of the model. The laser is positioned at a vertical

height that varies according to the degree of completion of the model. At each section, the laser traverses through the universe along horizontal and vertical lines called rays. The rays start at one edge of the universe and propagate through the universe, until they reach the opposite universe boundary, detecting the solid and non-solid regions of the model according to the data given in the STL format. In areas where a solid mass has been detected, the ray will not propagate and consequently there will be no incision by the laser.

(e) Merging. This step concerns the merging of the computer representations of the supports, the prototype and any other necessary prototype parts.

(f) Preparation. The process entails the selection of a number of operational parameters. These include the amount of time, in seconds, that the system waits before the adhesion or recoating of a successive layer and, in the case of the SLA process, the number of recoater blade sweeps and the sweep period.

(g) Building. The construction of the actual model.

(h) Part completion and draining. Once the laser drawing sequence has been completed for a given layer, steps (*d*)-(*g*) are repeated for subsequent layers. If the SLA process is being used, excess resin is drained from the bath at this point.

(i) Removal. The platform and the attached part are removed from the machine.

(j) Postcure. This step is only used for the SLA method of manufacture. At this point, the model is in its 'green state', that is, it is not completely polymerised and possesses a layer of

cured resin enclosing a section of uncured material. Postcuring completes the polymerisation process and improves the mechanical strength of the prototype. A model is postcured by placing it in an oven, when still in its 'green state', and bombarding the model with UV light of an appropriate wave length.

(k) Optional part finishing. The surface of the final model must be subjected to a degree of finishing. Due to the tessellated method of manufacture, the model will have a 'stepped' appearance. Shot blasting can be employed to remove any sharp edges and smooth the stepped profile. A polished finish may be achieved by first coating and curing the model with a photo sensitive resin, and then applying a fine abrasive paper to the surface. The model is then primed, and painted, for a highly realistic representation of the actual product. Models created using the LOM process are sealed to prevent distortion and delamination.

3.4.2.4 Generation of Rapid Prototyping Data.

The computational model, whose geometry the physical model is based upon, must possess a surface that is entirely composed of triangular facets. Once this tessellated model has been formed, a STL file is created. The 'STL' file contains the global co-ordinates of the vertices of each triangular facet, together with the unit normal that point externally away from the triangular plane of a facet. The text format of the data contained within an ASCII[xii] 'STL' file corresponds to that shown in Table 3-5 (page 138). The unit surface normal is used by the Rapid Prototyping machine to determine which are the internal and external section profiles of the model, and thereby, on which tessellated side of the object the model's mass is lying.

[xii] The STL file may also be of a binary format. The advantage with this type of format being the ability to store large amounts of data for a minimum file storage space. It is not possible to directly read and check binary data unless it is first decoded, or 'translated', into the ASCII format.

Although it is a fairly simple task to generate a surface using a CAD system, the conversion, or translation, of the geometric data to a format recognisable by the Rapid Prototyping machine can be an extremely difficult proposition. Hence, this stage of the process tends to be the most crucial. During the early development of Rapid Prototyping technology, it became apparent that not only was it extremely laborious to check STL data for discontinuities, it became totally unrealistic when the files contained data relating to tens of thousands of facets[3.16]. Algorithms have been developed, and are still being developed, that will correctly translate the data of a CAD model into the STL format. Such algorithms are implemented into computer programmes called 'translators'. The problems encountered during the translation of data has led to the defining of two rules that need to be satisfied for a correctly translated STL file. These are:

- **Vertex to Vertex Rule.**

The tessellated surface used by the STL file for the representation of a model's topology must be arranged such that it forms an enclosed volume, where every edge of a facet is connected to another facet edge. Another interpretation of this rule is that every facet apex must be connected to another facet apex; it is incorrect for a facet edge to be intersected by the apex of an adjoining facet. The violation of the rule leads to gaps being created on the tessellated surface. In such instances, the rays, along which the incision of the laser travels, pass through the gaps and towards the edge of the universe, resulting in the solid mass also extending outward from the gap and towards the edge of the universe.

- **Alignment of Unit Normal.**

The normal vectors must be so aligned that they point from the surface of the faceted model and away from the object's mass. Incorrectly aligned surface normals can produce such unwanted effects as walls of a zero thickness, or excessively contorted surfaces formed by the incorrect orientation of the facets. Twisted surfaces of this kind are called möbius strips[3.15,3.17].

3.4.3 The Physical Modelling of a Stable Minimal Surface.

In this thesis, L.O.M. has been chosen as the Rapid Prototyping process used for the construction of a stable minimal surface model. Rapid Prototyping is the preferred method of manufacture for the following reasons:

- Traditional prototyping processes, like CNC (Computer Numerical Control) machining, require the numerical surface to be approximated in some manner, usually by the use of a series of curved splines, or ruled surfaces. As a result, the surfaces generated from such an approach will not represent the numerical surface precisely.
- Processes which require some form of tooling are only as accurate as the size of the tool used for machining, and the degree of movement of the tool. It is not always possible to machine surfaces that are curved excessively as it makes it difficult, or impossible, for the tool to move.
- Machining requires the material to be held properly; a difficult proposition for models with highly irregular curved boundaries.

Rapid Prototyping avoids all of these problems by using a laser for the precise cutting of the material in a flat plane, irrespective of the orientation and curvature of the surface.

3.4.3.1 Construction of a Tessellated Model.

Since the form-found surface is already discretised using triangle elements, no faceting algorithm is required to approximate the surface geometry to a series of planar triangles. Consequently, there is no likelihood of an inaccurate surface geometry being produced.

The main problem in the construction of a form-found model lies in the requirement of the model to possess a volume, or thickness. A form-found surface is essentially a membrane of an infinitesimal thickness; the surface may be thought of as a 'cardboard shell' composed of triangles of a zero thickness. Formex algebra can be used for the creation of an enclosed tessellated model from the composition of the formices relating to the form-found surface and an enclosing support. The approach is analogous to the idea of putting a lid on a box. The form-found surface may be thought of as the '***lid***' that needs to be placed on the '***box***' to produce the necessary enclosed form. By creating a Formian scheme in much the same manner as that used for the construction of the initial surface illustrated in Section 3.2, the data relating to the configuration pattern of the triangle elements of the tessellated model may be found. The scheme 'BOXSTL' (Table 3-4) is presented as an illustration of the likely formex algebra manipulations required in the construction of a model:

```
BOXSTL='[:depth_1,depth_2,m,n,width,length,height:
.....
take box_ff
.....
u1=width/(4*m)
u2=length/(4*n)
u3=height/(4*m)
.....
square=[0,0,0;0,2,0;2,0,0]#..
[2,0,0;0,2,0;2,2,0]
rect=LAM(1,2)|square
segment1=ROSAD(2,2,2,180)|rect
base=RINID(m,n,4,4)|segment1
bot=TRAN(3,-depth_2)|(BT(u1,u2,u3)|base)
.....
side=VERAS(ric|4*m,0,-90)|base
sidea=TRAN(1,depth_1)|(BT(u1,u2,u3)|side)
surfb=TRAN(1,-4*m)|side
surfb=TRAN(1,-depth_1)|(BT(u1,u2,u3)|surfb)
side=sidea#surfb
.....
rect2=[0,0,0;2,0,0;0,0,-1]#[2,0,0;2,0,-1;0,0,-1]
rect3=BT(u1,u2,u3)|rect2
rect3_m=BT(u1,u2,u3)|(RIN(1,2,2)|[0,0,-1])
rect3_alt=RIN(1,2,2*u1)|[0,0,-depth_2]
rect3=NOV(rect3_m,rect3_al)|rect3
side_2=RINID(2*m,2,2*u1,4*n*u2)|rect3
.....
side_3=BT(u1,u2,1)|([0,0,0;0,2,0;0,2,-1]#[0,0,0;0,0,-1;0,2,-1])
side3_m=BT(u1,u2,1)|([0,0,-1]#[0,2,-1])
side3_alt=BT(u1,u2,1)|([0,0,-depth_2]#[0,2,-depth_2])
side_3=NOV(side3_m,side3_al)|side_3
side_3=LAM(1,length/2)|(TRAN(1,-depth_1)|(RIN(2,2*n,2*u2)|side_3))
.....
side_str=BT(u1,u2,u3)|([0,0,0;0,0,2;-1,0,0]#[-1,0,0;-1,0,2;0,0,2])
str_m=BT(u1,u2,u3)|([-1,0,0]#[-1,0,2])
str_alt=BT(1,u2,u3)|([-depth_1,0,0]#[-depth_1,0,2])
side_str=NOV(str_m,str_alt)|side_str
side_str=LAM(1,length/2)|(LAM(2,width/2)|(RIN(3,2*m,2*u3)|side_str))
.....
edge2=REF(1,0)|rect3
edge_m=[-2*u1,0,0]#[-2*u1,0,-depth_2]
edge_alt=[-depth_1,0,0]#[-depth_1,0,-depth_2]
edge=NOV(edge_m,edge_alt)|edge2
edge=RINID(2,2,(4*m*u1)+depth_1,(4*u2*n))|edge
.....
segment2=square
bot_stra=RIN(2,2*n,2)|(TRAN(1,4*m)|segment2)
bot_strb=RIN(2,2*n,2)|(TRAN(1,-2)|segment2)
mark=(RIN(2,(2*n)+1,2)|[(4*m)+2,0,0])#(RIN(2,(2*n)+1,2)|..
[-2,0,0])
mark=BT(u1,u2,u3)|mark
alter=TRAN(1,-depth_1)|(RIN(2,(2*n)+1,2*u2)|[0,0,0])
alter2=TRAN(1,(2*depth_1)+length)|alter
alter=alter2#alter
bot_strc=BT(u1,u2,u3)|(bot_stra#bot_strb)
bot_strc=NOV(mark,alter)|bot_strc
bot_str=TRAN(3,-depth_2)|bot_strc
.....
top_str=TRAN(3,height)|bot_strc
.....
```

A) **Defining the nominal parameters of the scheme.**

B) **Importing the formex representing the form-found surface, or '*lid*'.**

C) **Determination of the units in the normat directions of the form-found. surface.**

D) **Generation of the formices representing the configuration patterns of the elements forming the enclosing support, or '*box*'.**

Table 3-4 Scheme 'BOXSTL'.

box_sup= bot#side#side_2#side_3#side_str#edge#bot_str#top_str	***E)* Formation of the configuration pattern of the enclosing support, '*box*'**
box_stl=box_ff#box_sup	***F)* Formation of the configuration pattern of the tessellated model.**
CLEAR *USE VM*(2),*VH*(5,10,5,3,5,0,1,1,1) *SHOW* box_stl	***G)* Graphical depiction of the tessellated model.**
stlnod=**MED**|box_stl stlmem=**DIC**(stlnod)|box_stl supnod=**MED**|box_sup supmem=**DIC**(supnod)|box_sup box_sup=**RED**(supnod)|supmem box_stl=**RED**(stlnod)|stlmem	***H)* Amendment of the formex relating to the configuration pattern of the tessellated model to ensure the 'vertex to vertex' rule is met.**
KEEP box_stl,box_sup]'	***I)* Saving of formices containing relevant data.**

Table 3-4 Continuation of Scheme 'BOXSTL'.

Figure 3-39 showsp the tessellated enclosed model of the form-found surface discussed in Section 3.3. The tessellated model is represented by the configuration pattern of formex 'box_stl' (Table 3-4); the formex has been created by invoking the scheme **BOXSTL(1,0.5,4,4,10,10,10).** An external view of the same tessellated model is depicted in Figure 3-40.

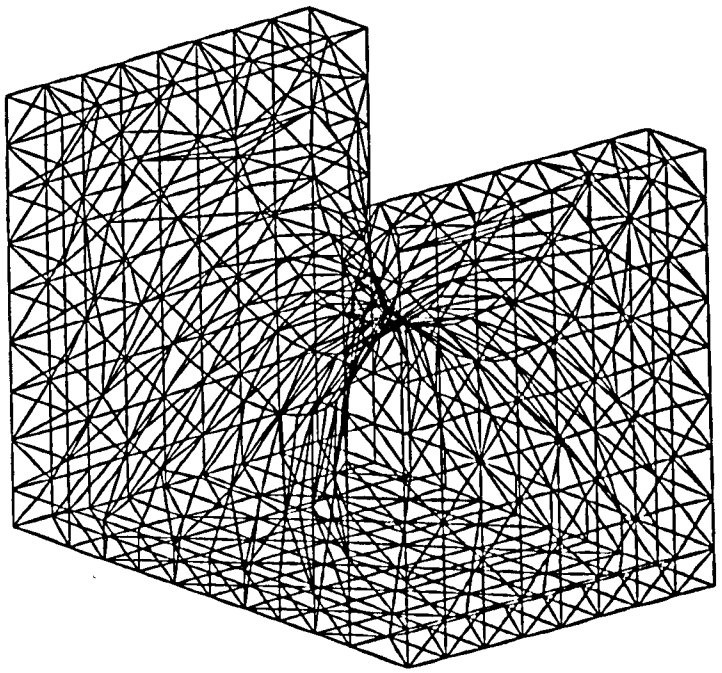

Figure 3-39 Configuration Pattern of the Tessellated 'BOX' model - Internal View.

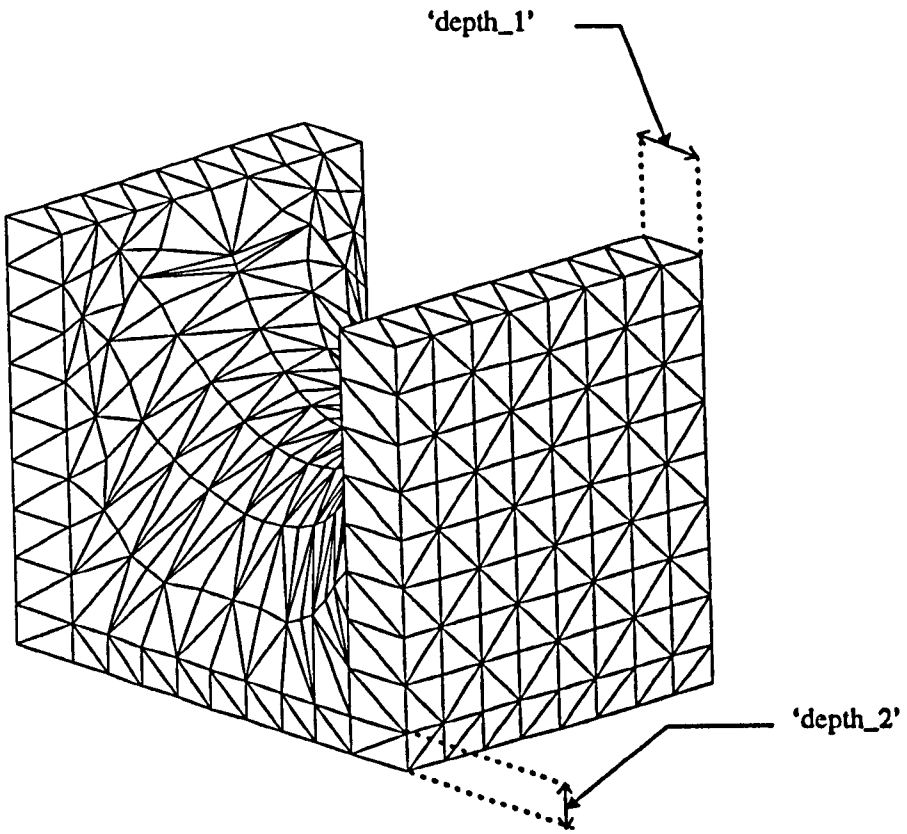

Figure 3-40 Configuration Pattern of the Tessellated 'BOX' model - External View.

The formex manipulations involved in stages *A*)-*I*) are explained with reference to the 'BOXSTL' scheme.

STAGE *A*) Initially, the parameters used to determine the dimensions of the '*box*' are defined. In this case, the nominal parameters 'depth_1' and 'depth_2' refer respectively to the value of the thickness of the enclosing support connected to the side and base of the form-found surface. The remaining parameters are used to acquire the dimensions and number of elements contained within the form-found surface; as explained in Section 3.2.

STAGE *B*) The formex relating to the configuration pattern of the stable minimal surface, 'box_ff', is loaded into the Formian programming environment, after the prior conversion of the form-found geometric data into a formex binary file using the MORFORM programme.

STAGE *C*) Because the formex manipulations depend on the reference system of the normat lines aligned according to the position of the global Cartesian axes of the initial surface used in form-finding, the value of the units in these directions must be determined from information supplied by the nominal parameters.

STAGE *D*) The constituent parts of the ***'box'***, and any supports needed to prevent the deformation of the model, are described by individual formex expressions.

STAGE *E*) The composition of the formices of stage ***D*)** produce the formex describing the complete configuration pattern of the **'box'** used for the enclosing of the minimal surface model; in this example formex 'boxsup'.

STAGE *F*) This stage involves the generation of the single formex obtained from the composition of the **'box'** and **'lid'**. Such a formex describes the configuration pattern of the tessellated Rapid Prototyping model

STAGE *G*) The implementation of Formian graphical commands allows the configuration pattern of the tessellated model to be checked.

STAGE *H*) The use of normat lines referenced according to the Cartesian axes of a form-found surface implies that the normat points are composed of real numbers. This can lead to formices being slightly incorrectly referenced, due to the influence of round-off errors during the manipulation of a formex[xiii]. Thus, the facets of the enclosing support, or **'box'**, may possess a vertex that is not exactly joined to the opposing vertex of the facet of the form-found surface. This will result in the violation of the 'vertex-to-vertex' rule and cause

[xiii] It is for this reason that integers are the preferred format for normat points.

interpretation errors when the STL data is transferred to the Rapid Prototyping machine. Round off errors are prevented by using the **MED** function which removes those normat points, contained within a formex, that are essentially positioned on top of a previous normat point. Therefore, to satisfy the vertex to vertex rule, the **MED** and **DIC** functions are used to disassemble the tessellated model into its basic constituent parts, the nodal co-ordinates and the element numbering scheme, and then use the redictum function **(RED)** for the subsequent reassembling of the model from these formices.

STAGE *I*) Saving of the formex representing the configuration pattern of the tessellated model. The data contained within the formex must be translated into the STL format according to the procedure given in section 3.4.3.2.

3.4.3.2 Conversion of Data to the STL Format.

During the construction of the tessellated model, significant consideration must be attached to the clockwise, or anti-clockwise, orientation of the points joining the planar vectors aligned along with sides of a discrete element. This is needed to ensure that the normal vector, calculated from the vector cross product of the planar vectors, points from the face of the facet and away from the model's mass. Further, it is noted that formex algebra manipulations can generate elements with nodes numbered in contrasting orientations; this is an additional complication. A simple example of this problem is the application of the lambda **(LAM)** function in the derivation of a formex found from the reflection of a triangular configuration pattern a plane perpendicular to its side. The ensuing formex will consist of two triangular elements that possess nodes that are numbered clockwise for one element, and anti-clockwise for the other.

Clearly, there is a need to find a universal approach for the determination of the unit normal vector, irrespective of the nodal order of a facet and the formex algebra transformations used in the construction of the tessellated form. By considering the vector equation of a plane, it is possible to define the direction of a unit normal according to the value of the perpendicular distance of a facet from the origin (Appendix 3A.2). Thus, the unit normal vectors of a tessellated model will depend **only** on the location of the origin.

- **Relationship Between the Direction of a Unit Normal and the Location of the Origin.**

With regards to the universe from which a model's 2D planar sections are cut, the 'internal area' is the term used to define the area of the universe that contains the mass of the model, while the external area comprises the wastage material. If the origin is translated so that it lies within the internal area, the position vector of each node forming the vertex of a facet will point towards the side of the facet containing the mass of the model, i.e. the internal facet side. The unit normal vector is then calculated in a manner to ensure that it always points away from the opposite face of the facet, the external side, into the external area, as shown in Appendix 3A.2. Figure 3-41 illustrates the incorrect and correct positions of the origin for the circular planar section of a cylindrical solid:

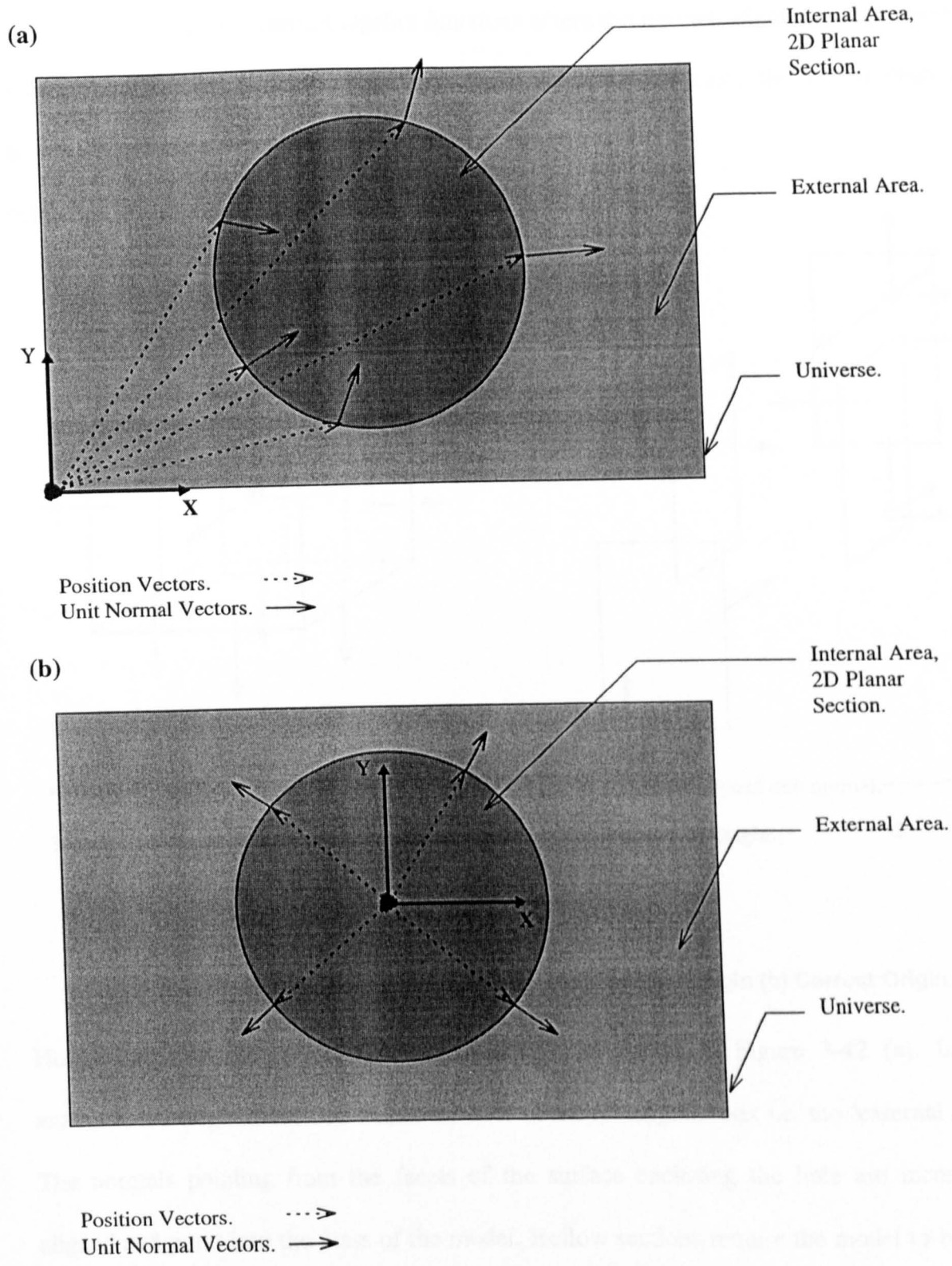

Figure 3-41 (a) Incorrect Origin position. (b) Correct Origin Position.

When the origin forms the vertex of an element, or a triangle element lies within the same plane as the origin, the perpendicular distance from the origin to the facet plane is equal to zero and the correct unit normal cannot be determined. Such cases are often associated with

surfaces generated from formex algebra functions where the normat origin also represents a normat point of the discretised surface. Should this be the case, the origin must be translated to a suitable position.

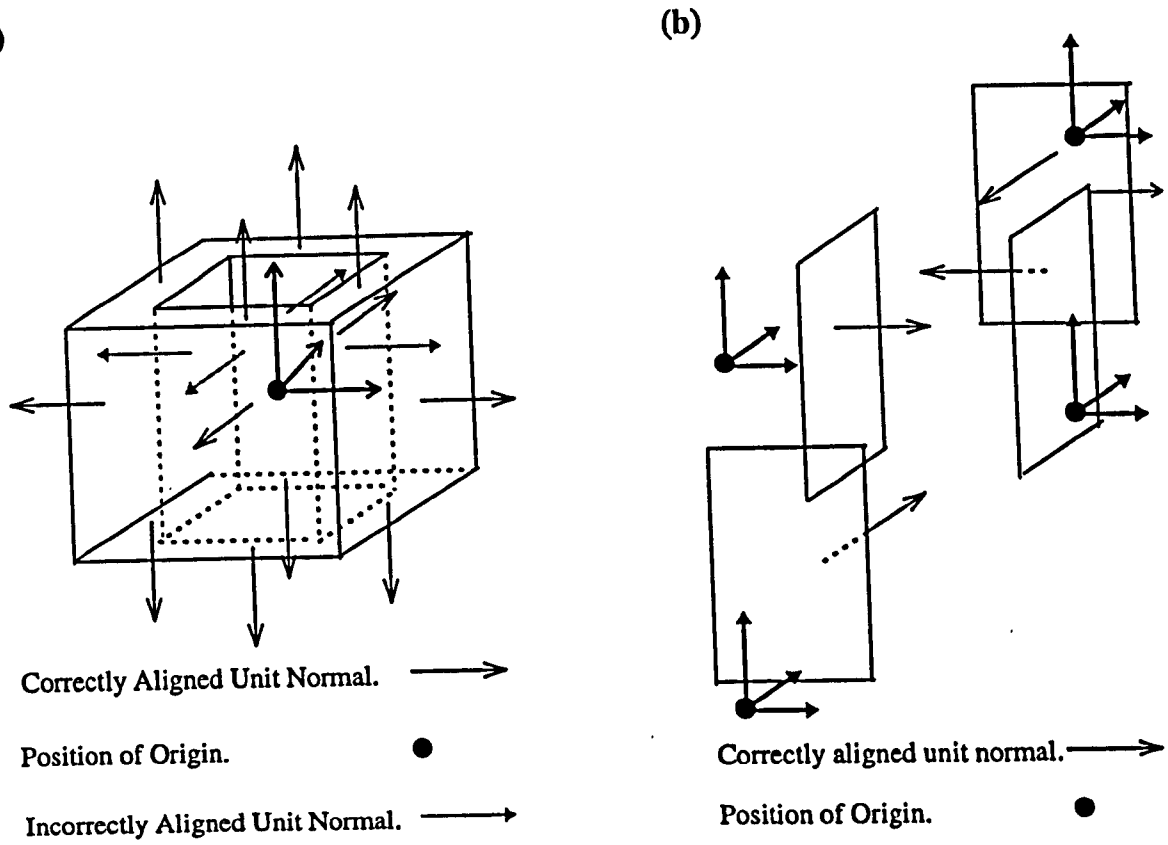

Figure 3-42 Construction of a Hollow Model (a) Incorrect Origin (b) Correct Origin.

Hollow sections present an additional problem, as shown in Figure 3-42 (a). In this example, the origin is located within the hole of the rectangular box i.e. the 'external area'. The normals pointing from the facets of the surface enclosing the hole are incorrectly aligned and point into the mass of the model. Hollow sections require the model to be split into individual faces, and the origin translated to suitable positions to enable the STL data to be correctly calculated for each face. This is illustrated for the faces enclosing the hole (Figure 3-42 (b)). Once the STL data for each face has been obtained, the data is combined with that of the other components, or faces, to give the complete STL file.

- **Example of the Generation of STL Data.**

The formex file representing the configuration pattern of the tessellated surface shown in Figure 3-40 is translated into the 'STL' format using the MORFORM programme. According to Section 3.4.3.2, the process requires a suitable location for the translation of the origin.

In this example, the origin cannot be translated so that all the position vectors of the vertices of the tessellated model are pointing to the internal faces of the facets (Figure 3-43 (a)). Figure 3-43(b) shows that the unit normals of the form-found surface, or '*lid*', are correctly aligned, provided that the origin is translated to the point 5,5,-80. However, this implies that the unit normals of the base of the tessellated model will be incorrectly aligned. The problem may be alleviated by determining the STL file for each of the formices representing the enclosing support and the form found surface i.e. the origin is translated to the point 5,5,-80 for formex 'box_ff' and to 5,5,3 for formex 'box_sup'. These individual STL files are then merged to give the model's complete STL file, as shown in Table 3-5.

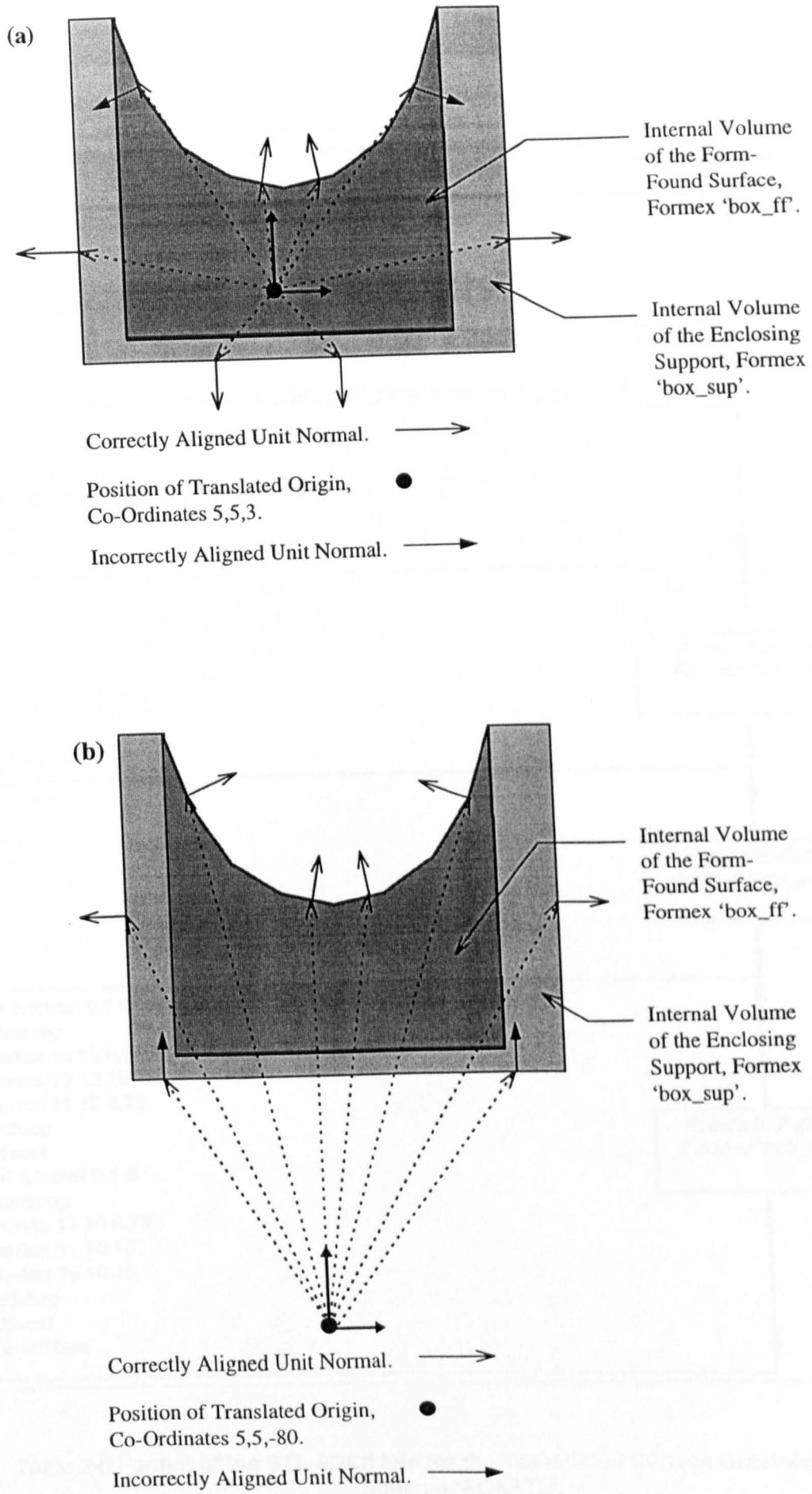

Figure 3-43 (a) Origin Position 5,5,3. (b) Origin Position 5,5,-80.

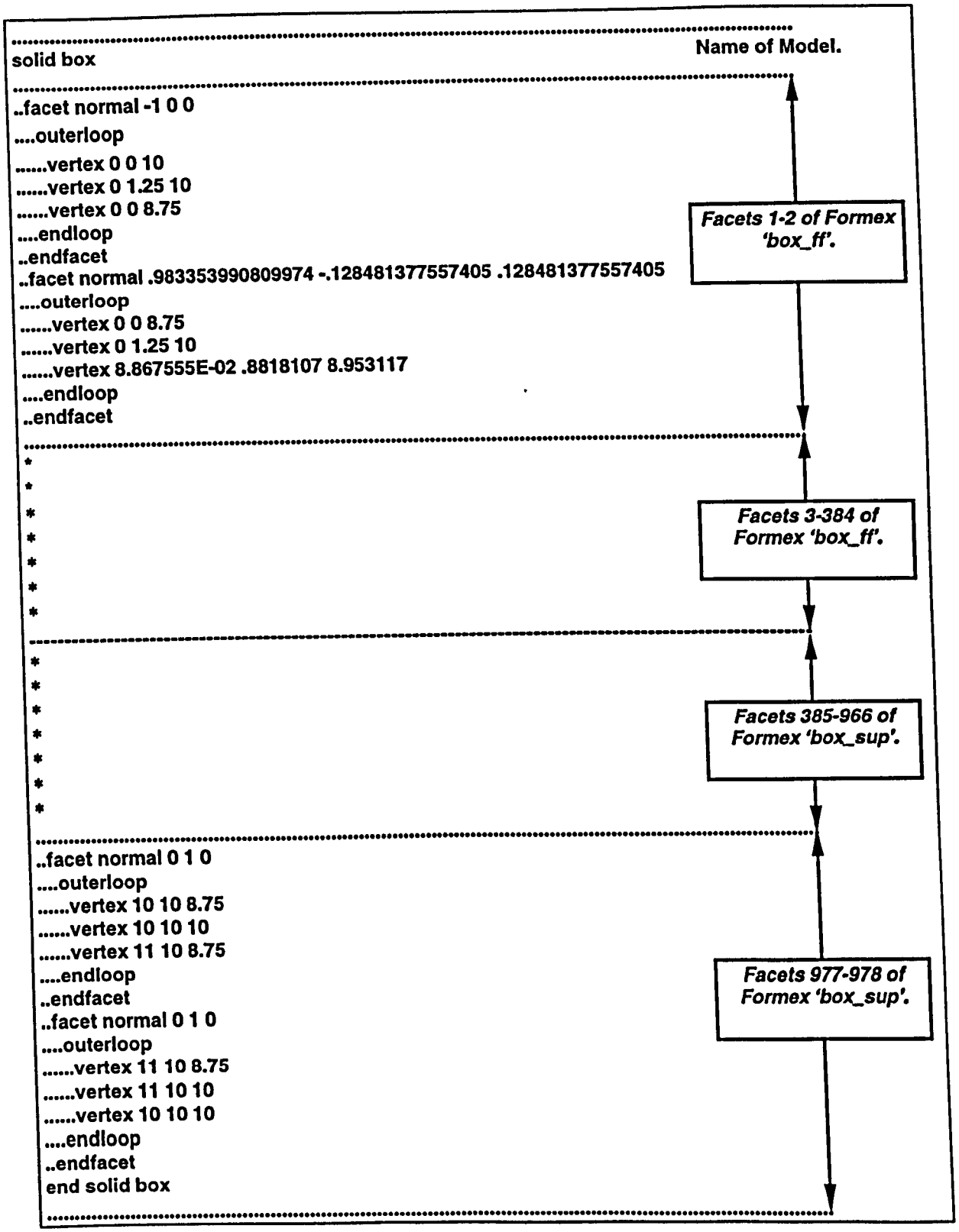

Table 3-5 Format of the STL ASCII File for the Tessellated Surface Obtained from the Scheme 'BOXSTL'.

3.4.3.3 Example of a Stable Minimal Surface Physical Model.

The STL file presented in Table 3-5 is used for the manufacture of the model shown in Figure 3-44. The scale of the model is 1:100.

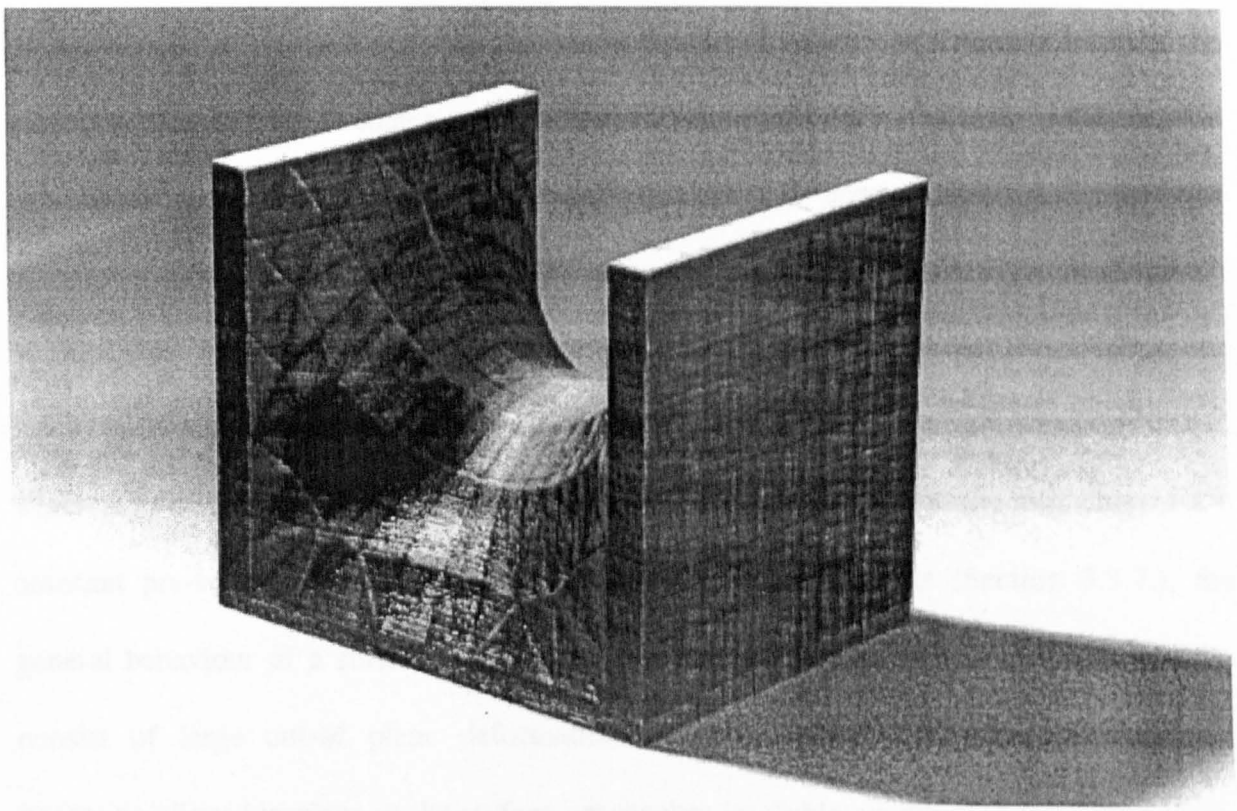

Figure 3-44 Solid Model of the 'BOX' Form-found Surface.

3.5 Summary.

In this Chapter the three main steps involved in the computational form-finding of a stable minimal surface have been introduced. These steps were accomplished using three computer programmes: Formian, the form-finding 'equation solver' and AutoCAD. These programmes were integrated through the use of the programme MORFORM. It was shown how formex algebra statements, of a generic formulation, are employed to create a configuration pattern that may be altered quickly, according to the user's requirements. Subsequently, it was illustrated that the grouping together of a series of generic formex statements within a scheme leads to an efficient and convenient means of generating and storing all the data required by the form-finding equation solver. Such a process requires the user to follow six distinct stages, each stage involving a sequence of formex manipulations that satisfy the syntax and rules of formex algebra. The power of the technique was adequately demonstrated by the example presented in Section 3.3.6. The "form-found" surface was generated with no prior knowledge of the final shape, other than the geometrical arrangement of its boundaries. From a very crude initial discretised surface, which in no way represented the final equilibrated stable minimal form, the ideal shape for a constant pre-stress was "found". From the analysis of the results (Section 3.3.7.), the general behaviour of a surface undergoing a form-finding analysis was shown to initially consist of large out-of plane deformations, which gradually decrease in magnitude, becoming aligned in-plane as the surface approaches its stable equilibrated state. The ability to asses the configuration of a numerical form-found surface using a solid model was documented. The process required the creation of data relating to an enclosed tessellated model using a Formian scheme. Furthermore, the data required the origin of the tessellated model to be suitably positioned, in order to ensure that the data was correctly transferred to the Rapid Prototyping machine using the MORFORM programme.

APPENDIX 3

3A.1 -Derivation of Element "Pseudo Cable Forces".

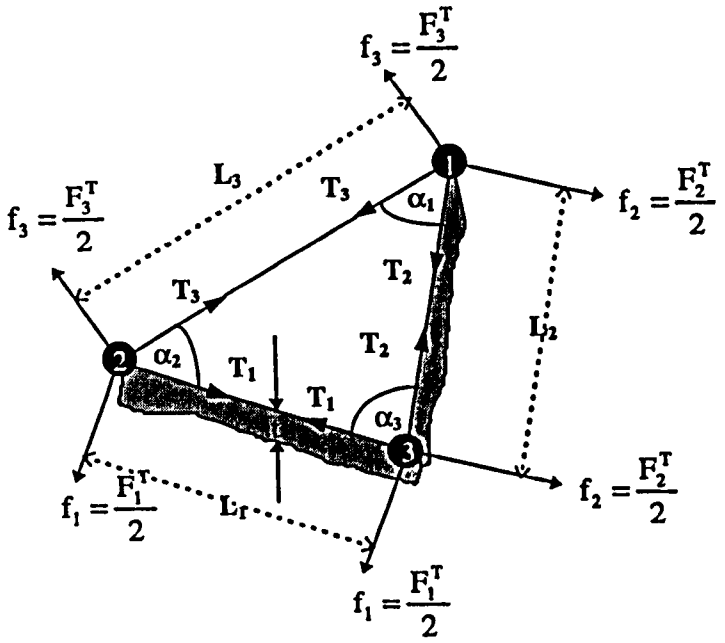

Figure 3A-1 Orientation of "Pseudo Cable Forces."

The constant stress σ_S acting perpendicular to the sides of the element is replaced by the total force F_K^T acting along side k of the element (k represents the side adjacent to node i of the element, k and i are integers ranging from 1 to 3). The force acting at a node i of the element is given by f_k.

Node 1.

Static equilibrium parallel to length L_3.

$$T_3 + T_2 \cos\alpha_1 = f_2 \cos(90 - \alpha_1) = f_2 \sin\alpha_1 \qquad \text{(3a.1)}$$

Static equilibrium perpendicular to length L_3.

$$T_2 \sin\alpha_1 + f_2 \sin(90-\alpha_1) = f_3 \qquad \textbf{(3a.2)}$$

$$T_2 \sin\alpha_1 + f_2 \cos\alpha_1 = f_3 \qquad \textbf{(3a.3)}$$

$$\frac{\text{equation(3a.1)}}{\cos\alpha_1} - \frac{\text{equation(3a.3)}}{\sin\alpha_1} \text{ gives:}$$

$$\frac{T_3}{\cos\alpha_1} - \frac{f_2\cos\alpha_1}{\sin\alpha_1} = -\frac{f_3}{\sin\alpha_1} + \frac{f_2\sin\alpha_1}{\cos\alpha_1}$$

$$T_3 \sin\alpha_1 - f_2\cos^2\alpha_1 = -f_3\cos\alpha_1 + f_2\sin^2\alpha_1$$

$$T_3 \sin\alpha_1 = \frac{\sigma_s t}{2}(L_2 - L_3\cos\alpha_1) \qquad \textbf{(3a.4)}$$

In accordance to the "cosine rule", the sides L_1 and L_3 may be expressed as:

$$L_1^2 = L_2^2 + L_3^2 - 2L_2L_3\cos\alpha_1 \qquad \textbf{(3a.5)}$$

$$L_3^2 = L_1^2 + L_2^2 - 2L_1L_2\cos\alpha_3 \qquad \textbf{(3a.6)}$$

After substitution of L_1^2 from equation (3a.5) into equation (3a.6), rearrangement gives:

$$L_2 - L_3\cos\alpha_1 = L_1\cos\alpha_3 \qquad \textbf{(3a.7)}$$

substituting for the left hand side of equation (3a.7) into equation (3a.4) gives:

$$T_3 \sin\alpha_1 = \frac{\sigma_s t}{2}(L_1\cos\alpha_3) \qquad \textbf{(3a.8)}$$

In accordance to the "sine rule",

$$\frac{L_1}{\sin\alpha_1} = \frac{L_3}{\sin\alpha_3}$$

Hence,

$$T_3 = \frac{\sigma_s L_3 t}{2\tan\alpha_3} = \frac{F_3^T}{2\tan\alpha_3} \qquad \text{(3a.9)}$$

Because of symmetry, further relationships can be arrived at for the remaining "pseudo cable" forces T_1 and T_2.

Ill-conditioning of equation (3a.9) arises for the instance when $\alpha \to 90$, $\tan\alpha \to \infty$ .The distribution of the "pseudo cable" forces within the element are then described by Figure 3A-2 :

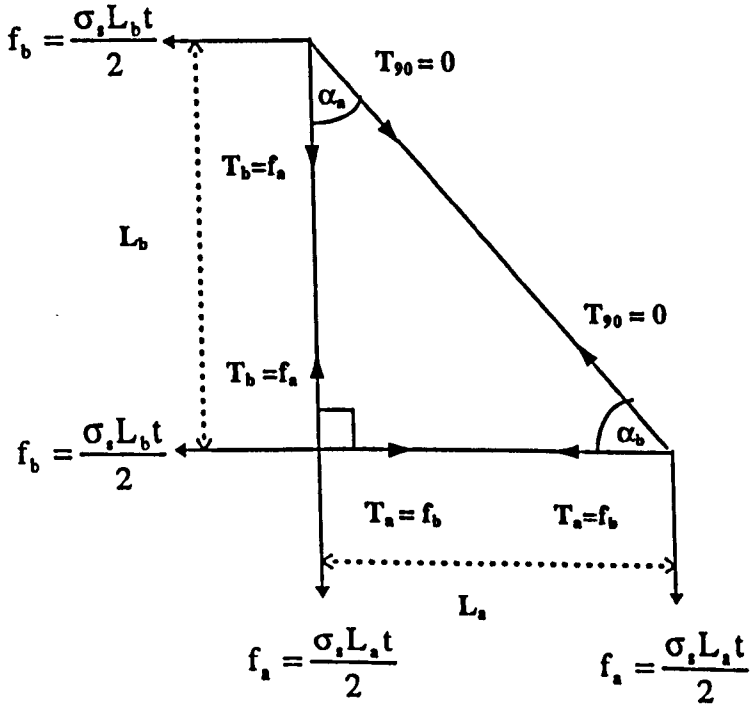

Figure 3A-2 Orientation of "Pseudo Cable Forces" for a Right Angled Triangular Element.

3A.2 - Procedure for the Calculation of a Correctly Aligned Unit Normal Vector.

The vector cross product of any two vectors produces the vector $\vec{V}_N$ This vector is perpendicular to the plane containing the vectors used by the cross product, and is in a direction governed by a 'right handed set' (Figure 3A-3). With respect to Rapid Prototyping, the rule implies that for every facet of the tessellated model, the vertices must be ordered so that the vector $\vec{V}_N$ normal to $\vec{V}_{AB}$ and $\vec{V}_{AC}$ points away from the mass of the model.

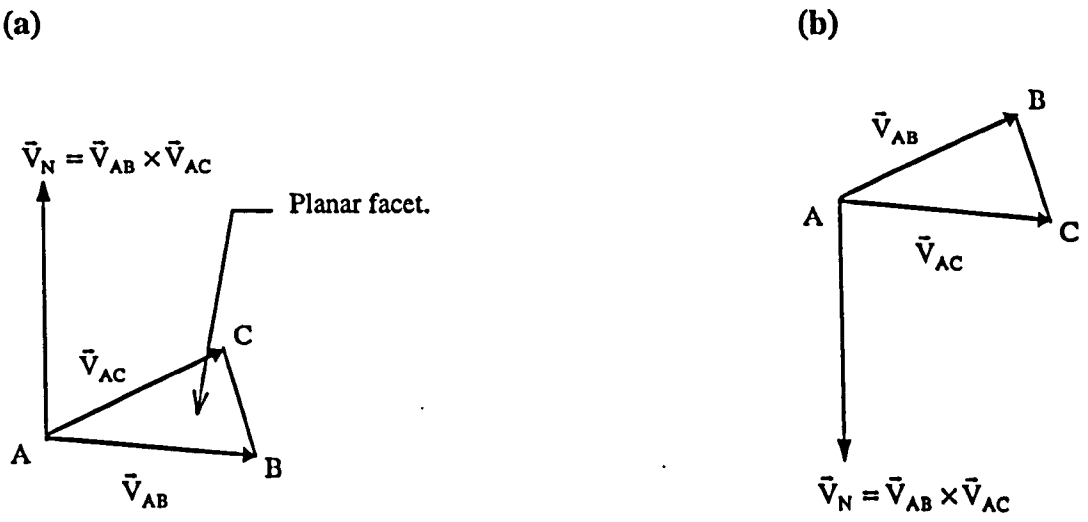

Figure 3A-3 Direction of $\vec{V}_N$ for Vertices Ordered (a) Clockwise (b) Anti-Clockwise.

The direction of the normal vector $\vec{V}_N$ may be defined independently of the clockwise, or anti-clockwise, order of the nodes defining a facet of the tessellated model, by considering the vector equation of a plane. Consider Figure 3A-4 which depicts the planar section of the top of a tessellated model that is to be constructed using Rapid Prototyping. It can be seen that the 'internal area' of each section represents a slice of the model's mass, and the successive adhering of such sections produces the total mass of the model.

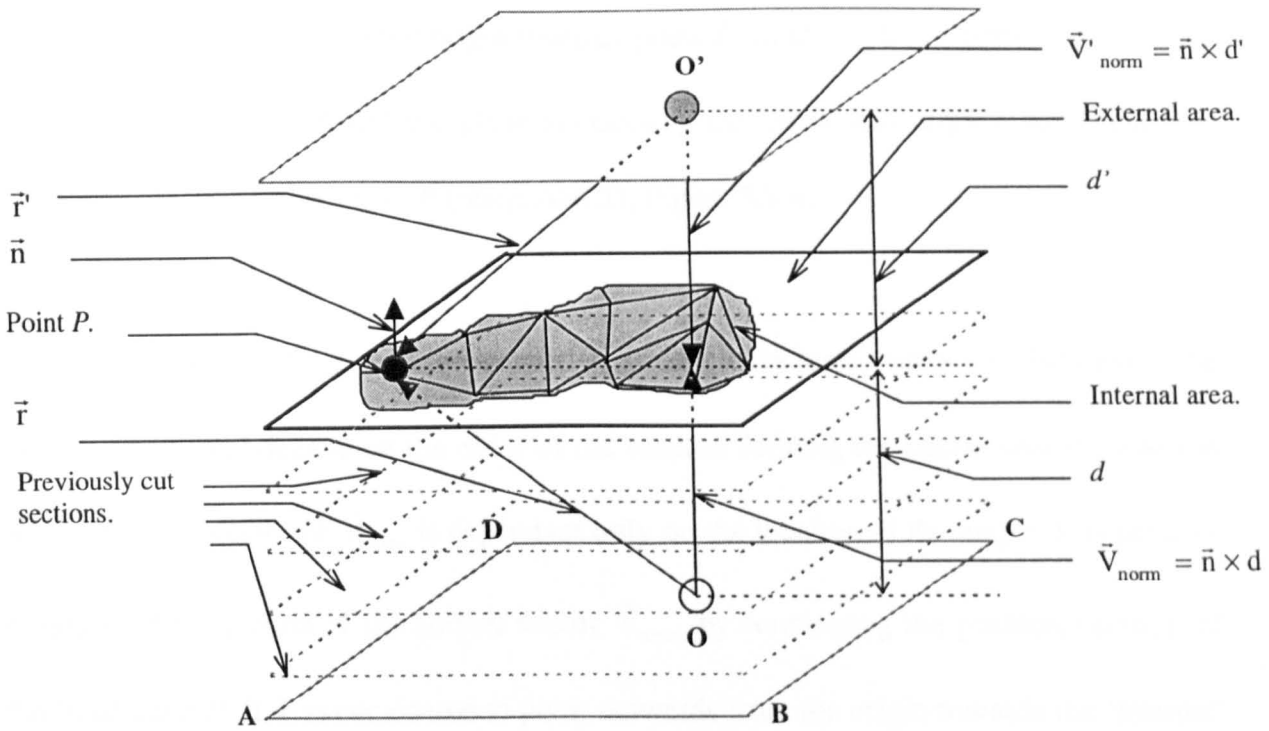

Figure 3A-4 Final Section of a Tessellated Model Constructed using Rapid Prototyping.

The vector equation of a plane is obtained from the equation :

$$\vec{r}.\vec{n} = d \qquad \textbf{(3a.10)}$$

This gives the equation of a plane, distance d from the origin and perpendicular to the unit vector $\vec{n}$; calculated from vector $\vec{V}_N$ of Figure 3A-3. The vector $\vec{r}$ represents the position vector of any fixed point P i.e. the vertex of a facet lying within the plane containing the facet of the tessellated model.

The vector $\vec{V}_{norm}$, representing the perpendicular distance of the point P from the origin, is given by:

$$\vec{V}_{norm} = d \times \vec{n} \qquad \textbf{(3a.11)}$$

$\vec{V}_{norm}$ will always point from the origin towards point *P*, in a direction perpendicular to the plane containing point *P*, and the plane intersecting the origin and aligned parallel to the plane containing the fixed point *P* (plane ABCD, Figure 3A-4).

The unit vector of $\vec{V}_{norm}$ will be aligned parallel to the unit vector $\vec{n}$. However, the direction of $\vec{n}$ will depend on the order of the vertices defining the planar vectors, whereas that of the unit vector of $\vec{V}_{norm}$ is dependant **only** on the location of the origin. It is possible to deduce the direction of the normal vector $\vec{V}_{norm}$ by considering the position vector $\vec{r}$ of the fixed point *P*. If $\vec{r}$ is considered to point outwards from the origin towards the 'internal' surface of a facet of the tessellated model, then the normal vector will point away from the opposing facet face, the 'external' surface. The implication of this statement is best illustrated using Figure 3A-4, for the instance when the origin is **incorrectly** translated to position **O'**. The plane containing point *P* represents the final section of the Rapid Prototype model, hence **O'** is considered to be positioned **outside** of the mass of the model. In this instance, the position vector is $\vec{r}'$ which points to the 'external face'. As a consequence, the perpendicular distance obtained from equation (3a.10) is *d'* which is opposite in sign to that of *d*. Hence, the vector $\vec{V}'_{norm}$, calculated from equation (3a.11), can be seen to be a vector that is equal and opposite to $\vec{V}_{norm}$, and aligned such that it wrongly points **into** the mass of the solid.

Because the direction of $\vec{V}_{norm}$ is not altered when the sign of *d* is positive, the unit normal vector $\vec{n}$, calculated from vector $\vec{V}_N$, (Figure 3A-3), need only be altered in cases where the sign of *d* has been found to be negative from equation (3a.10). In such circumstances, the

correct surface unit normal is given by multiplying the unit vector $\vec{n}$ by -1; provided the origin is suitably placed so that the position vectors $\vec{r}$ point to the 'internal' facets of the tessellated model (as illustrated for the example where the origin is given by O (Figure 3A-4)).

REFERENCES

3.1 D. Wakefield,
"Tensyl: The Development of an Integrated CAD System for Stressed Membrane Structures."
LSA 86, 1st International Conference on Light Weight Structures in Architecture, Sydney, 1986.

3.2 H. Nooshin, P. Disney and C. Yamamoto,
"Formian."
Multi-Science Publishing Co. Ltd., 1993.

3.3 H. Nooshin,
"Formex Configuration Processing in Structural Engineering."
Elsevier Applied Science Publishers, 1984.

3.4 D. Hadker,
"Formex Configuration Processing for Space Structures."
PhD Thesis, Department of Civil Engineering, University of Surrey, 1993.

3.5 T. S. Lewis and W. J. Lewis,
"An Integrated Approach to the Form-Finding of Structural Forms Possessing a minimal Surface Area."
University of Warwick Research Report CE52, November 1995.

3.6 C. Isenberg,
"The Science of Soap Films and Soap Bubbles."
Tieto Ltd., 1978, pages 8-9.

3.7 M. R. Barnes,
"Form-Finding and Analysis of Pre-stressed Nets and Membranes."
International Conference on Non-Conventional Structures,
Vol. 1, 1987, pages 327-338.

3.8 W. J. Lewis,
"Dynamic Relaxation Analysis of the Non-Linear Static Response of Pre-tensioned Cable Roofs."
Computers and Structures, Vol. 18, No. 6, 1984, pages 989-997.

3.9 T.S.Lewis and W. J. Lewis,
"Effectiveness of the Non-Linear Numerical Models for the Analysis of Light-weight Membranes."
SFB 230 Naturliche Konstruktionen, H9, 1994, pages 65-71.

3.10 K. Y. Tan,
"The Computer Design of Tensile Membrane Structures."
PhD, Dept. of Civil Engineering, Queensland University, 1989.

3.11 M. R. Barnes,
"Form and Stress Engineering of Tension Structures."
Structural Engineering Review, vol. 6, no. 3-4, Elsevier Science Ltd., pages 175-202, 1994.

3.12 J. Shan,
"Application of the Sub-Region Mixed Energy Principle to Numerical Modelling of Pre-Stressed Clad Cable Nets."
PhD Thesis, University of Warwick, Department of Engineering, 1990.

3.13 P. Singer, D. Strobel, R. Hordt and J. Bahndorf,
"A Method for Finding Minimal Surfaces."
2nd International Symposium SFB 230, Stuttgart, 1991, pages 137-142.

3.14 C. P. E. Zollikofer and M. S. Ponce de Leon,
"Tools for Rapid Prototyping in the Biosciences."
I.E.E.E. Computer Graphics and Applications, Vol. 16, no. 6, November 1995, pages 48-55.

3.15 P. F. Jacobs,
"Rapid Prototyping and Manufacture, Fundamentals of Stereolithography."
Society of Manufacturing Engineers, 1992.

3.16 J. H. Bϕhn, "Removing Zero Volume Parts from CAD Models for Layered Manufacture."
I.E.E.E. Computer Graphics and Applications, Vol. 16, no. 6, November 1995, pages 27-34..

3.17 S. Hildebrandt and A. Tromba,
"Mathematica and Optimal Form."
Scientific American Library, 1985.

CHAPTER 4

Verification of the Form-Finding Approach.

4.1 Introduction.

Although there is a significant amount of information relating to form-found surfaces obtained from the same discretised surface element as adopted in this thesis[4.1,4.2,4.3,4.4], the results tend to be limited to examples of light-weight structures that have been designed with constraints imposed on the surface deformations through the use of geodesic strings[4.3] (Chapter 6), or with a surface idealisation that includes a non-uniform pre-stress[4.3]. In conclusion, there is little literature relating to the generation of a numerical surface that accurately conforms to the configuration of a stable minimal surface. This Chapter intends to address this vacuum, and provide the reader with some measure of the accuracy of the numerical approach. The results of several form-found surfaces are studied, and assessed, in accordance with mathematical and experimental solutions. Also, some of the numerical examples are compared with similar surfaces obtained using different computational approaches. The thickness of all the surfaces is equal to 1 mm

Provided the boundaries enclosing a soap lamina are rigid, a soap film will always adopt the same geometry irrespective of the dimensions of the boundaries; the surface stress in a bubble is independent of its size (Chapter 1, Section 1.2, "Physical Modelling). (For instances where the lamina is bounded by flexible boundaries - as used by Frei Otto in his soap laminae experiments (Chapter 2, Section 2.2) - the lamina geometry will depend on the stiffness of the strings; flexible boundaries are discussed for those surfaces presented in Example 5.2.6 and Example 5.2.7 (Chapter 5)). Hence, to successfully model a stable

minimal surface, an acceptable margin of error for the residual forces of the numerical model is required; a residual that is independent of the magnitudes of the internal forces induced by the dimensions of the mesh and the assumed surface stress of the structure. (Previously, the criterion $ER \leq 0.5$[i], was used in the form-finding of the BOX example contained in Chapter 3, Section 3.3.6). Consequently, alternative criteria are suggested, and assessed, with the intention of selecting an appropriate universal criterion.

4.2 Alternative Convergence Criteria.

Convergence criteria used in numerical approaches developed by other authors include:

- A minimisation of the surface area[4.5], or a negligible change in the surface area between successive iterations[4.6]. (In this thesis, the criterion $A_{\%}$ is used to define the reduction in surface area of the **"initial surface."**)
- A maximum admissible size for the nodal displacements between successive iterations[4.6].
- The percentage of the error residual ER to the maximum pseudo cable force T_k[ii], $ER_{T\%}$
- The percentage of the error residual ER to the force per unit length F_k[iii], $ER_{F\%}$.

The criterion $ER_{T\%}$. was first suggested in a research report published by Gosling & Lewis[4.7] and adopted as the criterion of convergence for the numerical algorithm documented in his thesis[4.8] (Chapter 4, Section 4.5.2). It was concluded that provided $ER_{T\%} \leq 0.025$, there was little discrepancy between the configuration of a numerical surface and a soap lamina. $ER_{F\%}$ is used in practice for assessing the convergence of solutions obtained from a

[i] ER refers to the maximum value of the components of the out-of-balance forces.
[ii] The pseudo cable force is given by equation(3.7), Chapter 3, Section 3.3.3.
[iii] The force per unit with is given by equation (3.5), Chapter 3 Section 3.3.3.

programme utilising Haug's numerical approach, (Chapter 2, Section 2.3.4 and Chapter 4 Section 4.5). Convergence is deemed to have occurred if [iv] $ER_{F\%} \leq 0.1$.

4.3 Verification of Numerical Results using Mathematical Solutions.

Case 4.3.1 'BOX' Surface (Examples 4.1 and 4.2).

Whether it be stable or unstable, a minimal surface always possesses a geometry where the mean of the principal curvature at every point is equal to zero; as given by equation 2.2 (Chapter 2, Section 2.2). Figure 4-1(a) shows the principal curvatures passing through the centre of the numerical surface described previously in Section 3.3.5. (This surface is referred to as example 4.1 from this point onwards). When viewed in plan, it is apparent that the principal curvatures satisfy the requirement of being aligned perpendicular to each other, as shown in Figure 4-1 (b). However, further analysis of the results indicates that the centre of the surface, through which the principal curvatures pass, is located at the point with co-ordinates 5, 5, 4.923. This observation implies that the principal curvatures do not possess the same radii of curvature; the condition of a zero mean curvature is satisfied within a margin of error. Ideally, the central node of the surface, node number 147 (Figure 4-1 (a)), would be positioned at a vertical height of 5 m i.e. the global Z co-ordinate of the central node of the numerical surface is in error by -1.4%. The result is best described in Figure 4-2, where section AA' has been inverted and plotted against section BB'. Although it could be concluded that the geometry obtained does not represent exactly that of a stable minimal surface, the results are good when taking into account the excessively crude nature of the initial surface used in the form-finding analysis; the initial surface consisting of three flat planes.

[iv] From collaborative investigations with SL, it transpired that this was the criterion of convergence adopted by the firm in the computational analysis of light-weight tension structures. An example of a structure constructed by the firm is given in (Chapter 2, Section 2.5.1).

(a)

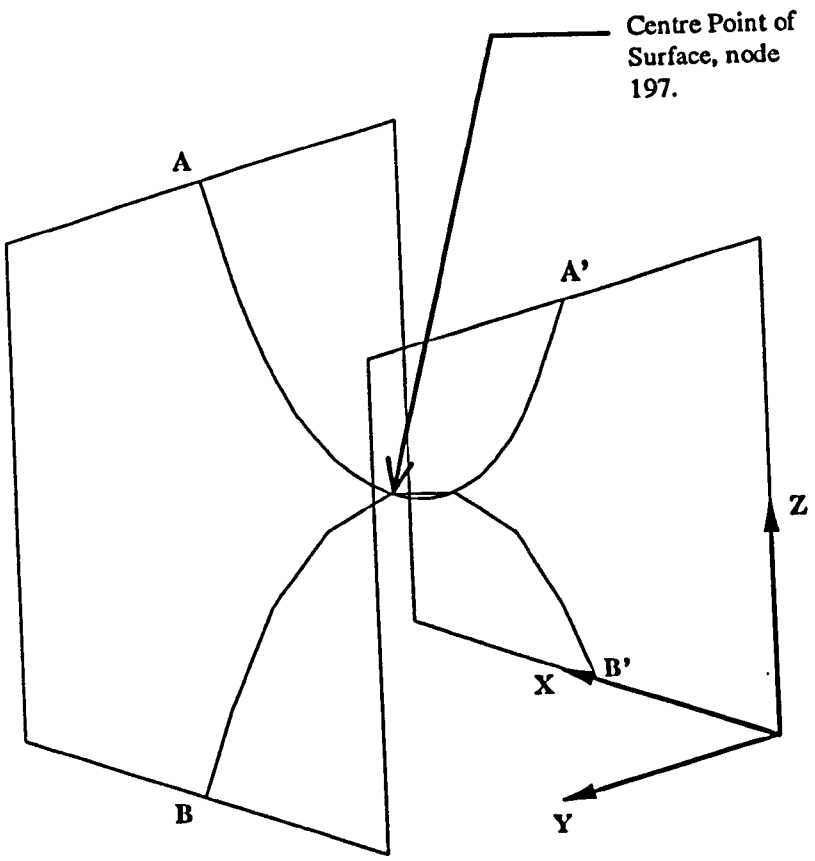

(b)

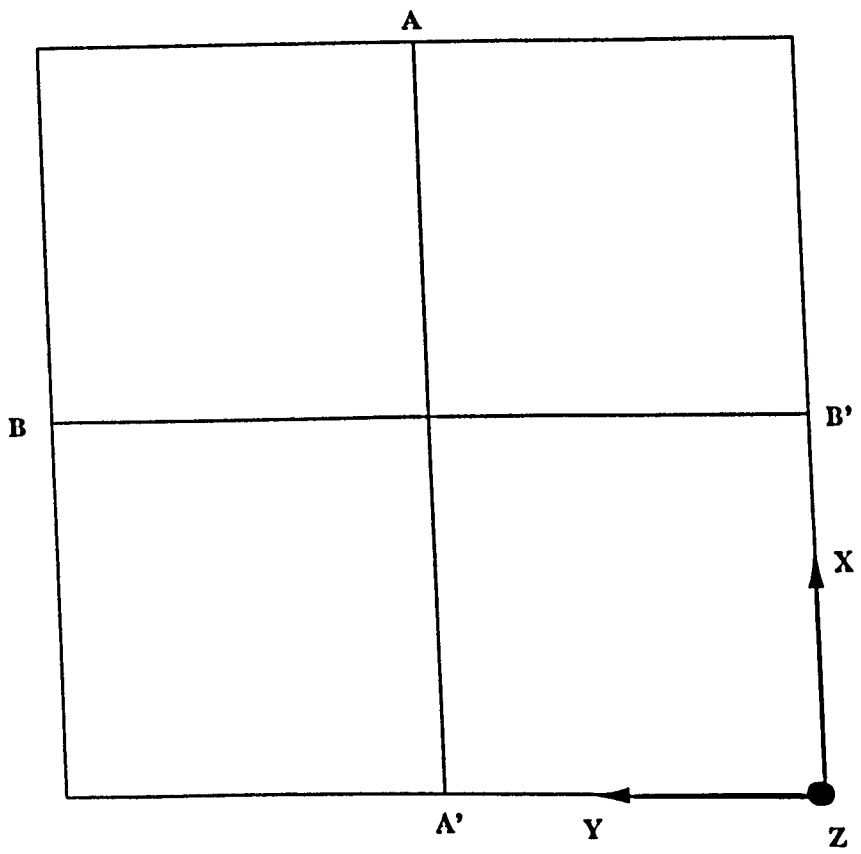

Figure 4-1 Principal Curvature of the Surface Presented in Example 4.1. (a) Perspective view. (b) Plan View.

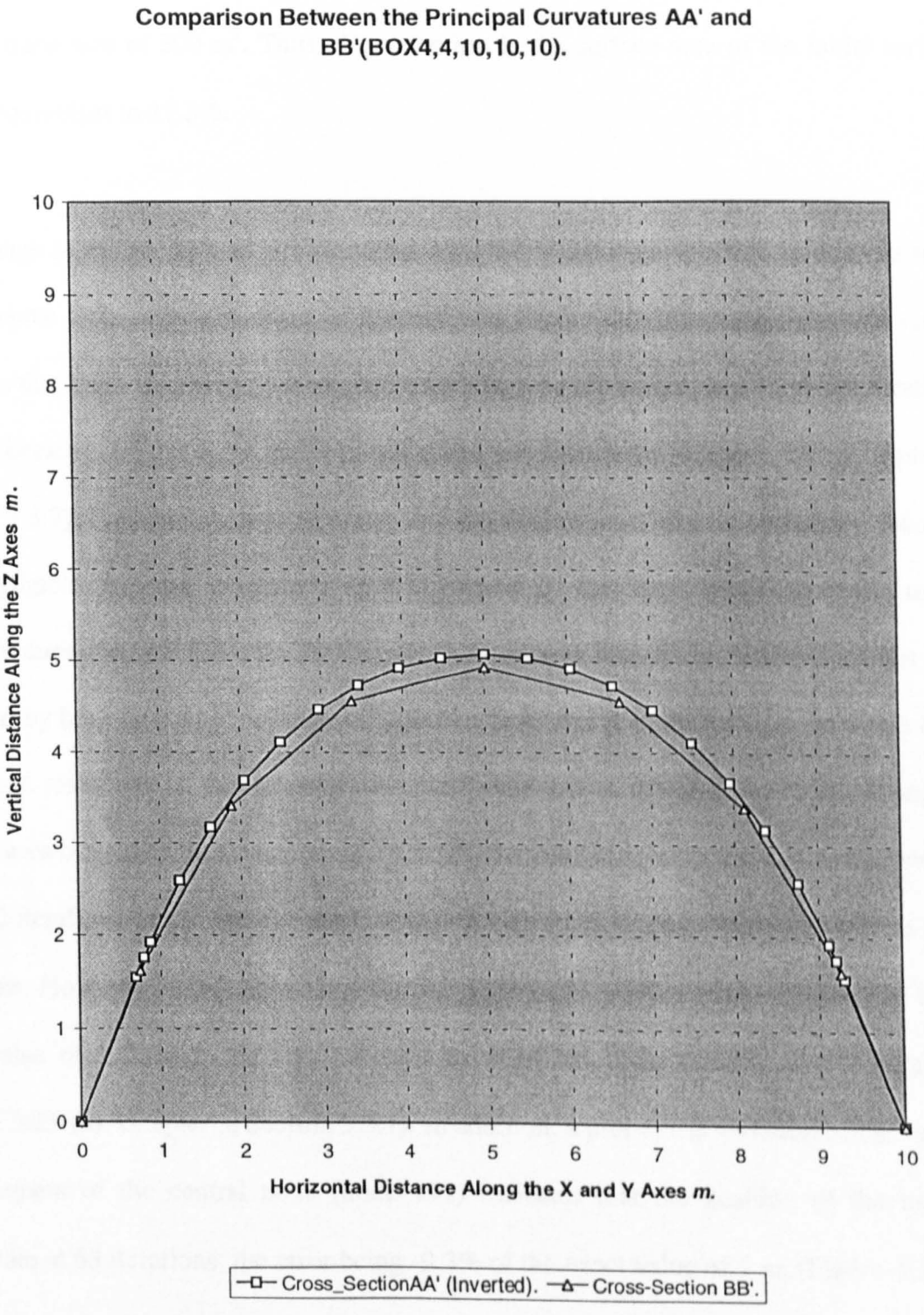

Figure 4-2 Principal Curvatures of the Surface Presented in Example 4.1.

Using Heron's formula, Appendix 4A.1, the total surface area of the faceted surface described in example 4.1 is calculated. The surface area is equal to 248 m^2, or 82.7% of the initial surface area of 300 m^2. Thus, the reduction in the surface area of the initial surface, $A_{\%}$, is equivalent to 17.3%.

The change in surface area of the structure depicted in example 4.1, during analysis using the Dynamic Relaxation algorithm, is illustrated in Figure 4-3 (a). Analysis of the results indicates that there is a rapid decrease in the surface area for the interval up to 63 iterations. This is because of the large scale out-of-plane displacements of stage (1) (Chapter 3, Section 3.3.7). Further iterations illustrate that the surface area remains essentially constant. The negligible variation in surface area is caused by the in-plane deformations of the elements during stages (2) and (3) (Chapter 3, Section 3.3.7). This phenomenon has been recorded by both Gosling[4.8] and Kneen[4.6]. Kneen describes it as the process by which those nodes not restrained at the boundaries move freely within the surface. If the change in surface area is used as the convergence criterion, the negligible variation in area between 63 and 850 iterations would seem to suggest that the optimum convergence point occurs at 63 iterations. However, at this point, it is clear that the surface is not in equilibrium due to the large value of 1.1E+3kN for ER; the final value of ER being 0.5 kN at 850 iterations, (Figure 3-29 (a), Chapter 3, Section 3.3.7). In addition, a plot of the variation of the vertical displacement of the central node (node 197) indicates that the position of the node is inaccurate at 63 iterations; the error being -9.3% of the exact value of 5 m, (Figure 4-3 (b)). Thus, the in-plane deformations can be considered to be significant in that they do affect the overall geometry of the surface, and further iterations are required to reduce the in-plane equilibrium and improve the surface geometry.

(a)

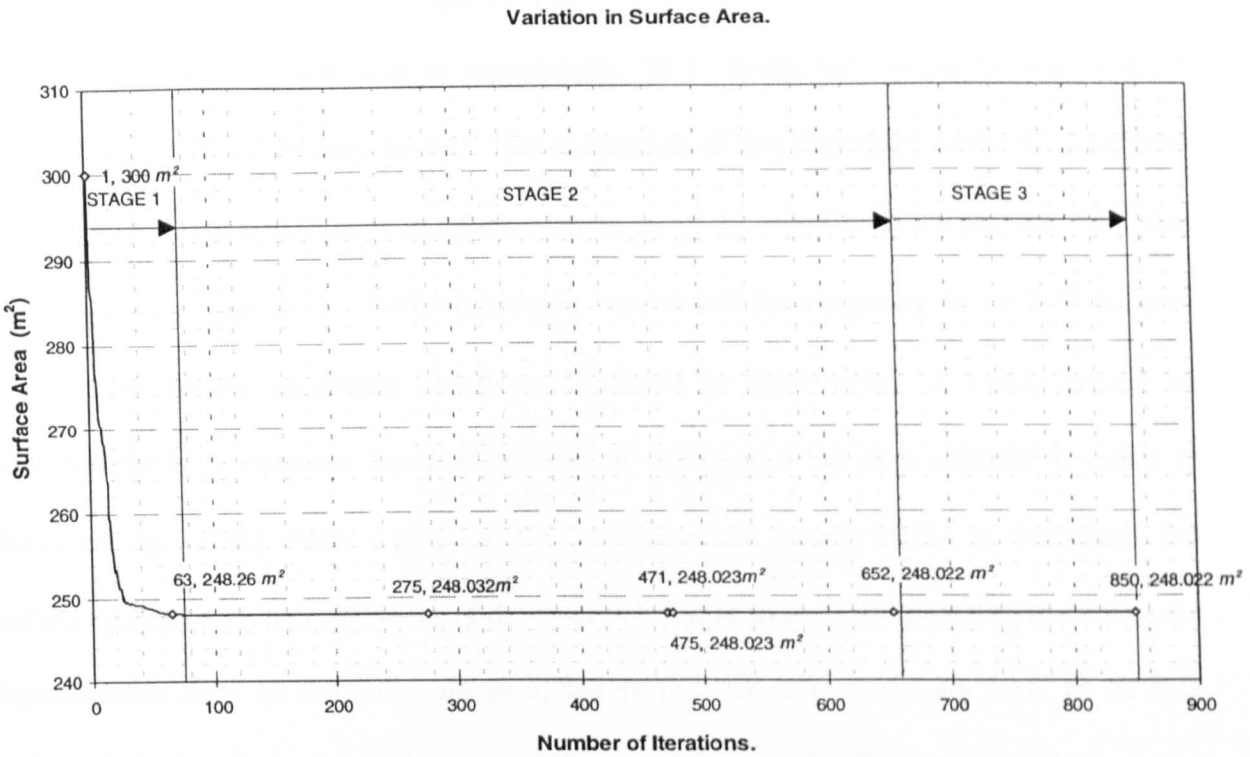

(b)

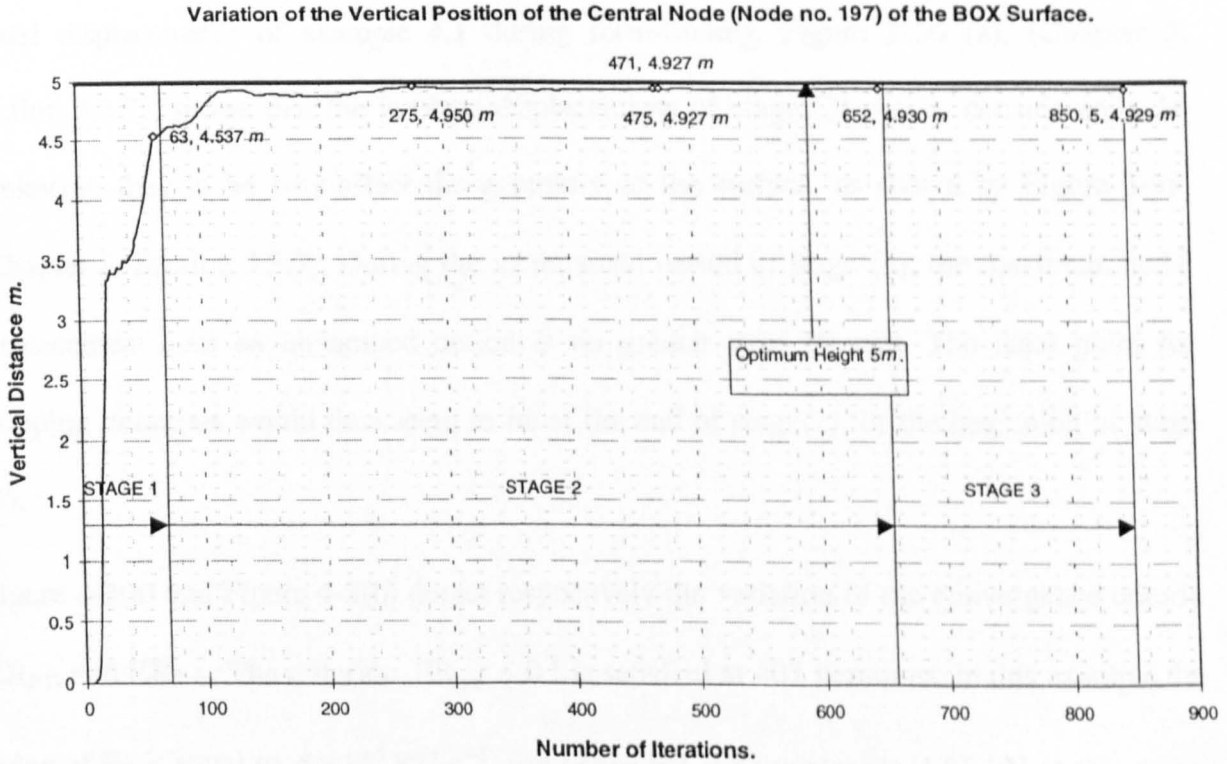

Figure 4-3 Variation of (a) Surface Area of the Surface Presented in Example 4.1 (b) Vertical Height of the Central node of the Surface Presented in Example 4.1, node number 197.

If a surface is unstable, then according to Bernoulli's principle of virtual work (Chapter 2, Section 2.2), the application of a displacement will cause the large scale displacement of the system and its irrecoverable loss of equilibrium. (In form-finding the displacements are a product of the out-of-balance forces). The magnitude of the maximum nodal displacement between successive iterations is an arbitrary measure of the stability of the surface, as it also depends on the values of the fictitious lumped masses and the weighting factor λ (λ is equal to unity for all the numerical solutions described in this thesis). A better means of measurement is to consider the displacement of the system between successive peaks in kinetic energy (K.E.). After a peak in K.E., the potential energy (P.E.) is minimised, the surface updated and the movement of the system brought to rest. By assessing the effect the displacements have on the deformation of the surface from its stationary state to its next peak in K.E., i.e. the undamped interval (Chapter 3 Section 3.3.7), it is possible to assess the P.E. and hence the stability of the surface. Examination of the trace of the maximum nodal displacements of example 4.1 during form-finding, Figure 3-36 (a), (Chapter 3, section 3.3.7), shows that the in-plane displacements of stage (3) can be considered to be irrelevant; they in no way affect the geometry of the surface, as shown by Figure 3-39, (Chapter 3, Section 3.3.7). During the incremental period of stage (3), the maximum nodal displacement over an undamped period is no greater than 30 mm. The ideal point for stopping iterations would thus seem to be at the end of stage(2), or the beginning of stage (3).

Figure 4-3(a) and Figure 4-3(b) depict respectively the variation of the convergence criteria $ER_{F\%}$ and $ER_{T\%}$. The criterion $ER_{F\%} \leq 0.1$ is satisfied at 407 iterations; in this example the value of F_K is equal to $5\times10^{3}\text{KNm}^{-1}$ and hence ER is equivalent to 4.85 kN at this point, (Figure 3-29, Chapter 3 Section 3.3.7). In contrast, $ER_{T\%} \leq 0.025$ is satisfied at 475

iterations for the last undamped interval of the stage (2) incremental period. Thus, it can be said that at 475 iterations, both the aforementioned criteria are satisfied.

(a)

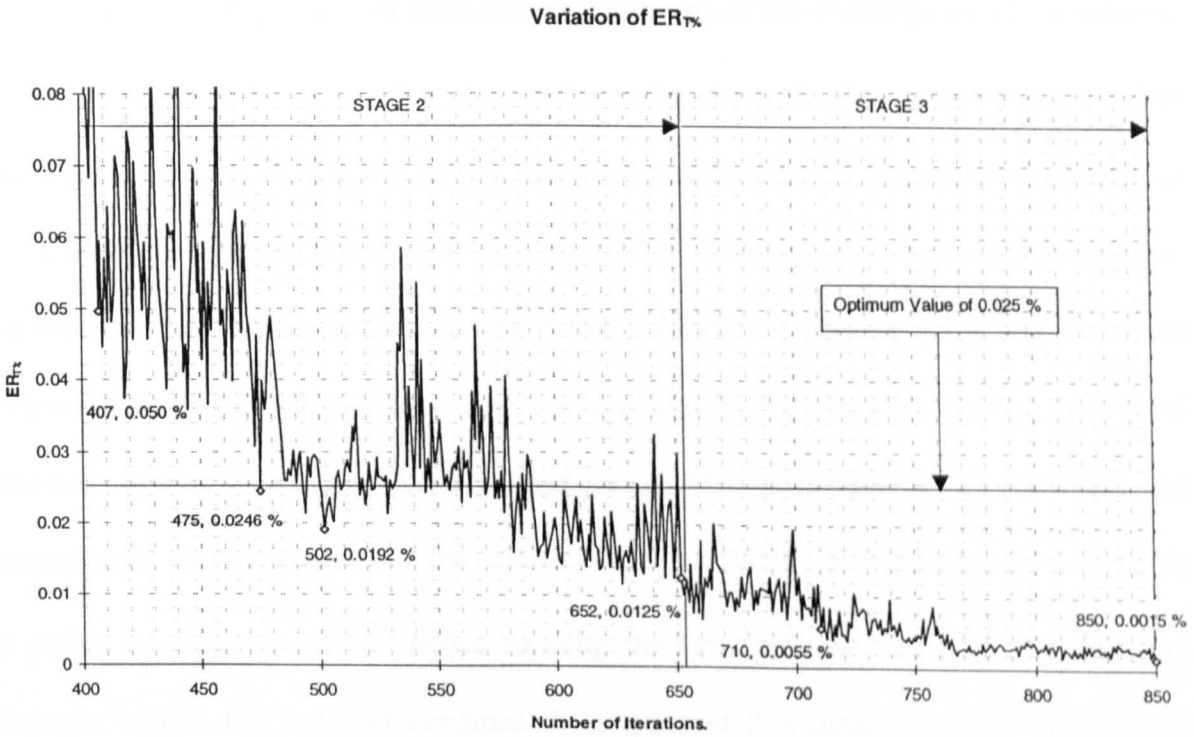

(b)

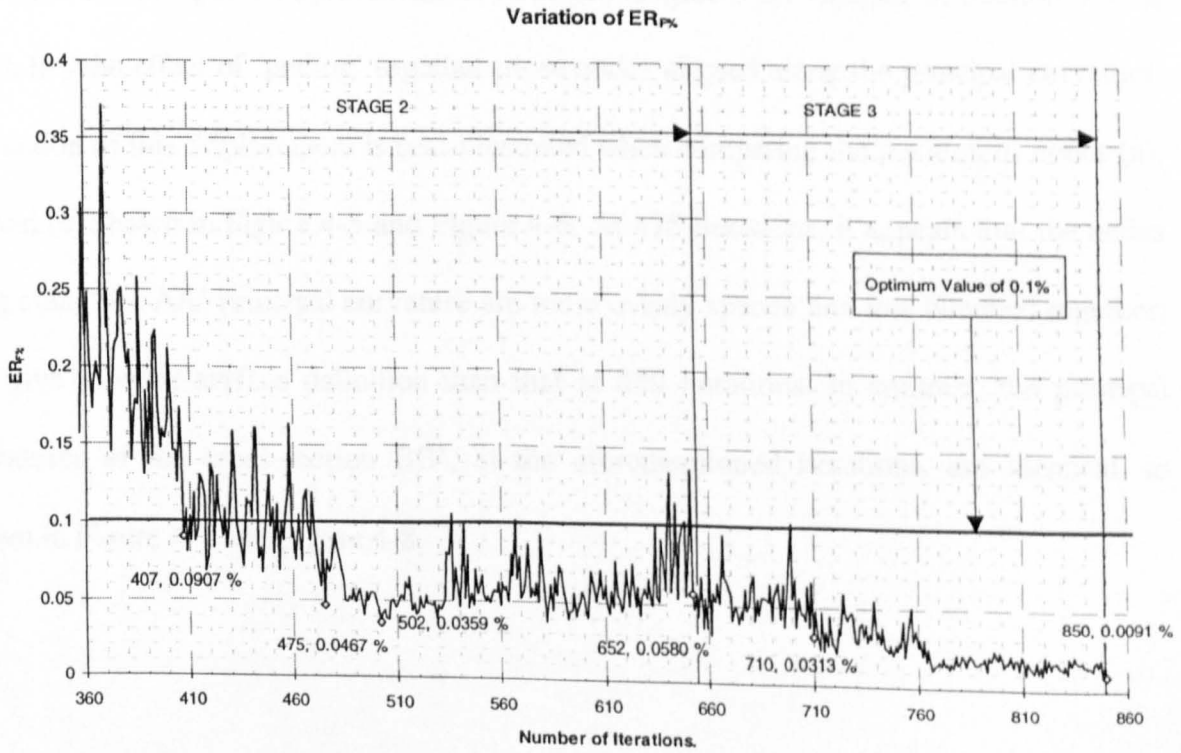

Figure 4-4 Variation of (a) $ER_{F\%}$ (b) $ER_{T\%}$ (Example 4.1).

The value of 0.0125 for $ER_{T\%}$ represents the end of stage (2), or the beginning of stage (3). It is known that the surface remains unaltered after this point; the geometry conforms to that of example 4.1 and the principal curvatures of Figure 4-2. Hence, it can be concluded that the criterion $ER_{T\%} \leq 0.0125$ is an adequate measure of the convergence of the solution for this example. It is known that the maximum **in-plane displacement** of the surface during the undamped interval 471 to 652 iterations is equivalent to 400 mm for node 82, as shown in Figure 3-29 (b) (Chapter 3, Section 3.3.7). Although this displacement might at first appear to be excessively high, it was stated in Chapter 3 Section 3.3.7, and illustrated in Figure 3-34, that the displacement does not appear to be significant in altering the overall geometry of the surface during the undamped period. The verification of this statement, and an assessment of the accuracy of the criterion $ER_{T\%} \leq 0.025$, is completed by comparing the actual co-ordinates of the nodes forming the principal curvatures of the structure (Example 4.1) at 475 and 850 iterations. It is apparent that there is a slight discrepancy between the positions of those nodes lying along the AA' principal curvature. This is due to the direction of in-plane displacement of node 82, (Figure 3-34 Chapter 3, Section 3.3.7), which has the effect of 'pulling' together those nodes aligned along the principal curvature. The action of this displacement is best illustrated when comparing the position of nodes (a), (b) and (c) shown in Figure 4-5 and Figure 4-6. At 475 iterations, it appears that the nodes lying along the AA' principal curvature are more evenly spaced and less bunched together, and give a better surface definition than that at 850 iterations. In contrast, the principal curvatures of the cross-section BB', at the aforementioned iterations, are identical, as shown in Figure 4-7 and Figure 4-8.

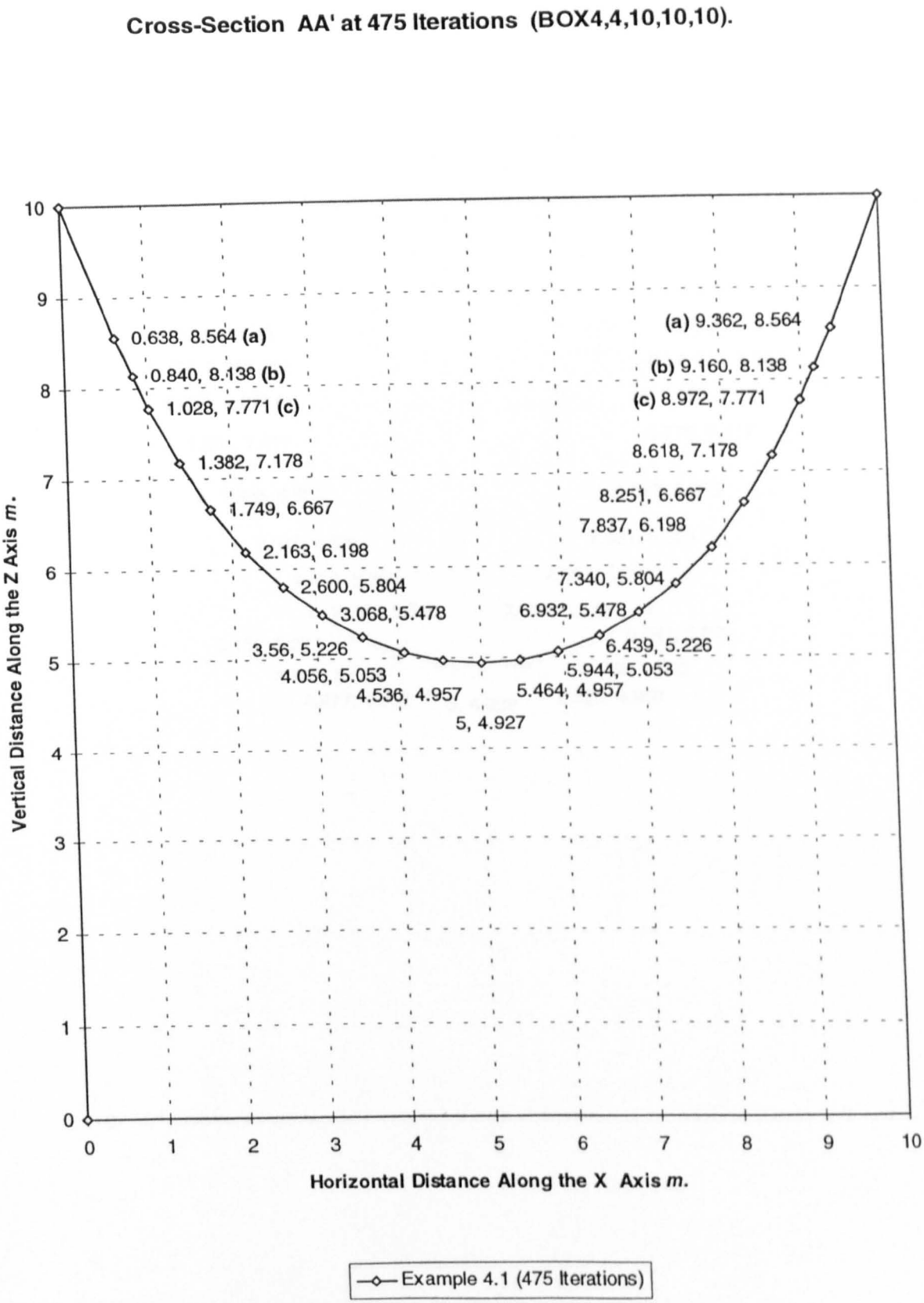

Figure 4-5 Principal Curvature AA' of the Surface Presented in Example 4.1 (475 Iterations).

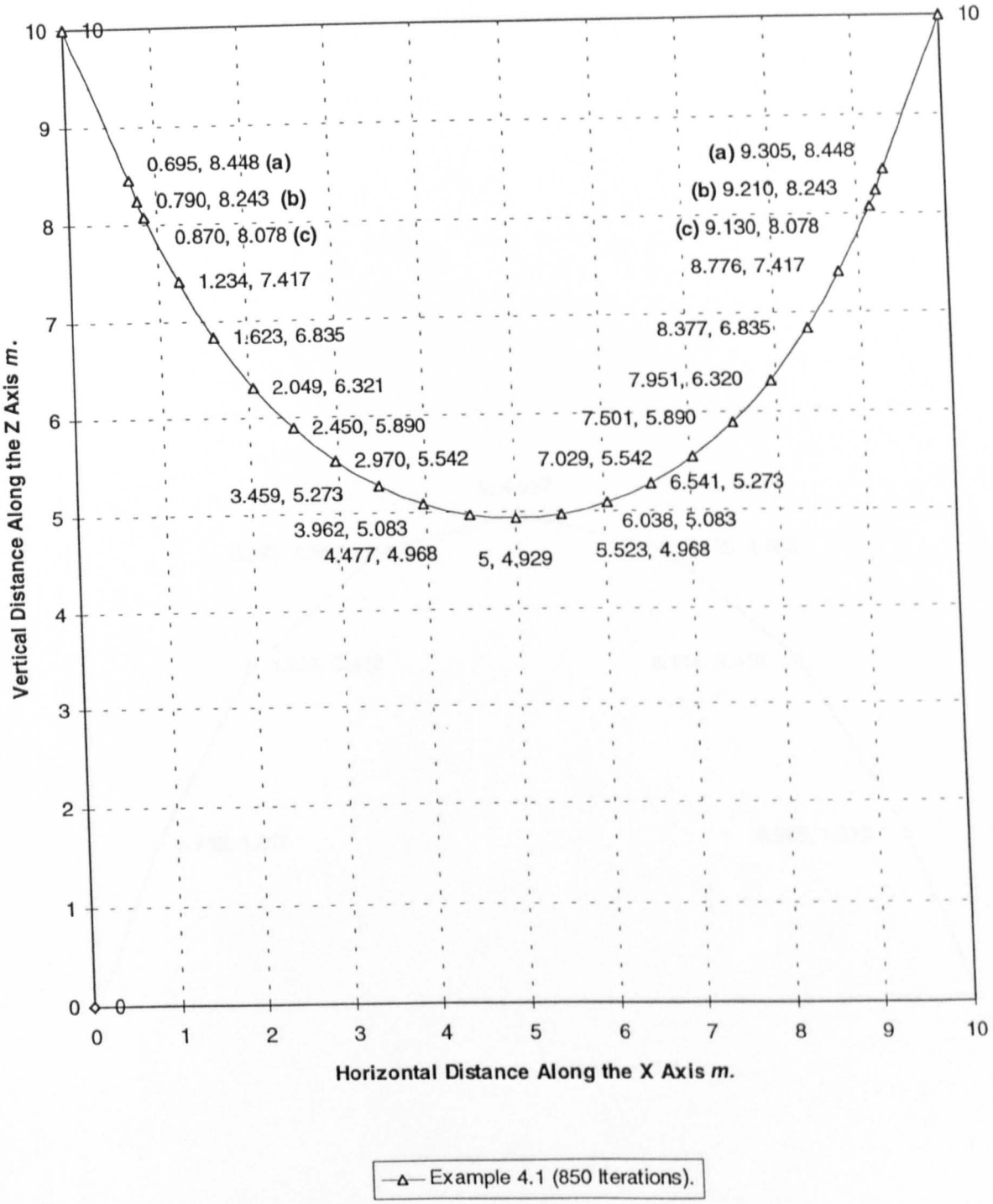

Figure 4-6 Principal Curvature AA' of the Surface Presented in Example 4.1 (850 Iterations).

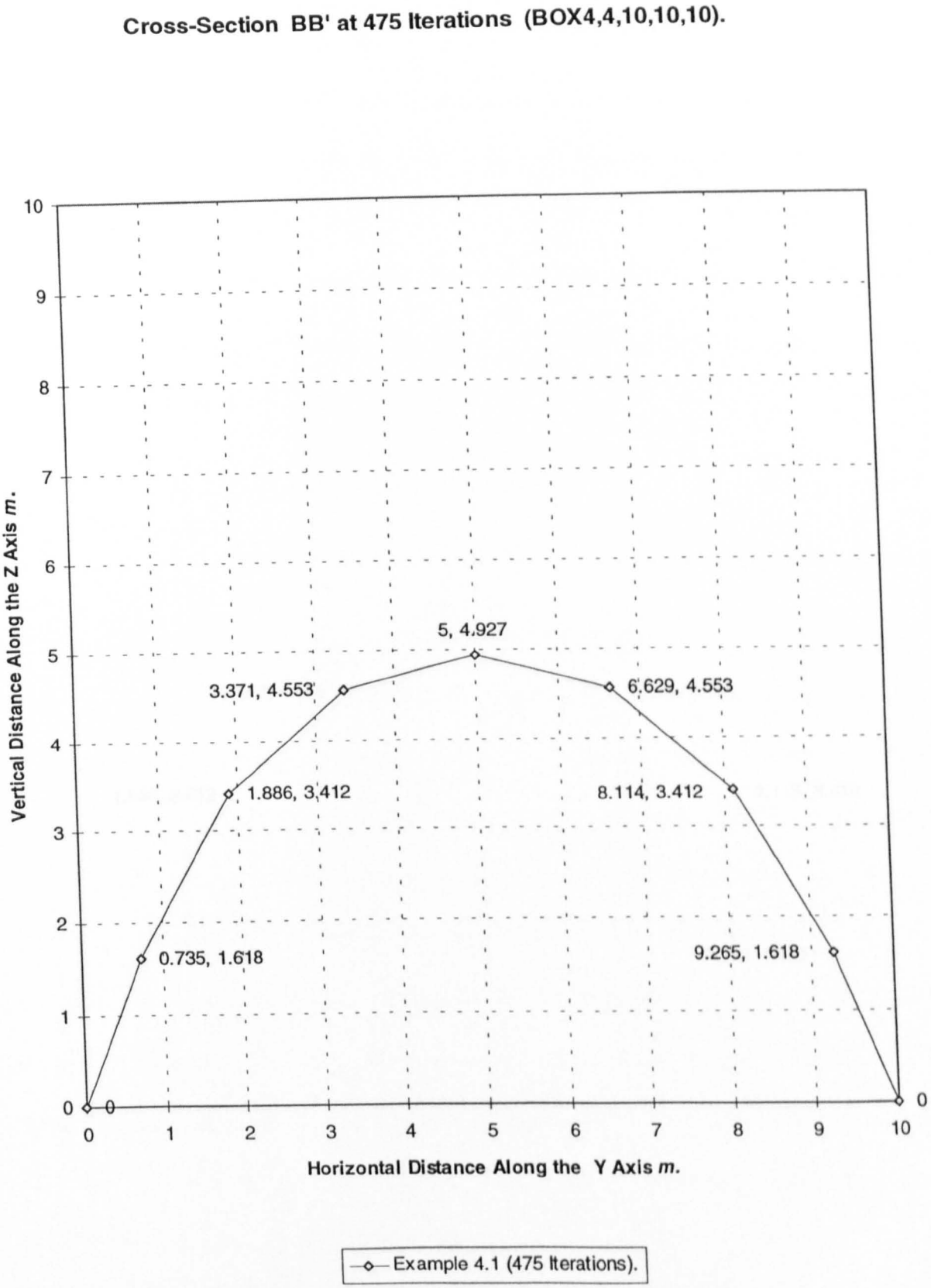

Figure 4-7 Principal Curvature BB' of the Surface Presented in Example 4.1 (475 Iterations).

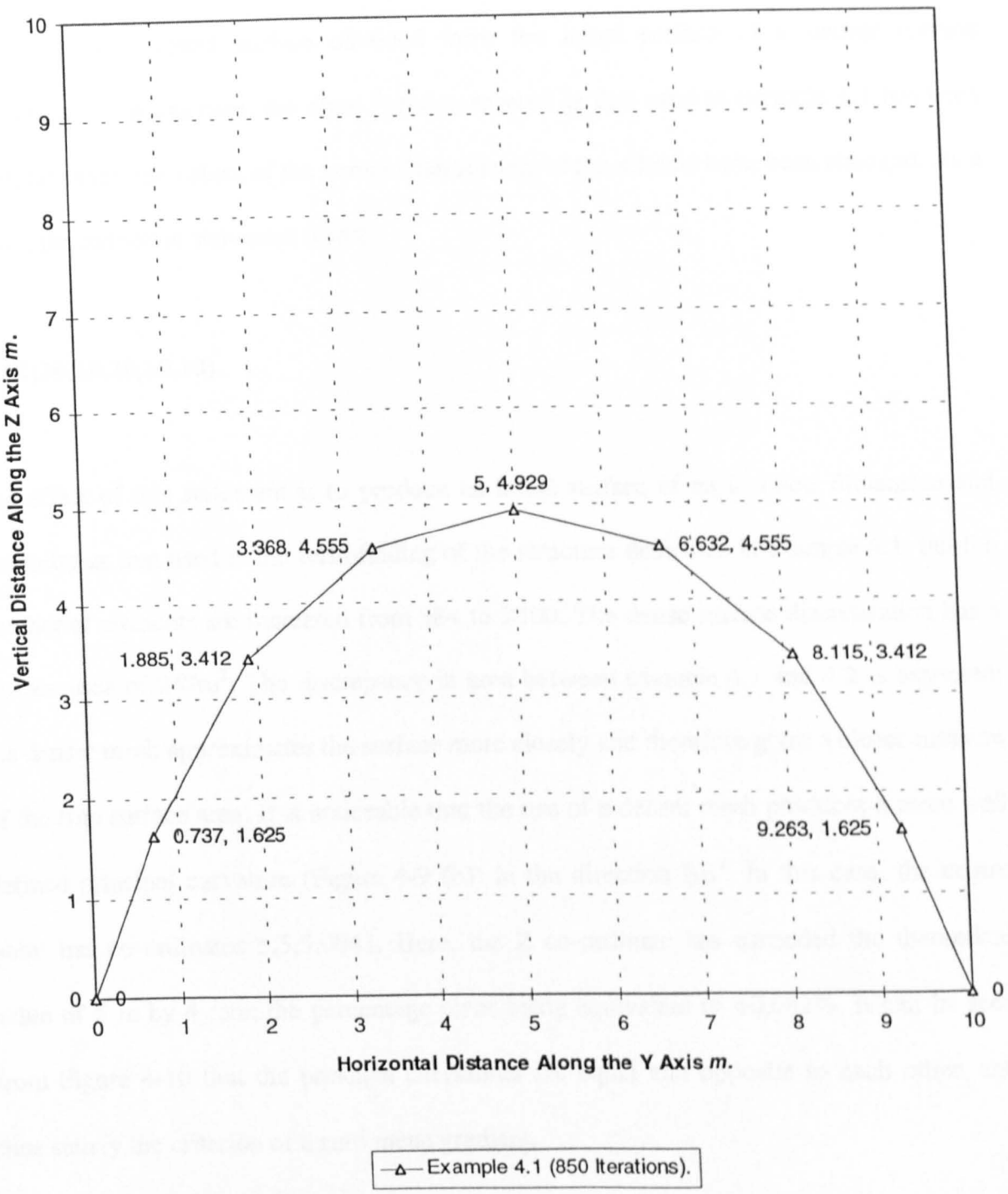

Figure 4-8 Principal Curvature BB' of the Surface Presented in Example 4.1 (850 Iterations).

The inaccuracy of the surface geometry in example 4.1 is not a product of an incorrectly formulated algorithm. Instead, it is due to the number of elements used in the surface discretisation. It is shown in the following example, example 4.2, how the accuracy of the solution may be improved quite easily through the use of a Formian scheme. Figure 4-9 (a) shows the form-found surface obtained from the initial surface of a denser surface discretisation. In this case, the same Formian scheme as that used in example 4.1 has been used; however, the values of the nominal parameters of the scheme have been changed. As a result, the induction statement reads:

BOX(10,10,10,10,10).

The effect of this statement is to produce an initial surface of an identical dimension and geometry as that used in the form-finding of the structure described in example 4.1, but the number of elements are increased from 384 to 2400. The dense surface discretisation has a surface area of 247m^2. The discrepancy in area between example 4.1 and 4.2 is expected; the denser mesh approximates the surface more closely and therefore gives a closer measure of the true surface area. It is noticeable that the use of a denser mesh produces a more well defined principal curvature (Figure 4-9 (b)) in the direction BB'. In this case, the centre point has co-ordinates 5,5,5.0041. Here, the Z co-ordinate has exceeded the theoretical value of 5 m by 4 mm; the percentage error being equivalent to +0.082%. It can be seen from Figure 4-10 that the principal curvatures are equal and opposite to each other, and thus satisfy the criterion of a zero mean gradient.

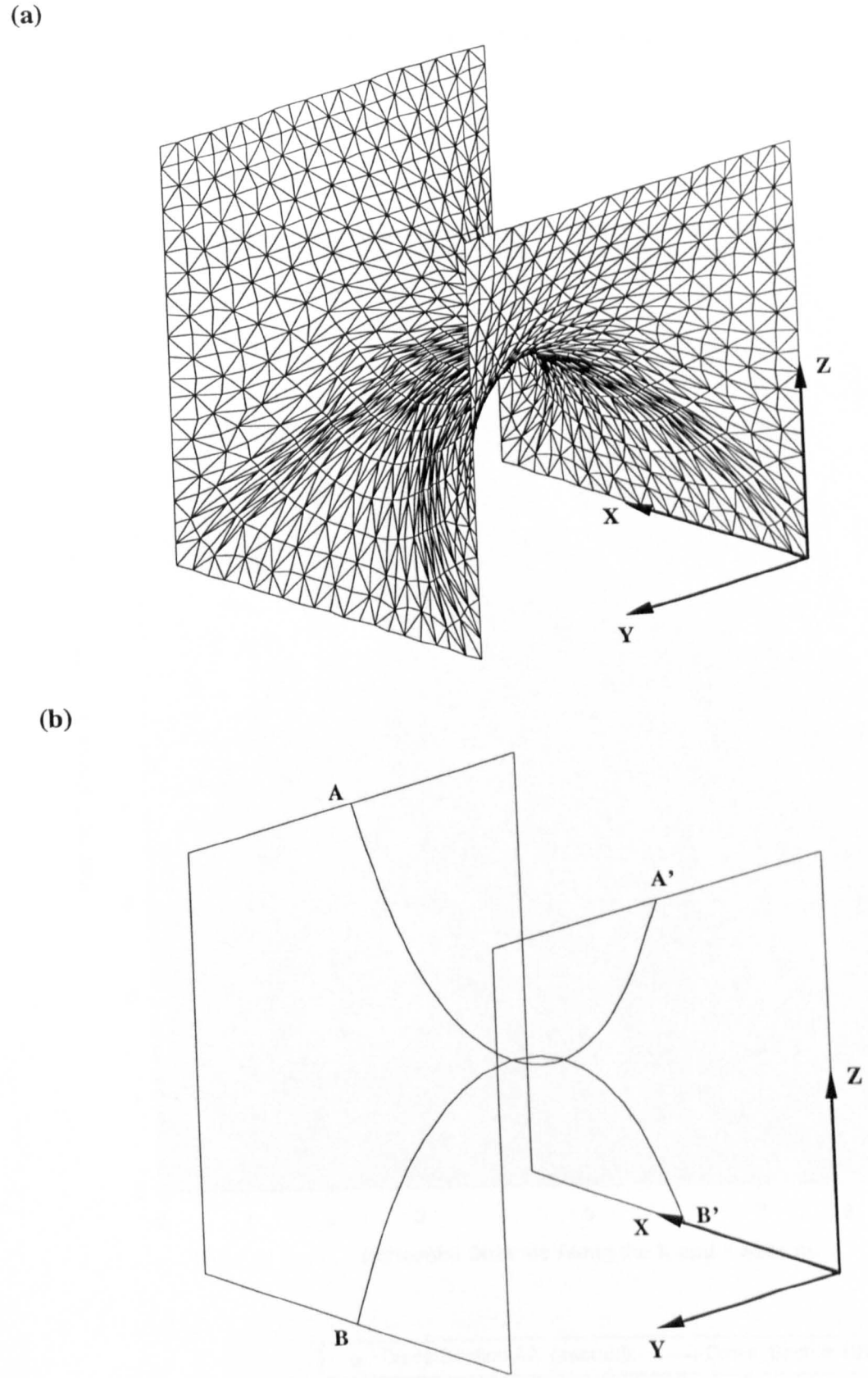

Figure 4-9 Example 4.2 (a) Form-Found Surface. (b) Principal Curvatures.

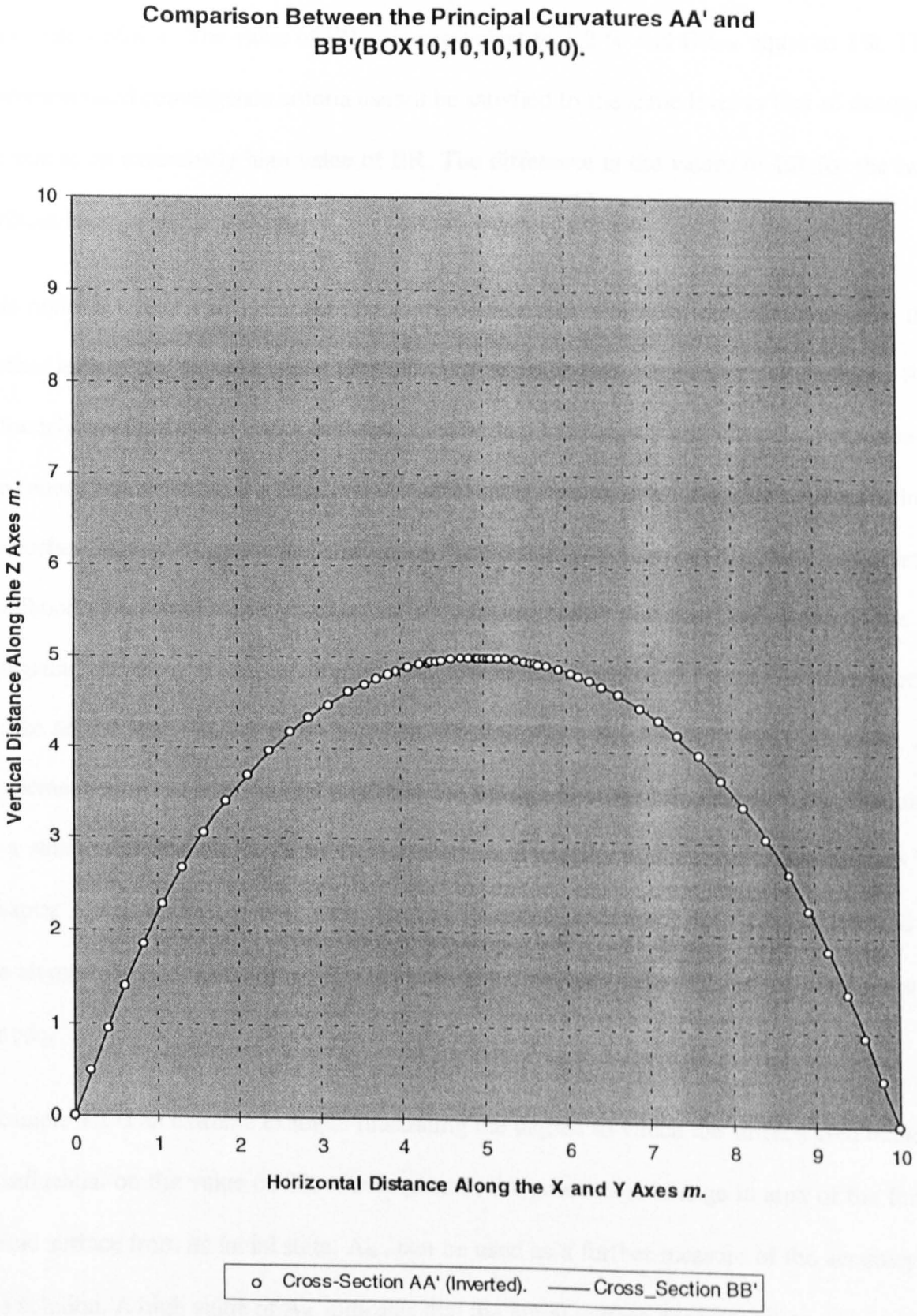

Figure 4-10 Principal Curvatures of the Surface Presented in Example 4.2.

The numerical solution has been obtained after 1000 iterations; the convergence criterion being $ER \leq 50KN$. The value of $ER_{T\%}$ is equivalent to 1.2 % and $ER_{F\%}$ equal to 1%. The aforementioned convergence criteria cannot be satisfied to the same level as that of example 4.1 due to an excessively high value of ER. The difference in the values of ER for the two surfaces is explained as follows:

It is noticeable that during form-finding the surface area will decrease. Consequently, the surface area of the elements must also reduce through the contraction of the elements. For extremely poorly defined initial surfaces, such as in examples 4.1 and 4.2., the surface area can reduce dramatically. If a large number of elements are used in the surface discretisation, the surface area of the individual elements will be small, and consequently, there is a greater likelihood of some elements contracting to such an extent that they are on the verge of collapsing and form an almost straight line (The effect is shown in Figure 4-9 (a) where it can be seen that the elements are bunched together along the BB' principal curvature). As an element contracts, the internal angles of the triangle become increasingly acute, resulting in a small value for the TAN of the internal angle and, in accordance to equation (3.7), Chapter 3, Section 3.3, a large value for the "pseudo" cable force acting along the side of the element. Hence, elements of this kind introduce onerous values for the residual force at a node.

Example 4.2 is an extreme example illustrating the degree to which the surface area reduces is influential on the value of ER. Consequently, the percentage change in area of the form-found surface from its initial state, $A_{\%}$, can be used as a further measure of the accuracy of the solution. A high value of $A_{\%}$ indicates that the initial surface has undergone a large scale deformation; the solution is likely to have an excessively high value of ER due to the poor aspect of some elements.

Case 4.3.2 Catenoid Surface - Stable Equilibrium (Examples 4.3 and 4.4).

The analytical solution to a catenoid may be obtained from the Euler-Lagrange equation. The equation describes the profile of a catenoid and is given by[2.9]:

$$r = a\cosh\frac{l}{a} \tag{4.1}$$

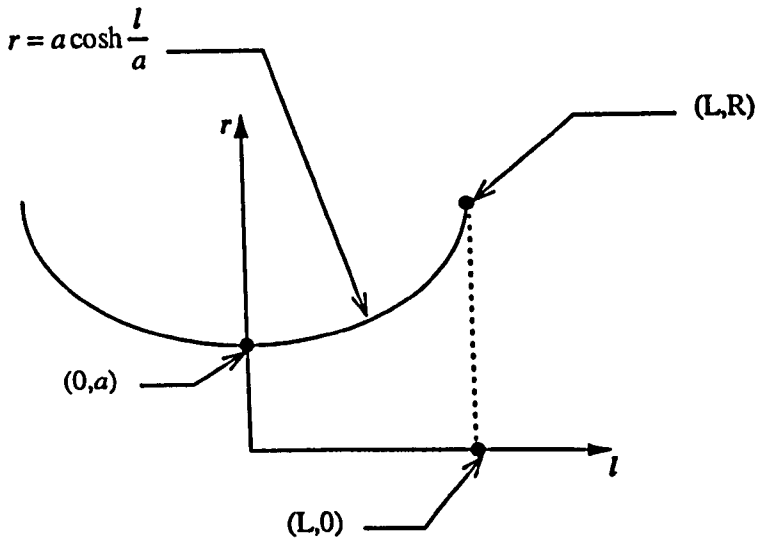

Figure 4-11 Cross-Section Profile of a Catenoid.

The parameters r and l are variables which relate to values of the cross-section radius of the catenoid and the height of the catenoid from its centre. Parameters a, R and L are constants representing the radius of the catenoid at its mid-point, the radius of the boundary rings and the total distance from the mid-point of the catenoid to the boundary. These parameters are fully defined in Figure 4-11. Equation (4.1) cannot be solved directly for a. The value of the constant a is found using a suitable iterative numerical approach, whereby various values of a are substituted into equation 4.1, until a gives the required boundary radius R for a known length L.

For the case of a catenoid of a height equal to the radius of its boundaries, the numerically found value of a is given by:

$$a = 0.848 \times R \qquad (4.2)$$

Using equations (4.1) and (4.2), the cross-section radius r for a catenoid possessing a boundary ring radius, R, of 40 m and a height, 2L, of 40 m are calculated for various values of l. The values of r, obtained from equation (4.1), are referred to as the "theoretical values", and are recorded in Table 4-2. The scheme[v],

CATENOID(24,10,40,40)

is used for the generation of the initial surface described in Figure 4-12 (a); the geometry of which is used in the form-finding of the surface described in example 4.3. The first parameter of the CATENOID scheme defines the number of 'm' divisions along the circumference of the catenoid, while the second parameter is responsible for dictating the number of divisions 'n' along the length of the catenoid. The remaining parameters define the height (2L) and radius (R) respectively, as shown in Figure 4-12 (a). The magnitude of the surface stress used in example 4.3 is $5 \times 10^6 \text{kNm}^{-2}$. Different values of the convergence criterion, ER and $ER_{T\%}$, as (defined in Section 4.2), are used for stopping iterations; this enables an assessment to be made concerning the influence of these values on the accuracy of the numerical solution and the number of iterations necessary for convergence (NIT). Further, the values of the criterion $ER_{F\%}$ are stated, and thereby give an additional indication of the convergence of the solution; the criterion is not used for stopping iterations.

[v] The formulation of the scheme is given in Appendix 4A.2

The "theoretical" surface area of a catenoid may be found from the equation:

$$A = 2\Pi a \left[L + \frac{a}{2} \sinh\left(\frac{2L}{a}\right) \right] \qquad (4.3)$$

the derivation of which is given in Appendix 4A.3. For the instance where L = 20 m and a = 33.92 m, equation (4.3) gives a "theoretical" value of 9584 m^2 for example 4.3. The "numerical" values of the surface area are presented in Table 4-1 . By examining the cross-section profile CC', shown in Figure 4-12 (b), a comparison between the "theoretical" cross-section profile and the cross section of the numerical model may be made. Table 4-2 gives the values for the vertical and horizontal co-ordinates of the numerical solution to the catenoid, while Figure 4-14 and Figure 4-15 show the plotting of these co-ordinates against the "theoretical" values of *r* and *l*. (It should be noted that the global Z axis is aligned in the direction of *l*, and the *X* axis in the direction of *r* Figure 4-12(b)).

Convergence Criterion.	Surface Area	NIT	$A_{\%}$	ER	$ER_{T\%}$	$ER_{F\%}$
$ER_{T\%} \leq 0.025$	9555 m^2	75	0.1	3.7 kN	1.5×10^{-2}	7×10^{-2}
$ER_{T\%} \leq 0.0125$	9555 m^2	78	0.1	2.2 kN	9×10^{-3}	4×10^{-2}
$ER \leq 0.1KN$	9555 m^2	187	0.1	8×10^{-2} kN	3×10^{-4}	1.6×10^{-3}
$ER \leq 0.001KN$	9555 m^2	335	0.1	9×10^{-4} kN	4×10^{-6}	1.8×10^{-5}

Table 4-1 Convergence Criteria used in Example 4.3.

Theoretical Values (R=40 m, L=20 m, a=33.92 m, Area = 9584 m^2)		Example 4.3 (NIT = 75).	Example 4.3 (NIT = 78).	Example 4.3 (NIT =187).	Example 4.3 (NIT = 335)
l	r	r	r	r	r
-20	40	40	40	40	40
-16	37.76	37.72	37.72	37.73	37.73
-12	36.04	36	36	36.00	36.00
-8	34.88	34.78	34.78	34.77	34.78
-4	34.16	34.05	34.05	34.05	34.05
0	33.92	33.81	33.81	33.81	33.81
4	34.16	34.05	34.05	34.05	34.05
8	34.88	34.78	34.78	34.77	34.78
12	36.04	36	36	36.00	36.00
16	37.76	37.72	37.72	37.73	37.73
20	40	40	40	40	40

Table 4-2 Theoretical and Numerical Results (Section CC' - Example 4.3).

The small value of $A_{\%}$ indicates that the initial surface, used in obtaining the numerical solution described in example 4.3, is an extremely close approximation of the form-found surface, and accounts for the small number of iterations necessary for convergence. (The geometry of the initial surface for the cross-section CC' is described in Figure 4-13). Furthermore, the accuracy of the initial surface allows for a far lower value of ER to be reached when compared to that used in example 4.2 and 4.1; the elements do not deform excessively and are of a good aspect. It is noticeable that there is little, or no difference in the geometry of the surface at 75 and 335 iterations; reducing the value of ER, and hence $ER_{T\%}$, does not significantly improve the surface definition. In addition, the surface area is in error by -0.3% of the "theoretical" value; the error may be improved by using a denser surface discretisation.

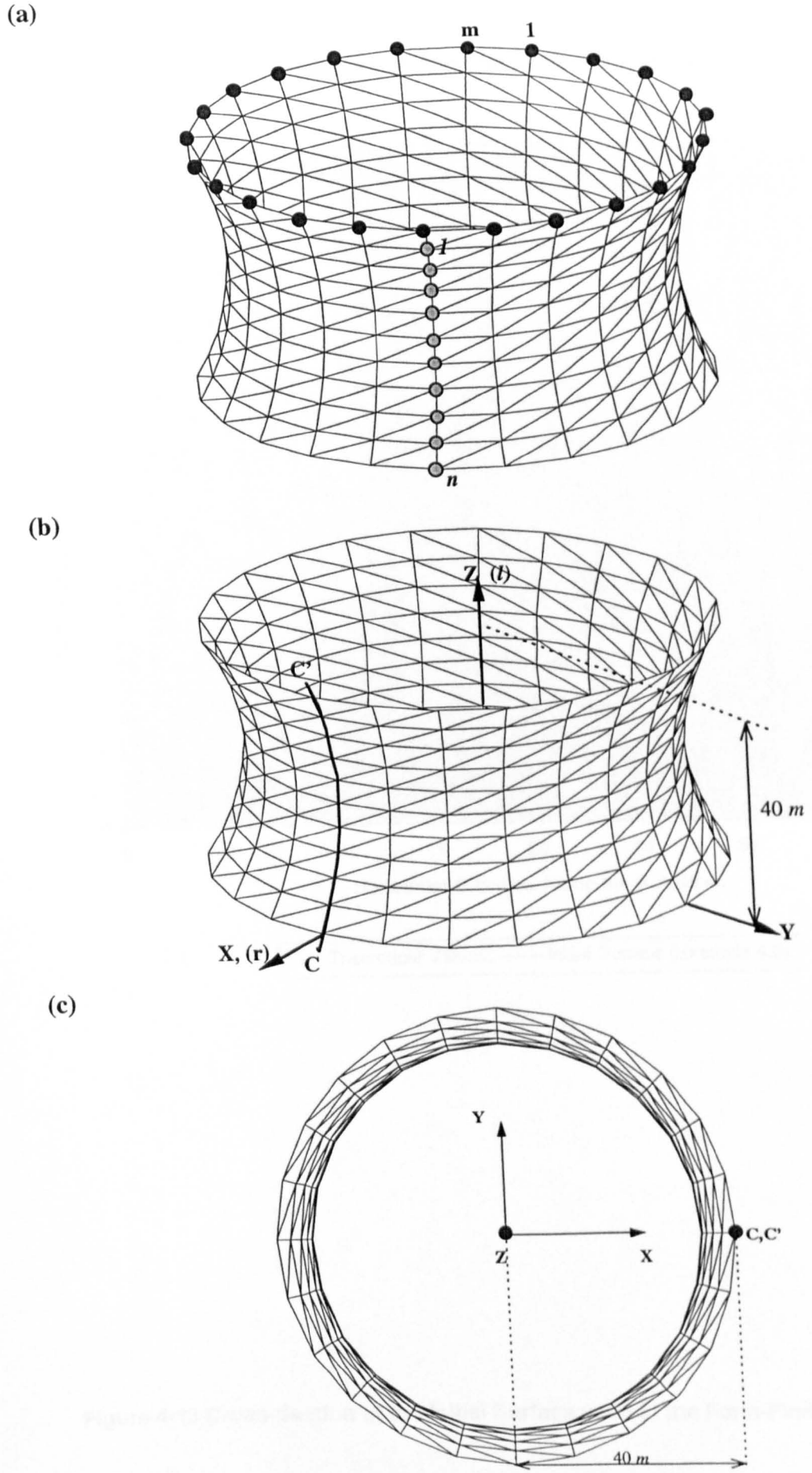

Figure 4-12 Example 4.3. (a) Initial Surface. (b) Form-Found Surface. (c) Form-Found Surface - Plan View (355 Iterations).

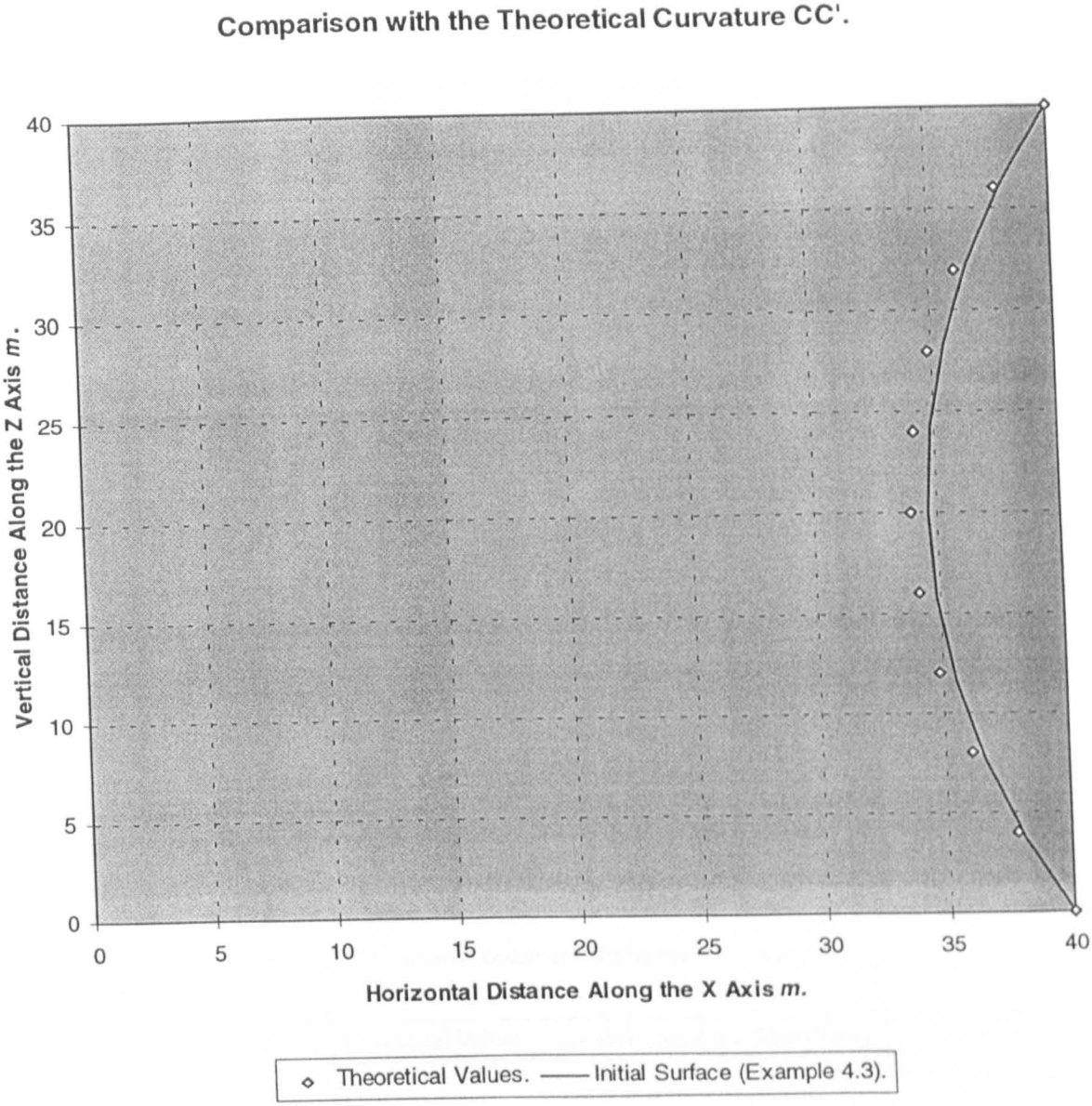

Figure 4-13 Cross-Section of the Initial Surface used in the Form-Finding of Example 4.3.

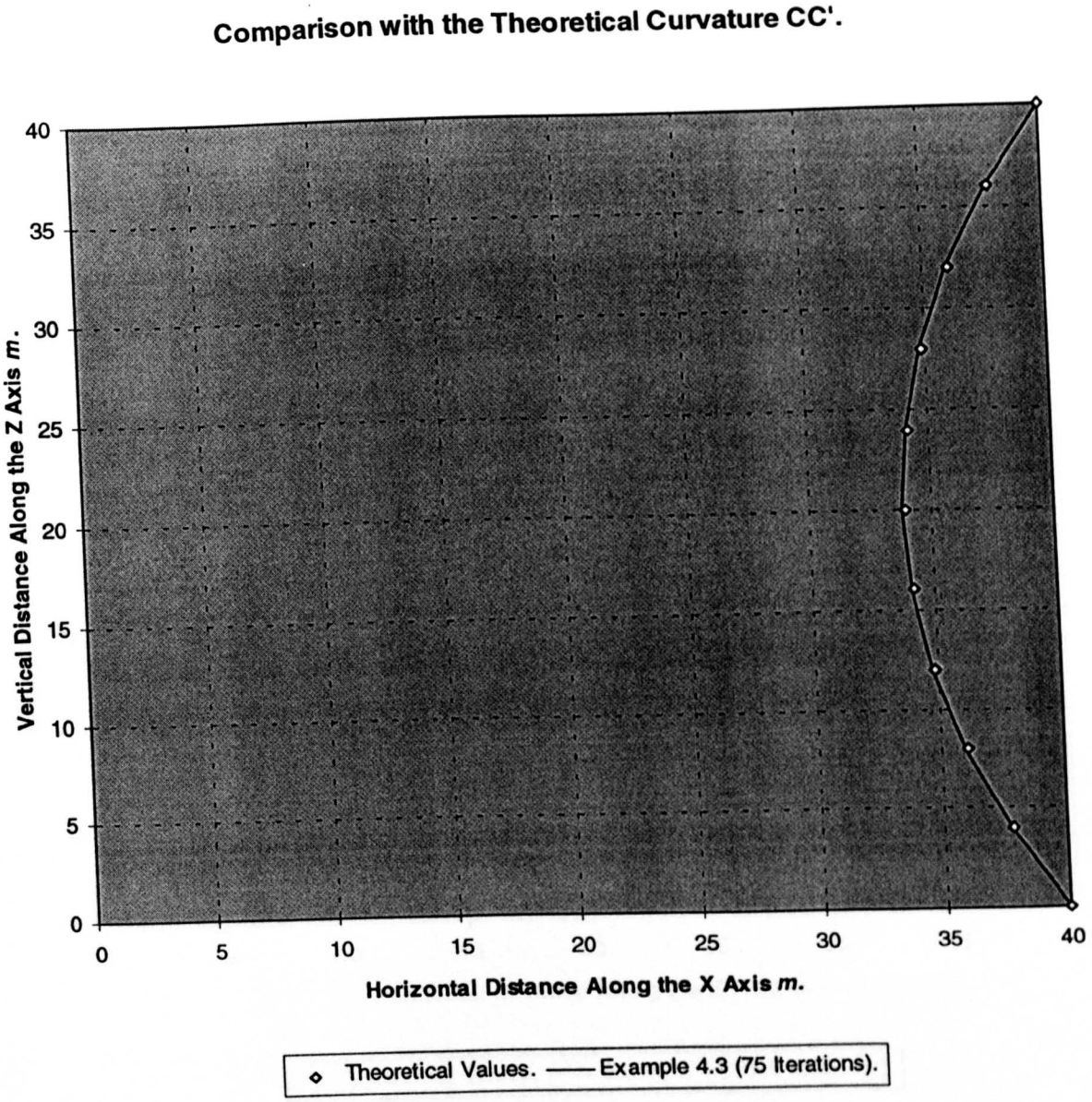

Figure 4-14 Theoretical and Numerical Solution to Example 4.3 (75 Iterations).

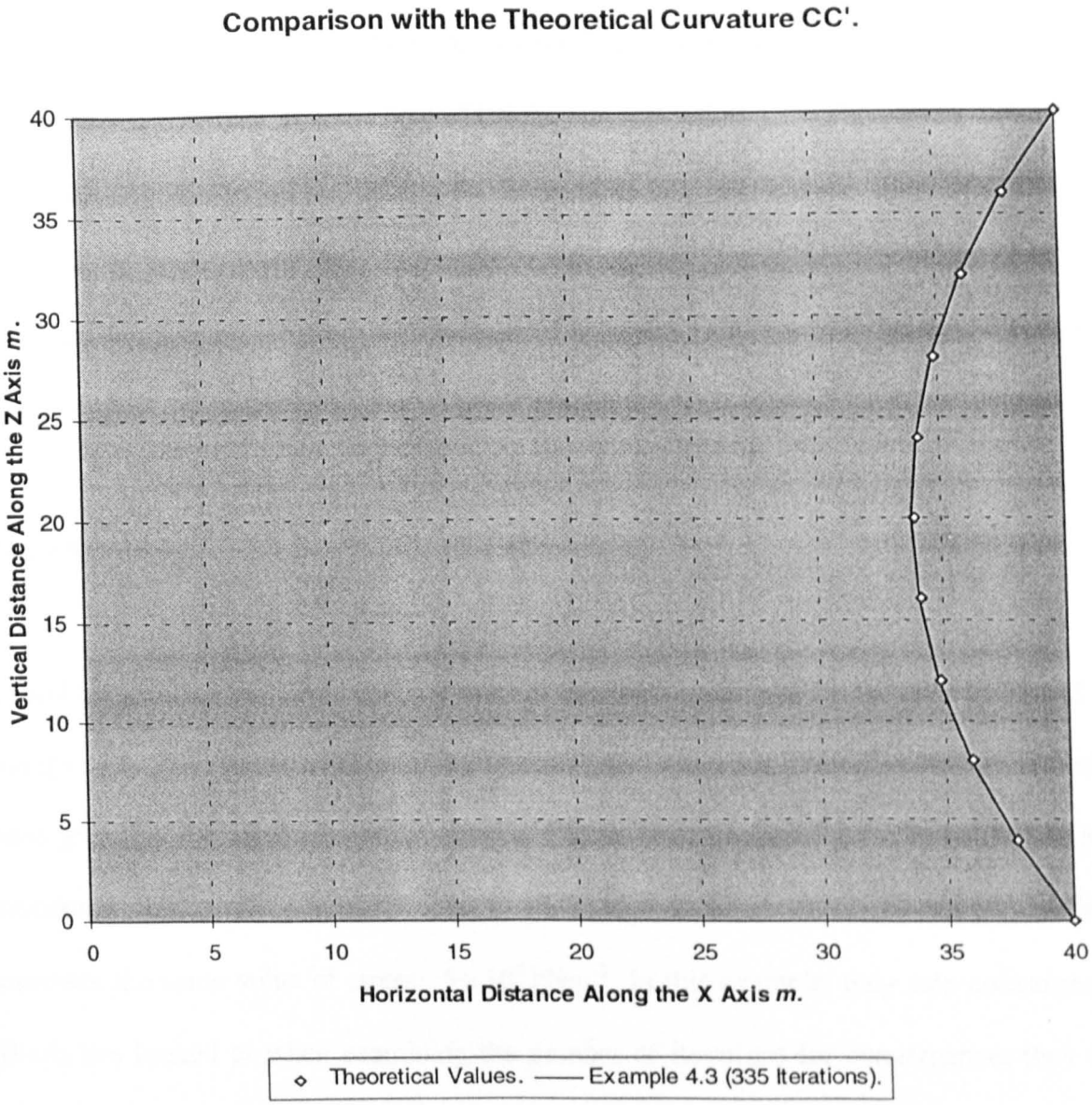

Figure 4-15 Theoretical and Numerical Solution to Example 4.3 (335 Iterations).

Results concerning a catenoid of a boundary ring radius (R) and height (2L) equal to unity, were published in a paper by Ishii & Suzuki[4.10] in 1991. In addition, Singer et al[4.11] documented the analysis of a catenoid of height 1 m and radius 1 m. The papers differed, in that Singer et al only published results concerning the surface area obtained from his numerical approach, while Ishii & Suzuki compared the accuracy of the geometry of his numerical solution with that of the "theoretical" solution. Ishii & Suzki's surface was based on an identical discretisation as that used in example 4.3. The scheme:

CATENOID(24,10,1,1)

is used to generate the initial surface used in the form-finding of the surface presented in example 4.4. The results corresponding to example 4.4 are scrutinised in accordance with those given by the aforementioned authors, (Table 4-4). The configuration of the surface considered in example 4.4 is identical to that given in Figure 4-12 (b) and the surface possesses the same value of stress; $5\times10^{6}\,kNm^{-2}$. In this example, only two convergence criteria are looked at when examining the number of iterations for convergence; they are $ER_{T\%} \leq 0.025$ and $ER \leq 0.001kN$ (Table 4-3).

Convergence Criterion.	Surface Area	NIT	$A_{\%}$	ER	$ER_{T\%}$	$ER_{F\%}$
$ER_{T\%} \leq 0.025$	$5.97\,m^2$	75	0.1	$9\times10^{-2}\,kN$	1.5×10^{-2}	1.8×10^{-3}
$ER \leq 0.001KN$	$5.97\,m^2$	246	0.1	$6.3\times10^{-4}\,kN$	1.1×10^{-4}	1.3×10^{-5}

Table 4-3 Convergence Criteria used in Example 4.4.

Theoretical Values (R=1 *m*, L=0.5 *m*, *a*=0.848 *m*, Area = 5.99 m^2).		Suzuki	Singer	Example 4.4 (NIT =75).	Example 4.4 (NIT = 246)
l	*r*	*r*	Area (m^2)	*r*	*r*
-0.5	1	1	5.99	1	1
-0.4	0.944	0.943		0.943	0.943
-0.3	0.902	0.900		0.900	0.900
-0.2	0.872	0.869		0.870	0.869
-0.1	0.854	0.851		0.851	0.851
0	0.848	0.845		0.845	0.845
0.1	0.854	0.851		0.851	0.851
0.2	0.872	0.869		0..870	0.869
0..3	0.902	0.900		0.90	0.900
0.4	0.944	0.943		0.943	0.943
0.5	1	1		1	1

Table 4-4 Theoretical and Numerical Results (Section CC' - Example 4.4).

Although the same value of ER ≤ 0.001kN is used in both examples 4.3 and 4.4, the number of iterations required for convergence of the surface described by example 4.4 is less, due to the inducement of smaller pseudo cable forces through the reduction in the mesh size due to the overall smaller size of the catenoid. This is reflected by the increased value of $ER_{T\%}$ at 246 iterations. Thus, the criterion ER can be said to depend on the applied surface stress, the dimensions/mesh size of the surface and the value of the thickness of the membrane. $ER_{F\%}$ is also a somewhat arbitrary constant as it too depends on ER and, importantly, it is also related to the force per unit width F_K ; a constant which is similarly related to the properties of stress and membrane thickness. It can be seen that the number of iterations for the criterion $ER_{T\%} \leq 0.025$ is identical for example 4.3 and 4.4. This is because the criterion, unlike the other two criteria, is a **non-dimensional** measure of the convergence of the solution. A stable minimal surface should adopt the same geometry irrespective of the dimensions of the boundary; it depends only on the configuration, or geometrical

arrangement, of its boundaries i.e. both example 4.4 and 4.3 are described by equation (4.1). Consequently, $ER_{T\%}$ is a more universal measure of the convergence of the solution. Figure 4-16 shows the plot of the maximum nodal displacements for Example 4.4. The plot shows that the displacements do not affect the surface configuration after 75 iterations when the criterion $ER_{T\%} \leq 0.025$ has been satisfied, i.e. iterations thereafter can be considered to belong to stage (3) of the form-finding analysis. (There are no Stage (1) deformations as the initial surface closely approximates the form-found surface, and hence there are no large out-of-plane forces and displacements.)

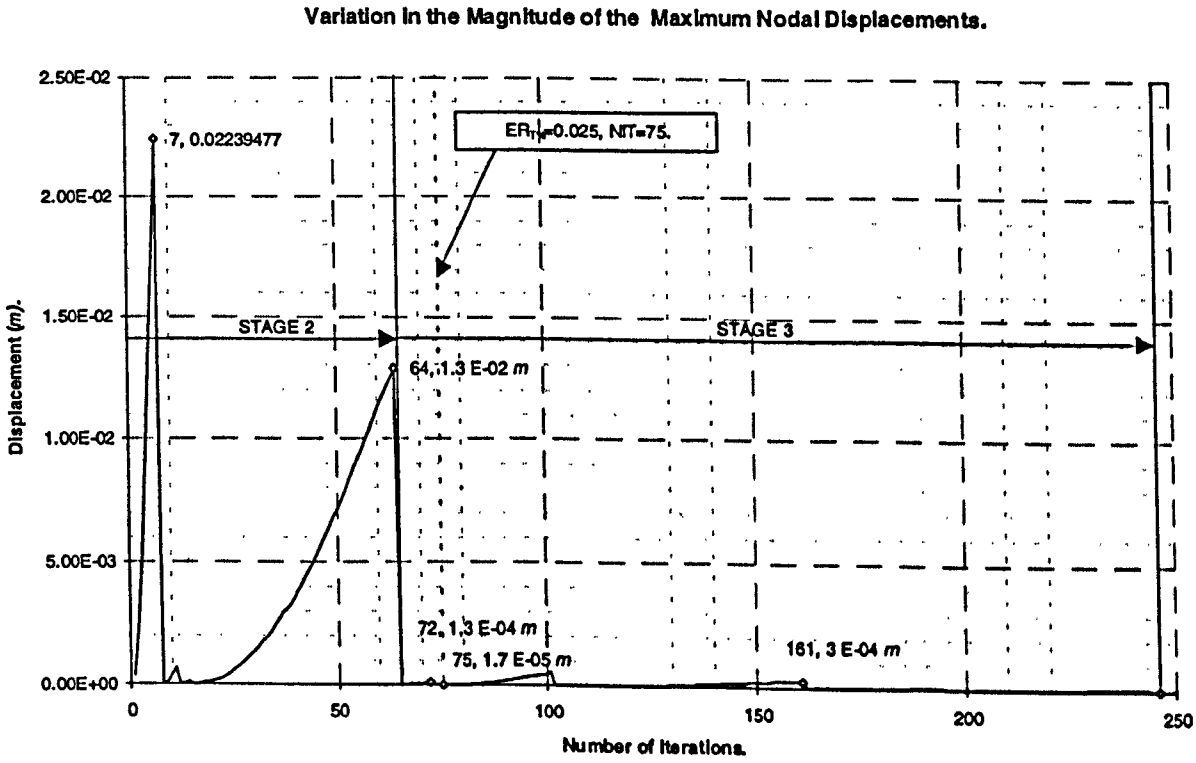

Figure 4-16 Variation of the Maximum Nodal Displacements - Example 4.4.

In summary, the stable minimal surfaces produced by the author, and depicted in examples 4.3 and 4.4, show an excellent agreement with both the numerical results of Ishii & Suzki and Singer et al., together with those for the values of the "theoretical" cross-section

profile. In both examples, the surface area is in error by just -0.3%; although this value is small, it can become significant when the dimensions are as large as those used in example 4.3. In each example, there was no noticeable change in the surface geometry after 75 iterations; at this point the criterion $ER_{T\%} \leq 0.025$ was satisfied. The examples illustrated how the use of a well defined initial surface was advantageous in reducing the number of iterations and the magnitude of the out-of-balance forces. The accuracy of the initial surface was described by the negligible change in the surface area for a number of iterations; a property described by the extremely small value of $A_{\%}$.

Case 4.3.3 Catenoid Surface - Unstable Equilibrium (Example 4.5).

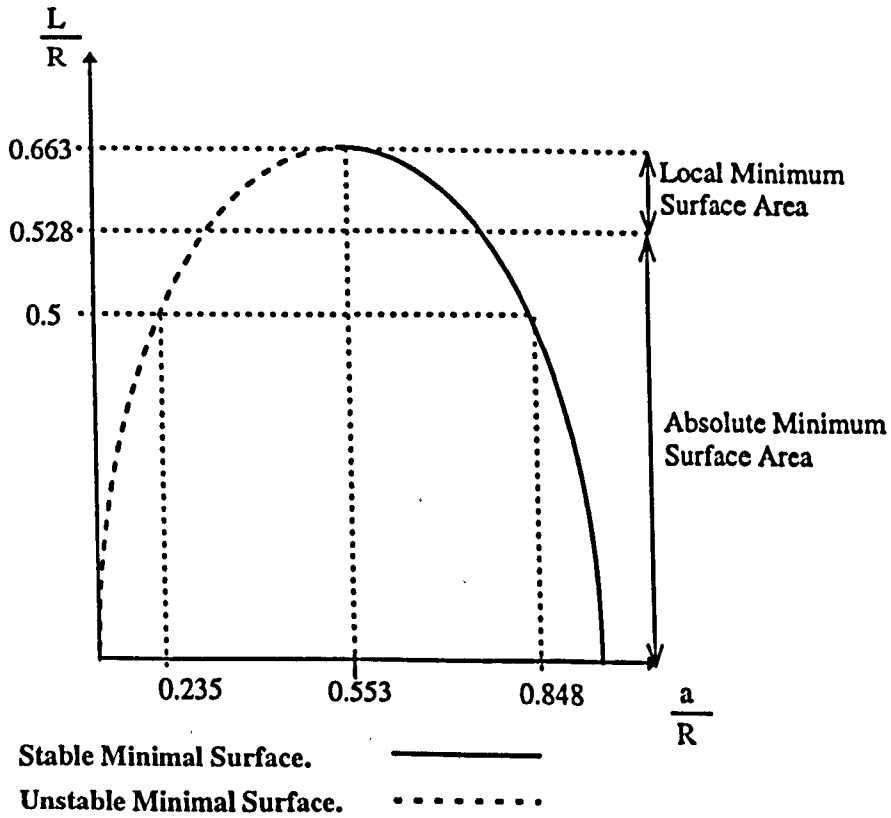

Figure 4-17 Variation of *a* and the Surface Area of a Catenoid with the Distance (L).

It has been stated in Chapter 2, Section 2.2, that a minimal surface is not necessarily a stable minimal surface, and hence, does not exclusively span a surface of minimum area. It can be shown that there is another numerical solution to a for a boundary identical to that discussed in examples 4.3 and 4.4:

$$a = 0.235 \times R \qquad 4.4$$

This gives the equation for a catenary that describes an **unstable** minimal surface for the instance when R = 2L; where L= $\frac{1}{2}$ of the height of the catenoid. An unstable surface is defined as that surface, where the application of a small amount of displacement causes the equilibrium of the form to be irrecoverably lost, causing the surface to adopt a new geometry once it has come to rest at a more stable equilibrium. This explains why unstable minimal surfaces cannot be modelled using a soap film; any perturbation will cause the soap lamina to break. An unstable minimal surface does not possesses a minimum surface area. Assuming the same boundary configuration as used in example 4.4, R=1 m, L=0.5 m, and taking a to be 0.235 m, equation (4.3) gives a "theoretical" surface area of 6.85 m^2; a value greater than that of the stable minimal surface described by example 4.4. Depending on the parameter L, two values of a exist for a catenoid, Figure 4-17[4.12]. The stable state for a minimal surface of a specified height, is given by the larger value of a; the smaller value gives the unstable minimal surface. With respect to Goldschmidt's theory[4.13], as long as the height of separation of the two rings is less than $1.056 \times R$ and a suitable value of a is used, i.e. the right hand curve depicted in Figure 4-17, the Euler-Lagrange equation gives the absolute minimum surface area i.e. a catenary of revolution. For heights above this value, but less than $1.325 \times R$ [vi], the Euler-Lagrange equation gives a surface that has an area that is only a local minimum; the absolute minimum is given by the area of the two rings. For a

[vi] The derivation of this value is given in Appendix 4A.4

height greater than $1.325 \times R$ the surface will jump discontinuously into two discs. Bach et al[4.14] has proven this theory experimentally, showing that the maximum separation of two boundary rings is $1.3 \times R$. If two circular rings are placed in a soap solution and gradually pulled apart, it is easy to imagine that the soap lamina (stable minimal surface) will become increasingly more 'wasted' at its mid-point. This effect is illustrated by the right hand curve shown in Figure 4-17, it describes a gradual reduction in the value of a for the stable soap film as the height L is increased. When the distance between the rings is equivalent to the maximum attainable height of a catenoid, only one value of a will exist; the numerical value of which is given by $0.553 \times R$. (The derivation of this value is given in Appendix 4A.4). At the maximum attainable height, the surface is quasi stable, any slight perturbation will cause the breaking of the soap laminae. At this point, the Euler-Lagrange equation will describe a minimal surface that possesses a surface area that is only a local minimum. Such a surface is described in the following example, which also illustrates Goldschmidts theory.

The scheme:

CATENOID(24,20,1.325,1)

gives an initial surface that differs from the previous examples by possessing 20 elements along the height of the catenoid. The increased surface discretisation is necessary to model the high curvature anticipated in the final solution. Due to the unstable nature of the solution, the displacements have been reduced by using a smaller value of 5×10^3 kNm^{-2} for the surface stress. Table 4-6 presents a comparison between the "theoretical" results and those obtained from the Dynamic Relaxation algorithm. The criteria used for stopping iterations are given in Table 4-5.

Convergence Criterion.	Surface Area.	NIT	$A_{\%}$	ER	$ER_{T\%}$	$ER_{F\%}$
AREA ≤ 7.544m²	7.54 m²	14	1.6	2.6×10^{-2} kN	4.23	0.5
ER ≤ 0.0035kN	7.49 m²	26	2.2	3.3×10^{-3} kN	0.5	0.07
Goldschimdts Solution.						
NIT = 65	6.46 m²	65	16.8	0.5 kN	90.8	10

Table 4-5 Convergence Criteria used in Example 4.5.

Theoretical Values R=1 m, L=0.663 m, a= 0.553 m, Area =7.544 m².			Example 4.5 (NIT = 26)	
l (m)	r (m)	Z Co-ordinate.	Z Co-ordinate.	r(m)
-0.663	1	0	0	1
			0.045	0.938
-0.530	0.827	0.133	0.094	0.877
			0.148	0.817
-0.398	0.702	0.265	0..207	0.761
			0..271	0.708
-0.265	0.617	0.398	0.341	0.661
			0.416	0.662
-0.133	0.568	0.53	0.495	0.593
			0.578	0.575
0	0.553	0.663	0.663	0.568
			0.745	0.575
0.133	0.568	0.796	0.830	0.593
			0.909	0.622
0.265	0.617	0.928	0.984	0.661
			1.054	0.708
0.398	0.702	1.061	1.118	0.761
			1.177	0.818
0.530	0.827	1.193	1.231	0.877
			1.280	0.938
0.663	1	1.325	1.325	1

Table 4-6 Theoretical and Numerical Results (Section CC'- Example 4.5).

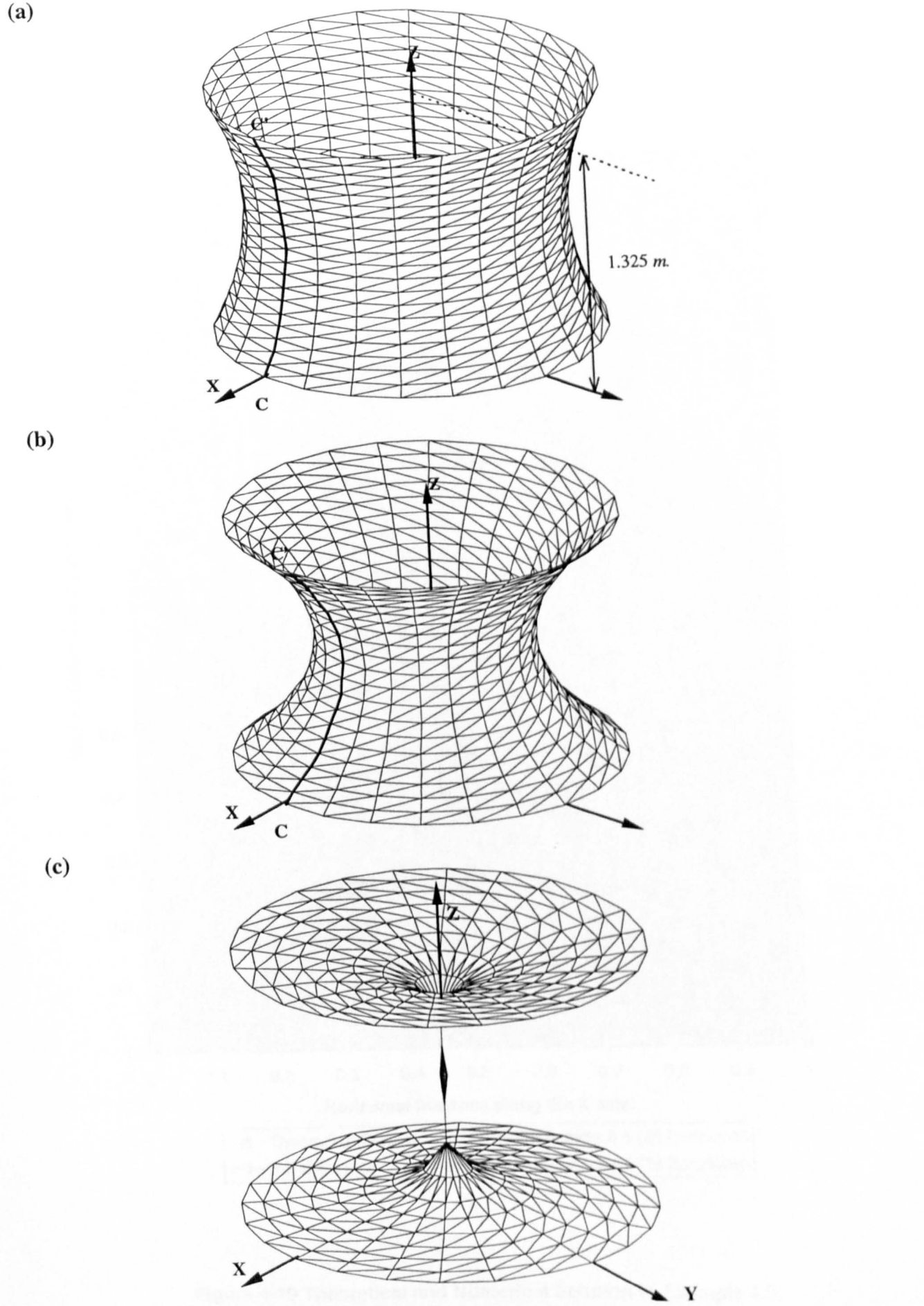

Figure 4-18 Example 4.5. (a) Initial Surface. (b) Form-Found Surface-Unstable Minimal Surface (26 Iterations). (c) Goldschmidt's Solution (65 Iterations).

Comparison with the Theoretical Curvature CC'.

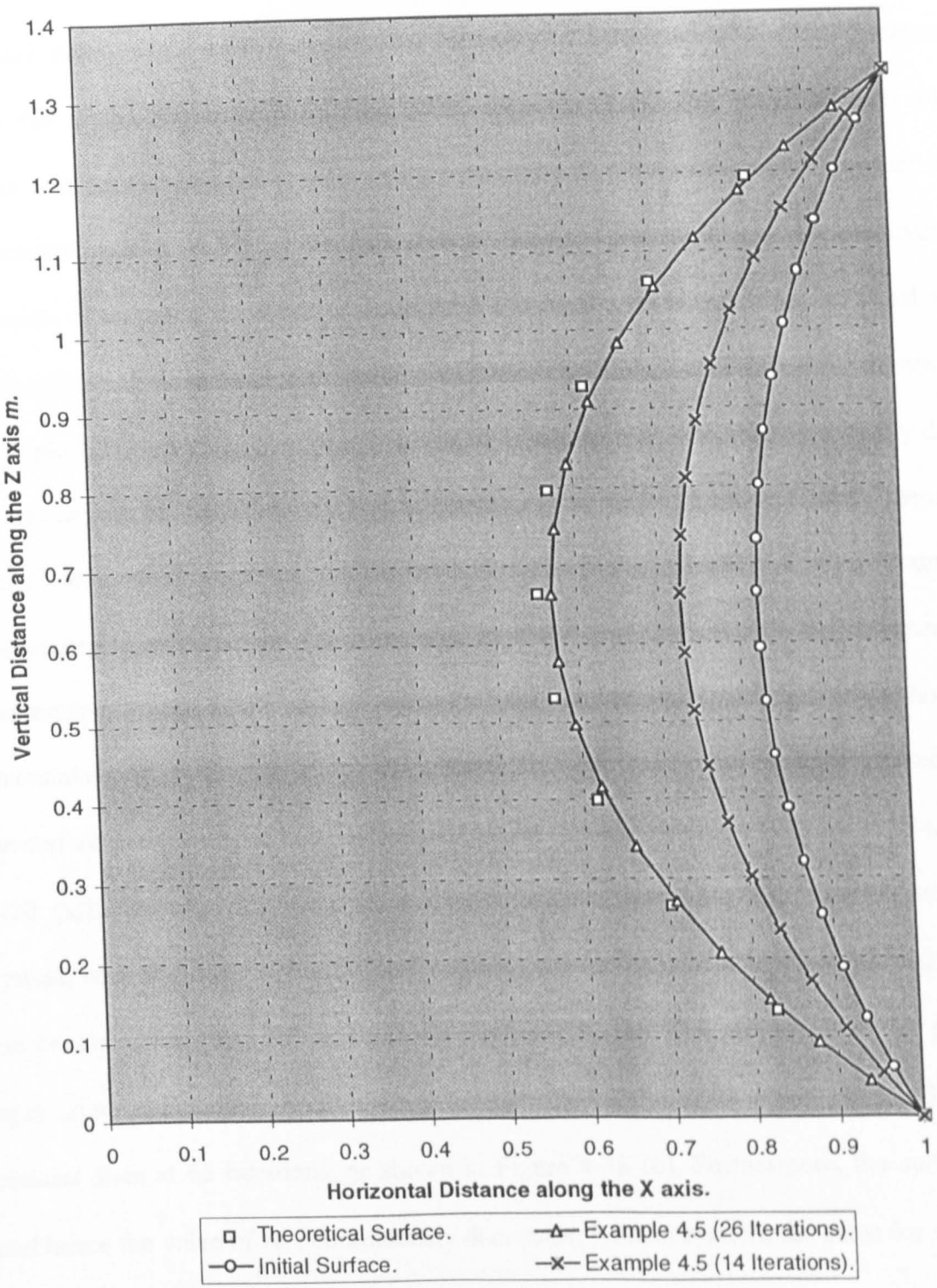

Figure 4-19 Theoretical and Numerical Solution to Example 4.5.

Figure 4-18 (b) shows the numerical solution after 26 iterations, the surface is not equilibrated to the same degree as that in the previous examples, with $ER_{T\%}$ being equal to 0.5; a value far greater than that encountered in examples 4.3 and 4.4. This is due to the unstable nature of the solution. Figure 4-19 shows that the numerical surface compares well with that of the "theoretical" solution. With respect to Table 4-6, it can be seen that the radius *a* at the mid-point of the catenoid is in error by -2.7%. In addition, the surface area is inaccurate to only -0.7% of the "theoretical" surface area (Table 4-5). A convergence criterion of stopping iterations as soon as the surface area is less than, or equal to, the "theoretical" area can be seen to produce an inaccurate surface configuration, (Figure 4-19 - Example 4.5 (14 iterations)). This is because the surface area modelled numerically depends on the degree of discretisation, and is hence only an approximation to the "theoretical" surface area. At 26 iterations, the surface has reached only its local equilibrium state; it has not reached its absolute one. Choosing a value of ER lower than 0.0035 kN as a measure of convergence results in the surface losing its local equilibrium. This is because although the potential energy of the system for the unstable state has been minimised, the movements of the surface are undamped and the surface has yet to reach its stable stationary state, (Figure 4-20 (a)). Consequently, successive displacements disrupt the local equilibrium of the system, such that the residual forces progressively increase in a direction aligned towards the centre of the catenoid, as shown in Figure 4-20 (b). The surface does not regain its equilibrium and stability, and becomes increasingly wasted at its centre, until it forms two circular discs at 65 iterations, as shown in Figure 4-18 (c). Furthermore, the surface area, and hence the value of $A_{\%}$, continuously decreases; it never remains the same for successive iterations. This is in stark contrast to the stable catenoid surfaces depicted in examples 4.3 and 4.4. It can be concluded therefore, that the solution is not exhibiting divergence but is

simply conforming to Goldschimdt's theory for an unstable minimal surface i.e. the absolute minimum surface area is given by the "theoretical" area of the two rings; 6.28m^2.

(a)

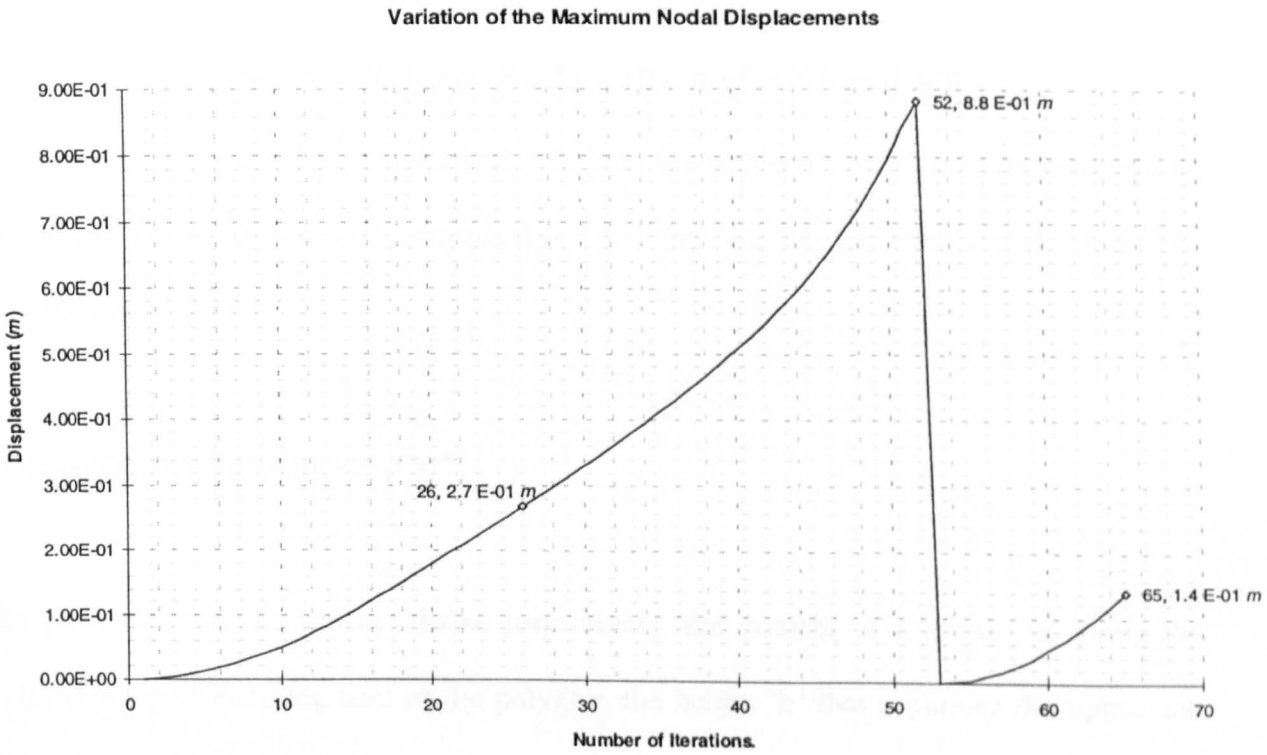

(b)

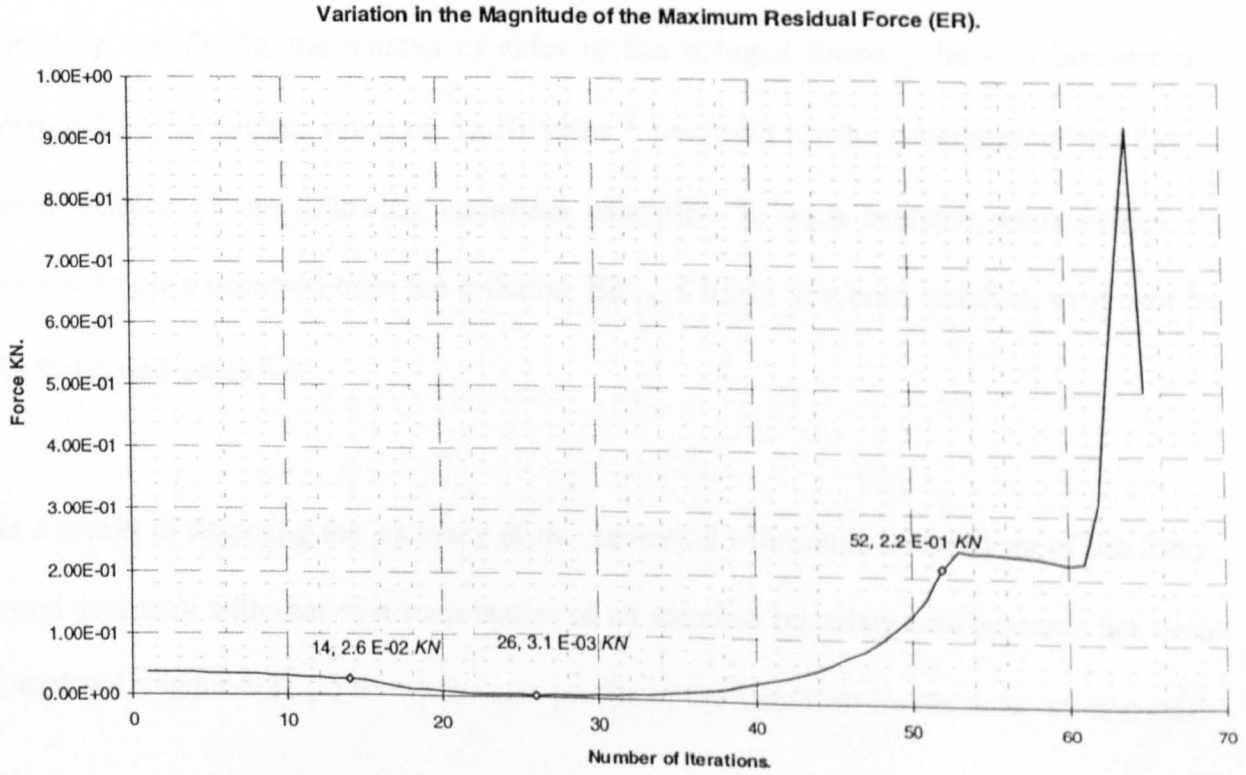

Figure 4-20 Variation of (a) Maximum Nodal Displacement (b) Criterion ER (Example 4.5).

4.4 Verification in Accordance with Experimental Results.

Case 4.4.1 Polygon Surface (Examples 4.6 and 4.7).

Examples 4.6 and 4.7 depict numerical solutions for stable minimal surfaces bounded by two decagons. In the case of example 4.6, the initial surface has been created from the induction statement:

POLYGON(8,9.783,4.365,25,10)[vii],

The parameters of the scheme define respectively, the number of intervals 'n' along the inclined plane of each segment of the polygon, the height 'h' that separates the upper and lower boundaries, the horizontal distance 'r' from the centre to the outer edge of the top boundary, the horizontal distance 'R' from the centre to the outer edge of the lower boundary and finally, the number of sides of the polygon forming the two boundaries, (Figure 4-21). A surface stress of $5\times10^{3}\,\mathrm{kNm}^{-2}$ was used for the generation of the form-found surface of the following numerical examples. In each example, convergence is deemed to have occurred once the criterion $ER_{T\%} \leq 0.025$ has been satisfied, as shown in Table 4-8 and Table 4-9.

As a means of assessing the accuracy of the numerical solution, a comparison of the form-found geometry with that of a soap lamina of an identical boundary configuration has been completed. Figure 4-22 (a) shows the side profile of the soap film for the cross-section DD'

[vii] The formulation of the scheme is given in Appendix 4A.5.

of example 4.6. Two further parameters require defining: 'b' is the horizontal distance, parallel to cross-section DD', measured from the centre to the outer edge of the top boundary while B is a similar distance that defines the position of the lower boundary, measured form the centre to the point D, (Figure 4-21 (c)). Traditionally, a soap lamina is bounded by a single piece of wire that has been deformed to form the desired boundary geometry. If the wire boundary is of a low rigidity, the interaction from the soap film can distort the boundary. Consequently, the lower boundary used in the experimental solution, (Figure 4-22 (a)), was constructed using wire of a significant thickness to improve its rigidity. The impracticality of deforming the wire by hand led to the cutting of the wire into individual sections, before the reassembling and welding of the sections to form the appropriate decagon configuration.

Table 4-7 contains the values of the aforementioned parameters for the numerical and experimental results. Using an enlarged print of Figure 4-22(a), various points have been measured and plotted against those for example 4.6, Figure 4-23. It is apparent that the experimental solution is not exactly symmetrical about the point $\frac{y}{2B} = 0.5$; point D' is positioned at $\frac{y}{2B} = 0.96$ and consequently, length DD' is in fact 252.5 mm, an error of -4%. This inaccuracy is due to the impossibility of ensuring the sides of the frame enclosing the soap lamina are identical in length and are aligned at exactly 72 degrees to each other. However, it is clear that there is a good agreement between the numerical and experimental solutions to the left of the centre-point, as shown in Figure 4-23.

It is possible to gauge the accuracy of the curvature to the right of the centre point by taking B to be the distance from the centre of the experimental surface to point D'.

(Previously, B was measured from the centre to point D). This gives a value of 121 mm for B. The assumption of this value implies that the aspect ratio $\frac{h}{b}$ and the ratio $\frac{b}{B}$ has to change. Consequently, a new initial surface has been generated for new values of 'r' and 'h', resulting in example 4.7. (The initial surface is created from the scheme presented in Table 4-7). Figure 4-22 (c) depicts the side profile of the generated numerical surface. Again, there is good agreement between the numerical and experimental solutions. Detailed examination of the photograph suggests that where the right hand side lower boundary is not supported, i.e. from the point $\frac{y}{2B} = 0.5$ to point D', the boundary has slightly displaced under its own weight and due to some interaction from the soap film. This explains why the curvature of the experimental model has been underestimated, and lies below that of the numerical model depicted in Example 4.7.

	R	r	B	b	h	h/B	b/B	SCHEME
Experimental Results (Unaltered Value for B).	125 mm	22 mm	131.5 mm	23 mm	49 mm	0.373	0.175	N.A.
Example 4.6	25 m	4.365 m	26.23 m	4.590 m	9.783 m	0.373	0.175	POLYGON(8,9.783,4.365,25,10)
Experimental Results (Modified Value for B).	125 mm	22 mm	121 mm	23 mm	49 mm	0.405	0.190	N.A.
Example 4.7	25 m	4.740 m	26.23 m	4.984 m	10.623 m	0.405	0.190	POLYGON(8,10.623,4.74,25,10)

Table 4-7 Dimensions of the Numerical and Experimental Solutions to Examples 4.6 and 4.7.

Convergence Criterion	Surface Area	NIT	$A_{\%}$	ER	$ER_{T\%}$	$ER_{F\%}$
$ER_{T\%} \leq 0.025$	2120 m^2	548	2.4	3.3×10^{-3} kN	2.4×10^{-2}	6.6×10^{-2}

Table 4-8 Convergence Criteria used in Example 4.6

Convergence Criterion	Surface Area	NIT	$A_{\%}$	ER	$ER_{T\%}$	$ER_{F\%}$
$ER_{T\%} \leq 0.025$	2140 m^2	544	2.7	3.4×10^{-3} kN	2.4×10^{-2}	6.8×10^{-2}

Table 4-9 Convergence Criteria used in Example 4.7.

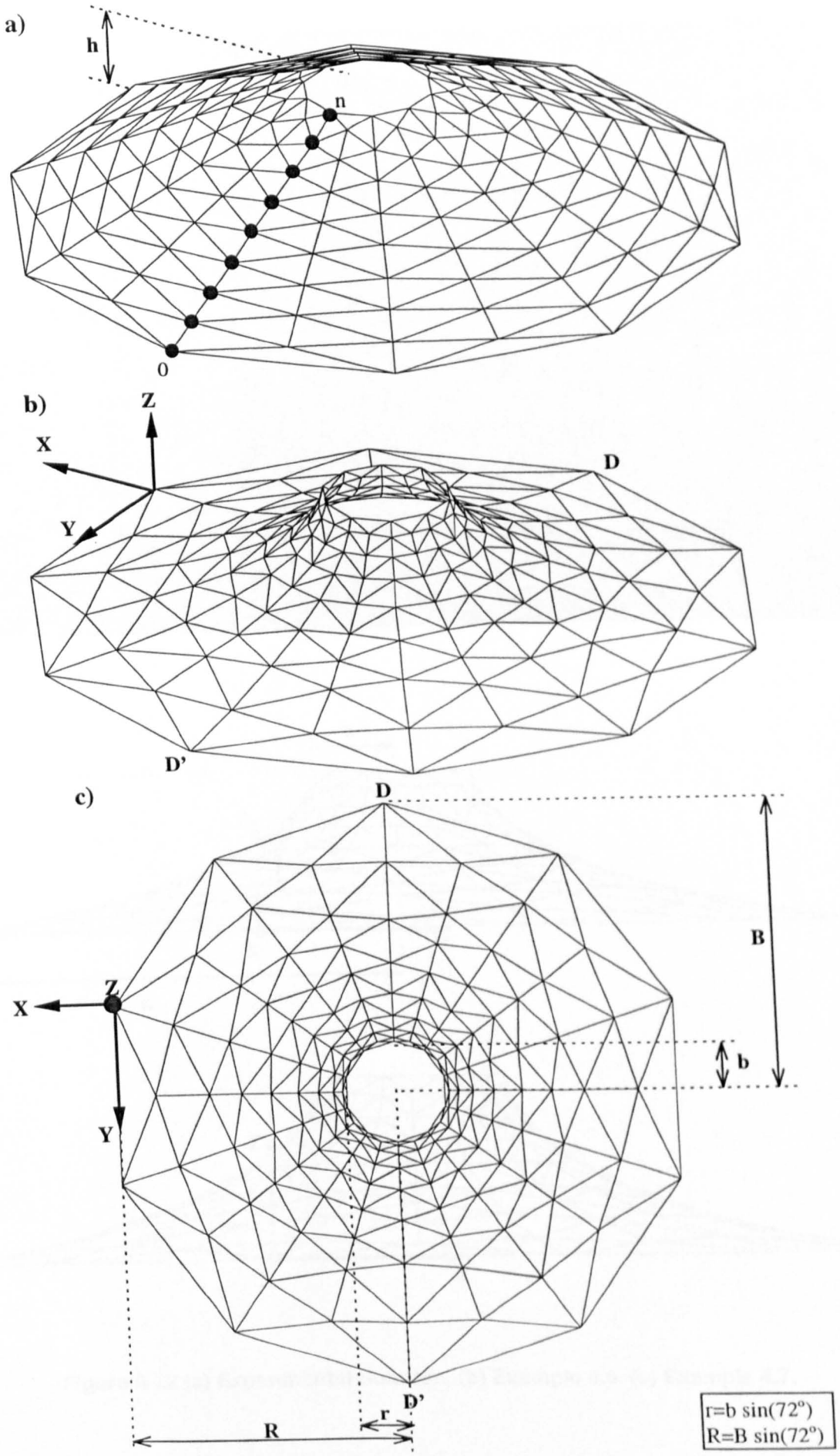

Figure 4-21 Example 4.6. (a) Initial Surface. (b) Perspective View. (c) Plan View.

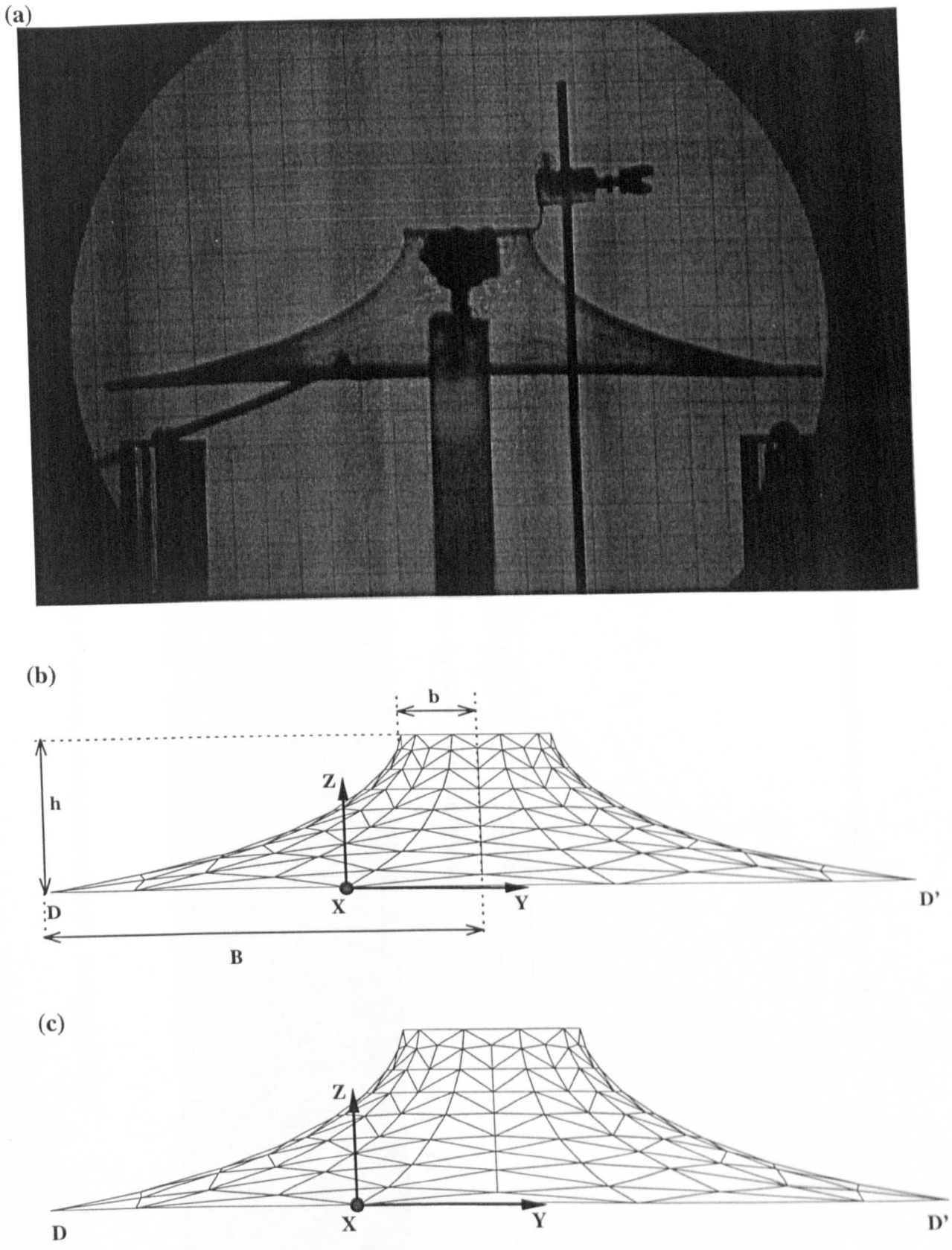

Figure 4-22 (a) Experimental Solution. (b) Example 4.6. (c) Example 4.7.

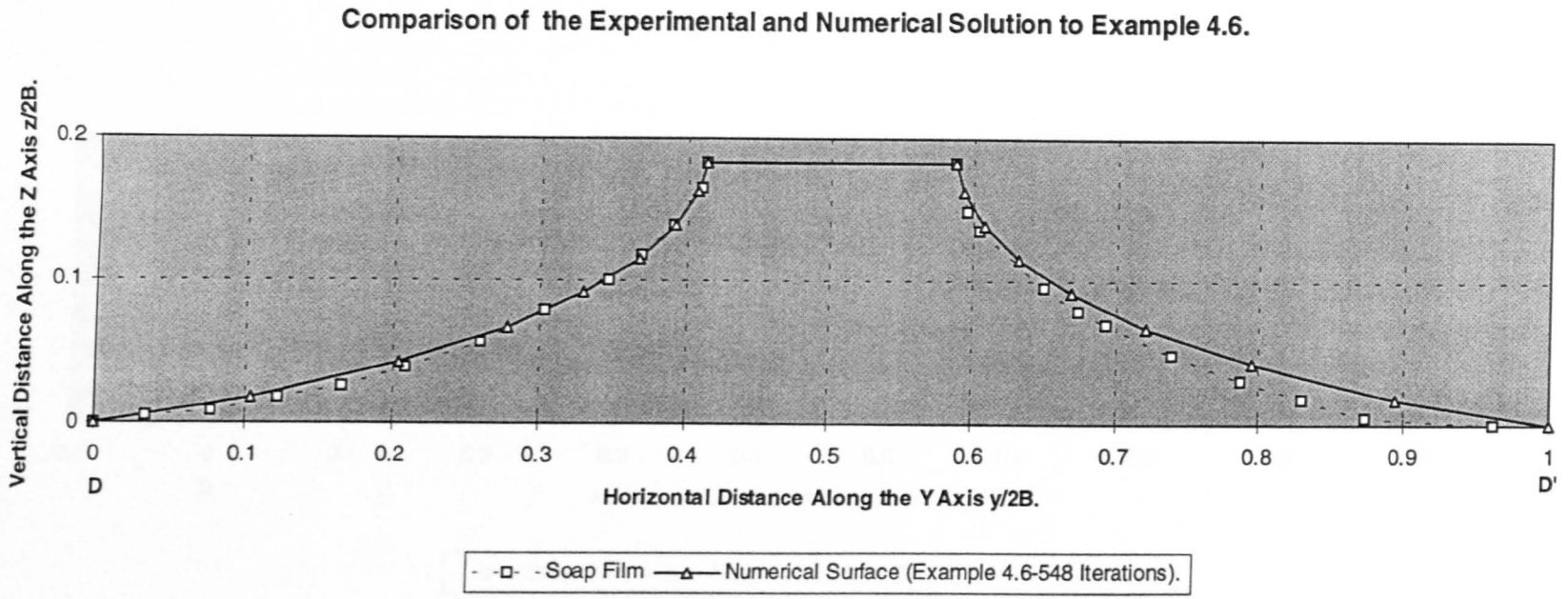

Figure 4-23 Comparison of Cross-Section DD' for Example 4.6.

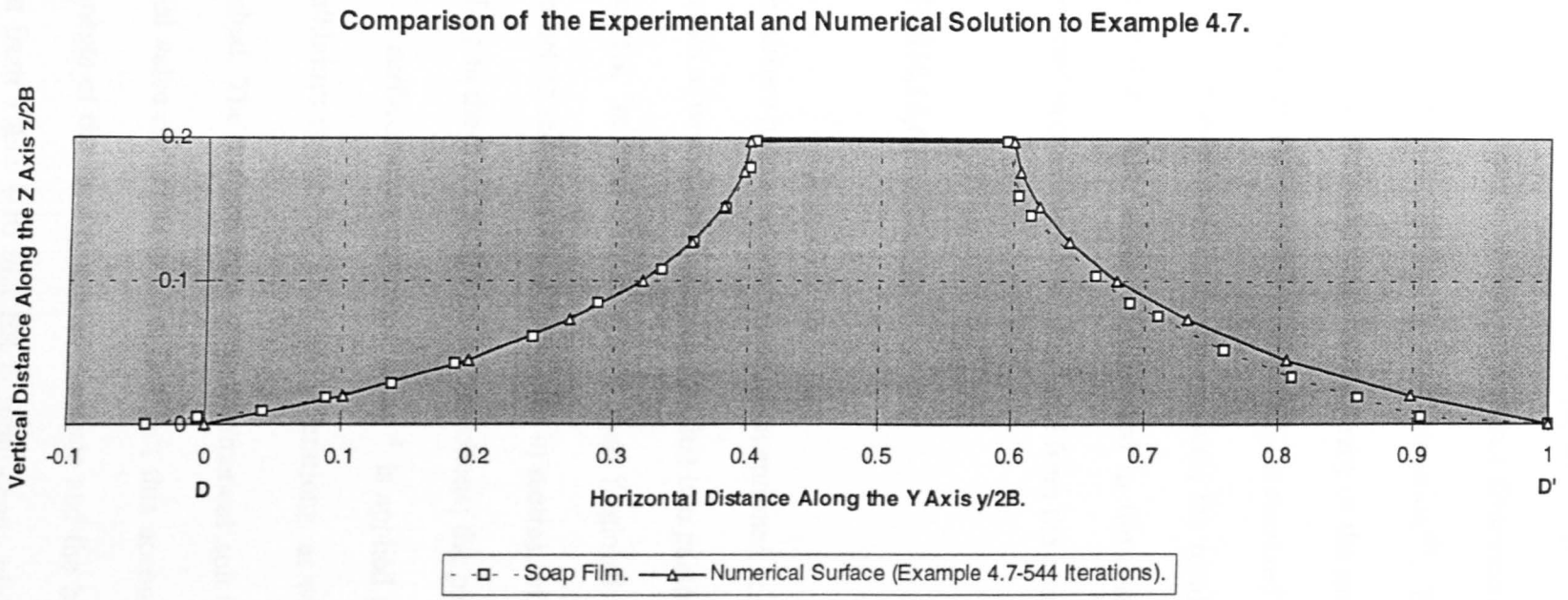

Figure 4-24 Comparison of Cross-Section DD' for Example 4.7.

Case 4.4.2 Weir Surface (Example 4.8)

Figure 4-26 (a) and Figure 4-27 (a) depict the experimental solution to a stable minimal surface possessing a boundary of planar dimensions 126×188.7 mm, and a vertical depth of 63.5 mm for the triangular side elevation[viii]. The figures describe the front and end elevations of the soap film. The accuracy of the numerical model, presented in example 4.8, (Figure 4-26 (b) and Figure 4-27 (b)), is assessed through comparisons of the geometry of the experimental and numerical surfaces; the results being documented in Figure 4-28 and Figure 4-29. The initial surface used in the form-finding of the stable minimal surface presented in example 4.8 is generated from the scheme:

WEIR(6,16,63.5,188.7,63)[ix]

The surface produced from the aforementioned scheme is illustrated in Figure 4-25 (a), and consists of two inclined planes. The first two parameters of the scheme define the number of elements, 'm' and 'n', in the X and Y global directions respectively. The subsequent parameters relate to the dimensions, in metres, of the 'height', 'length' and 'width' of the surface in the X, Y and Z global directions; the parameters are fully defined in Figure 4-25 (a). A surface stress of $5\times10^{6}\,\mathrm{kNm^{-2}}$ is applied to the initial surface during form-finding. Equilibrium is satisfied after 1148 iterations, at which time the criterion $ER_{T\%} \leq 0.025$ is reached. The surface area of the numerical solution has decreased significantly from its initial value of 33760 m^2 to 27300 m^2; this accounts for the excessive deformation of the elements of the final discretised surface and the high value of $A_{\%}$, (Table 4-10). It can be seen from Table 4-10 that ER is significantly high; this is due to the inducement of very

[viii] The author would like to acknowledge that the experimental solution was obtained from work conducted by Dr . P. Gosling, and recorded in his 1992 thesis (ref. 4.8).

[ix] The formulation for the scheme is given in Appendix 4.A6.

large "pseudo cable" forces in elements with a poor aspect ratio. (This effect was previously described in the form-finding of Example 4.2, Section 4.3).

The results presented in Figure 4-28 and Figure 4-29 show excellent agreement between the numerical and experimental solutions. This is a significant result; it is apparent that the dynamic relaxation algorithm is capable of producing a numerical model that accurately represents the ideal soap film solution, for the particular instance where an extremely ill defined initial surface has been used for form-finding. In a thesis written by Gosling, it was described how accurate results, for a similar numerical solution to Example 4.8, required careful modelling of the initial surface through the definition of the surface geometry using hermitian polynomials[x4.8].

Convergence Criterion.	Surface Area.	NIT	$A_{\%}$	ER	$ER_{T\%}$	$ER_{F\%}$
ER ≤ 0.025	27300 m^2	1148	19.1	17 kN	2.4×10^{-2}	3.4×10^{-1}

Table 4-10 Convergence Criteria used in Example 4.8.

[x] An example of an initial surface generated using herimtian plynomials is presented in example 4.10, Section 4.5.

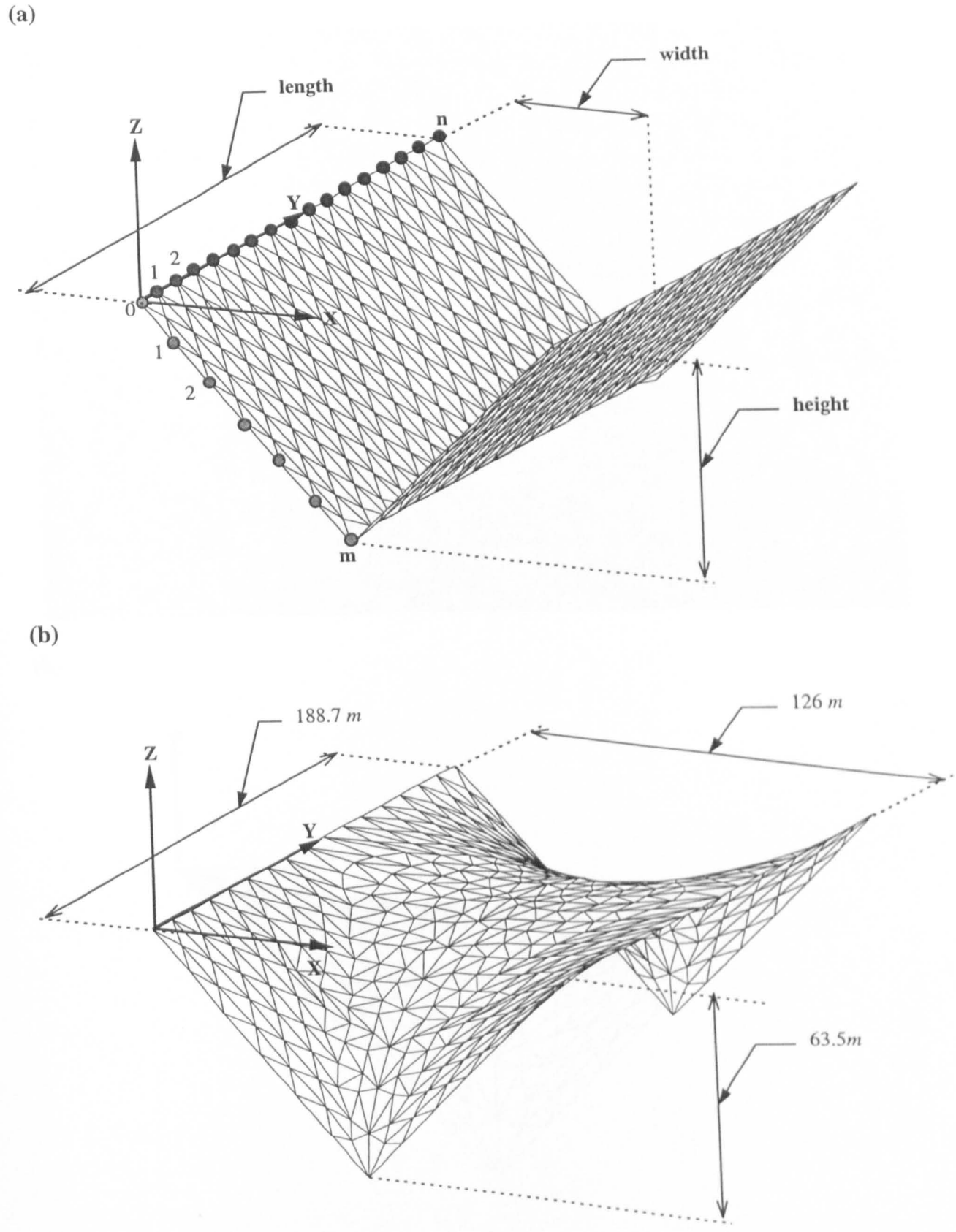

Figure 4-25 Example 4.8 (a) Initial Surface (b) Form-Found Surface.

(a)

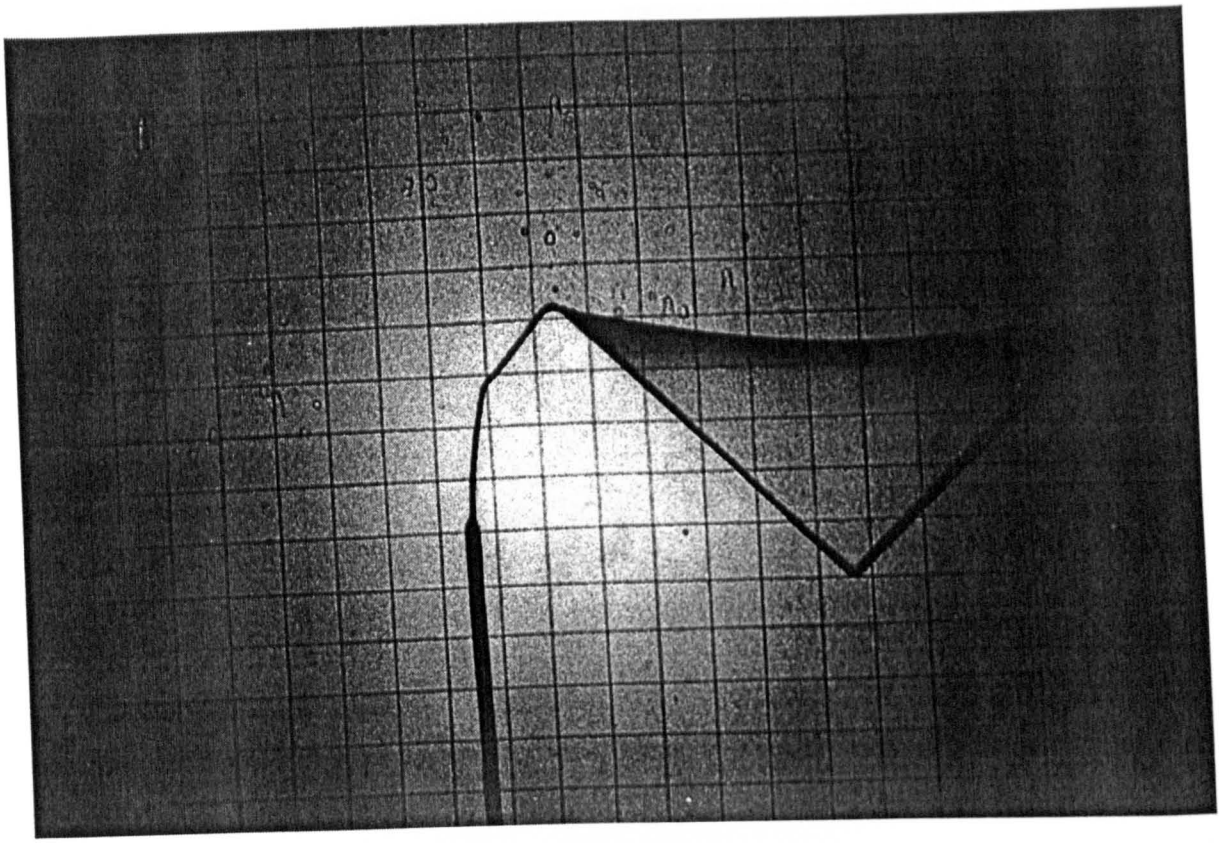

(b)

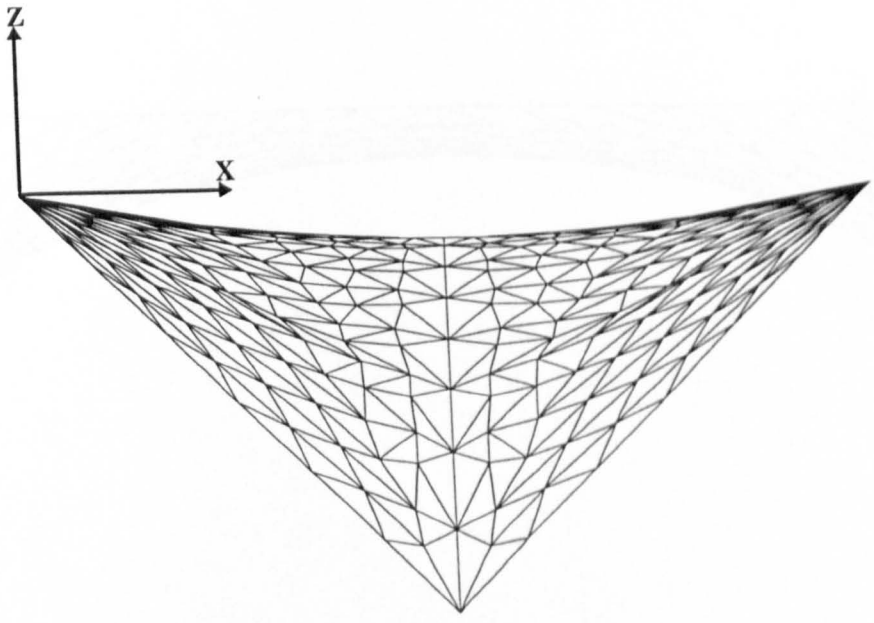

Figure 4-26 ZX Plane (a) Experimental Solution (b) Numerical Solution (Example 4.8).

(a)

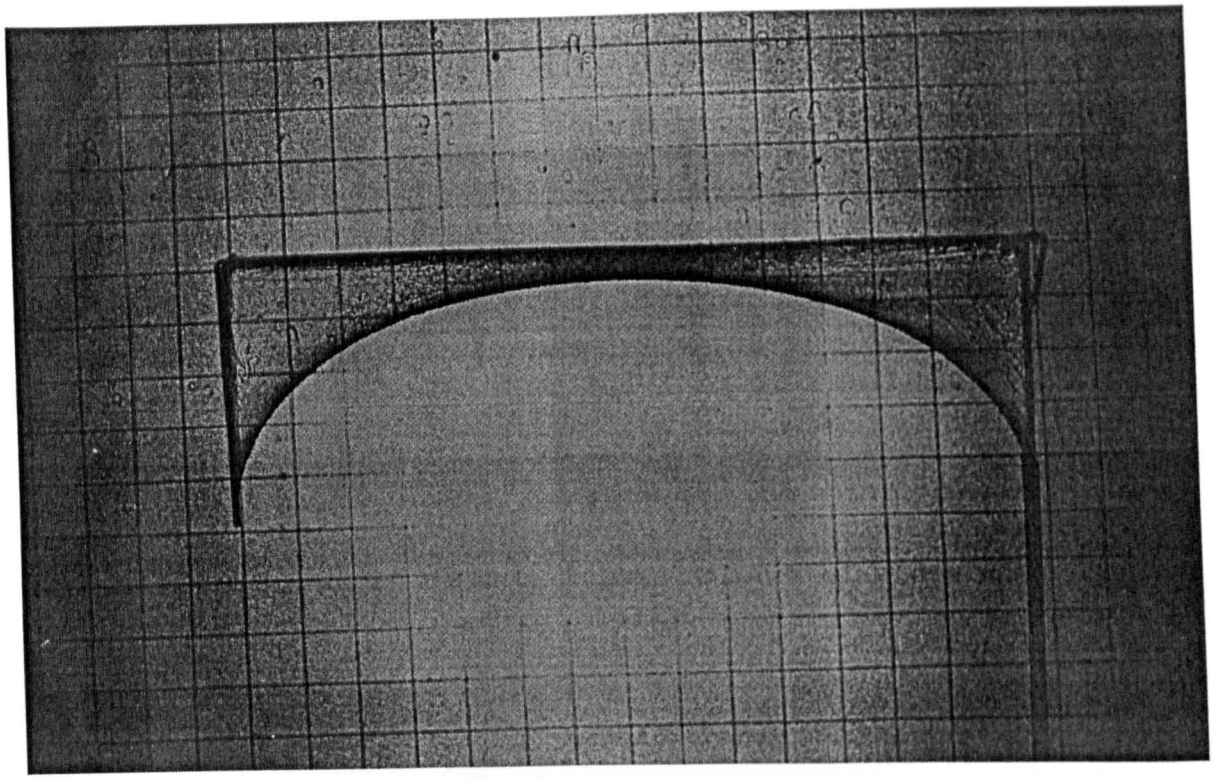

(b)

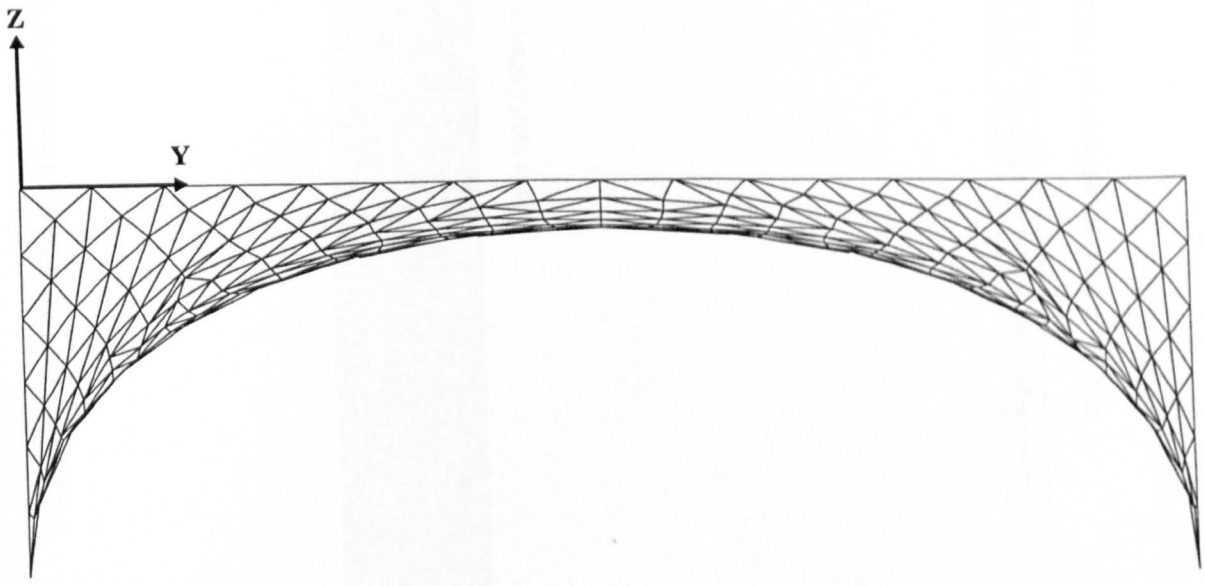

Figure 4-27 ZY Elevation (a) Experimental Solution. (b) Numerical Solution (Example 4.8).

Comparison of the Experimental and Numerical Solution to Example 4.8.

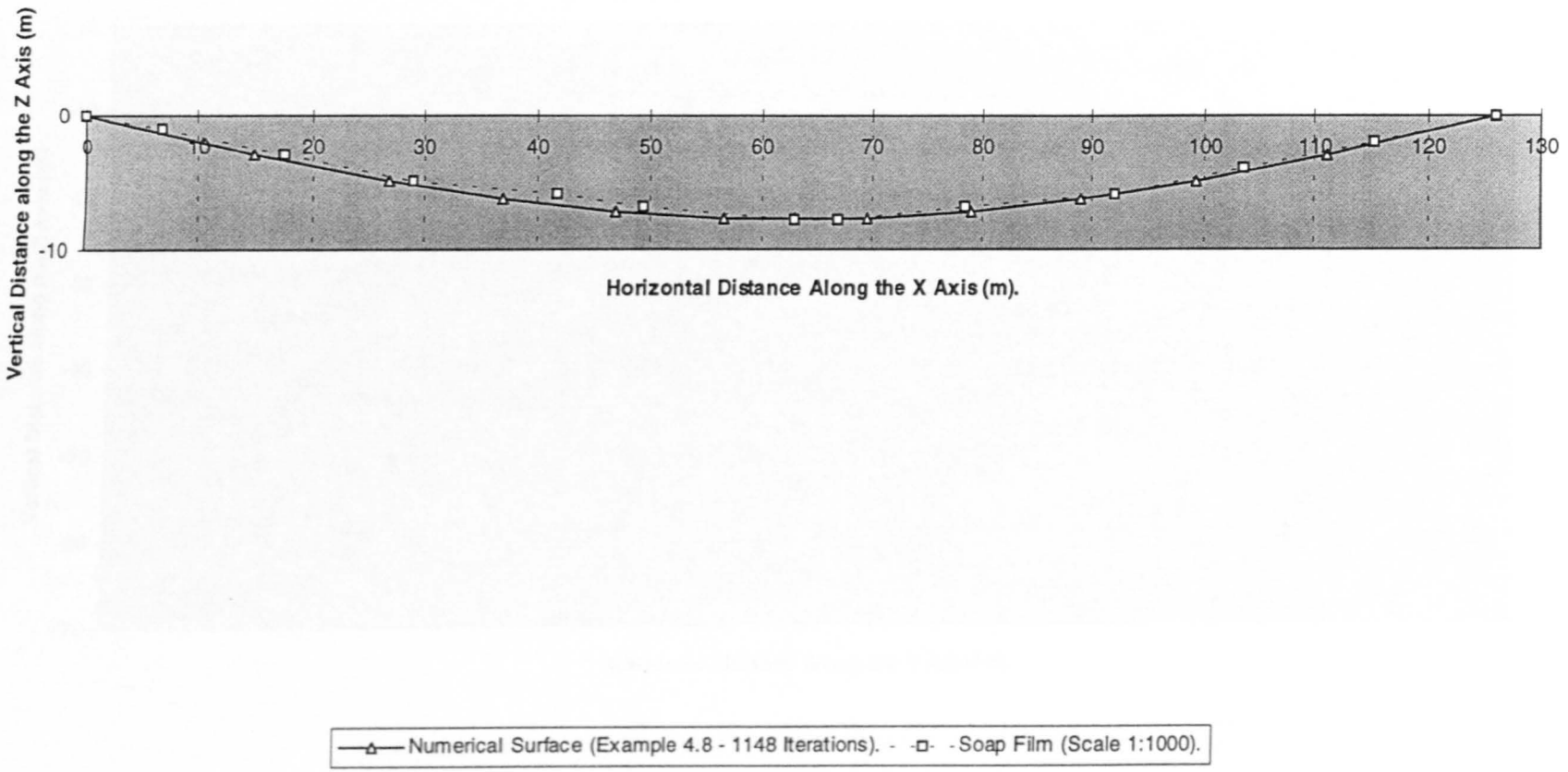

Figure 4-28 Comparison of the ZX Elevation of Example 4.8.

Comparison of the Experimental and Numerical Solution to Example 4.8.

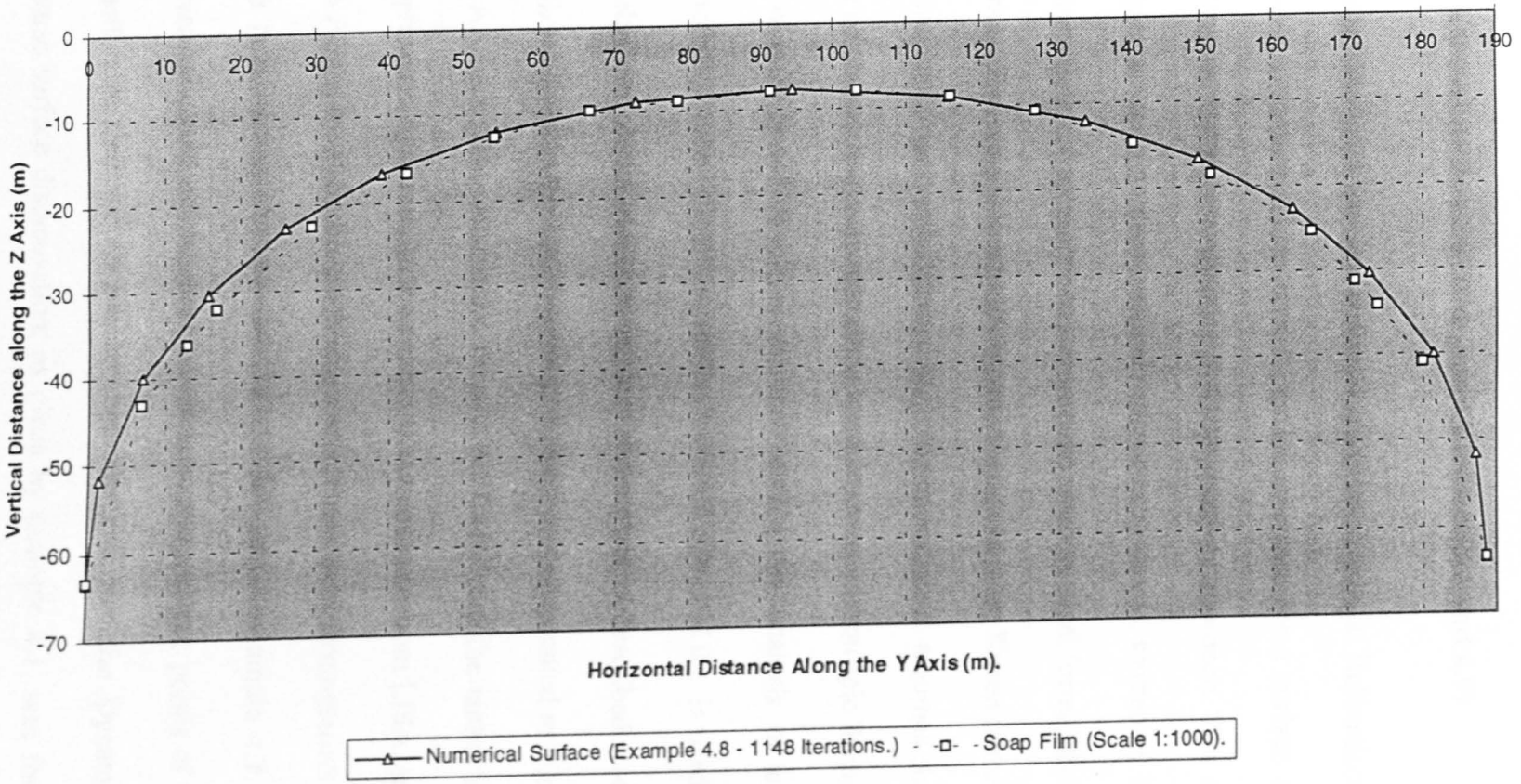

Figure 4-29 Comparison of the ZY Elevation of Example 4.8.

4.5 Verification in Accordance with the Results Obtained using Alternative Computational Methods.

Case 4.5.1 Box Surface (Examples 4.1, 4.2 and 4.9)

The configuration of the BOX surface obtained from the Dynamic Relaxation algorithm, (examples 4.1 and 4.2), has been compared with that obtained for a surface of the same boundary configuration, but generated using a stiffness matrix approach. This comparative study was accomplished using a computational analysis programme, written by Haug, called LISA.(Little documentation is available concerning the mathematical formulation of Haug's numerical approach). The programme has been used extensively by Kneen in the design of a variety of light-weight structures in Australia[4.6]. The programme assumes the surface is discretised using quadratic iso-parametric elements that are of an isotropic linear material. A force per unit width[xi] $F_K = 1\text{kNm}^{-1}$ is assumed during the analysis of example 4.9; convergence is satisfied once $ER \leq 1\text{N}$ i.e. the criterion $ER_{F\%} \leq 0.1$ is used. The form-found solution obtained by the author using this programme is described in example 4.9, (Figure 4-30 (a)), and the principal curvatures of this structure presented in Figure 4-30 (b). The curvatures AA' and BB' of the BOX surface, obtained from the author's 'integrated' form-finding approach, have been plotted against those obtained from LISA, and the results are presented in Figure 4-35 and Figure 4-36 . For a dense mesh arrangement, the solution obtained by the from-finding approach adopted in this thesis, example 4.2, is extremely close to that given by LISA. Indeed, the co-ordinates of the centre points of the numerical surfaces obtained form the two approaches are identical. For the Dynamic Relaxation algorithm, a sparse surface discretisation, as given by example 4.1, was found to take a significantly shorter time to converge than LISA. An equivalent time for convergence was

[xi] The use of a convergence criterion based on F_K is discussed in Section 4.2.

exhibited by a relatively dense surface discretisation (example 4.2) when compared to example 4.9. However, the surface discussed in example 4.2 contains four times as many elements as the solution obtained from LISA, (example 4.9). Hence, the solution procedure using Dynamic Relaxation could be considered to be of a greater efficiency.

Singer et al[4.11] published results relating to a surface conforming to an identical boundary as that presented in examples 4.1 and 4.2. The solution was obtained through a minimisation of the surface area. Visually, the surface quite clearly did not possess a zero mean curvature at its centre point. In addition, the accuracy of Singer's solution is suspect as the area of his solution was given as $250m^2$; a value greater than that for examples obtained from the Dynamic Relaxation algorithm.

(a)

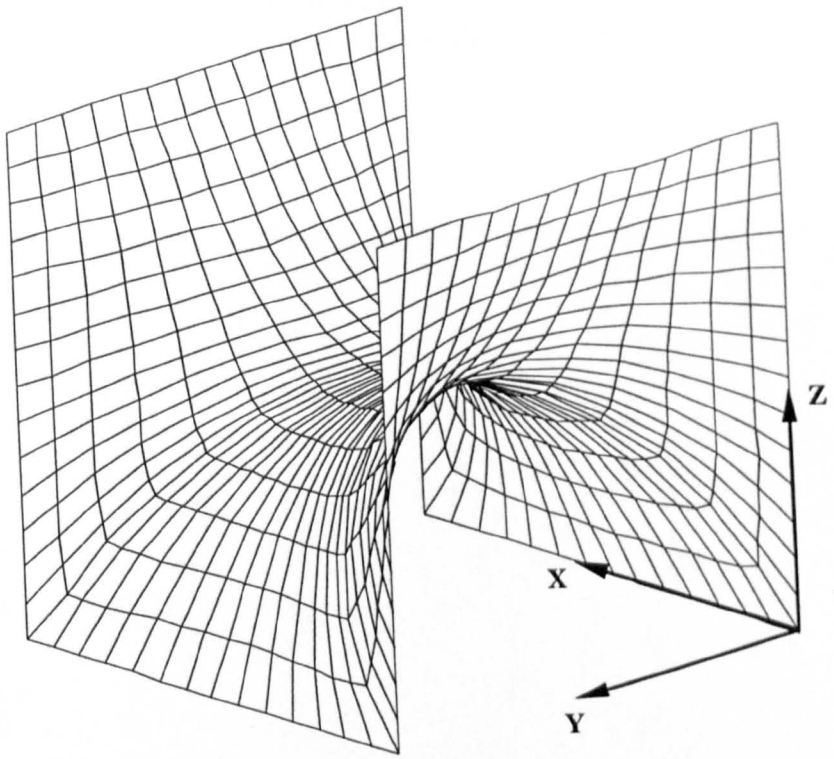

(b)

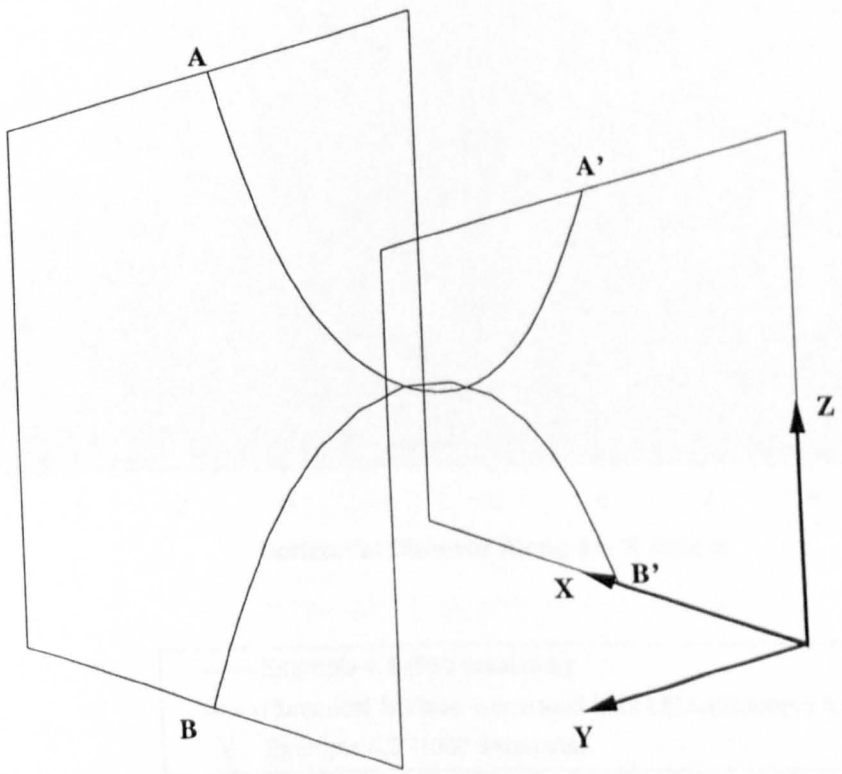

Figure 4-30 Form-Found Surface Obtained Using LISA - Example 4.9 (a) Perspective View. (b) Principal Curvature.

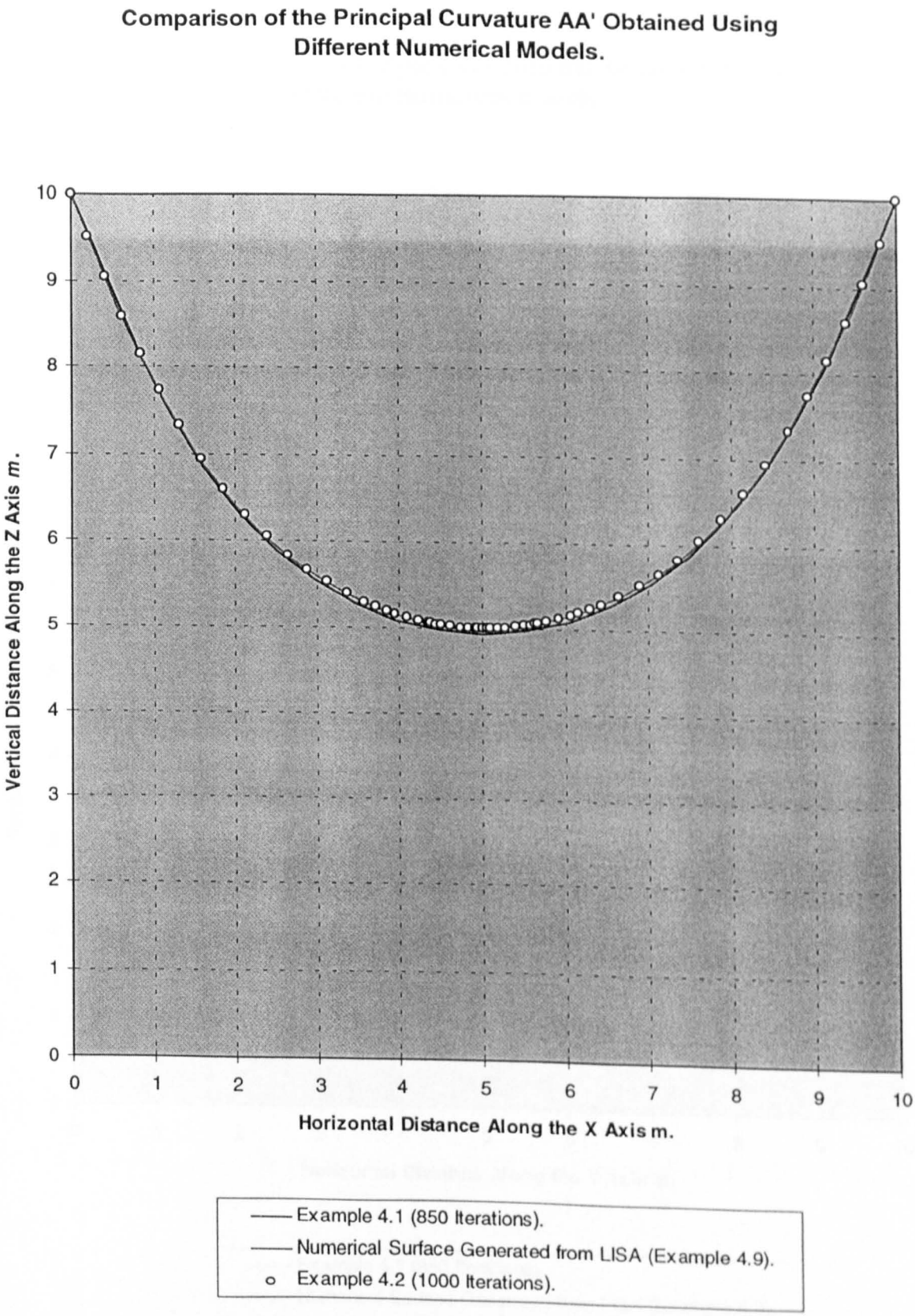

Figure 4-31 Comparison of the Cross-Section AA' ('BOX' Surface) for Different Numerical Models.

Comparison of the Principal Curvature BB' Obtained Using Different Numerical Models.

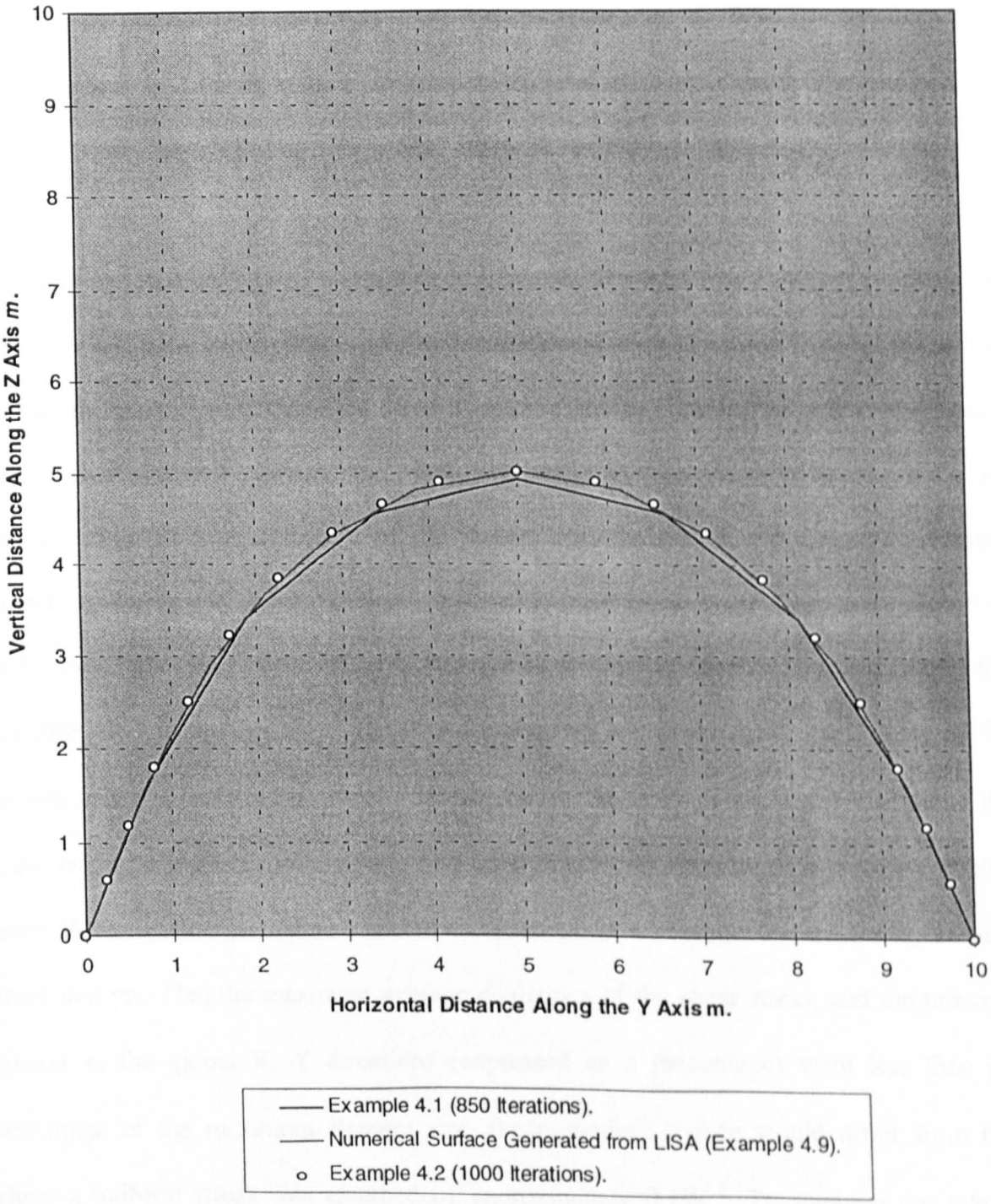

Figure 4-32 Comparison of the Cross-Section BB' ('BOX' Surface) for Different Numerical Models.

Case 4.5.2 Ellipsoid Saddle Surface (Example 4.10).

The final model used for the verification of the form-finding approach is one that has been used previously in investigations by Gosling[4.8]. It consists of a saddle shaped structure whose boundary is of a convex simple projection[xii] of an ellipse onto the X Y plane. The initial surface has **not** been generated using Formian, instead, it has been created from data used previously by Gosling in the analysis of the aforementioned surface[4.8]. The assumptions and approximations of Gosling's numerical approach are summarised below:

The main limitation of Gosling's approach (the essence of which was originally proposed by Barnes[4.4]) lies in the assumption that an element undergoes small strains. This is reflected in the transformation matrix based on Mohr's circle of strain. Further, "pseudo cable" forces were calculated from a stiffness matrix that was based on the geometry of the element at an interval when the kinetic energy of the system had peaked. If the element deformed excessively during successive iterations, the pseudo cable forces were incorrectly related to the "current" geometry of the element. In order to obtain convergence, Gosling relaxed the condition of constant stress by allowing the element to deform while the values of the "pseudo cable" forces were frozen. Subsequently, the stresses necessary to induce the forces in the "current" geometry were evaluated after a stipulated number of kinetic energy peaks. Although the procedure violated the concept of a constant surface stress, Gosling stated that provided the maximum average deviations of the shear stress, and the principal stresses in the global X, Y directions (expressed as a percentage) were less then the percentage of the maximum element size, the numerical surface would differ from that where a uniform stress was assumed by approximately 0.1%[4.8]. To improve the rate of convergence and reduce the stress deviations, Gosling used Hermitian polynomials to

[xii] The term is described in Chapter 2, Section 2.2.

describe an initial surface that approximated the shape obtained from a soap lamina experiment; the soap lamina[xiii] of a geometry conforming to that described in example 4.10 is depicted in Figure 4-35 (a). The method relied on entering values for the co-ordinates at the start and end of the polynomial curve, together with a value for the slope at these points[4.8].

Figure 4-34 shows the numerical model produced from the form-finding approach adopted in this thesis, (example 4.10). To reiterate, the initial surface (Figure 4-33) has been created from data obtained from a Hermitian polynomial approximation, and **not** from using formex algebra. The surface contains 1124 elements and possesses a uniform stress of $5\times10^{+6}\,kNm^{-2}$. Convergence is deemed to have occurred once the criterion $ER_{T\%} \leq 0.025$ is satisfied; a value also used by Gosling in his solution. Figure 4-36 shows the cross-section EE' for the solution generated by the author together with that produced by Gosling. It is clear that the author's method produces a surface almost identical to that given by Gosling's approach. However, convergence has been attained after 634 iterations, whereas that of Gosling's has taken 840 iterations; a marginal improvement. From Figure 4-36 and Figure 4-33, it can be seen how closely the initial surface approximates the final solution. This is reflected by the small value of $A_{\%}$, (Table 4-11). It has been stated by Gosling[4.8] that the discrepancy between the experimental and numerical models is due to the physical boundaries deviating from the theoretically assumed boundary curve. It can be seen from Figure 4-35 (b) that the difficulty in reproducing the experimental model numerically lies mainly in a poorly defined boundary that is not symmetrical about the Z X plane. This has caused the elements used in the numerical solution to deform irregularly i.e. they are not symmetrical about the Z X plane, as described in Figure 4-34 (b). This effect, together with

[xiii] The author would like to acknowledge that the experimental solution, and the data relating to the initial surface used in the form-finding of example 4.10, were obtained from work conducted by Dr. P. Gosling, and recorded in his 1992 thesis (ref. 4.8).

the increased dimensions of the numerical model used by the author - Gosling's numerical model possesses dimensions in mm whereas those used in example 4.10 are in metres and, hence, the surface described in example 4.10 is 1000 times larger than Goslings solution- explains the inability for the author's solution to satisfy a lower value of ER.

Convergence Criterion.	Surface Area	NIT	$A_{\%}$	ER	$ER_{T\%}$	$ER_{F\%}$
$ER_{T\%} \leq 0.025$	20380 m^2	634	1.9	14 kN	1.8×10^{-2}	0.3

Table 4-11 Convergence Criteria used in Example 4.10.

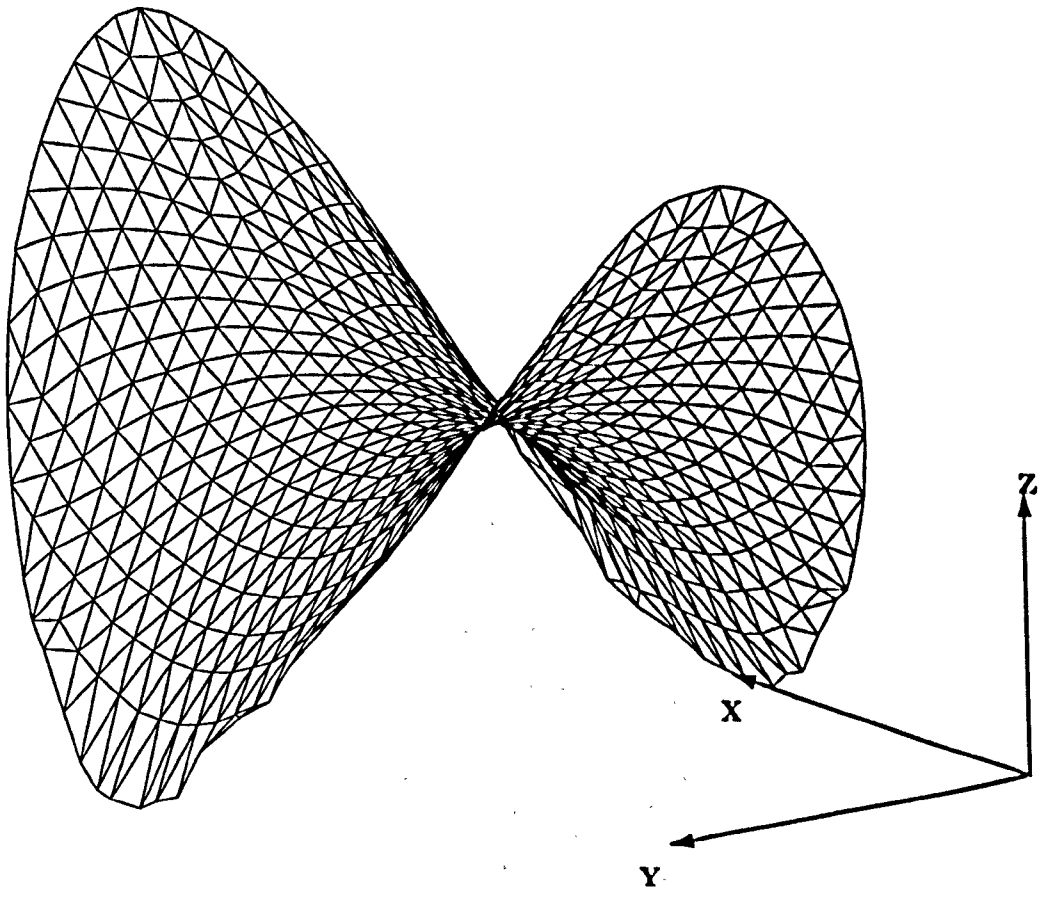

Figure 4-33 Initial Surface Generated form Hermitian Polynomials (Example 4.10).

(a)

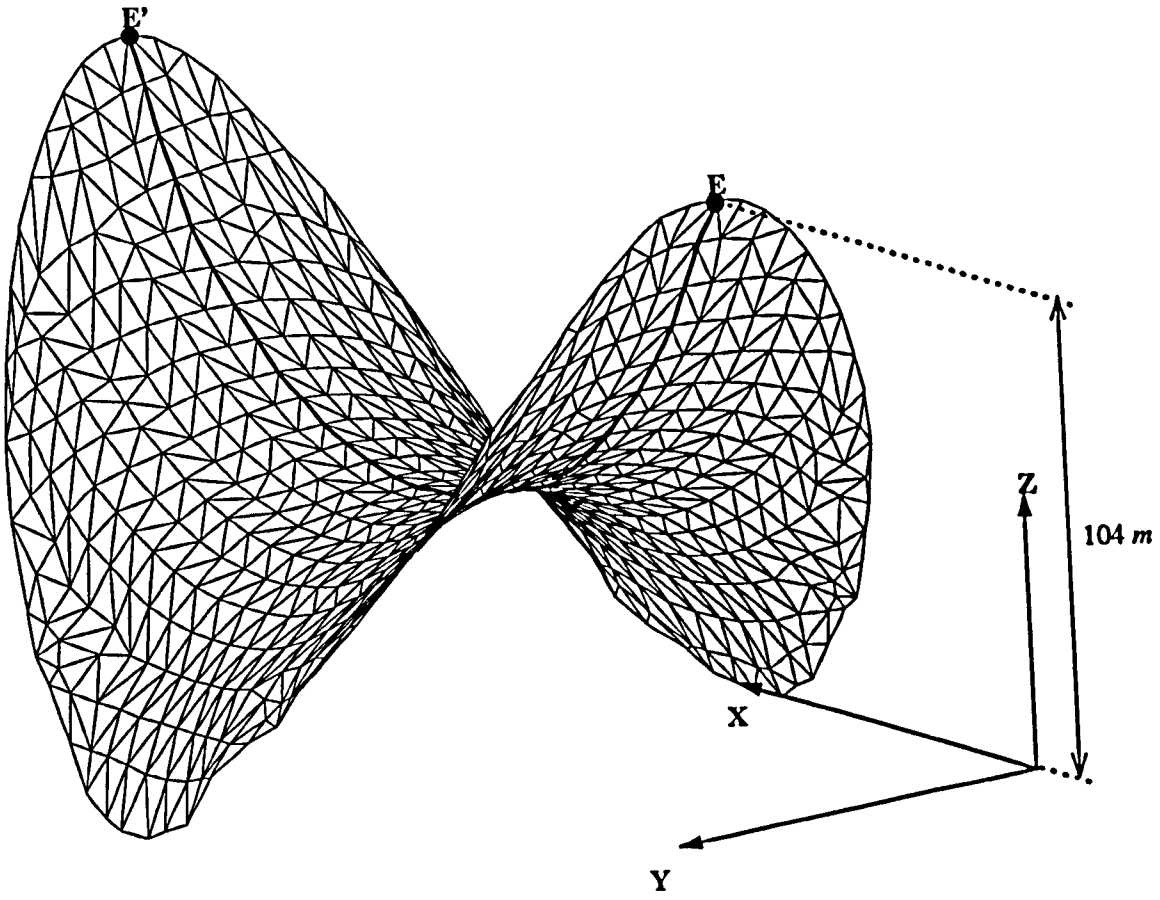

(b)

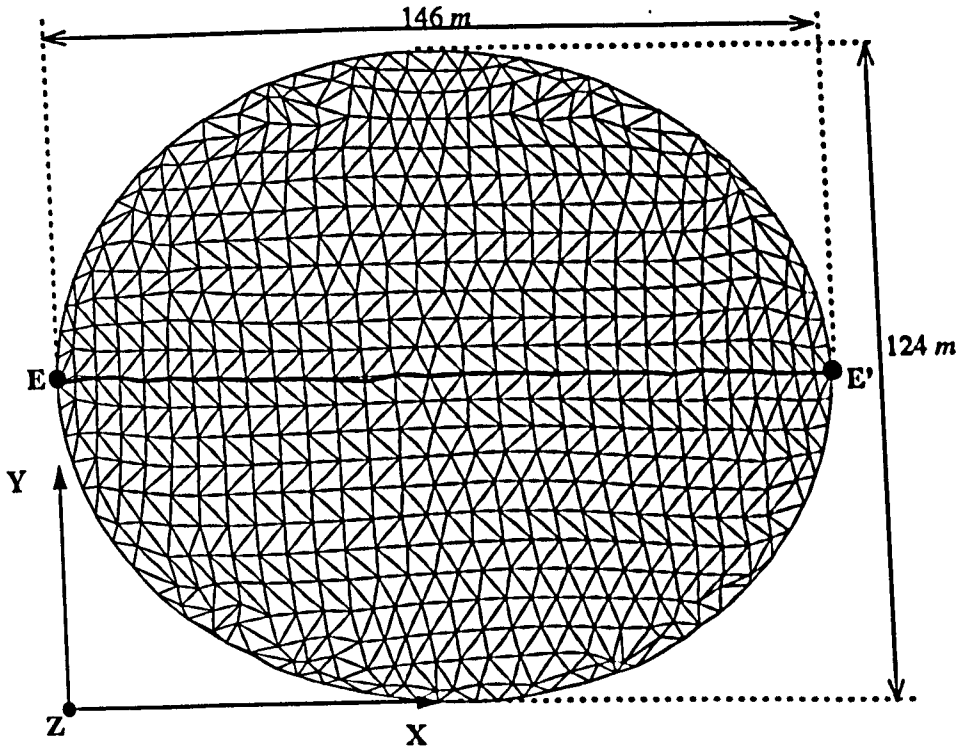

Figure 4-34 Example 4.10 (a) Perspective View. (b) plan View.

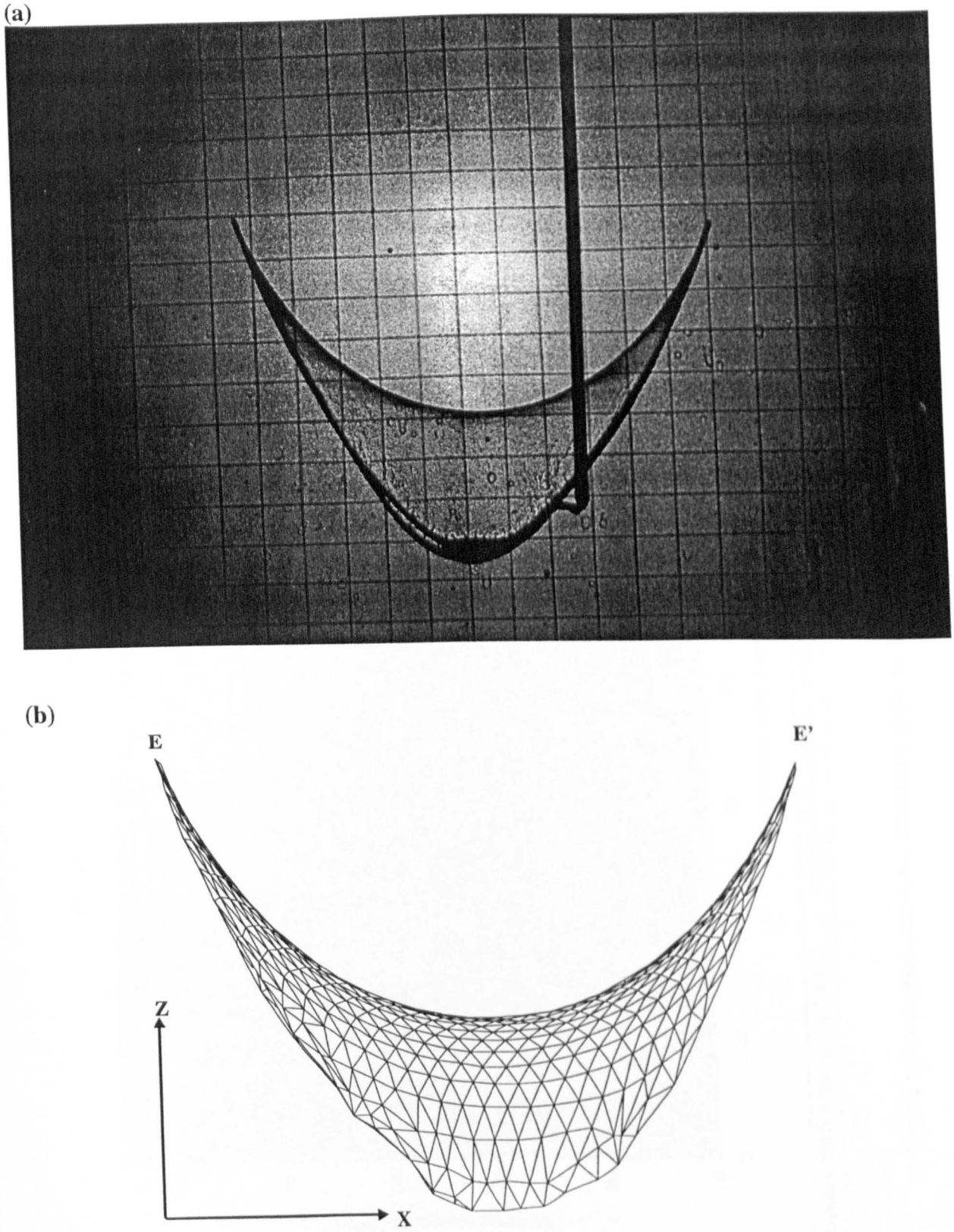

Figure 4-35 Cross-Section EE' (a) Experimental Solution (b) Form-Found Surface (Example 4.10 - 634 Iterations).

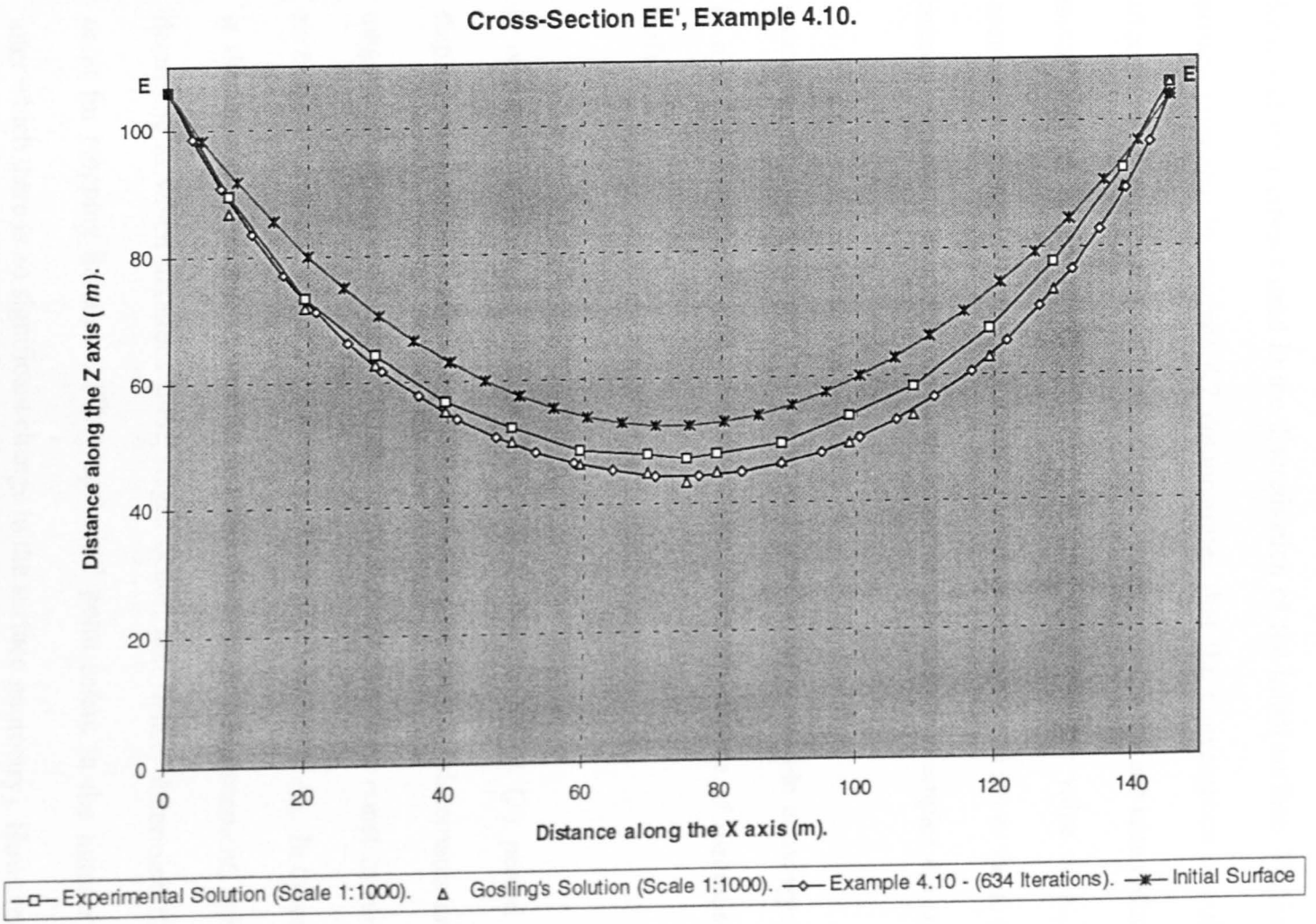

Figure 4-36 Comparison of the Geometry of Cross-Section EE' for Different Models.

4.6 Discussion of Results and Selection of Suitable Convergence Criteria.

- Examples 4.1 and 4.2 show that the accuracy of a form-found surface will depend on the density of the elements used in the discretisation of the initial surface. Furthermore, the surface presented in example 4.2 demonstrates that the convergence criterion, ER, is affected by the degree to which the elements deform, as the surface area reduces from its initial state. It can be concluded therefore, that the lower the value of $A_{\%}$ the more accurate the geometry of the initial surface, and, consequently, a lower value of ER and a reduced number of iterations can be achieved; as described in examples 4.3 and 4.4.

- Examples 4.1 and 4.5 show that the surface area is not a suitable convergence criterion as it is only an approximate value that depends on the degree of discretisation of the surface.

- It is shown in examples 4.1 and 4.4 that during the stage (3) period of analysis; displacements do not influence the overall geometry (the displacements are of a small magnitude and aligned in-plane). Stage (3) is characterised by a constant surface area for successive iterations, which is reflected by the constant value of $A_{\%}$. In these examples, it is shown that by plotting values of the maximum nodal displacement, it is possible to determine at which iterations these stages occur, and hence, determine the 'optimum' point for stopping iterations. (The 'optimum' point refers to the number of iterations after which there is no significant change in the surface geometry). However, this is not a practical solution; it requires the completion of a form-finding analysis in order to know the best moment at which to stop iterations. Nevertheless, the plot is a useful indication of the stability of the solution for the following reason:

A stable surface shows a characteristic decrease in the nodal displacement peaks, as described when comparing the plots for examples 4.4 and 4.5. In contrast, an unstable minimal surface (example 4.4) tends to undergo a continuous reduction in the surface area - again reflected by the value of $A_{\%}$ - with no apparent decrease in the maximum nodal displacements over the total incremental period of analysis.

- Examples 4.2, 4.3 and 4.4 show that the values of ER and $ER_{F\%}$ are arbitrary criteria that depend on the deformation of the elements - as particularly demonstrated in the form-finding of the surface presented in examples 4.2 and 4.8 - and the dimensions and assumed properties of surface stress and thickness, (examples 4.3, 4.4, and 4.10). The adoption of such criteria dose not produce a universal measure of stability and could give a misleading indication that the numerical solution has been reached.

- $ER_{T\%}$ is a non-dimensional measure of the convergence of the solution, as illustrated in examples 4.2, 4.3 and 4.10. Further, in all examples, it is noticeable that $ER_{T\%}$ generally satisfies the criterion $ER_{F\%}$ to a greater extent . For these reasons, $ER_{T\%}$ is the preferred measure of convergence. The dilemma is in choosing what value of $ER_{T\%}$ to adopt as the universal convergence criterion. A wide range of values has been obtained for $ER_{T\%}$, namely:

  1.7 % for a highly deformed, though accurate, stable minimal surface, (example 4.2).

  0.5% for an unstable minimal surface, (example 4.5).

  0.0125% and/or **0.025%** for all remaining examples of stable minimal surfaces.

It is clear that examples 4.2 and 4.5 differ in that the value of $A_{\%}$ for the excessively deformed stable minimal surface presented in example 4.2 is higher, and remains constant for a large number of iterations; unlike that for the unstable surface (Example 4.5) which does not remain constant even for successive iterations. Hence, a surface possessing what might seem a high value of $ER_{T\%}$ can be considered to be in static equilibrium provided $A_{\%}$ is significantly high, and remains constant for a period of iterations. (Both example 4.2 and 4.8 are extreme examples of a poorly defined surface; generally a surface will not undergo the same degree of deformation and reduction in surface area as in these examples and will tend to be lower than 19 %). Furthermore, it is apparent that in all examples, the accuracy of the numerical solution is not significantly improved by using a value lower than 0.025 for $ER_{T\%}$, and, in fact, the selection of such a criterion can be considered to be detrimental to the overall efficiency of the algorithm.

It is suggested that all numerical solutions should aim to satisfy the criterion $ER_{T\%} \leq 0.025$ In addition, $A_{\%}$ should be used as a further measure of the accuracy of the solution i.e. a high value of $A_{\%}$ would suggest that a value of $ER_{T\%}$ greater than 0.025 is acceptable, while a low value of $A_{\%}$ would suggest that a lower value of $ER_{T\%}$ may be achieved for an increased number of iterations if so desired. Further, it is clear that in order to get a more accurate solution, the initial surface must be closer to the form-found surface.

4.7 Summary

This chapter illustrated that the form-finding algorithm used by the author is efficient in producing numerical surfaces that accurately depict stable minimal surfaces, judged by comparisons made with those surfaces generated using analytical equations, soap film experiments and alternative numerical algorithms. Furthermore, the ability to alter the initial surface easily through the use of Formian schemes is shown to be a major advantage in cases where adjustments to the surface geometry or surface discretisation are required. A convergence criterion of $ER_{T\%} \leq 0.025$ is suggested for use in determining the convergence of a stable minimal surface together with the criterion $A_{\%}$.

APPENDIX 4

4A.1 Heron's Formulae

For any triangle with lengths a, b, c the surface area is given by:

$$A = \sqrt{(s(s-a)(s-b)(s-c))}$$

where:

$$2s = a + b + c$$

4A.2 "Catenoid" Formian Scheme.

```
CATENOID='[:m,n,height,radius:
    sum=(2*radius*radius-(height*height))/(2*radius*radius)
    angle=(ACOS|sum)
    x=radius*(COS|(angle/2))
    y=radius-x
    angleu=angle/(2*n)
    rot=(angle/2)+90-angle
    length=radius*2*3.14
    lengthu=length/(2*m)
    arc=5*((angle*3.14)/360)/(2*n)
    a=RINIT(N,M,2,2)|([radius,0,0;radius,2,0;radius,2,2]#..
        [radius,0,0;radius,0,2;radius,2,2])
    b=VERAD(0,0,rot)|BC(1,angleu,1)|a
    c=VERAT(0,0,-90)|b
    d=TRAN(1,radius)|VERAS(0,0,-90)|c
    e=TRAN(3,height/2)|d
    f=TRAN(1,-y)|e
    g=TRAN(1,radius)|f
    surface=BC(1,360/(2*m),1)|g
    USE VM(2), VH(0,0,1,0,5,0,0,5,1)
    CLEAR
    show surface
    totnod=MED|surface
    totmem=DIC(catnod)|surface
    KEEP totnod,mem]'
```

4A.3 Analytical Solution to the Determination of the Surface Area of a Catenoid.

The length of a small chord δs of a curve $y = f(x)$ is given by:

$$\delta s = \sqrt{1+\left(\frac{dy}{dx}\right)^2}\,dx$$

The surface area of a solid formed by rotating the curve about the x axis is given by:

$$A = 2\Pi \int_{c2}^{c1} y\delta s$$

where c1 and c2 represent the value of y over which the surface area is to be calculated, substituting for δs into the above equation gives:

$$A = \int_{c2}^{c1} 2\Pi y \sqrt{1+\left(\frac{dy}{dx}\right)^2}\,dx \qquad \textbf{(4a.1)}$$

Substituting for equation **(4.1)**[xiv] into **(4a.1)** gives:

$$A = 2\times 2\Pi \int_{0}^{L} a\cosh\frac{l}{a} \sqrt{1+\left(\frac{d(a\cosh\frac{l}{a})}{dl}\right)^2}\,dl \qquad \textbf{(4a.2)}$$

where L is the distance from the mid-point of the catenoid to a circular boundary. Through the integration of equation **(4a.2)** the following expression is obtained:

[xiv] The equation is given in Section 4.3 for Case 4.3.2.

$$A = \left[2\Pi a^2 \sinh\left(\frac{l}{a}\right)\left(1+\left(\sinh\left(\frac{l}{a}\right)\right)^2\right)^{\frac{1}{2}} + 2\Pi a^2 \sinh^{-1}\left(\sinh\left(\frac{l}{a}\right)\right)\right]_0^L \qquad \textbf{(4a.3)}$$

Simplifying **(4a.3)** gives equation **(4.4)**; as documented in Section 4.3 for Case 4.3.2.

$$A = 2\Pi a\left[L+\frac{a}{2}\sinh\left(\frac{2L}{a}\right)\right] \qquad \textbf{(4.4)}$$

4A.4 Derivation of the Maximum Height, H_{MAX}, of a Catenoid.

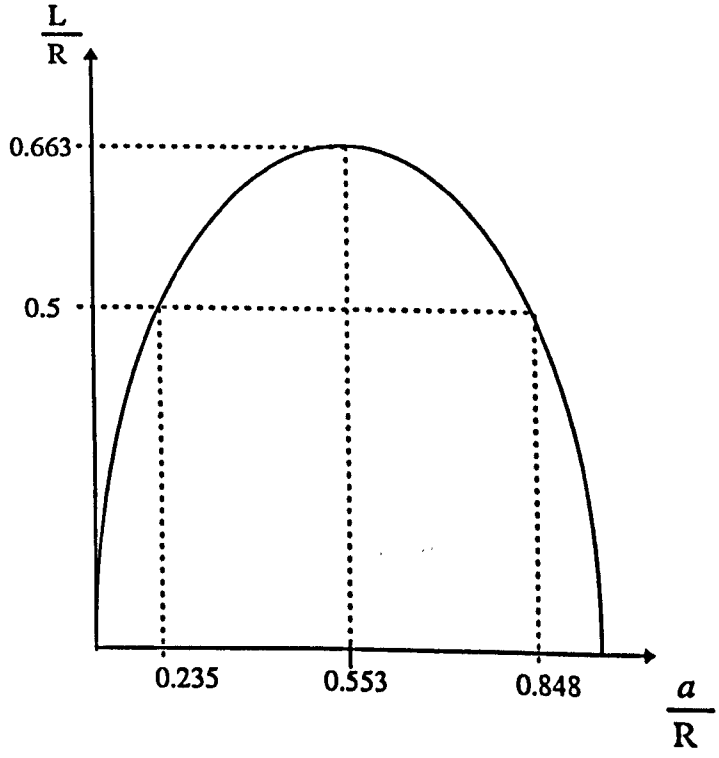

Figure 4A-1 Variation of *a* with L - Derivation of the Maximum Catenoid Height.

For the instance when *r* is equivalent to the radius R of the boundary rings of the catenoid[xv] and the length is equal to the distance L, equation **(4.1)** gives:

$$R = a\cosh\left(\frac{L}{a}\right) \qquad \textbf{(4a.4)}$$

[xv] The height of a catenoid is given by 2×L.

From Figure 4A-1 it can be seen that the maximum value of L is for the instance when $\frac{dL}{da}$ is equal to zero. Differentiating equation **(4a.4)** w.r.t. *a* gives,

$$0 = \cosh\frac{L}{a} + a\left(\frac{d\left(\cosh\frac{L}{a}\right)}{da}\right) \qquad \textbf{(4a.5)}$$

where,

$$\frac{d\left(\cosh\frac{L}{a}\right)}{da} = \left(\frac{a\frac{dL}{da} - L}{a^2}\right)\sinh\frac{L}{a} \qquad \textbf{(4a.6)}$$

At the maximum length, $L=L_{MAX}$ and $\frac{dL}{da} = 0$. Substituting these values into equation (4a.6) allows equation (4a.5) to be reduced to:

$$\frac{L_{MAX}}{a} = \coth\frac{L_{MAX}}{a} \qquad \textbf{(4a.7)}$$

The numerical solution to equation (4a.7) is given by,

$$\frac{L_{MAX}}{a} = 1.2$$

Substituting this value into equation (4a.4) gives:

$$R = \frac{L_{MAX}}{1.2}\cosh(1.2)$$

The maximum length is thus equal to:

$$\boxed{L_{MAX} = 0.6627 \times R} \qquad \textbf{(4a.8)}$$

Hence, the maximum catenoid height H_{MAX} is given by $2 \times L_{MAX}$ or,

$$\boxed{H_{MAX} = 1.325 \times R} \qquad \textbf{(4a.9)}$$

and the cross-section radius at H_{MAX} is given by:

$$a = 0.553 \times R \qquad \textbf{(4a.10)}$$

4A.5 "Polygon" Formian Scheme.

```
POLYGON=['n,height,r,r2,side:
 mid=n+1
 end=n-1
 rot=360/side
 nrot=rot/2
 base=2*(r2*(TAN|nrot))
 width=base/2
 b1=(r2-r)/(2*n)
 b2=(width-r*(TAN|nrot))/n
 mid=width/b2
 ext=2*mid-n
 b3=height/(2*n)
 a1=2*n
 a2=ext+n
 triangl1=LIB(I=0,end)|[(0-(I*2)),(0+I),(0+(I*2));..
        (-1-(I*2)),mid,(1+(I*2));(-2-(I*2)),..
        (1+I),(2+(I*2))]
 triangl2=LIB(I=0,end)|[0-(I*2),(A2-I),(0+(I*2));..
        (-2-(I*2)),((A2-1)-I),(2+(I*2));(-1-(I*2)),..
        mid,(1+(I*2))]
 triangl3=[0,0,0;0,A2,0;-1,mid,1]
 triangl4=[-A1,n,A1;-(A1-1),mid,A1-1;-A1,ext,A1]
 triangla=LIB(I=1,N-1)|[-((2*I)-1),mid,(2*I)-1;-(2*I),I,2*I;..
        -((2*I)+1),mid,(2*I)+1]
 trianglb=LIB(I=1,N-1)|[-((2*I)-1),mid,(2*I)-1;-(2*I),A2-i,2*I;..
        -((2*I)+1),mid,(2*I)+1]
 segment=triangl4#triangl1#triangla#trianglb#triangl2#triangl3
 surf=BT(b1,b2,b3)|segment
 surface=ROSAD(-r2,width,side,rot)|surf
 totnod=MED|surface
 mem=DIC(totnod)|surface
 CLEAR
 USE VM(2),VT(2),..
    VH(20,0,20,0,0,0,0,0,1)
 SHOW surface
 KEEP mem, totnod]'
```

4A.6 "Weir" Formian Scheme.

```
WEIR = a'[ :m,n,height,length,width:
    tri1=[0,0,0;2,0,-2;1,1,-1]
    tri1=RINAX(0,0,0,2,0,-2,m)|tri1
    tri2=[1,1,-1;2,0,-2;3,1,-3]
    tri2=RINAX(1,1,-1,3,1,-3,(m-1))|tri2
    tri3=[1,1,-1;3,1,-3;2,2,-2]
    tri3=RINAX(1,1,-1,3,1,-3,(m-1))|tri3
    tri4=[0,2,0;1,1,-1;2,2,-2]
    tri4=RINAX(0,2,0,2,2,-2,m)|tri4
    tri5=[0,0,0;1,1,-1;0,2,0]
    lastnode=2*m
    tri6=[(lastnode-1),1,-(lastnode-1);lastnode,0,-lastnode;..
          lastnode,2,-lastnode]
    segment=tri1#tri2#tri3#tri4#tri5#tri6
    surf=RINAX(0,0,0,0,2,0,n)|segment
    surf=LAM(1,lastnode)|surf
    u1=width/lastnode
    u2=length/(2*n)
    u3=height/lastnode
    bound1=LAM(1,2*m)|(LAM(2,n)|(RINAX(0,0,0,2,0,-2,(m+1))|[0,0,0]))
    bound2=LAM(1,2*m)|(RIN(2,n+1,2)|[0,0,0])
    bound=PEX|(bound1#bound2)
    bound=BT(u1,u2,u3)|bound
    surface=BT(u1,u2,u3)|surf
    interior=MED|(LUX(bound)|surface)
    totnod=bound#interior
    memb=DIC(totnod)|bound
    mem=DIC(totnod)|surface
    USE VM(2),VP(0,0,30)
    CLEAR
    SHOW surface
    KEEP totnod,mem,memb]'
```

REFERENCES

4.1 M. R. Barnes,
"Pre-stressed Cable Networks."
Construction Research and development Journal, 1971.

4.2 M. R. Barnes,
"Applications of Dynamic Relaxation to the Design and Analysis of Tension Structures by Dynamic Relaxation."
2nd International Conference on Space Structures, Guildford, 1975.

4.3 M. R. Barnes,
"Form and Stress Engineering of Tension Structures."
Structural Engineering Review, vol. 6, no. 3-4, pages 175-202, 1994.

4.4 M. R. Barnes,
"Form-Finding and Analysis of Pre-stressed Nets and Membranes."
Proceedings of the International Conference on Non-Conventional Structures, Volume 1, 1987, pages 327-338.

4.5 L. Grundig,
"Minimal Surfaces for Finding Forms of Structural Membranes."
Computers and Structures, vol. 30, no. 3, pages 679-683 1988.

4.6 P. Kneen,
"Computer Aided Design of Tensioned Fabric Structures."
LSA 86, 1st International Conference on Light Weight Structures in Architecture, Sydney, 1986, proceedings vol. 2, pages 992-1009.

4.7 P. D. Gosling and W. J. Lewis,
"Computer Modelling of Stable Minimal Surfaces."
Research Report CE 32, Department of Engineering, University of Warwick, 1990.

4.8 P. D. Gosling,
"Numerical Modelling of Stable Minimal Surfaces."
PhD Thesis, Dept. of Civil Engineering, University of Warwick, 1992.

4.9 S. Hildebrandt,
"Minimal Surfaces- A Short History."
Forming Bubbles, IL (Institute of Light Weight Structures, University of Stuttgart.) No. 18,1987, pages 310-317.

4.10 K. Ishii and T. Suzuki,
"Shape of Membrane Structures."
Proceedings of IASS Symposium, part 2 on Tension Structures and Space Frames, Tokyo and Kyoto, 1972, pages 127-136.

4.11 P. Singer, D. Strobel, R. Hordt and J. Bahndorf,
"A Method for Finding Minimal Surfaces."
2nd International Symposium SFB230, Stuttgart, 1991, pages 137-142.

4.12 D. Trong Thi, A.T. Fomenko,
"Minimal Surfaces, Stratified Multivarifolds and the Plateau Problem."
American Mathematical Society, 1991, pages 32-34.

4.13 C. Isenberg,
"The Science of Soap Films and Bubbles."
Teito Ltd., 1978.

4.14 K. Bach, B. Burkhardt, F. Otto,
"Forming Bubbles."
IL (Institute of Light Weight Structures, University of Stuttgart.) No. 18,1987, pages 310-312.

CHAPTER 5

Further Examples of Numerical Solutions to Stable Minimal Surfaces.

5.1 Introduction.

The versatility of the form-finding approach is described within this chapter. A variety of surfaces with contrasting geometrical boundaries are generated. They illustrate possible structural configurations suitable for the definition of the geometry of a light-weight tension structure. All the numerical solutions contained within this chapter satisfy the criterion $ER_{T\%} \leq 0.025$[1]. The induction statements of the schemes used in the generation of the initial surfaces are presented in Table 5-1, (the composition of the schemes themselves are documented in Appendix 5), together with the number of iterations necessary for convergence (NIT) and the surface areas of the initial and form-found surfaces. In addition, the criterion $A_{\%}$ is also presented in Table 5-1 as a means of assessing the accuracy of the numerical solution (Chapter 4, Section 4.6). Some of the schemes used in the generation of an initial surface are of a paragenic formex formulation. The term refers to formex expressions that have been generated by applying a retronorm to a formex that has been transformed previously using a similar, or different retronorm (Chapter 3, Section 3.2.2.5). The technique allows one to create non-conventional geometrical configurations through different combinations of standard retronorm functions.

A new type of stable minimal surface is introduced within this Chapter. Unlike the numerical solutions to stable minimal surfaces described previously, the surfaces presented in examples 5.2.6, 5.2.7.1 and 5.2.7.2 are generated between flexible boundaries. The form-finding

[1] $ER_{T\%}$ relates to the percentage of the maximum residual nodal force component to the maximum 'pseudo' cable force, (Chapter 4, Section 4.2).

algorithm is amended to take account of flexible cables that possess a constant tension force. (The contribution to the tension force from the elastic straining of the cable is neglected - the force is purely geometric. However, the contribution from the geometric forces of the triangular membrane elements joined to the flexible cables is not neglected. Furthermore, it is necessary to further generate data relating to the node numbers forming the links of a flexible cable. This is not accomplished through using Formian, instead, the data has been entered by hand using a suitable data file editor). For these examples, the boundaries are not rigid and therefore a wire boundary is no longer appropriate to model this situation experimentally. To overcome this, the surface would be modelled by adopting cotton threads (attached to some fixed points) to represent the enclosing flexible boundary of the soap laminae and any cables spanning from the boundary over the surface. Soap laminae models of this type were used extensively by Frei Otto in the design of a wide range of light-weight tension structures (Chapter 2, Section 2.2). The numerical modelling of stable minimal surfaces possessing flexible cables differs from those where a rigid boundary encloses the surface, as the cables will influence the shape of the membrane, and if the magnitude of the cable force is not chosen judiciously, the cables can dictate the shape. To elaborate, consider once more a soap lamina enclosed by cotton threads. It is apparent that increasing the tautness of the threads will increase the rigidity of the boundary, and for the case where threads span across the surface of the lamina, the threads will 'lift' the surface i.e. the threads dictate the shape of the soap film. If the threads are relaxed, then the soap lamina will dictate the deformations i.e. the magnitude of the deformation of the threads and surface will depend on how lax the threads are initially.

In all the examples where a rigid boundary encloses the stable minimal surface (Table 5-1), the surface stress σ_S is equal to $5\times10^{+6}$ kNm^{-2}. For those surfaces that possesses flexible

cables (examples 5.2.6, 5.2.7.1 and 5.2.7.2 (Table 5-1)) the surface pre-stress is 1×10^{3} kNm^{-2}. The membrane thickness is equivalent to 1×10^{-3} m for all the examples.

5.2 Examples of Stable Minimal Surfaces.

EXAMPLE	INDUCTION STATEMENT	NIT	SURFACE AREA (m^2)		$A_{\%}$
			Initial	*Final*	
5.2.1 (Rigid Boundary).	SCHEME1(8,4,0.02,10,10)	564	119	112	6
5.2.2 (Rigid Boundary).	SCHEME2(10,20,5,10,70)	318	556	551	0.9
5.2.3 (Rigid Boundary).	SCHEME3(6,12,2.5,10,5)	687	112	106	5
5.2.4 (Rigid Boundary).	SCHEME4(5,10,40,23.094,5,6)	668	4236	4135	2
5.2.5.1 (Rigid Boundary).	SCHEME5(15,20,20,10,20,10)	679	535	484	10
5.2.5.2 (Rigid Boundary).	SCHEME5(10,18,20,6,20,0)	831	445	425	4
5.2.5.3 (Rigid Boundary).	SCHEME5(10,18,30,5,20,0)	517	650	621	4
5.2.6 (Flexible Boundary)	SCHEME6(8,0.02,5,3)	654	95	92	3
5.2.7.1 (Flexible Boundary)	SCHEME7(8,0.02,5)	679	96	91	5
5.2.7.2 (Flexible Boundary)	SCHEME7(6,0.02,5)	432	103	87	16

Table 5-1 Results Relating to the Numerical Solutions contained within Chapter 5.

Example 5.2.1

SCHEME1(m,n,p,width,length)

A hyperbolic paraboloid is an example of a doubly curved surface that is generated from a series of straight lines; it is often referred to as a ruled surface. Using a suitable normat arrangement, the basi-hyperbolic retronorm (**BHP**) can be used to transform a flat plane into a hyperbolic paraboloid[5.1]. The retronorm requires a value called the 'pitch', parameter 'p' of **SCHEME1**, for the definition of the curvature of the surface; the higher the value the more pronounced the curvature of the surface. A hyperbolic paraboloid can be subdivided into four quadrants, where each quadrant is separated from one another by the intersection of the two lines that pass through the centre point, 'saddle point', (origin of the normat - Figure 5-1) of the surface; these lines are horizontal and orthogonal to each other. This geometric property is exploited in the generation of the initial surface of example 5.2.1 (Figure 5-1). Here, one quadrant of a hyperbolic paraboloid is generated from the configuration pattern containing 'm' elements in the X global direction and 'n' elements in the Y axis direction. The quadrant is then reflected about a plane intersecting the Y axis at the normat point labelled 'n' (Figure 5-1 (a)) to give the desired configuration pattern. The configuration pattern is then scaled in the X and Y directions in accordance with the parameters supplied in the induction statement. The vertical height of the surface is given by $8\times(m\times n\times p)$, and hence depends on the configuration pattern of the surface before scaling. Invoking the statement **SCHEME1(8,4,0.02,10,10)** produces an initial surface with a vertical height of 5.12 m, and planar dimensions of 10 m×10 m. Figure 5-2 (c) illustrates the graphical rendering of the surface (example 5.2.1); the procedure enhances the aesthetic appeal of the structure, and highlights the structural "lightness" of the form. The marginal headroom offered by the structure would suggest that it would not be an appropriate means

of covering on its own. It is perhaps more suitable for providing cover over a conventional building, where the horizontal boundary edges would be ideally suited to the regular arrangement of a building.

Further post-processing has led to the construction of a rigid model of the numerical surface using the scheme **RPM1(8,4,0.02,10,10,0.5,1)**[ii]. The first five parameters of the scheme are identical to those used in the generation of the initial surface, and are necessary to determine the positions of the nodes joining the form-found surface, formex 'f_fin1', with those of the enclosing support, formex 'support' (Appendix 5, Section 5A.2). In addition, 'depth_1' and 'depth_ 2' correspond to the thickness of the model (Figure 5-3 (a)). Two rigid models of the numerical surface are illustrated in Figure 5-3 (c), both are of a scale 1:50.)

[ii] The process by which a physical model is constructed is included in Chapter 3, Section 3.4.

(a)

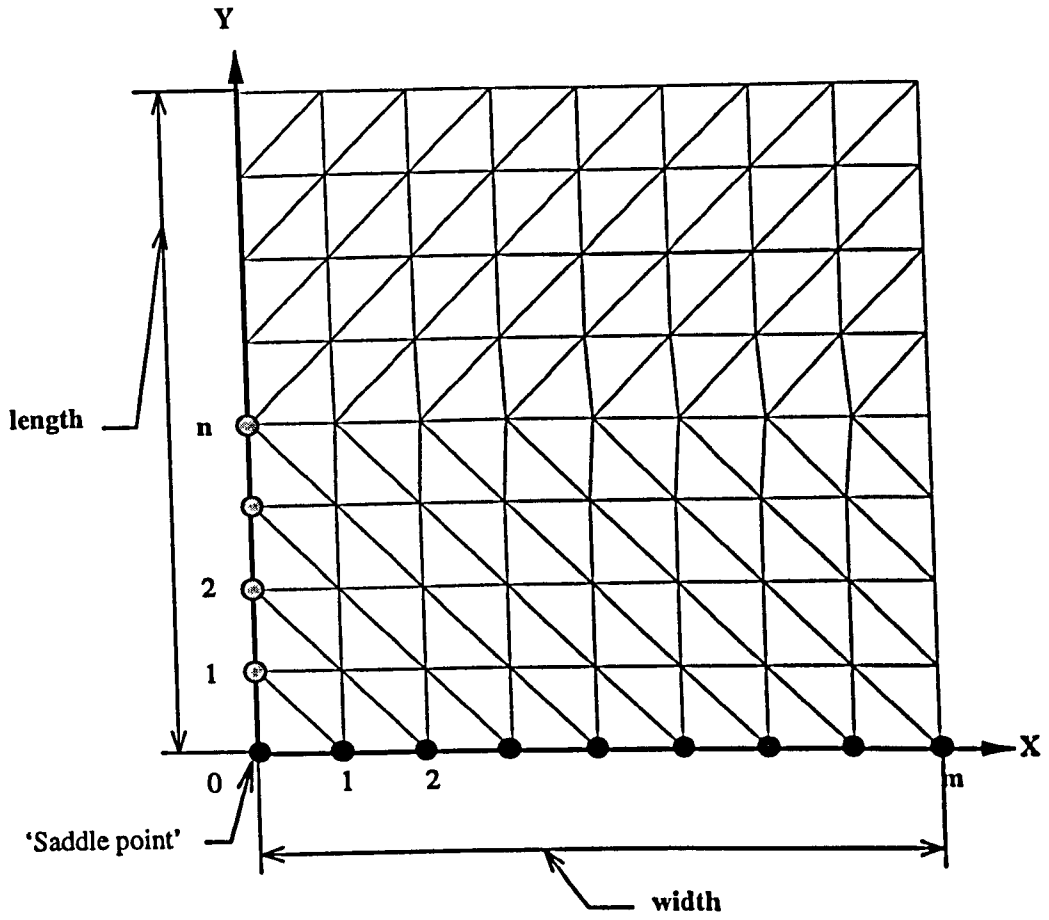

(b)

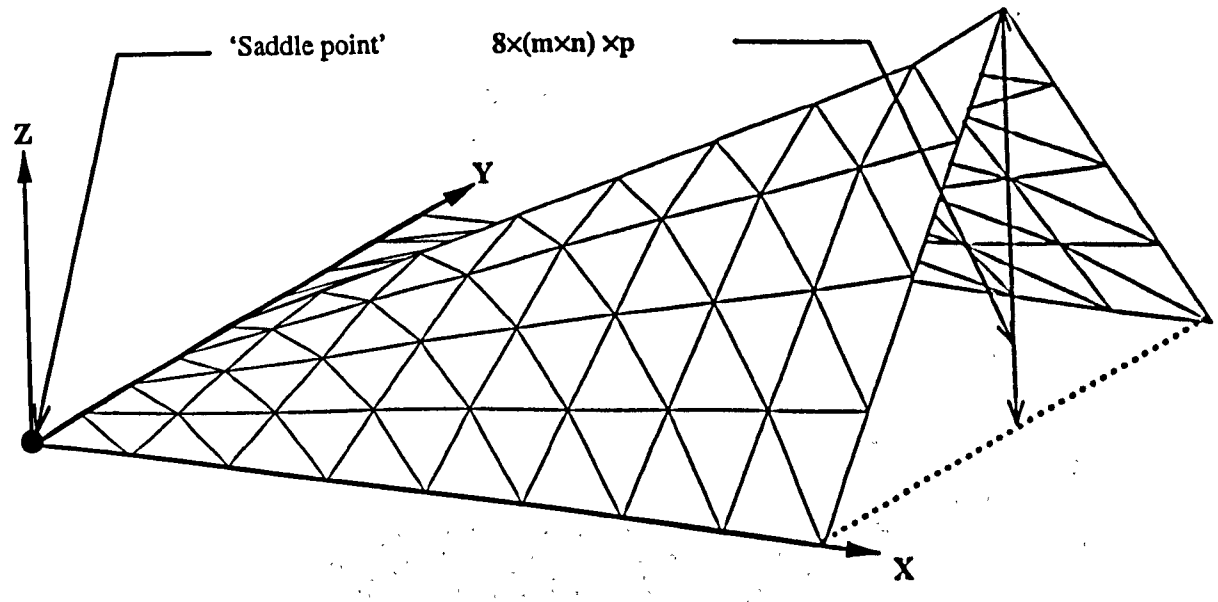

Figure 5-1 Initial Surface (Example 5.2.1) (a) Plan View. (b) Perspective View.

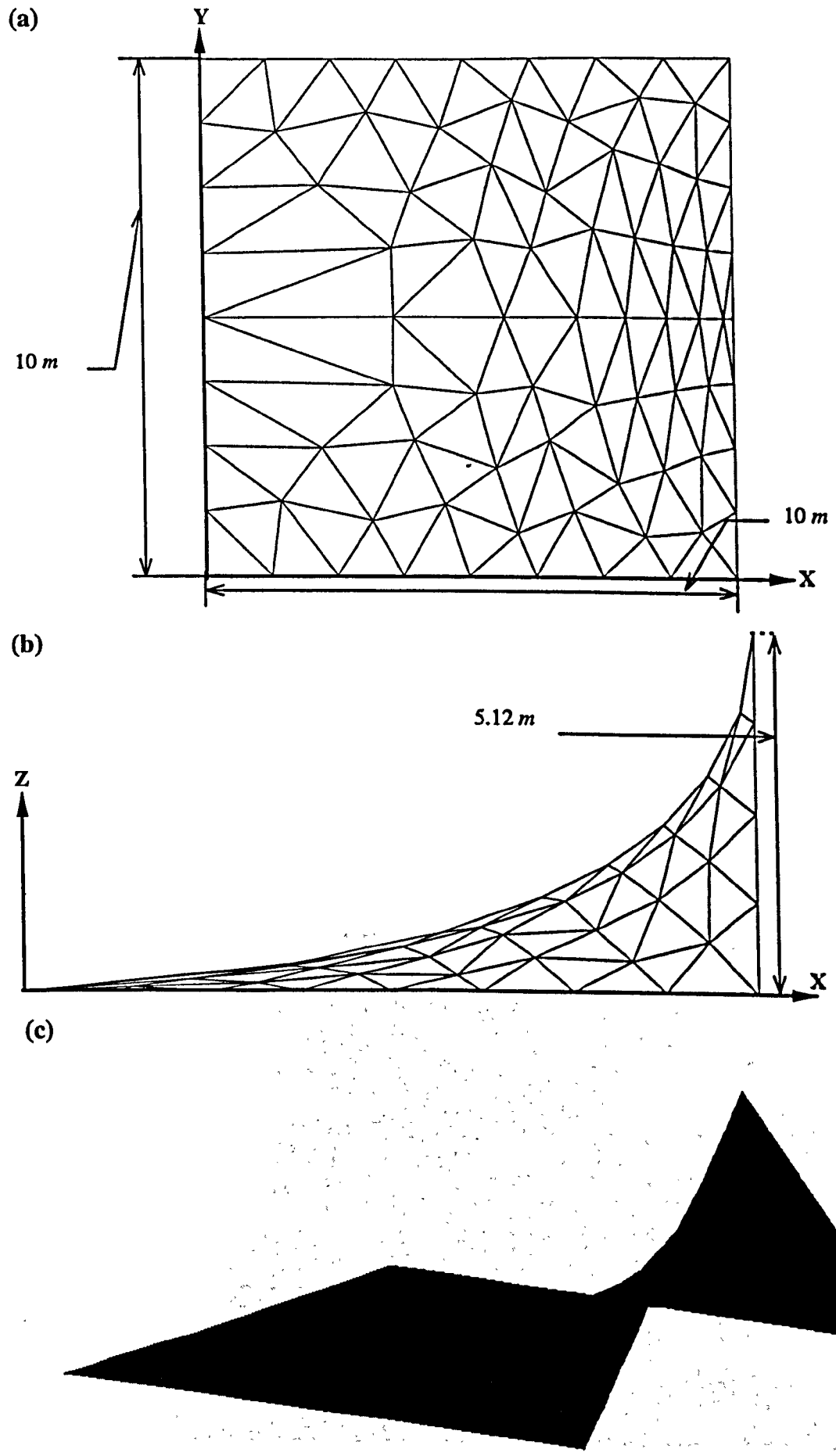

Figure 5-2 Example 5.2.1 (a) Plan View. (b) Side Elevation. (c) Rendered Perspective View.

(a)

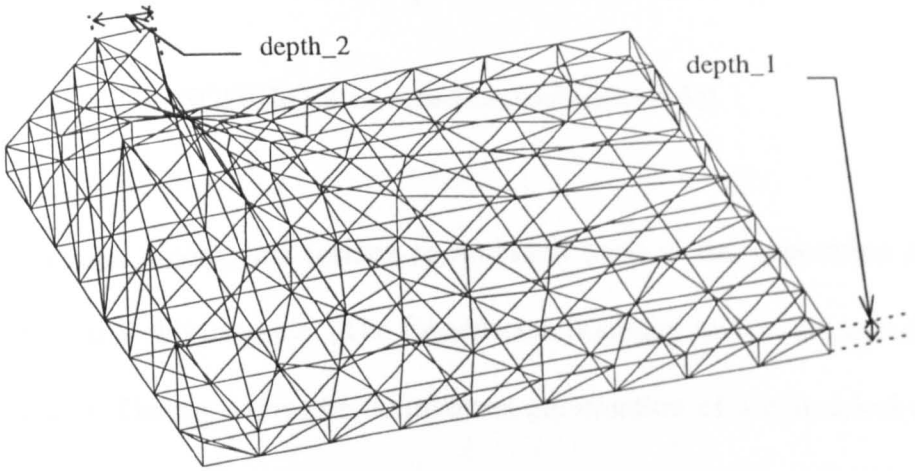

(b)

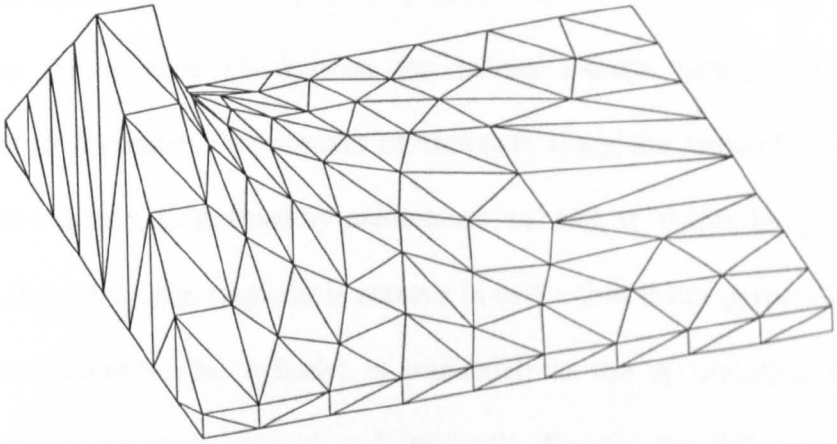

(c)

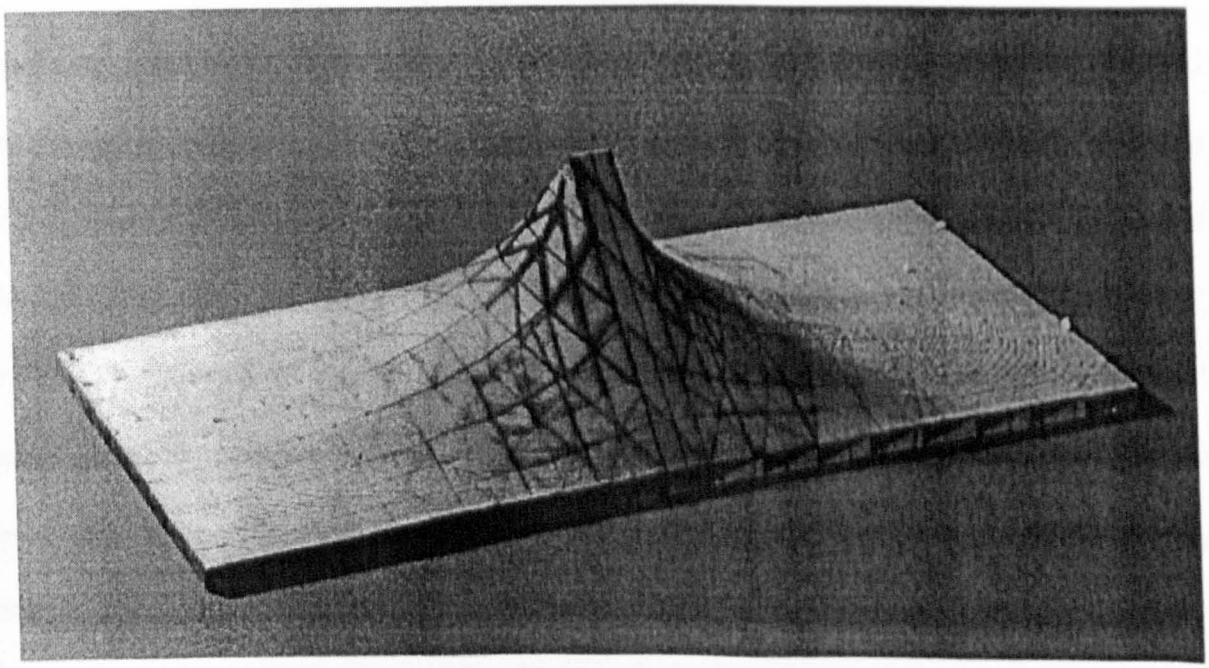

Figure 5-3 Rapid Prototype Construction (Example 5.2.1) (a) Tessellated Model - Internal View. (b) Tessellated Model - External View. (c) Physical Model.

Example 5.2.2

SCHEME2(m,n,radius,radius2,angle)

A simple example of a paragenic formex formulation used in the generation of an initial surface is presented in this example. (The formulation is similar to that discussed in Chapter 3, Section 3.2.2.5). The procedure firstly involves the creation of a cylindrical segment, or barrel vault, from the configuration pattern produced by the basi cylindrical retronorm (BC). The radius of the cylinder is specified by the parameter 'radius2' while the parameter 'angle' specifies the number of degrees the radius sweeps through in defining the circumference of the cylinder. The number of elements along the circumference and length of the cylindrical segment are defined by parameters 'm' and 'n' respectively (Figure 5-4 (a) and Figure 5-4 (b)). Next, the segment is rotated in order that it lies perpendicular to the Y global axes. Subsequently, the cylinder is translated in the X direction by an amount dependent on the parameters 'radius' and 'radius2'. Finally, the BC retronorm is again applied for the 360 degree rotation of the displaced cylinder about the Z axes thereby producing a doubly curved conical 'tent like' surface. The effect of the aforementioned geometrical transformations on the overall dimensions of the initial surface is described in Figure 5-4. It is apparent that parameters 'm' and 'n' will respectively dictate the number of elements in the radial and circumferal directions (Figure 5-4 (a)). In addition, 'radius' governs the value of the radius of the top boundary, while parameters 'radius2' and 'angle' define both the curvature of the surface's side profile, and the vertical distance separating the boundaries. As previously stated, the initial surface created from 'SCHEME2' is doubly curved, and is hence well defined; it approximates the final form-found surface closely, as reflected by the low value of $A_{\%}$ (Table 5-1), the small number of iterations (NIT) necessary

for convergence (Table 5-1), and the negligible distortion of the elements of the form-found surface (Figure 5-5 (b)).

The rigid model of example 5.2.2 is manufactured from data obtained through invoking the induction statement **RPM2(10,20,5,10,70,0.5).** The first five parameters correspond to those used in the induction statement (Table 5-1) responsible for the creation of the initial surface depicted in Figure 5-4. The final parameter relates to the depth, 'depth', of the enclosing support of the tessellated model. It is clear from the aforementioned induction statement that 'depth' is of a value of 0.5 m (Figure 5-6 (a)). The actual physical representation of example 5.2.2 is shown in Figure 5-6(c), and is of a scale 1:100.

(a)

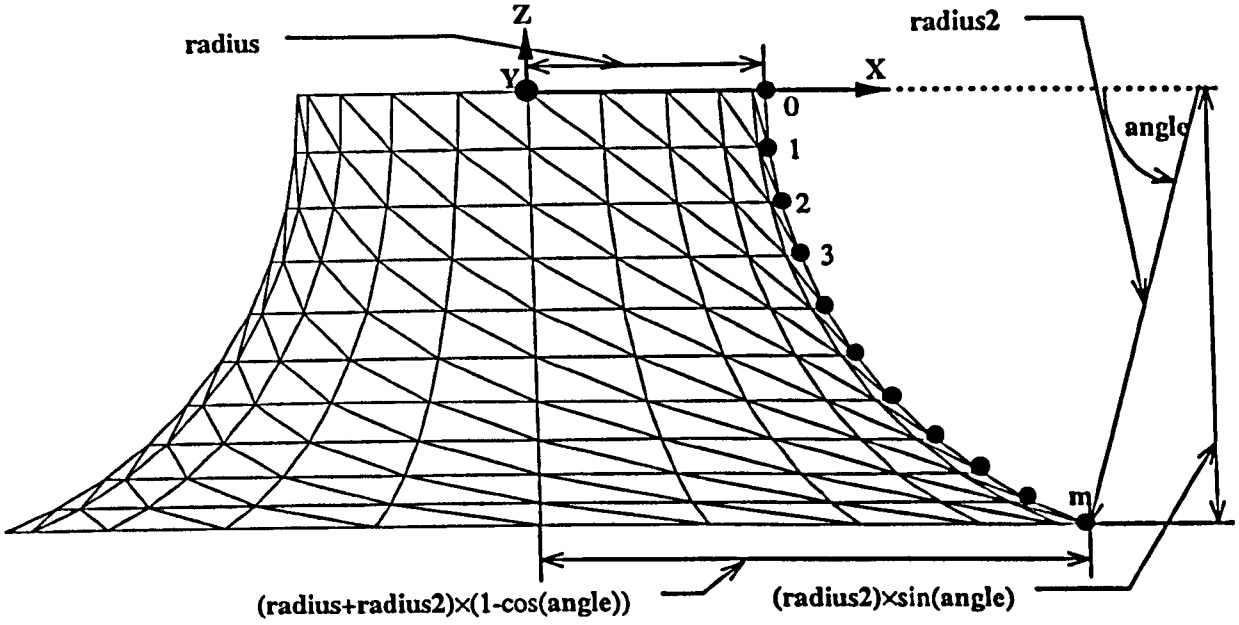

(b)

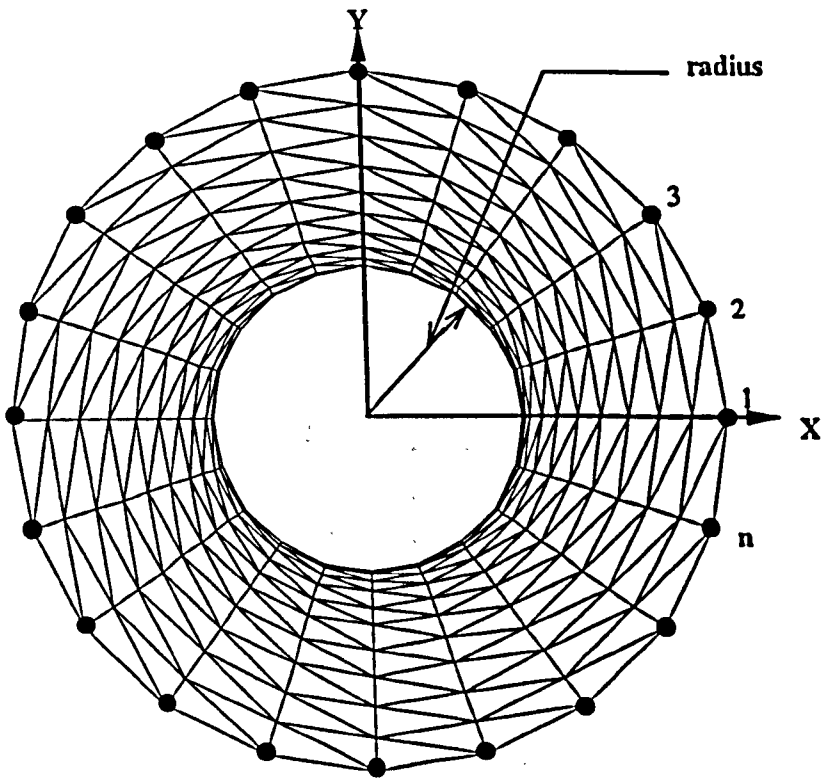

Figure 5-4 Initial Surface (Example 5.2.2) (a) Side Profile. (b) Plan View.

(a)

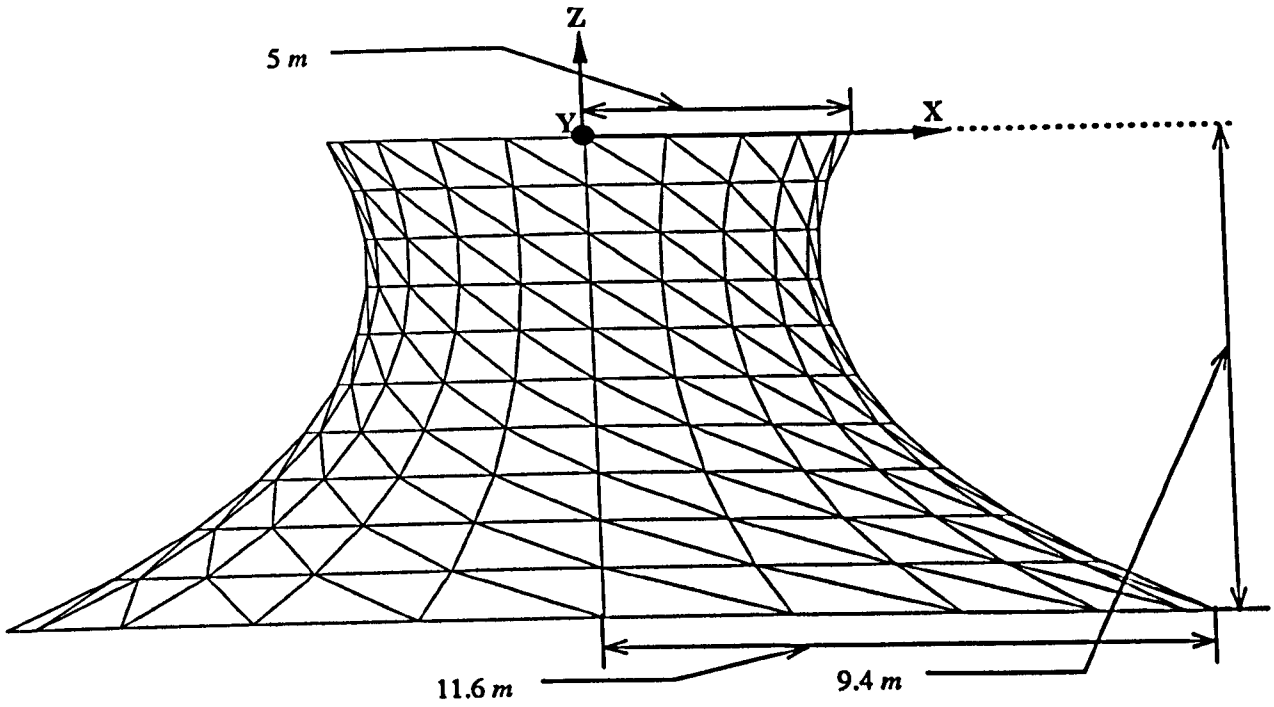

(b)

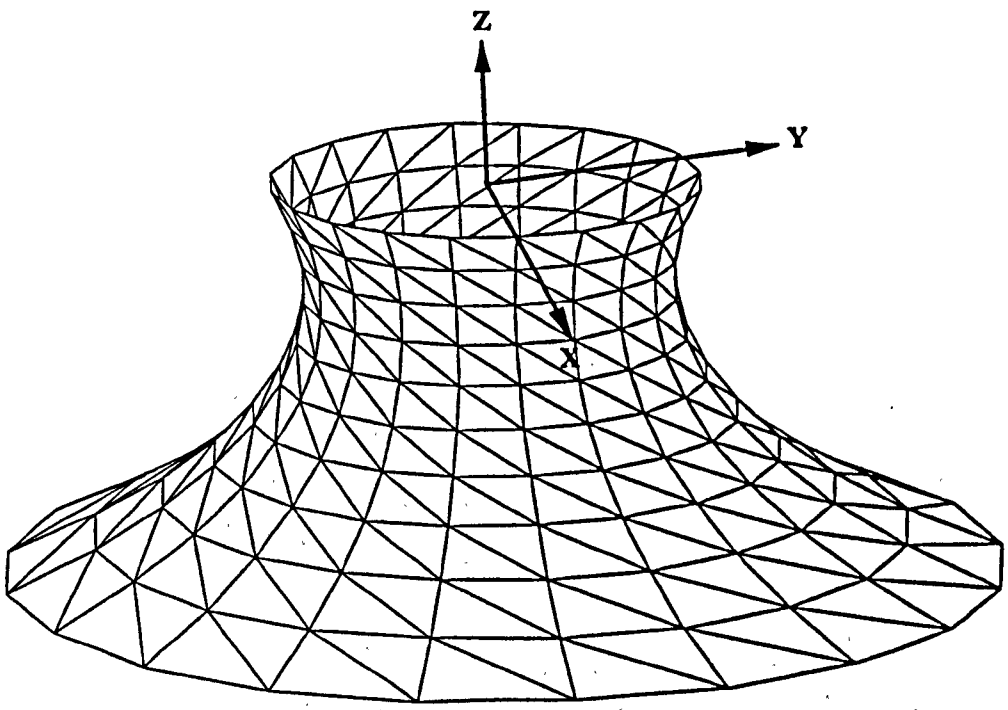

Figure 5-5 Example 5.2.2 (a) Side Profile. (b) Perspective View.

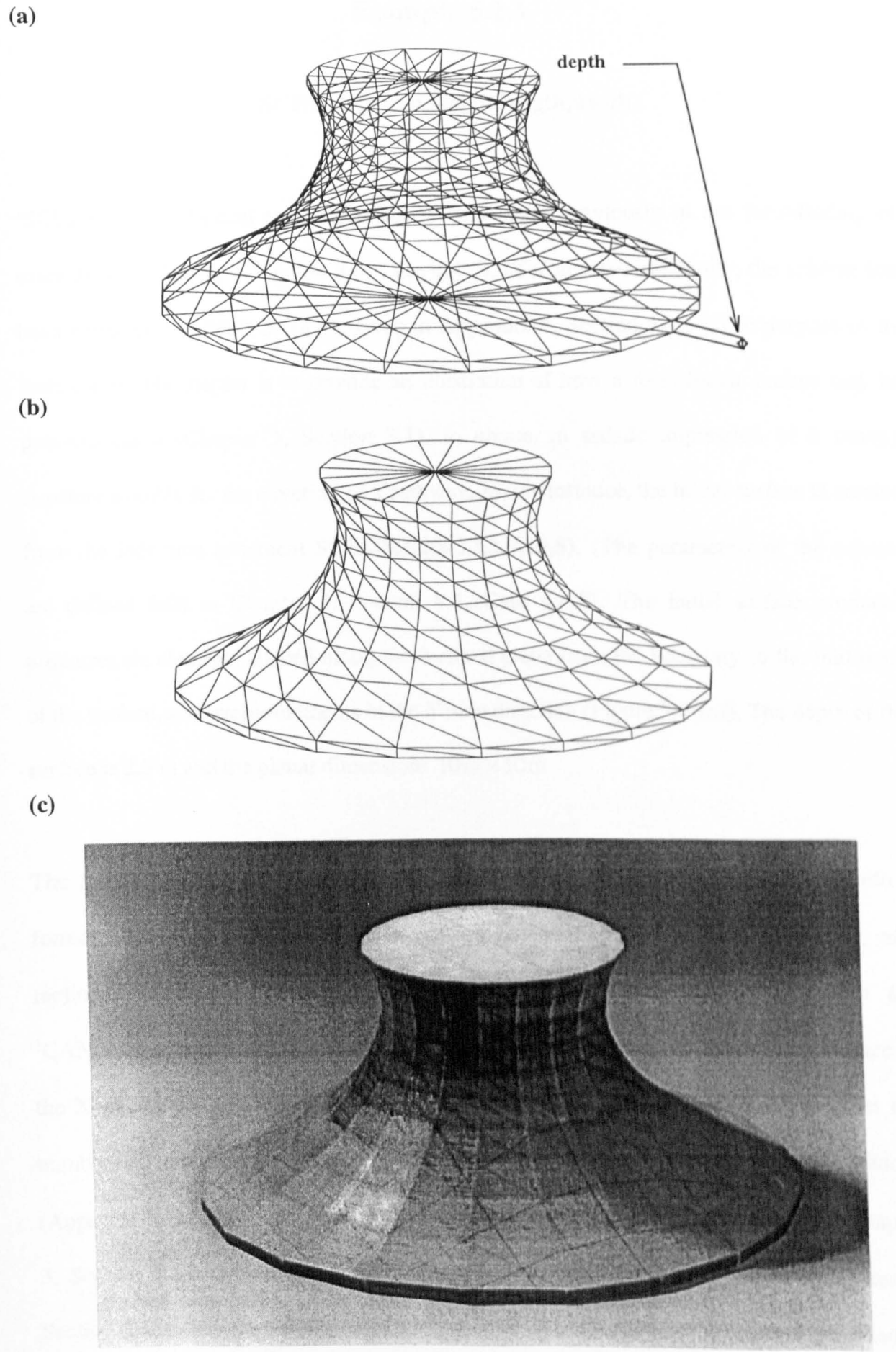

Figure 5-6 Rapid Prototype Construction (Example 5.2.2) (a) Tessellated Model - Internal View. (b) Tessellated Model - External View. (c) Physical Model.

Example 5.2.3

SCHEME3(m,n,height,length,width)

'SCHEME3' is identical to the scheme 'WEIR' used previously in the form-finding of example 4.8 (Chapter 4, Section 4.4, Case 4.4.2). (To preserve continuity, the scheme has been renamed 'SCHEME3' and is given in Appendix 5, Section 5A.5). The purpose of its inclusion in this chapter is to provide an illustration of how a form-found surface may be post-processed (Chapter 3, Section 3.1), to create an artistic impression of a canopy structure suitable for the covering of a pathway. In this instance, the initial surface is created from the induction statement **SCHEME3(6,12,2.5,10,5)**. (The parameters of the scheme are defined fully in Chapter 4, Section 4.4, Case 4.4.2). The initial surface produced possesses six elements aligned along the inclined plane from the boundary to the mid-point of the surface, and twelve elements in the Y axis direction (Figure 5-7 (a)). The depth of the surface is 2.5 m and the planar dimensions $10\text{m} \times 10\text{m}$.

The form-found surface depicted in example 5.2.3 (Figure 5-7 (b)) is converted into a formex expression using the MORFORM programme (Chapter 3, Section 3.1), and replicated four times using the scheme **CANOPY(5,4)**. The first parameter of the 'CANOPY' scheme relates to the planar dimension, 'width', of the form-found surface in the X direction - as used in the creation of the initial surface - while 'num' specifies the number of replications of the form-found surface. The formex expression 'canop' (Appendix 5, Section 5.A.6) is then saved through the use of the ***KEEP*** command (Chapter 3, Section 3.2.2.4), and converted into a format suitable for use by ACAD (Chapter 3, Section 3.1) using the MORFORM programme. The detailing of the surface depicted in

example 5.2.3 is shown in Figure 5-8, together with a rendered view of the surface; both effects have been accomplished using ACAD.

(a)

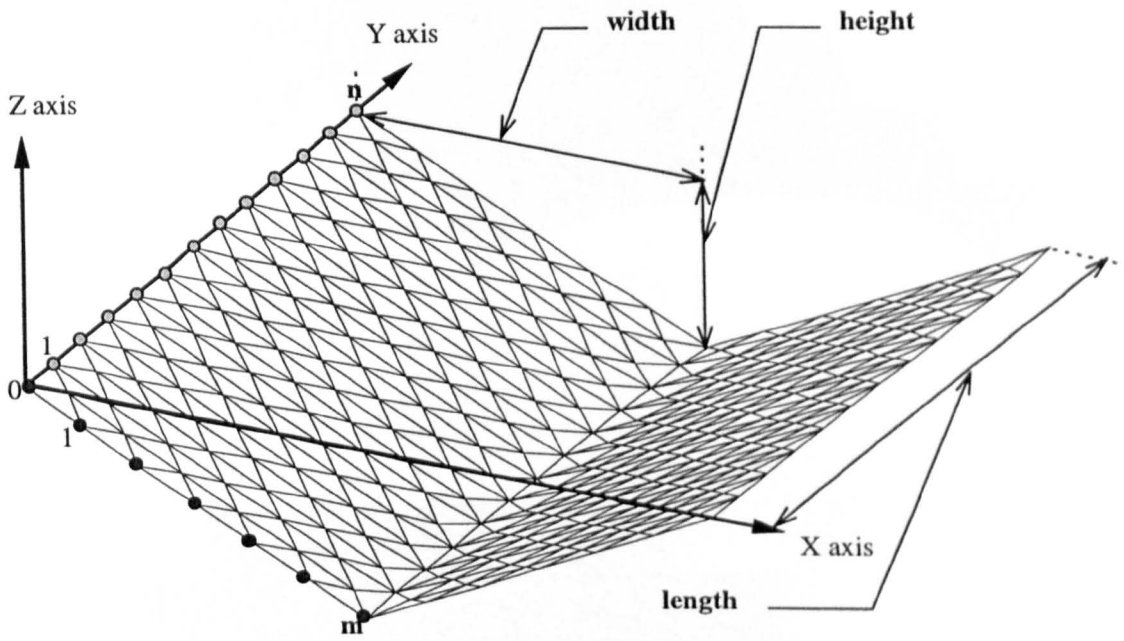

(b)

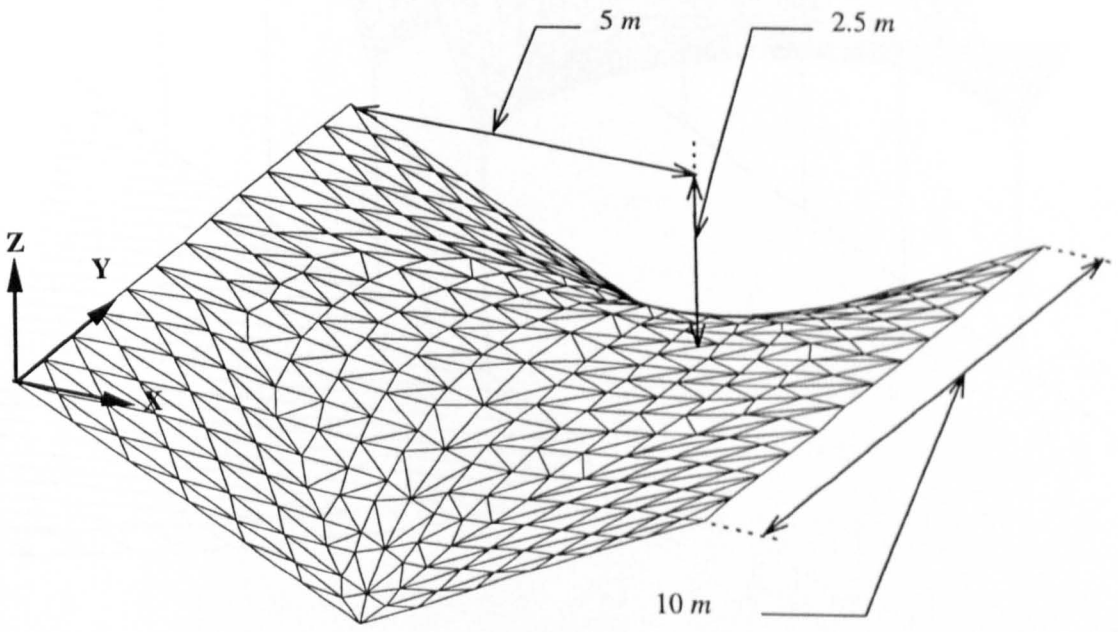

Figure 5-7 Example 5.2.3 (a) Initial Surface. (b) Form-Found Surface.

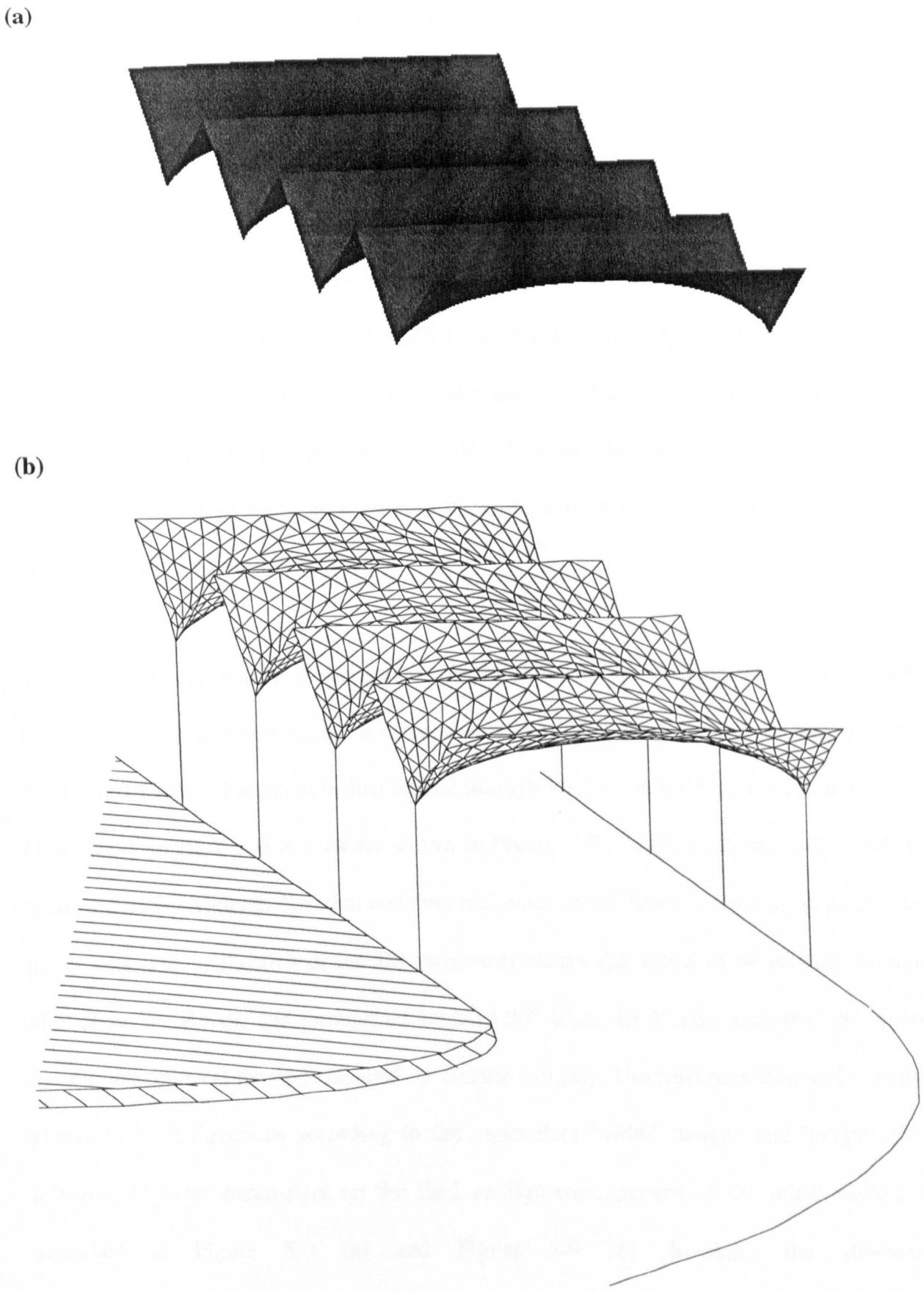

Figure 5-8 Post-Processing of Example 5.2.3 (a) Rendering. (b) Addition of Detailing.

Example 5.2.4

SCHEME4(m,n,width,length,height,num)

This example concerns the stable minimal surface created from a paragenic formex formulation that involves the basi-cylindrical retronorm (**BC**)and the basi-spherical retronorm (**BS**). (The basi-spherical retronorm is used to transform a configuration pattern to the geometry of a sphere). **'SCHEME4'** creates a surface consisting of a series of doubly curved segments arranged in a circular pattern (Figure 5-9 (a)). The number of segments depends on the parameter 'num'. A brief description of the geometric manipulations involved in the generation of the initial surface now follows (a more detailed explanation may be found in ref. 5.2):

The procedure for obtaining the surface firstly involves the creation of a barrel vault containing '2×m' elements along the circumference and 'n' elements along the length of the vault. The cylindrical segment is then rotated through 90° so that it lies parallel to the Z axis (The Cartesian X, Y and Z axes are shown in Figure 5-9). In the next stage, the vault is translated in the X global direction and then replicated 'num' times in a direction parallel to the Y axis. The application of the **BS** retronorm causes the vaults to be rotated through 360° about the Z axis, and through an angle of 90° about the Y axis, such that the vaults meet at the centre at the node labelled 'n' (Figure 5-9 (a)). The surface is then scaled in the global X, Y, Z directions according to the parameters 'width' 'length' and 'height'. The influence of these parameters on the final configuration pattern of the initial surface is described in Figure 5-9 (a) and Figure 5-9 (b). Invoking the statement **SCHEME4(5,10,40,23.094,5,6)** produces a discretised surface containing 1200 triangular elements and 706 nodes. During the form-finding analysis, movement is restricted along the 'spines' of the surface; where a single spine is given by the curve AB, and at the edges of

the segment that pass through the curve AB at the nodal points labelled 0 and n-1 (Figure 5-9 (a)). Analysis using the Dynamic Relaxation algorithm produces the surface presented in example 5.2.4 (Figure 5-10 and Figure 5-11). The form-found surface may be thought of as being representative of a hybrid membrane structure; that is, the structure composed of an exterior steel infrastructure bounded by a fabric membrane.(An example of such a structure is the "Auqapolis" pavilion, constructed for the 1975 World Expo at Okinawa, Japan, ref. 5.3).

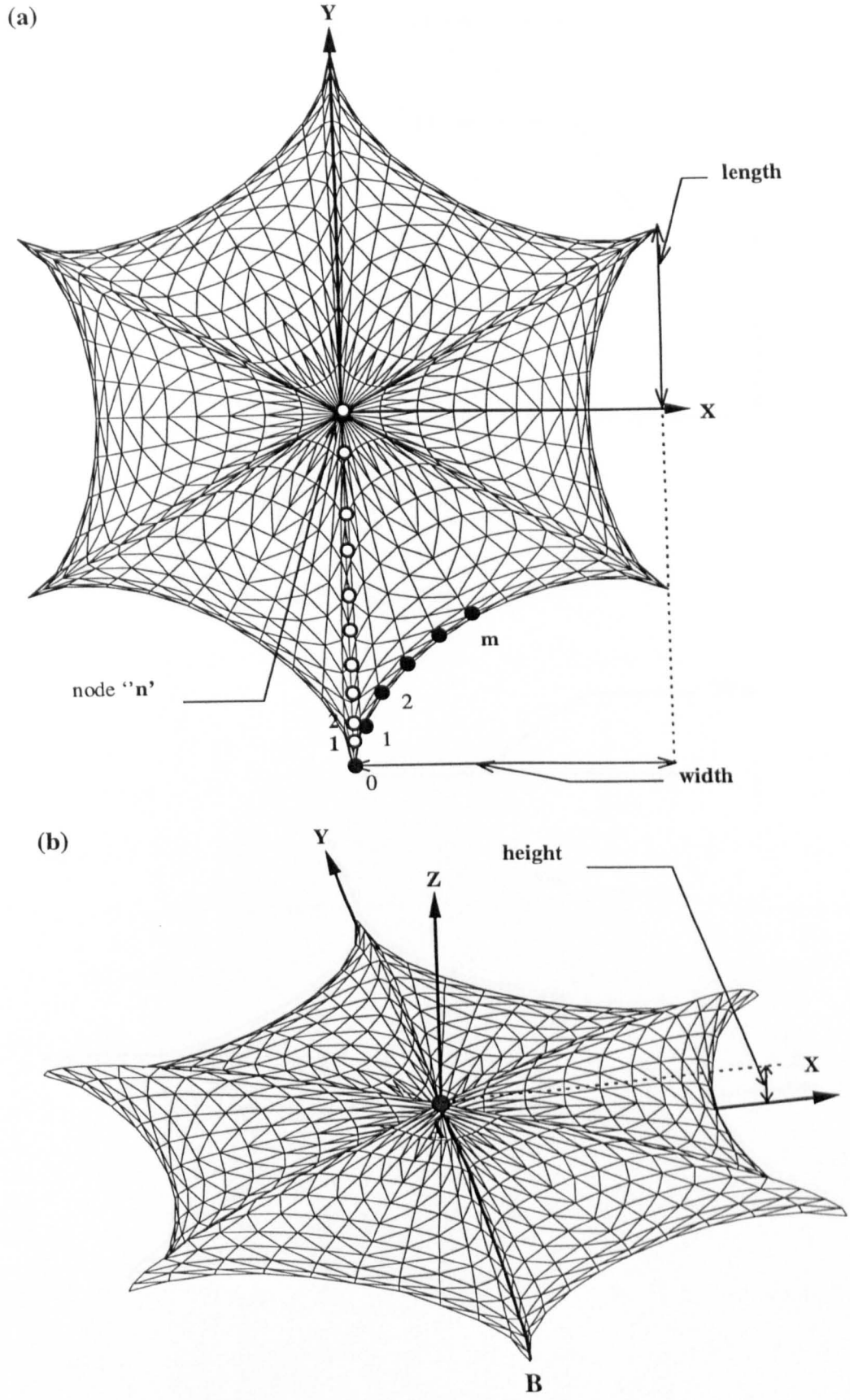

Figure 5-9 Initial Surface (Example 5.2.4). (a) Plan View. (b) Perspective View.

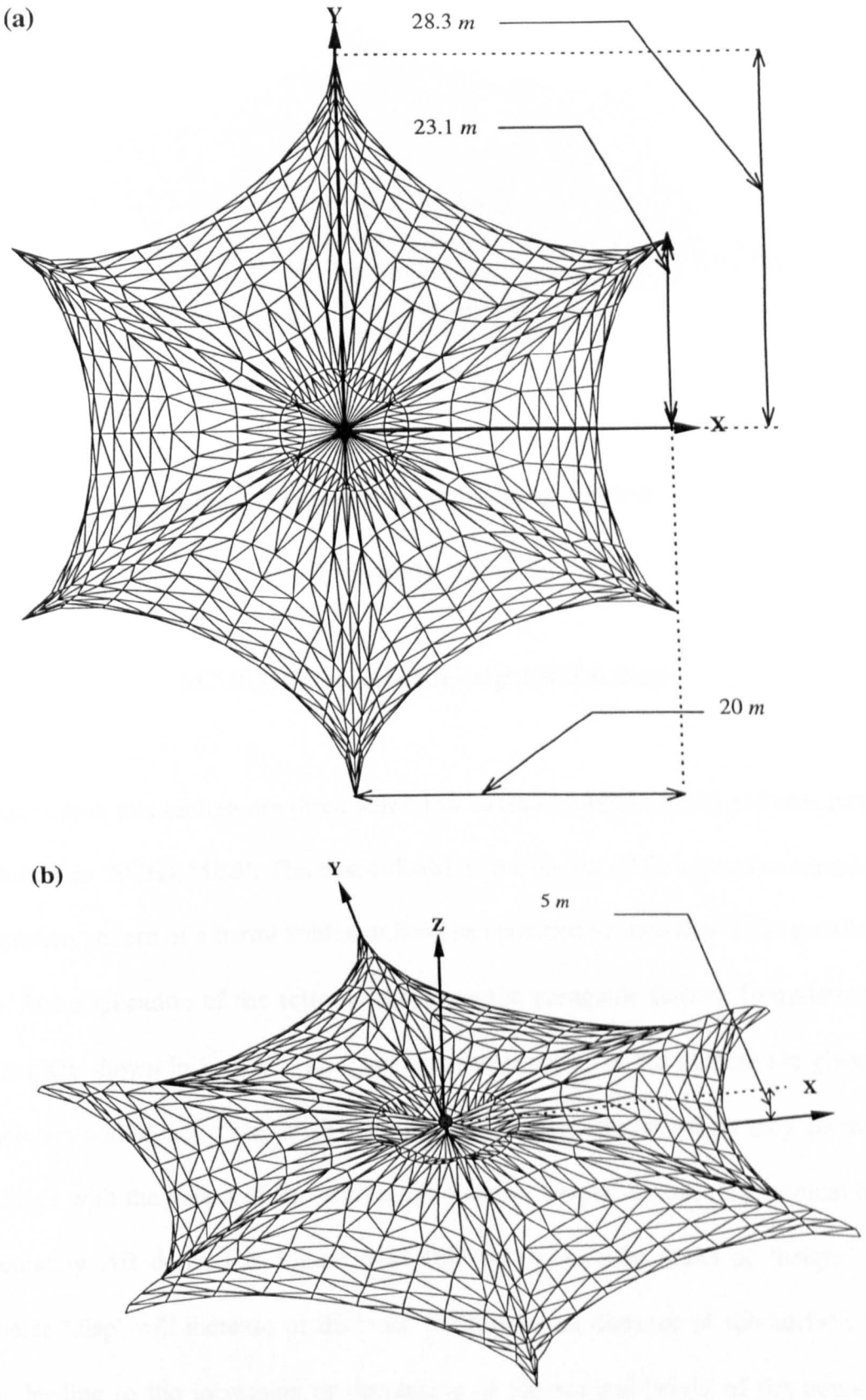

Figure 5-10 Example 5.2.4. (a) Plan View. (b) Perspective View.

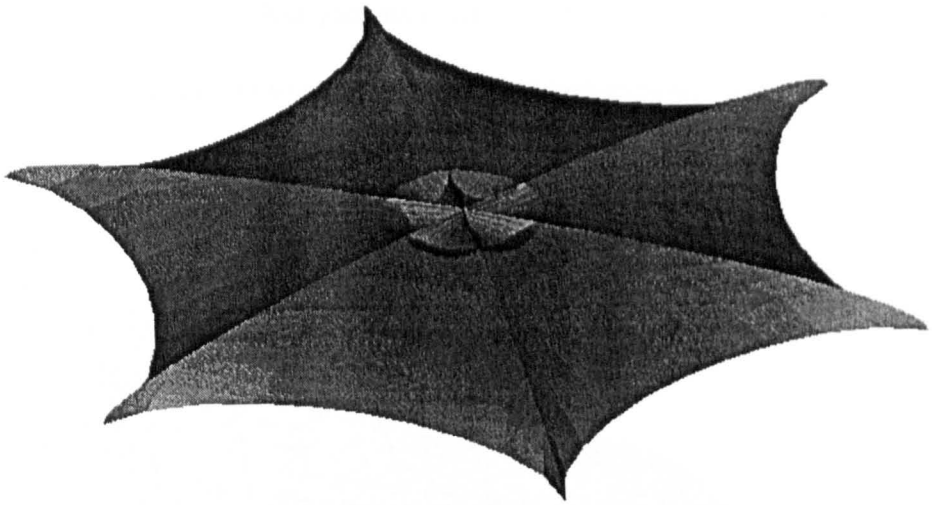

Figure 5-11 Example 5.2.4 - Rendered View.

Example 5.2.5

SCHEME5(m,n,length,height,width,disp)

Presented within this section are three numerical examples whose initial surfaces have been generated from **'SCHEME5'.** The basi-cylindrical retronorm (**BC**) is used to transform the configuration pattern of a barrel vault that has been positioned such that it lies parallel to the **X** axis. The application of the retronorm creates the paragenic formex formulation of the initial surface shown in Figure 5-12. The planar dimensions of the surface are given by the parameters ;'width' and 'length'. The degree of surface discretisation may be altered in accordance with the values of 'm' and 'n'. Parameter 'height' dictates the vertical height of the boundary AB defined in Figure 5-12 (b). For a constant value of 'height', altering parameter 'disp' will increase or decrease the horizontal distance of the surface from the origin, leading to the increasing or decreasing of the vertical height of the boundary CD. Parameter 'theta' is the angle of inclination of the surface and depends on parameters 'disp', 'height' and 'length'; it is **not** defined in the scheme. With regards to the side profile of the initial surface, increasing 'height' will in turn increase the curvature of boundary AB.

Examples 5.2.5.2 and 5.2.5.3 illustrate how the setting of 'disp' to zero also reduces the vertical height of boundary CD to zero (Figure 5-14 and Figure 5-15).

(a)

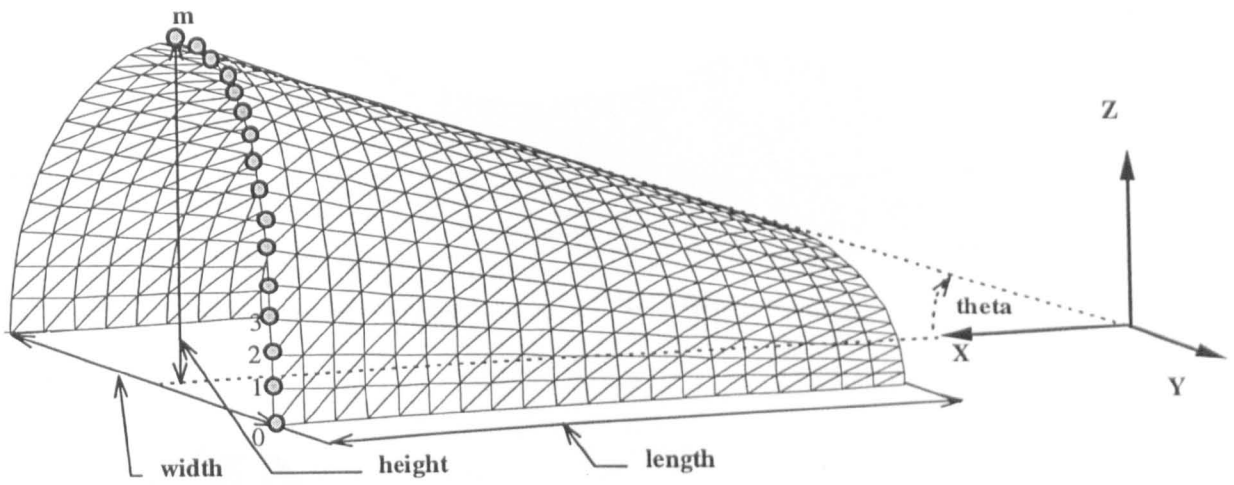

(b)

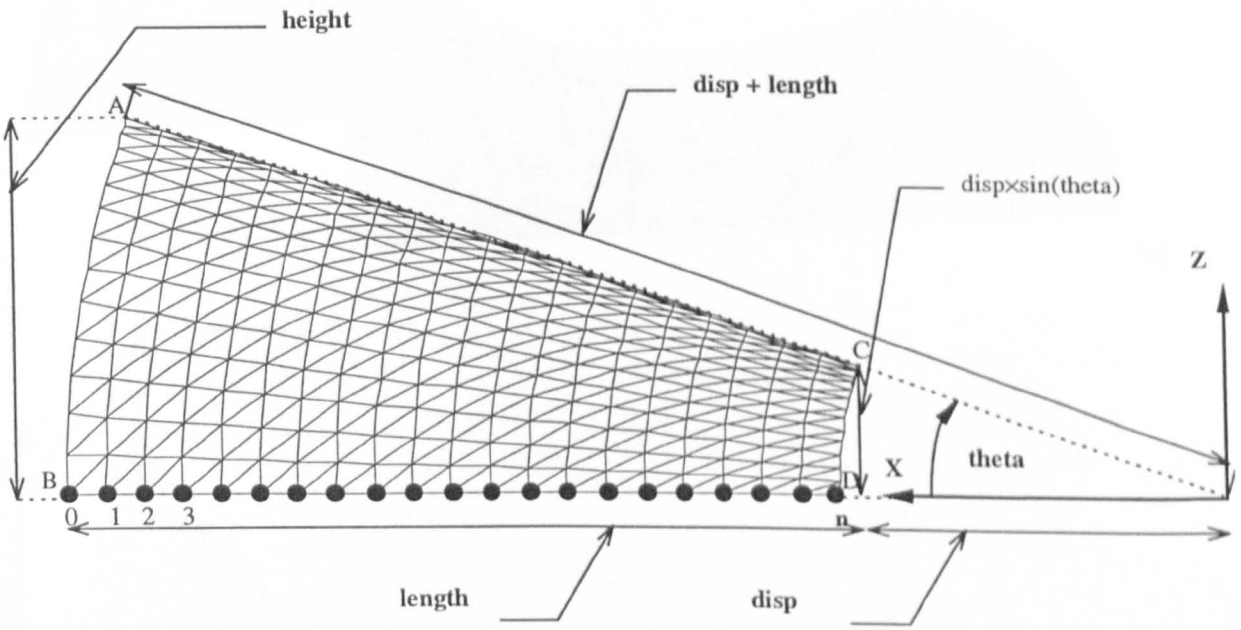

Figure 5-12 Paragenic Formex Formulation for the Initial Surfaces used in Examples 5.2.5.1, 5.2.5.2 and 5.2.5.3. (a) Perspective View. (b) Side Profile.

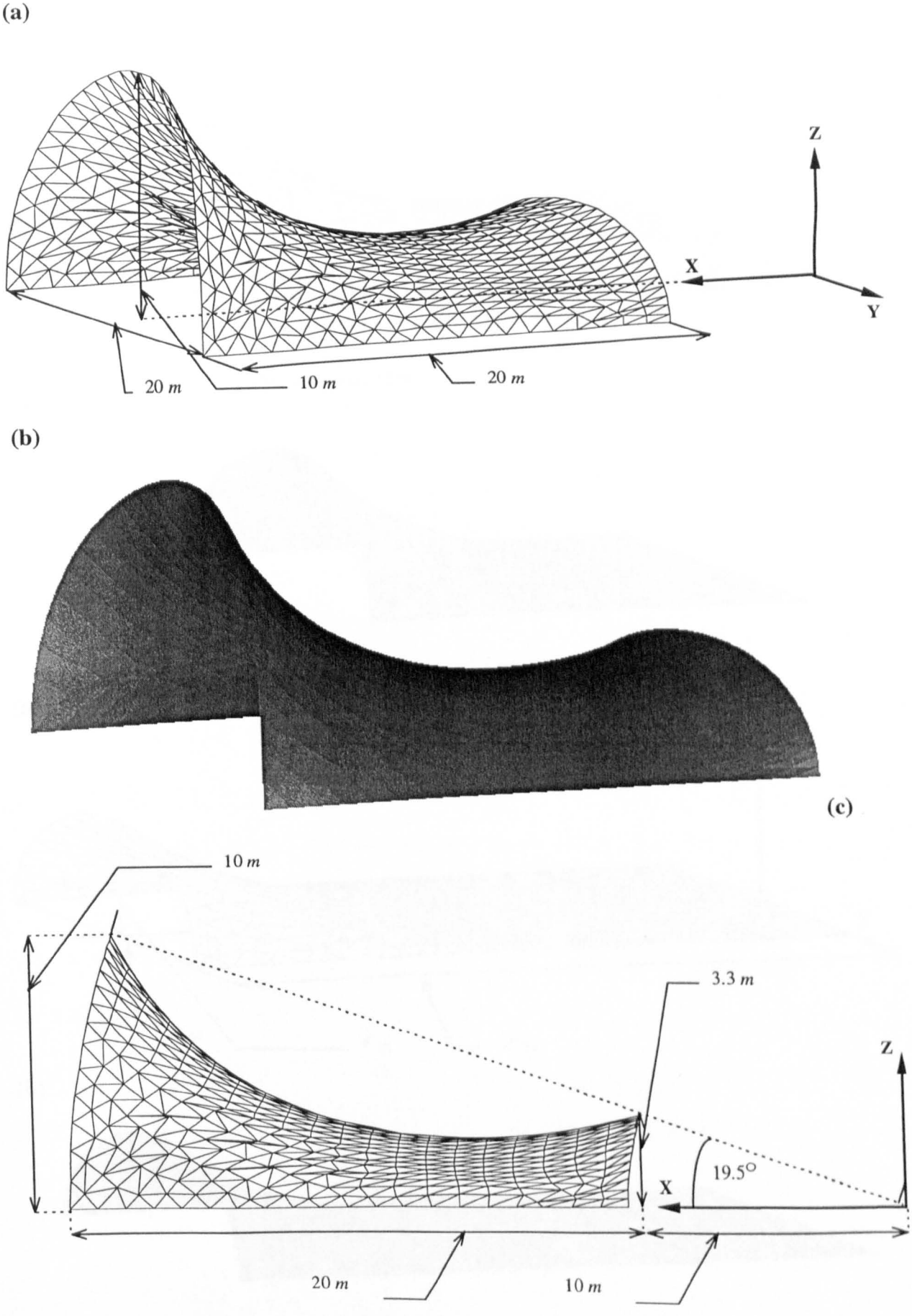

Figure 5-13 Example 5.2.5.1 (a) Perspective View. (b) Rendered View. (c) Side Profile.

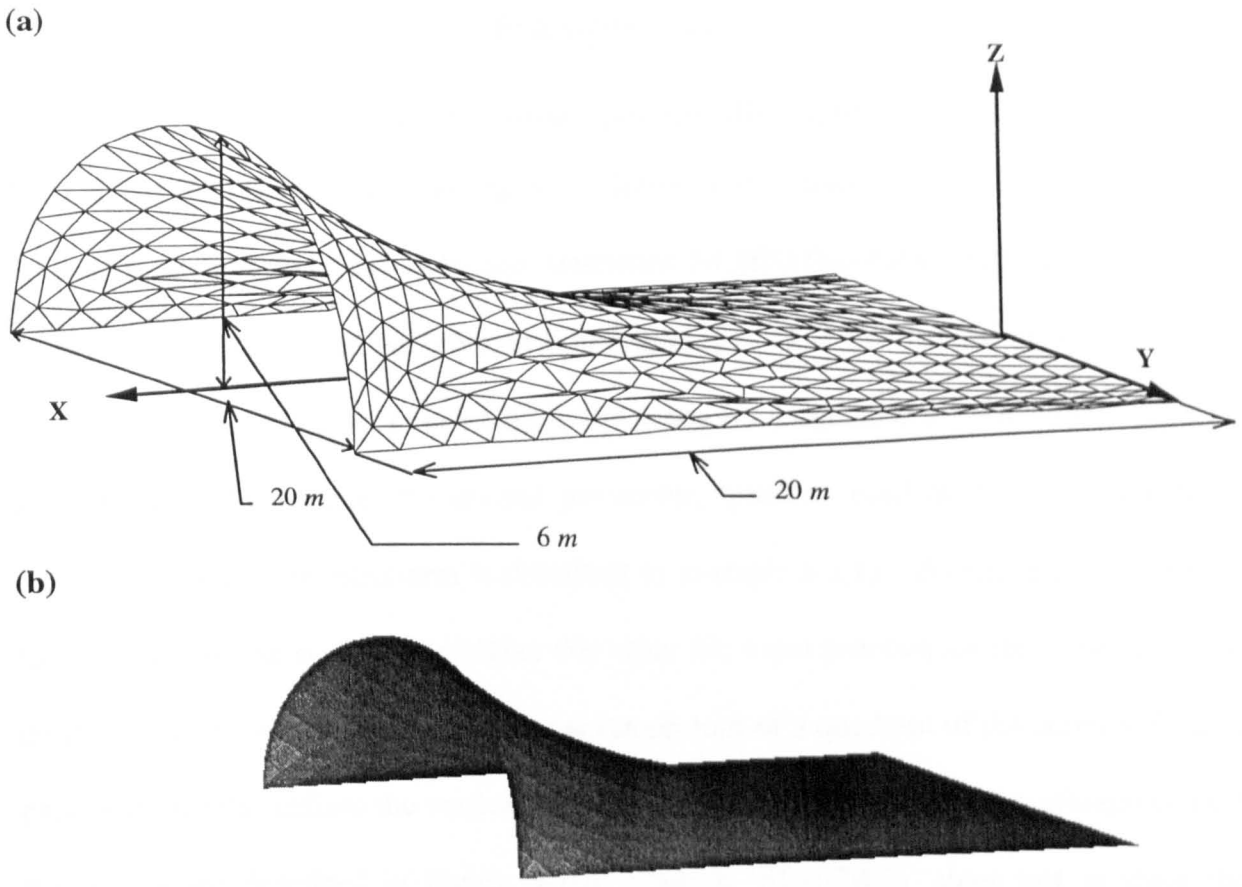

Figure 5-14 Example 5.2.5.2 (a) Perspective View. (b) Rendered View.

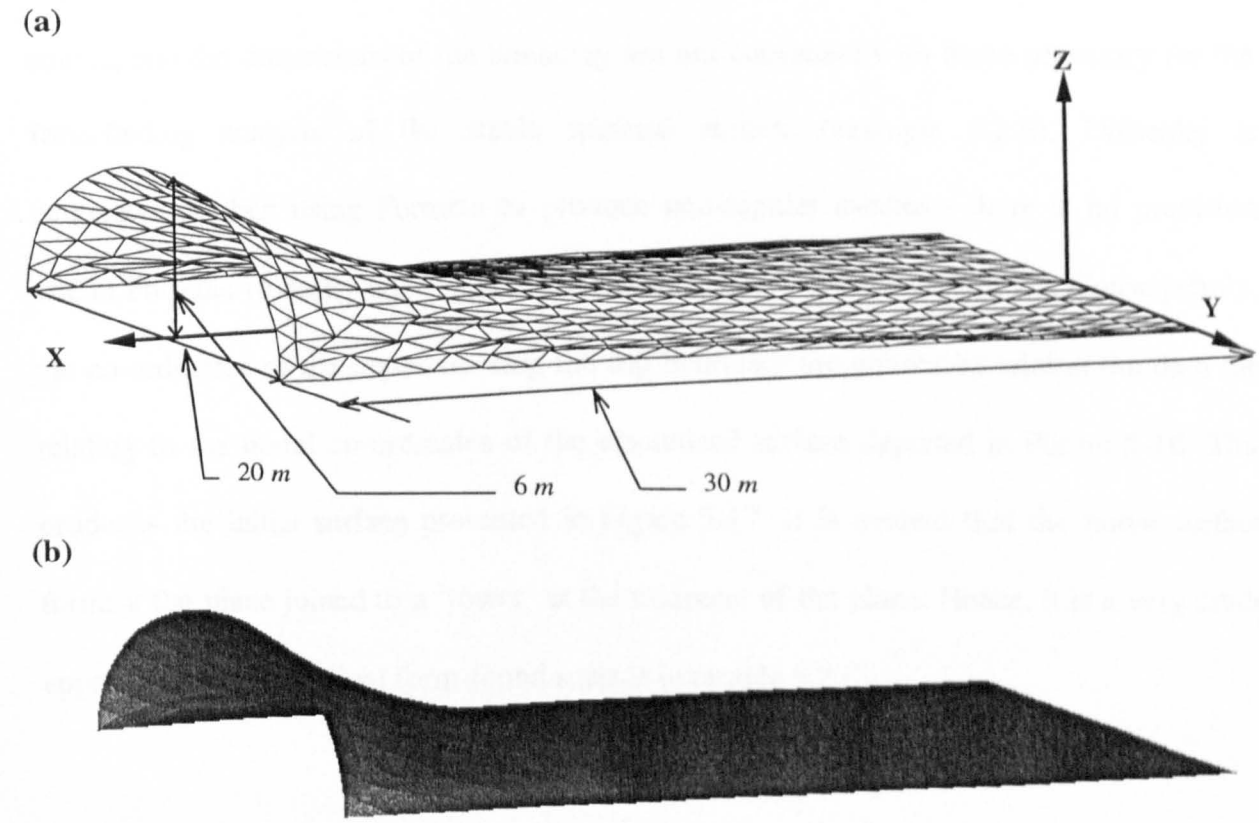

Figure 5-15 Example 5.2.5.3. (a) Perspective View. (b) Rendered View.

Example 5.2.6

SCHEME6(num,pitch,width,height)

Initially, the form-finding data relating to the initial surface used for the analysis in example 5.2.6 is generated from the induction statement **SCHEME6(8,0.02,5,3)**. The statement produces the configuration pattern shown in Figure 5-16. The first parameter of the scheme is used to define the number of elements 'num' along the diagonal line from the mid-point of a quadrant of the surface, the second parameter, 'pitch' - used by the basi hyperbolic retronorm (**BHP**) (the retronorm is described in example 5.2.1) - defines the curvature of the boundary of the surface; the higher the value the more pronounced the curvature. The third parameter, 'width', defines the planar dimensions of a quadrant of the surface. Finally, parameter 'height' defines the vertical distance of the upper boundary. (The aforementioned parameters are described in Figure 5-16). Scheme 'SCHEME6' **does not** produce the required initial surface. It can be seen from Figure 5-16 that the upper boundary forms a square, and the dimensions of the boundary are not consistent with those necessary for the form-finding analysis of the stable minimal surface (example 5.2.6). Difficulty is encountered when using Formian to produce non-regular meshes - there is no provision within Formian to easily alter local areas, or points, of a discretised surface. Consequently, the co-ordinates of the nodes forming the top boundary are altered by editing the data file relating to the nodal co-ordinates of the discretised surface depicted in Figure 5-16. This produces the initial surface presented in Figure 5-17. It is evident that the initial surface forms a flat plane joined to a 'tower' at the midpoint of the plane. Hence, it is a very crude approximation to the final form-found surface (example 5.2.6).

A stress σ_S equivalent to $1\times10^3 kNm^{-2}$ ($F_K=1kNm^{-1}$) is applied to the membrane, while a constant force of 6kN is applied to the exterior boundary cables and the interior cables subjected to a force of 1kN (Figure 5-18). The surface is fixed at the points shown in Figure 5-18. The numerical solution to the stable minimal surface presented in example 5.2.6 is illustrated in Figure 5-19 to Figure 5-23.

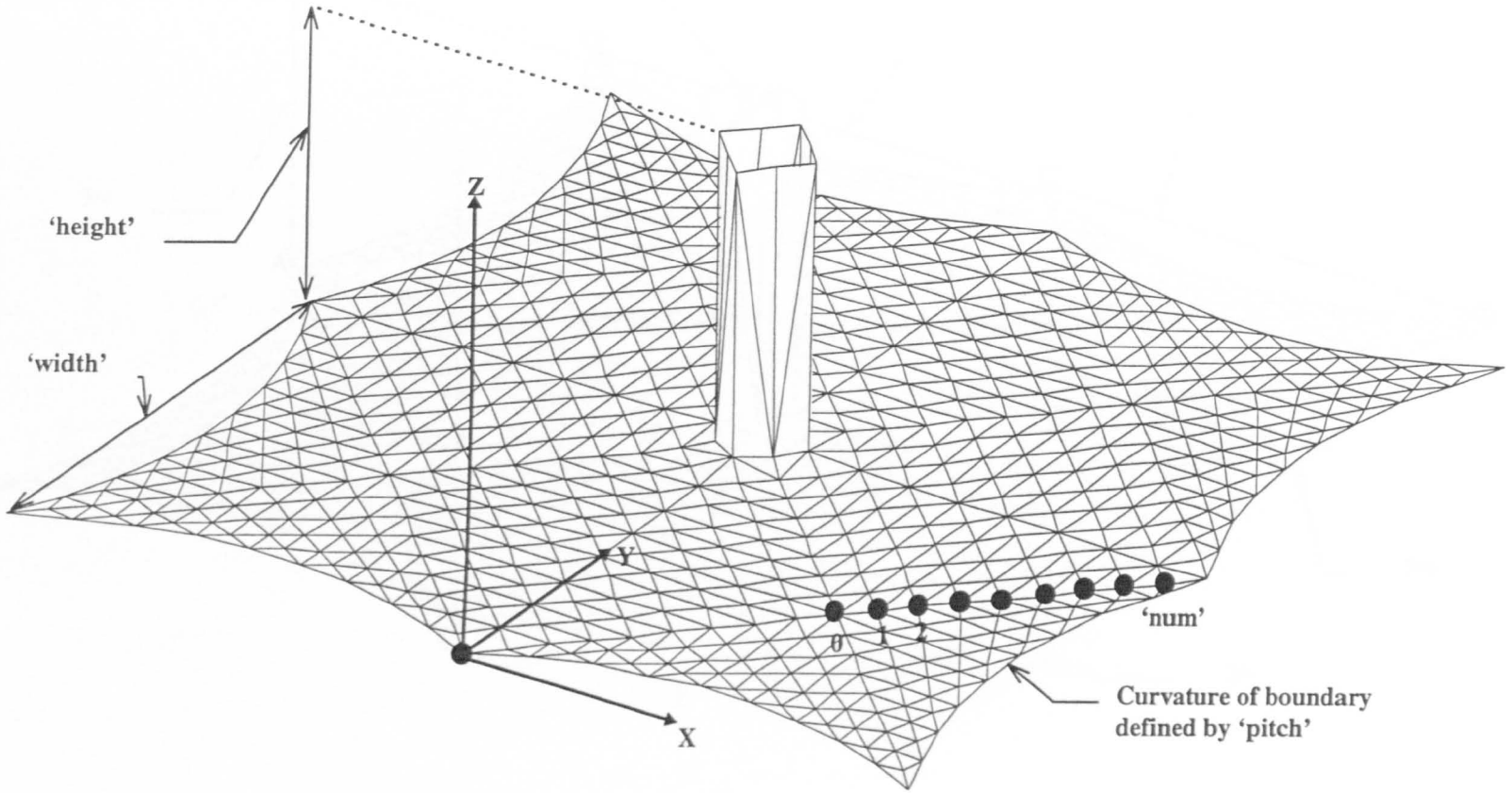

Figure 5-16 Surface Generated from the Formian Scheme "SCHEME6" (Appendix 5, Table 5A.9).

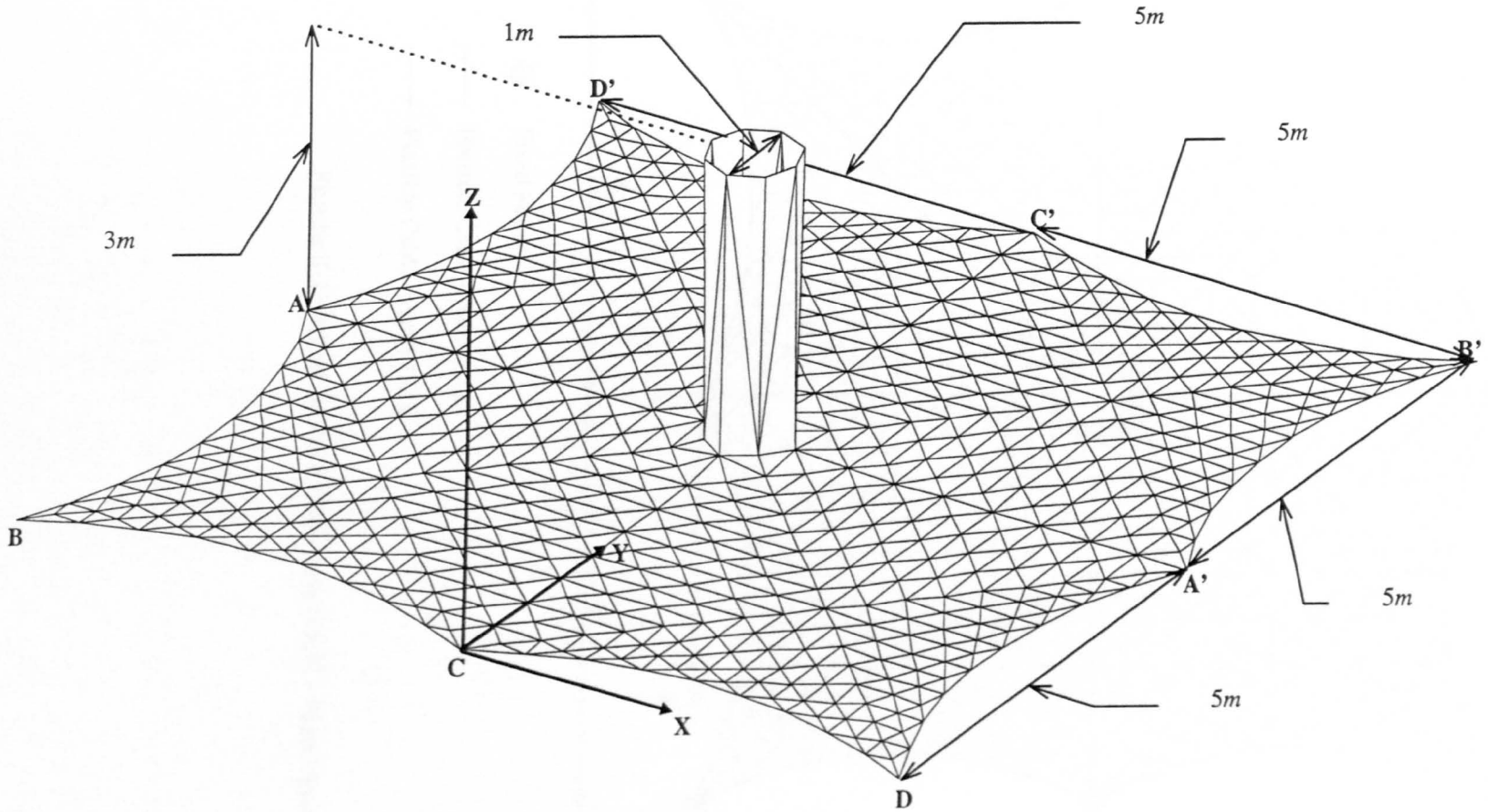

Figure 5-17 Modified Initial Surface (Example 5.2.6) - Perspective View.

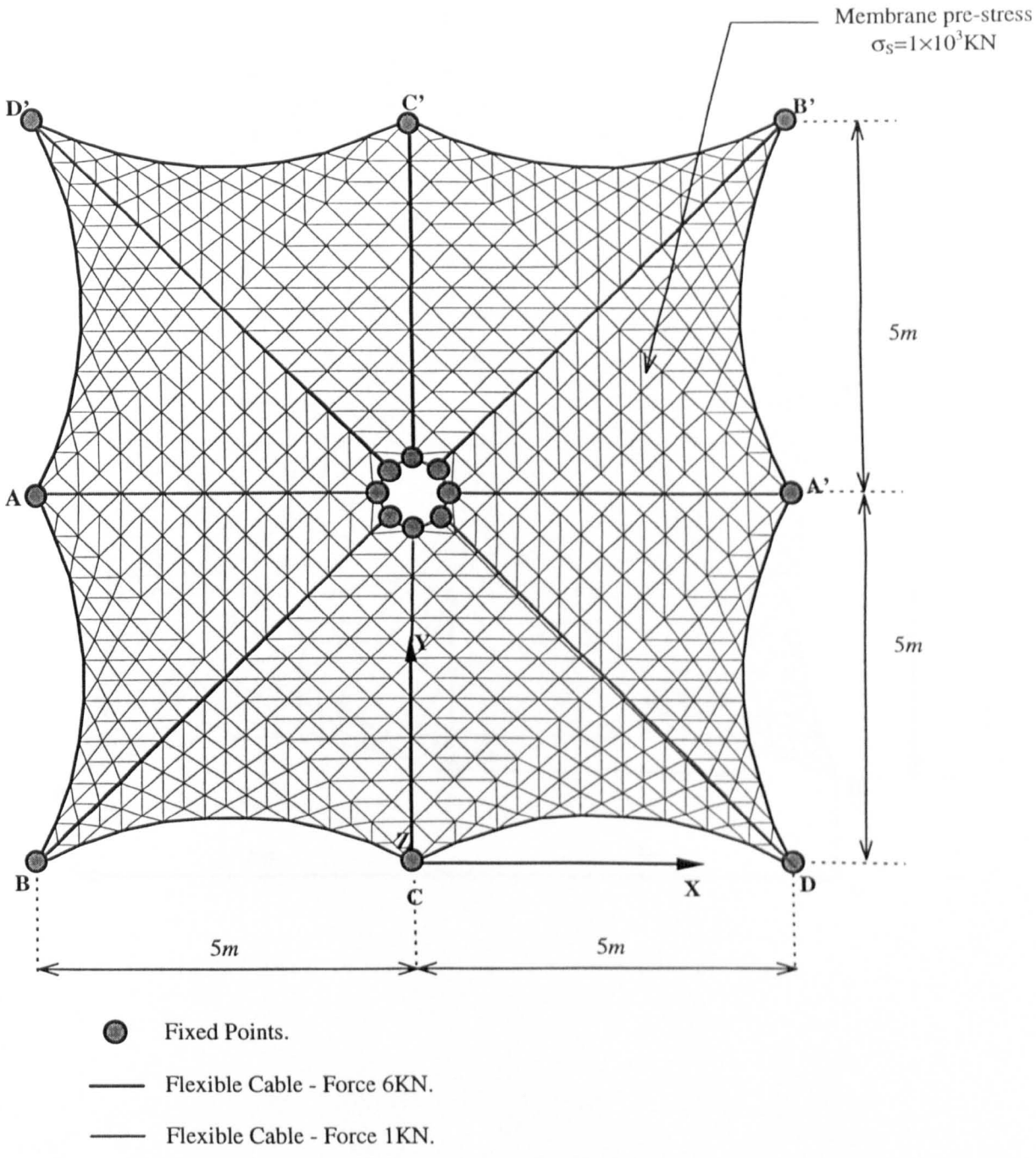

Figure 5-18 Initial Surface (Example 5.2.6) - Plan View.

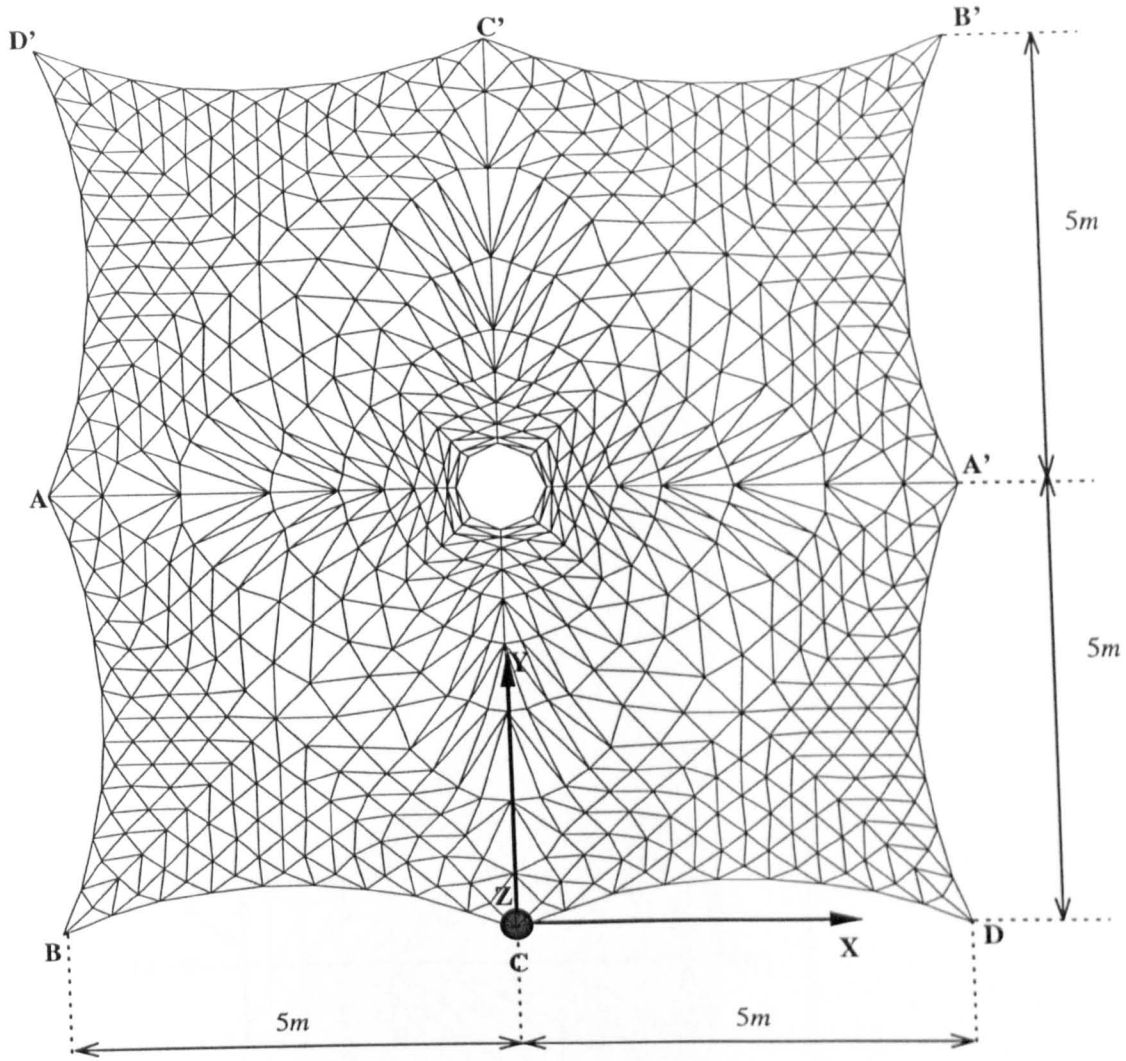

Figure 5-19 Example 5.2.6 - Plan View.

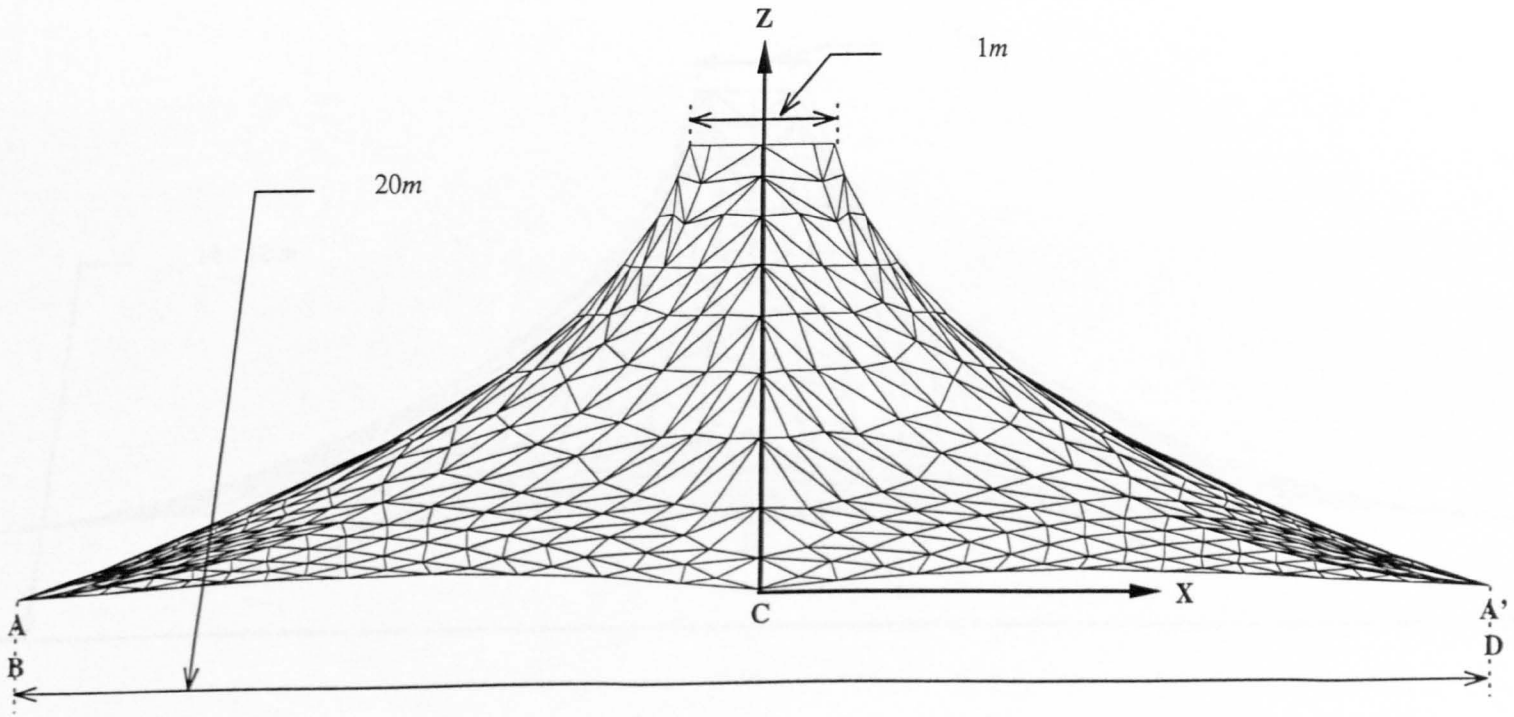

Figure 5-20 Example 5.2.6 - Side Elevation (Cross-Section AA').

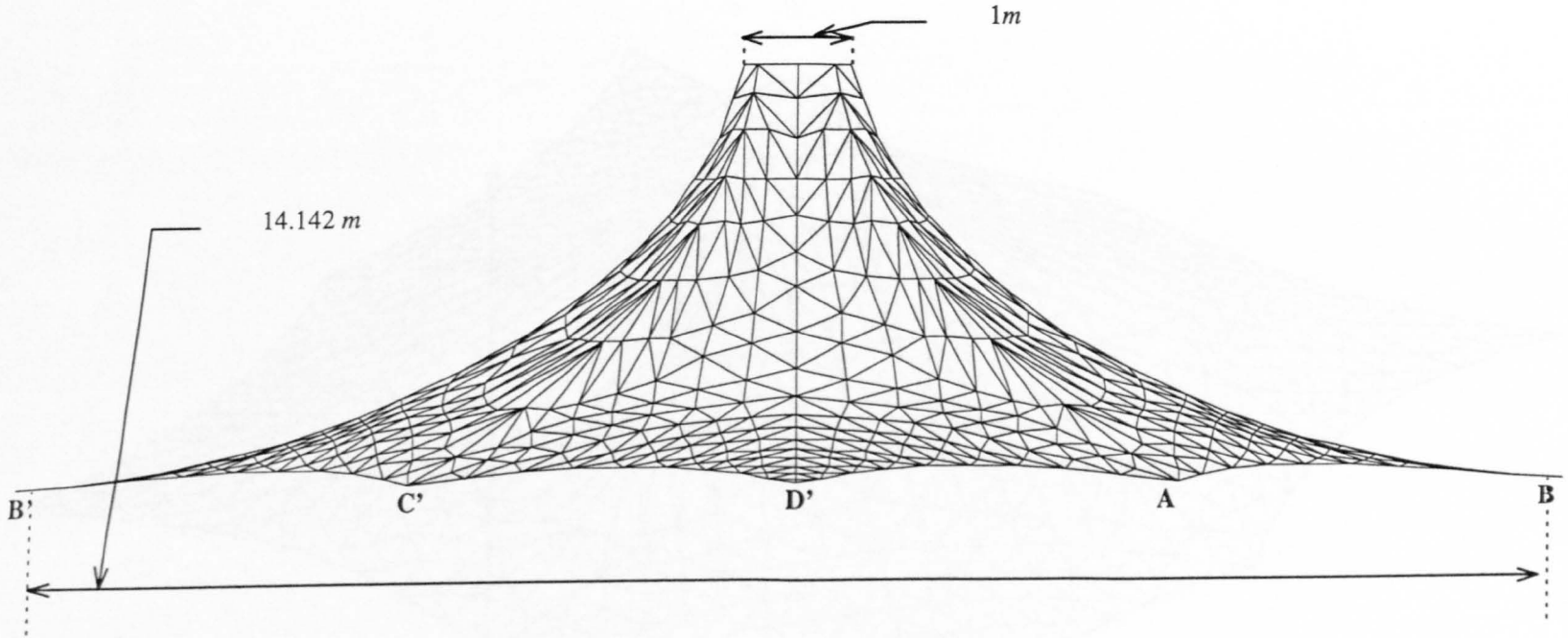

Figure 5-21 Example 5.2.6 - Side Elevation (Cross-Section BB').

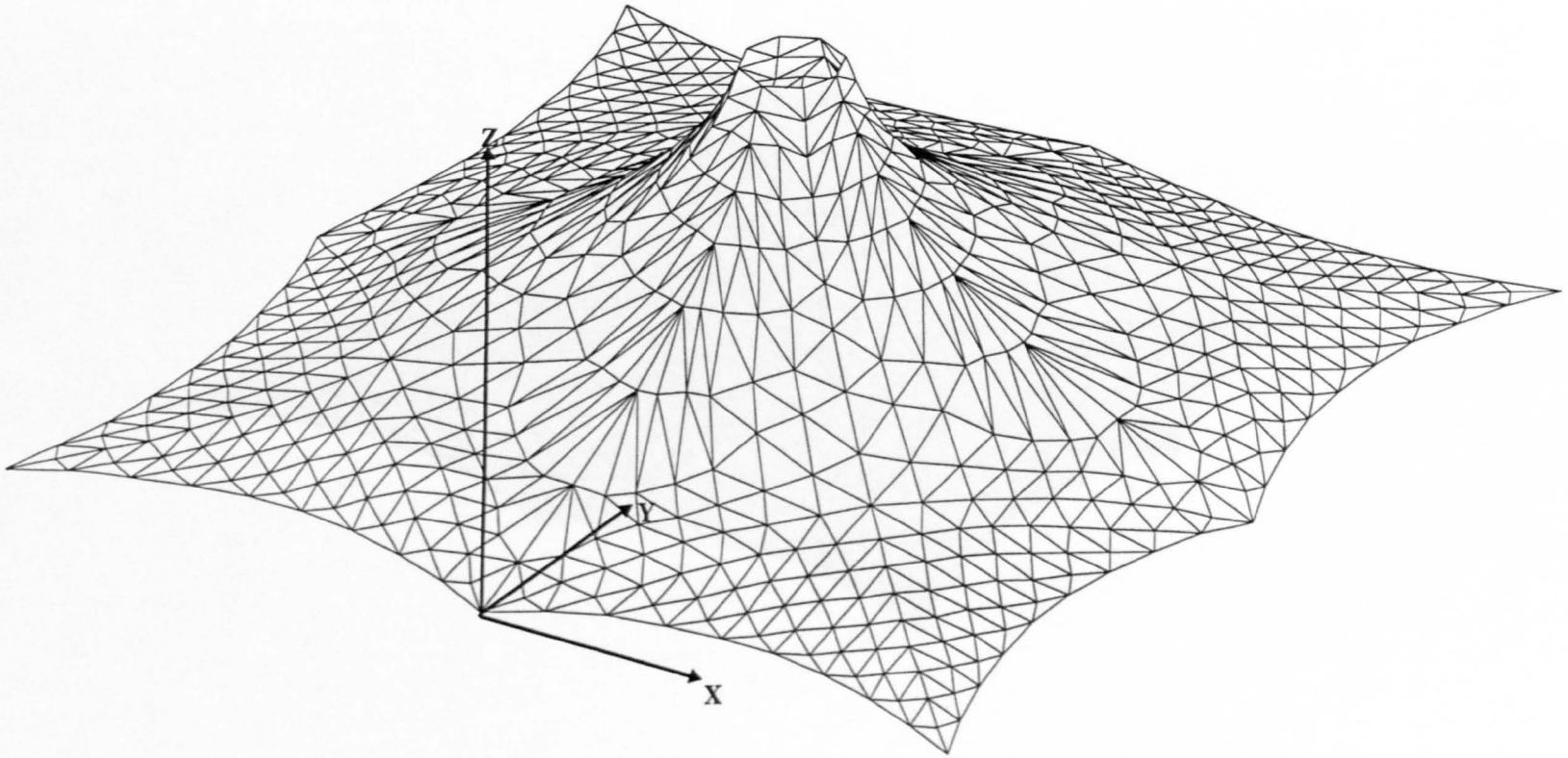

Figure 5-22 Example 5.2.6 - Perspective View.

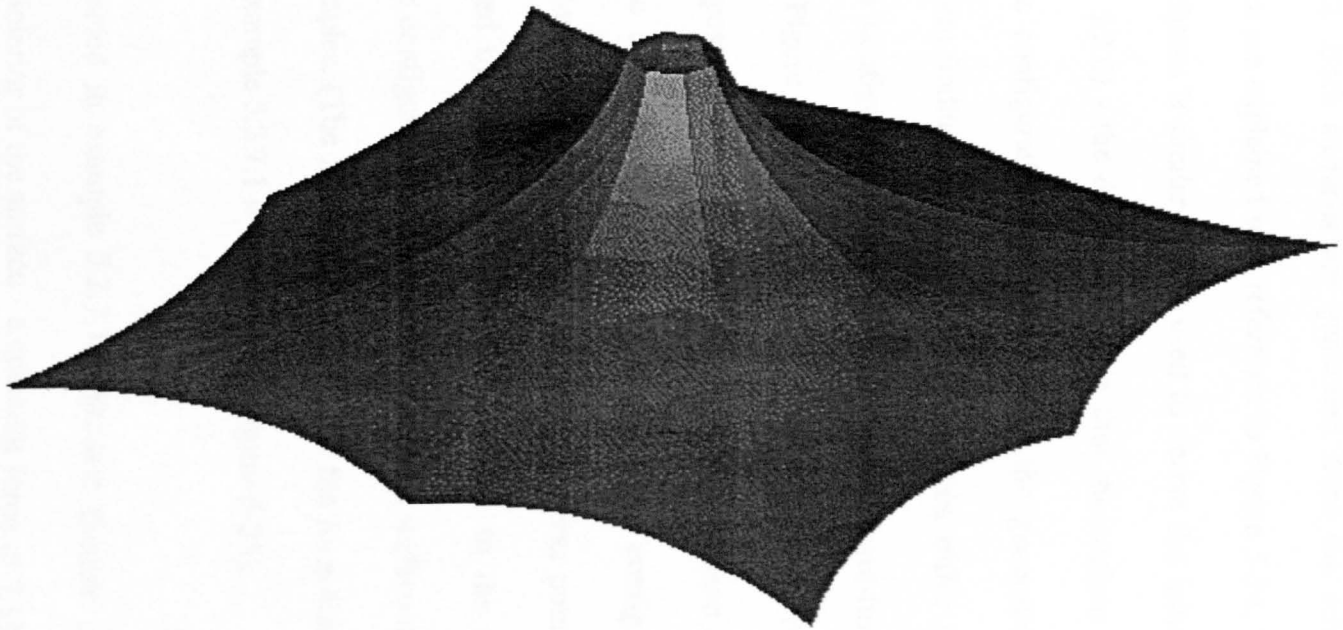

Figure 5-23 Example 5.2.6 - Rendered View.

Example 5.2.7

SCHEME7(num,pitch,width)

Flexible cables are introduced during the form-finding of the surfaces presented in examples 5.2.7.1 and 5.2.7.2. Both surfaces are generated from the scheme 'SCHEME7' - the parameters of which are explained with reference to Figure 5-24. The configuration pattern produced by the scheme is similar to that used to derive the initial surface in the previous example (example 5.2.6) - the difference being that the surface solely forms a flat plane (Figure 5-24). The configuration patterns used in the generation of the initial surfaces utilised for the form-finding of the following surfaces differ in the degree of surface discretisation. The configuration pattern used for the form-finding of the first surface (example 5.2.7.1, Figure 5-24) possesses 1296 elements while that of the second surface (example 5.2.7.2) possesses 796 - the induction statements used to generate these patterns are given in Table 5-1. Once the data relating to the configuration pattern has been computed, the surface is altered by raising four of the corner points of the plane to 5 m (an action accomplished by altering the data files relating to the nodal co-ordinates). The modification of the configuration pattern gives the initial surface used in the form-finding of the following examples. (The initial surface used for the form-finding of the stable minimal surface given by example 5.2.7.1 is illustrated in Figure 5-25).

The surface presented in example 5.2.7.1 possesses flexible cables that span both the boundary and the interior of the surface - a constant force of 7 kN is applied to the exterior boundary cables, while the interior cables are subjected to a force of 4 kN for the symmetric surface cables, and 8 kN for the valley cables (Figure 5-26). In contrast, the surface presented in example 5.2.7.2 only possess cable elements of force 7 kN along the boundary

of the surface. In both examples, movement is restricted at the eight corner nodes of the initial surface, and a pre-stress, σ_s , equivalent to 1×10^3 kNm^{-2} is applied to the membrane.

The geometries of the stable minimal surfaces described by the examples above are given in Figure 5-27 to Figure 5-34. Although these stable minimal surfaces possess the same boundary conditions and dimensions, it is noticeable that the introduction of the interior 'symmetric' and 'valley' cables is significant in altering the shape of the membrane (Figure 5-28 and Figure 5-32).

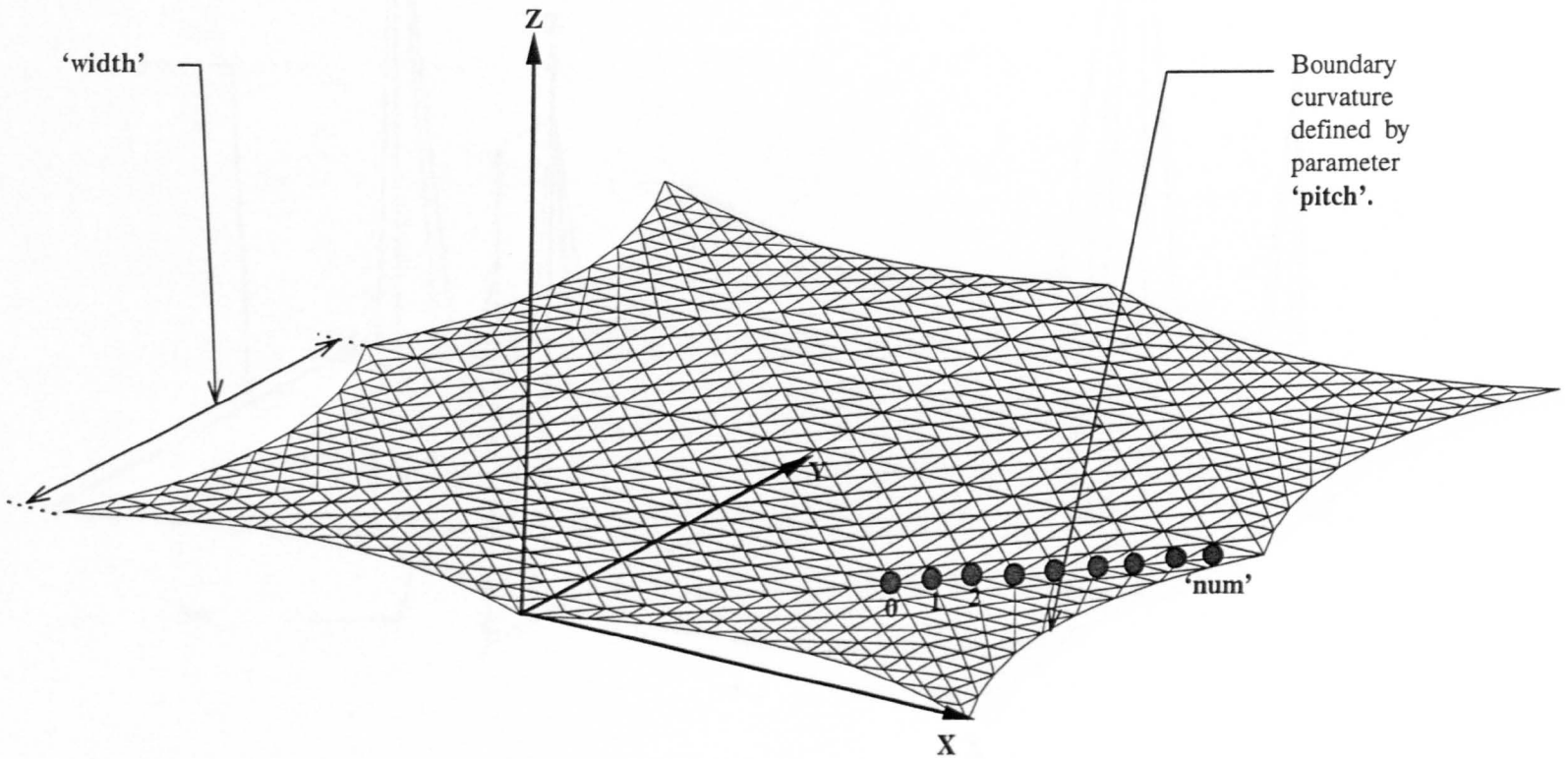

Figure 5-24 Surface Generated from the Formian Induction Statement "SCHEME7(8,0.02,5)."

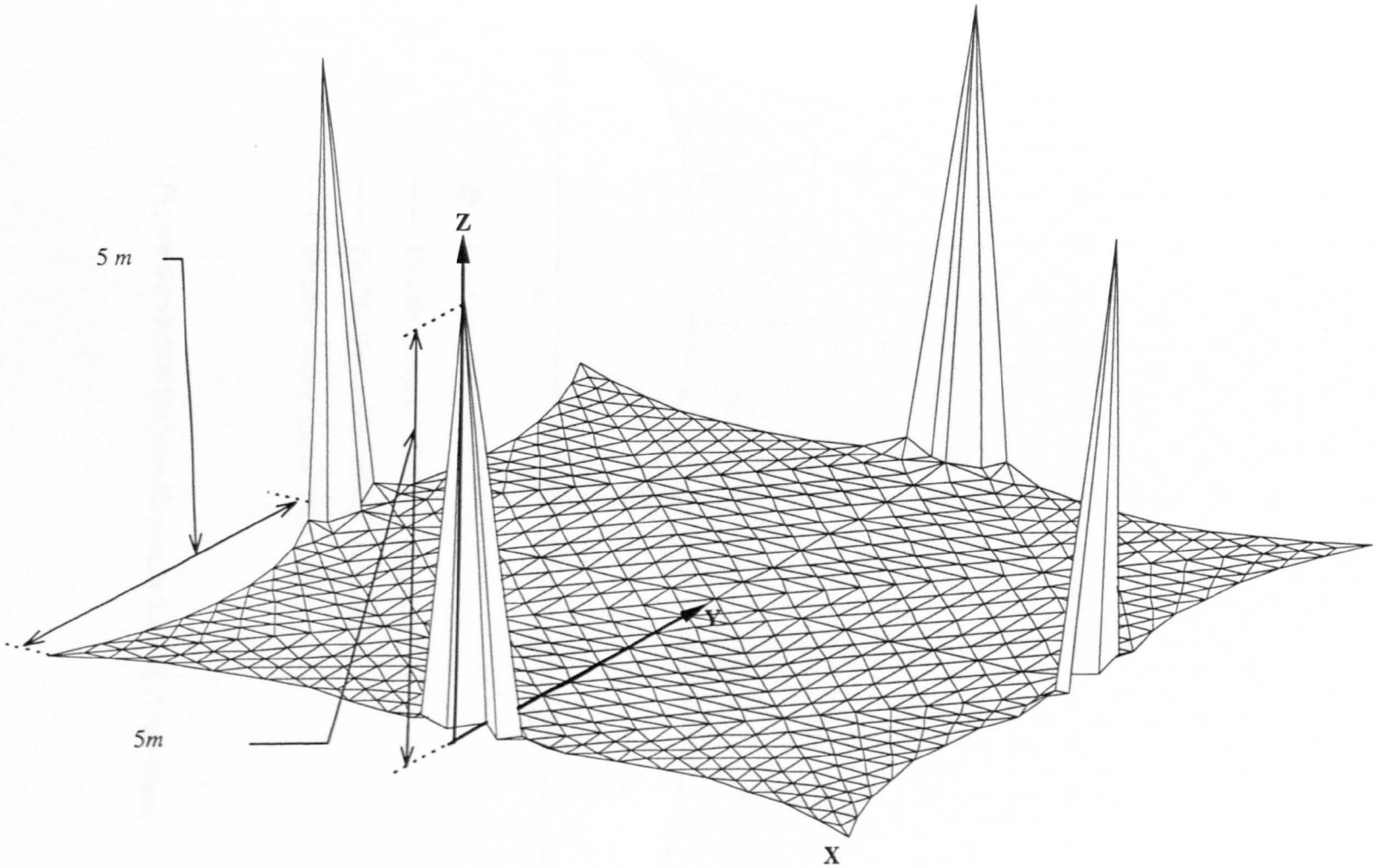

Figure 5-25 Modified Initial Surface (Example 5.2.7.1) - Perspective View

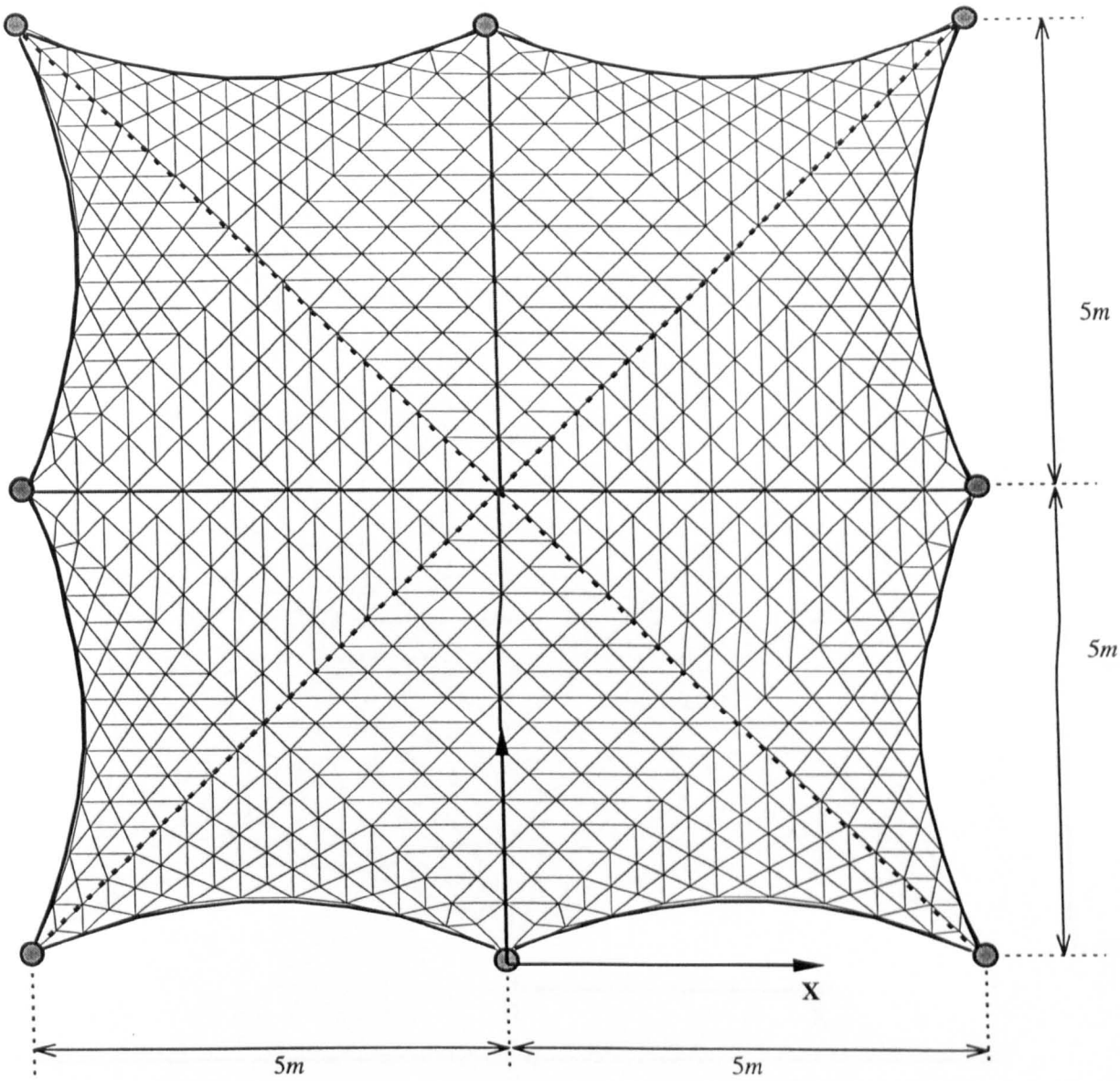

Fixed Points.

Flexible 'Boundary' Cable - Force 7KN.

Flexible 'Symmetric' Cable - Force 4KN.

Flexible 'Valley' Cable - Force 8KN.

Figure 5-26 Initial Surface (Example 5.2.7.1) - Plan View.

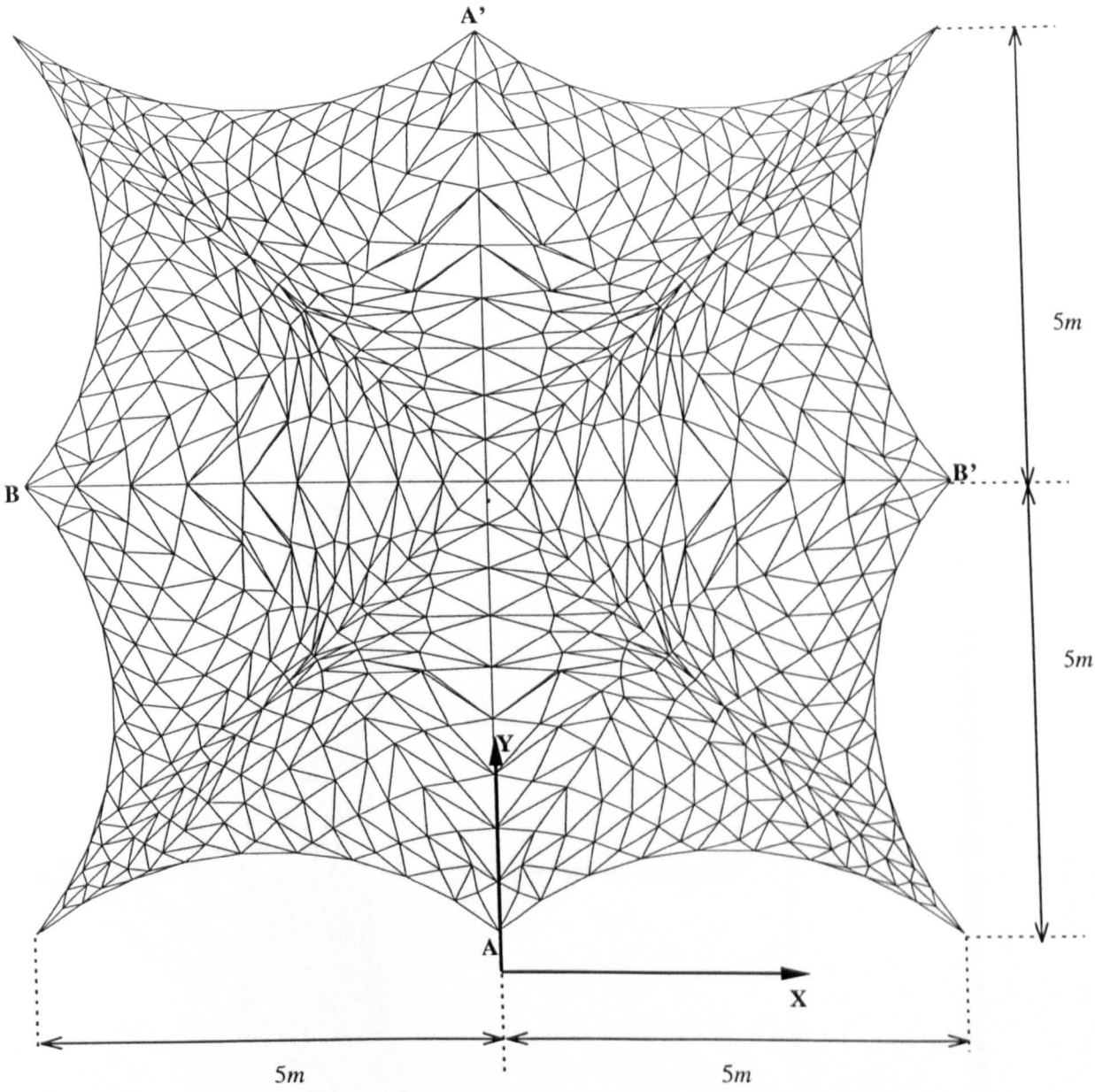

Figure 5-27 Example 5.2.7.1 - Plan View

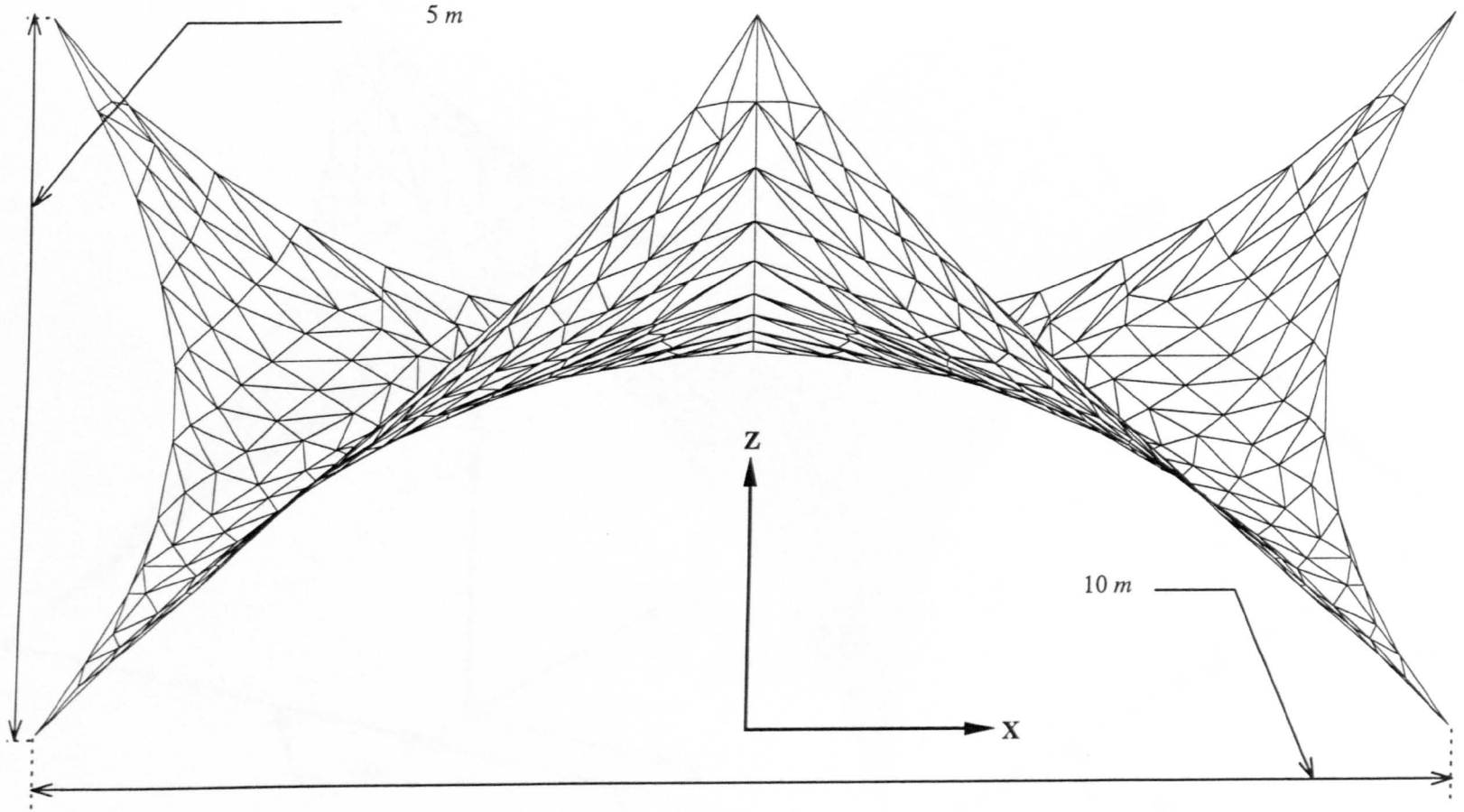

Figure 5-28 Example 5.2.7.1 - Side Elevation (Cross-Section BB').

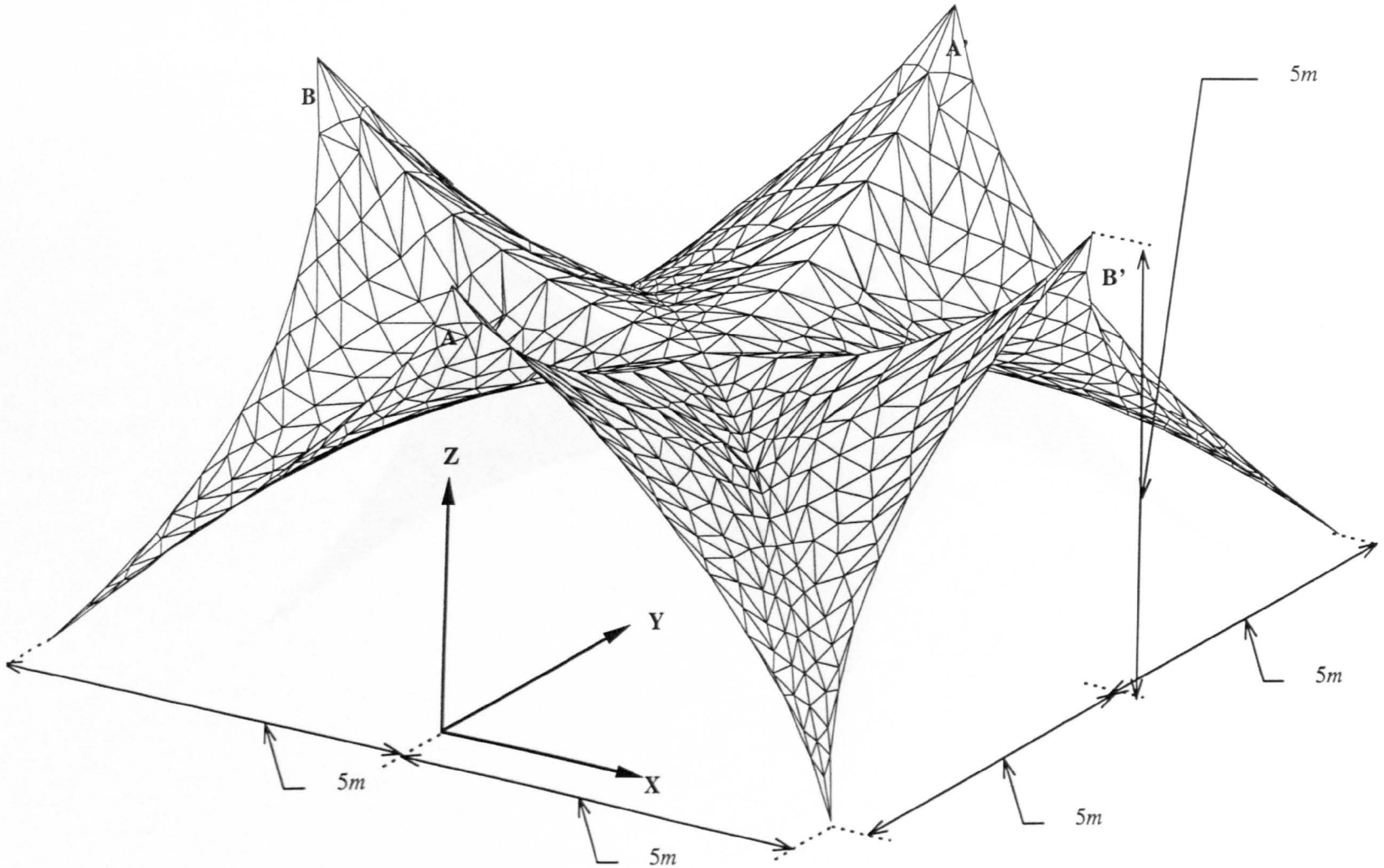

Figure 5-29 Example 5.2.7.1 - Perspective View.

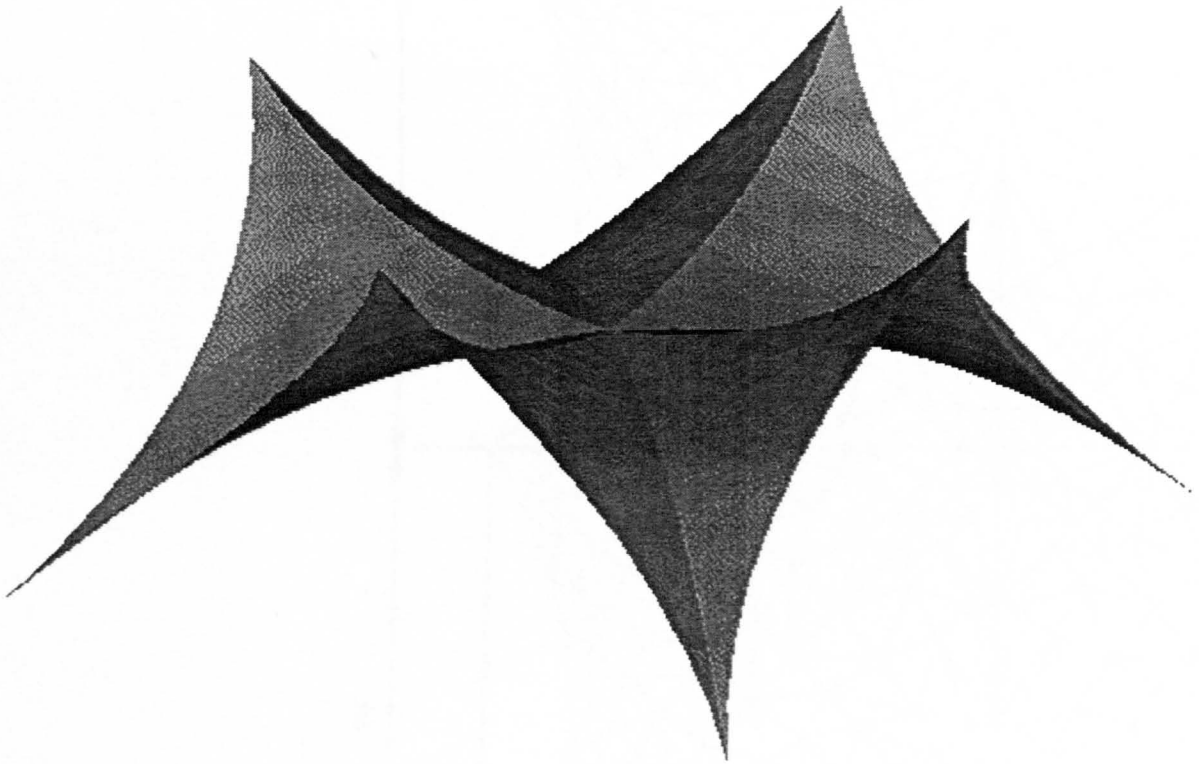

Figure 5-30 Example 5.2.7.1 - Rendered View.

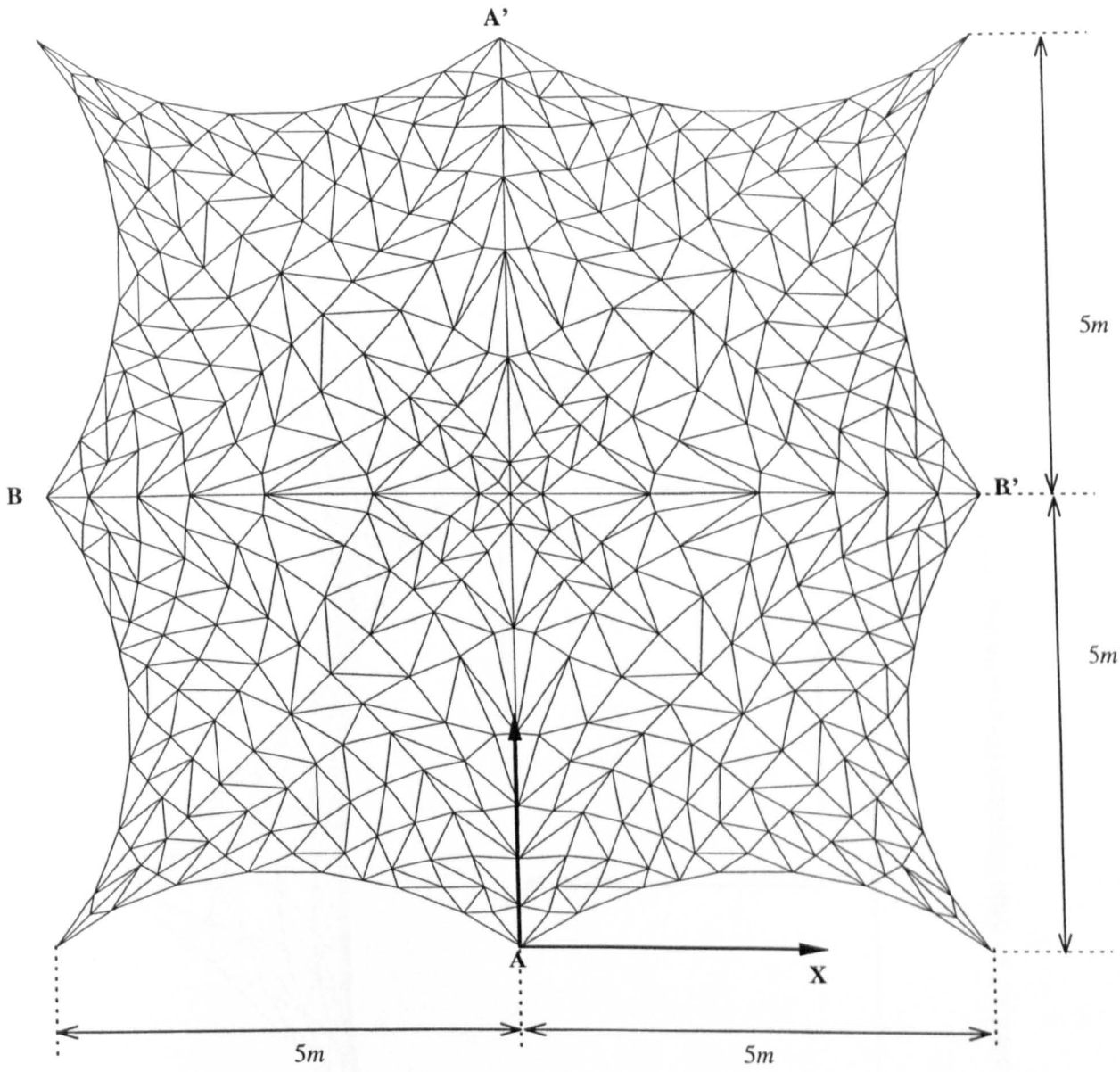

Figure 5-31 Example 5.2.7.2 - Plan View.

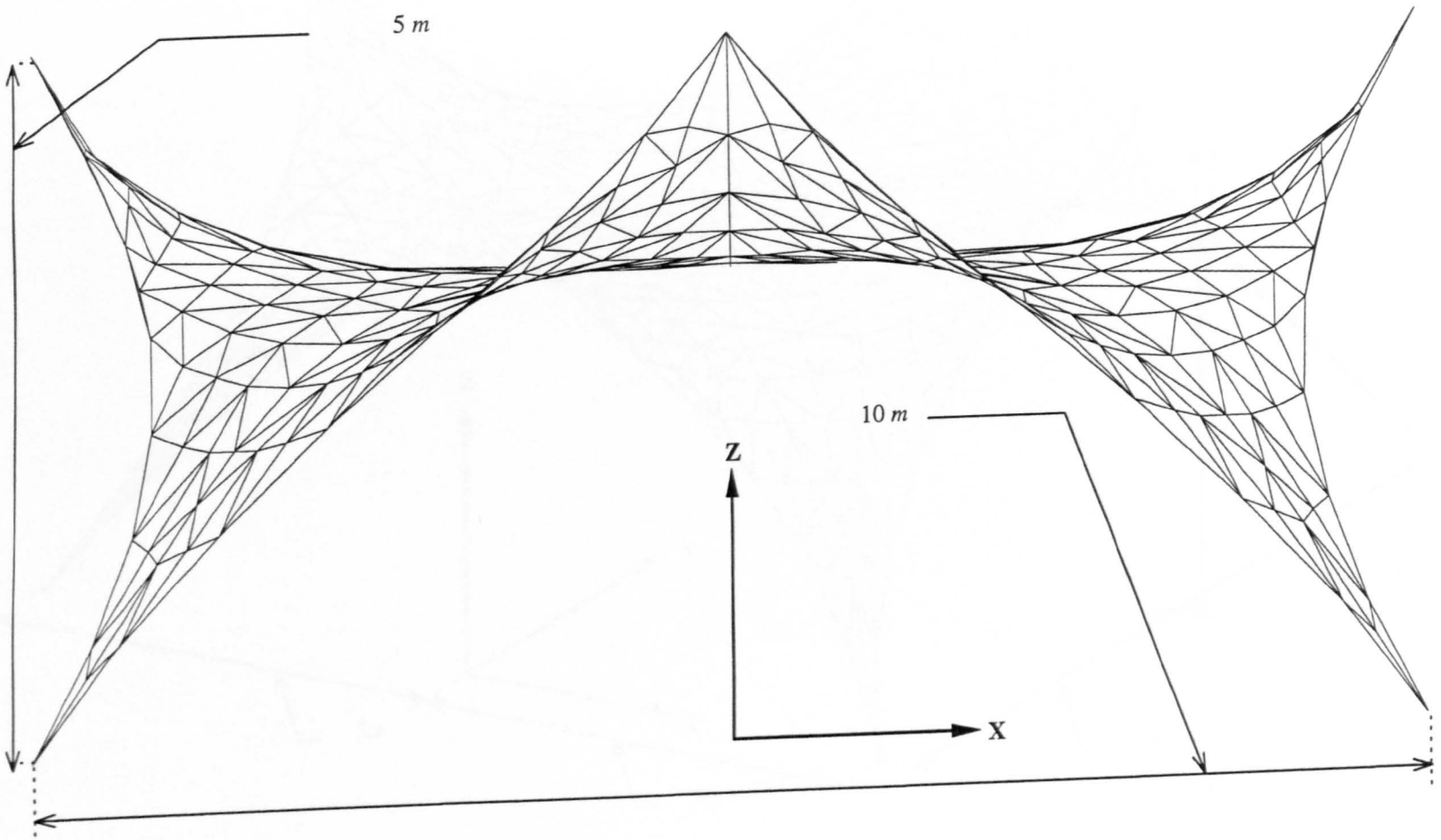

Figure 5-32 Example 5.2.7.2 - Side Elevation (Cross-Section BB').

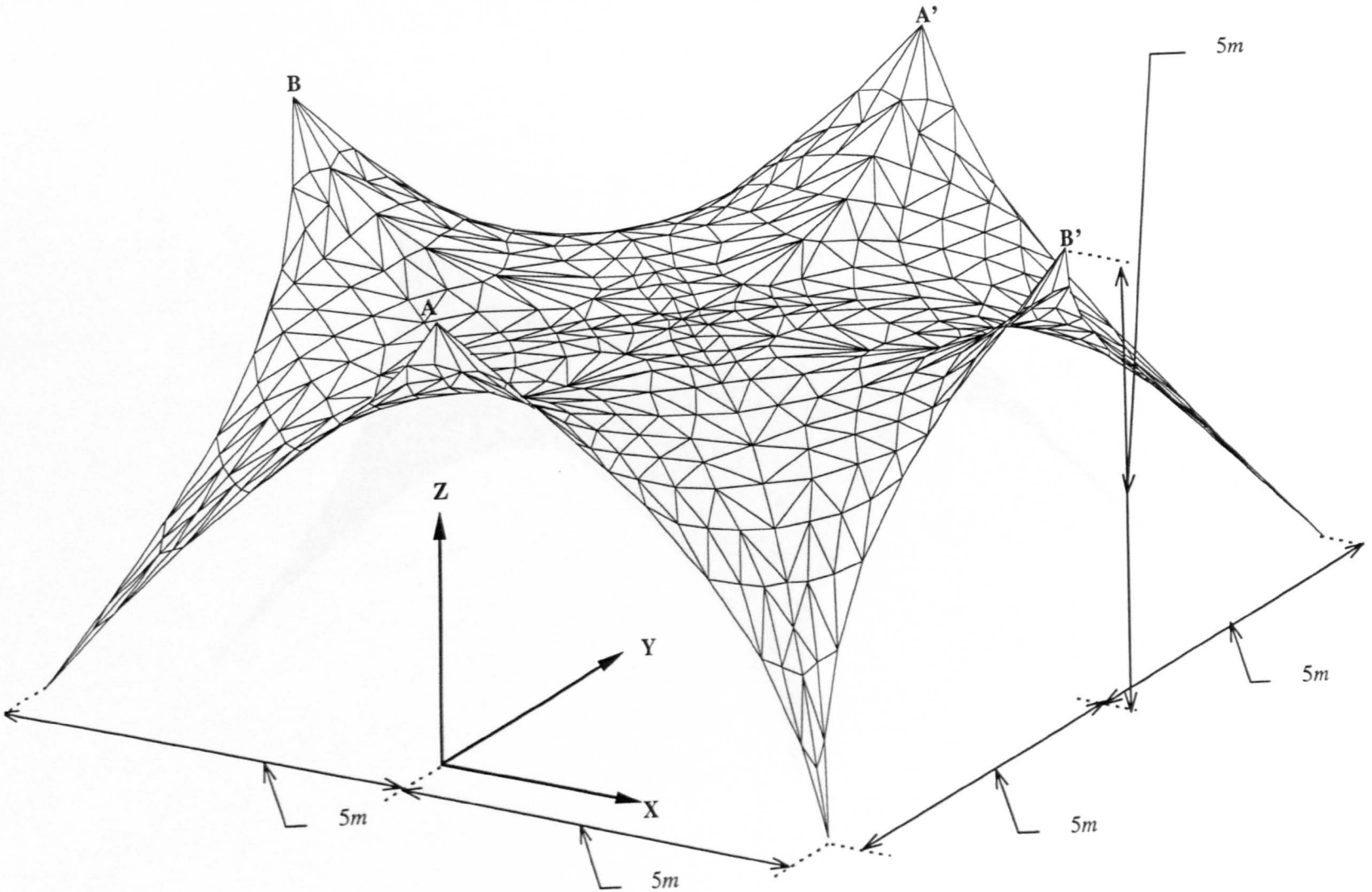

Figure 5-33 Example 5.2.7.2 - Perspective View.

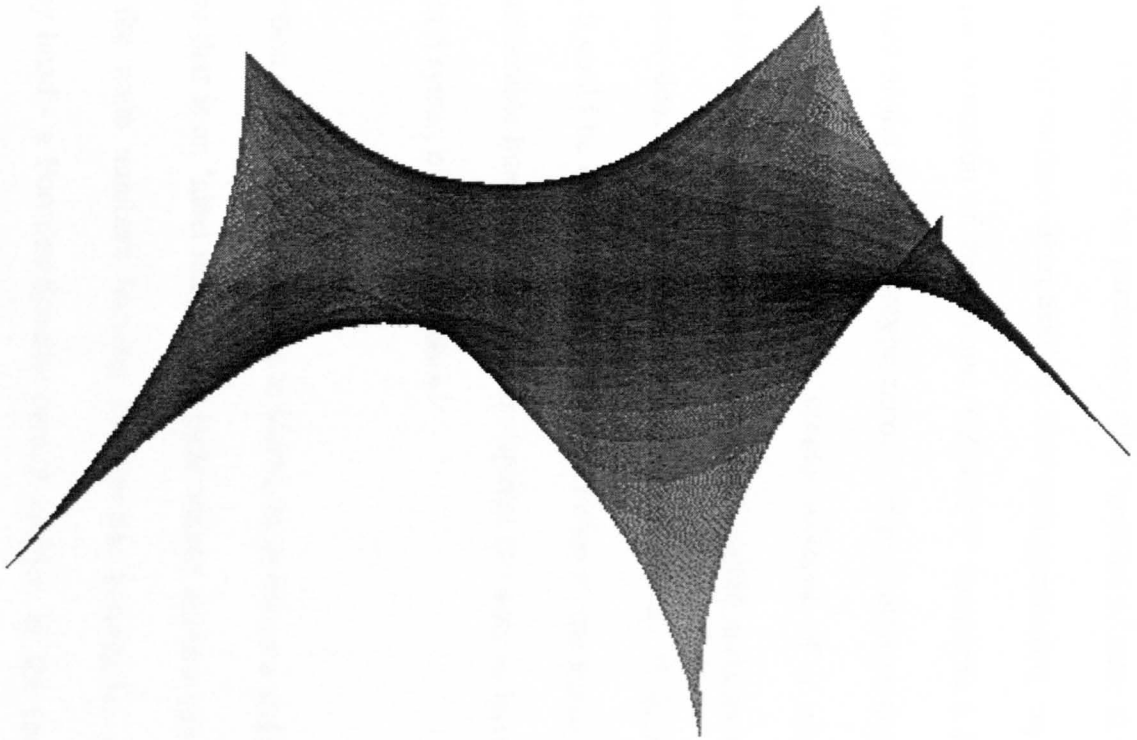

Figure 5-34 Example 5.2.7.2 - Rendered View).

5.3 Summary.

For the instance when a stable minimal surface is bounded by a rigid boundary, a scheme is equivalent to a self-contained 'module', responsible for the generation of all the data relating to an initial surface. It is illustrated, particularly by example 5.2.5, how a wide array of surfaces, of geometries suitable for the shape of a light-weight tension structure, can be created by the alteration of the parameters of a Formian scheme that relate to the boundary dimensions and the surface discretisation. The post-processing capabilities of Formian are explored in the formation of the scheme 'CANOPY' (example 5.2.3, Figure 5-8 (a)), and the manufacture of the rapid prototype models of the surfaces depicted in examples 5.2.1 and 5.2.2. Furthermore, the ability to create surfaces of a non-standard geometry is demonstrated by the paragenic formulations of the initial surfaces used in the form-finding of the surfaces described in examples 5.2.4 and 5.2.5. With respect to Table 5A.9, Appendix 5, it could be concluded that the generation of the initial surface (Example 5.2.6) can be a considerable intellectual task, and requires the user to have a full understanding of the concept and syntax of formex algebra.

The introduction of flexible boundaries is shown to produce a stable minimal surface of an elegant shape that is an 'ideal image' of a light-weight tension structure. Connectivity data relating to the node numbers forming the flexible boundaries of the initial surface is calculated by hand - a Formian Scheme cannot provide all the form-finding data for such surfaces. Flexible cables were shown to alter significantly the surface geometry, as shown by the discrepancy in the geometry between the surfaces depicted in examples 5.2.7.1 and 5.2.7.2. There is no means of easily modifying local areas, or points, of the initial discretised surface using Formian - modifications must be done by editing the appropriate data file with an editor (Examples 5.2.7.1 and 5.2.7.2).

APPENDIX 5

5A.1 "SCHEME1" Formian Scheme.

```
SCHEME1='[:m,n,p,width,length:
a=[0,2,0;2,2,0;2,0,0]#[2,0,0;0,2,0;0,0,0]
b=RINID(m,n,2,2)|a
c=BHP(1,1,1,p)|b
d=LAM(2,2*n)|c
u1=width/(2*m)
u2=length/(4*n)
u3=1
surf=BT(u1,u2,u3)|d
bound=(RIN(1,m,2)|[0,0,0])#(RIN(2,(n+1),2)|([0,0,0]#[2*m,0,0]))
bound=MED|bound
bound=BHP(1,1,1,p)|bound
bound=LAM(2,2*n)|bound
bound=MED|(bt(u1,u2,u3)|bound)
interior=LUX(bound)|surf
interior=MED|interior
totnod=bound#interior
mem=DIC(totnod)|surf
memb=DIC(totnod)|bound
CLEAR
USE VM(2),VT(2),VH(12*n,-6*n,6*n,0,0,0,0,0,1)
SHOW surf
KEEP totnod,mem,memb]'
```

5A.2 "RPM1" Formian Scheme.

```
RPM1='[:m,n,p,width,length,depth_1,depth_2:
TAKE f_fin1
seq=[(2*m),0,0;(2*m),2,0;(2*m),2,-depth_1]#..
      [(2*m),0,0;(2*m),0,-depth_1;(2*m)..
      ,2,-depth_1]
seq1=RIN(2,n,2)|seq
seq1a=BHP(1,1,1,p)|seq1
d1=[(2*m),2,-depth_1]
d1a=RIN(2,n,2)|d1
mark=BHP(1,1,1,p)|d1a
alter=[(2*m),2,-depth_1]
alternod=RIN(2,n,2)|alter
back=LAM(2,2*n)|(NOV(mark,alternod)|seq1a)
strip=BHP(1,1,1,p)|(RIN(2,n,2)|{[2*m,0,0;2*m,2,0;2*m+2,2,0],..
      [(2*m)+2,2,0;(2*m)+2,0,0;2*m,0,0]})
stripalt=BHP(1,1,1,p)|(RIN(2,n+1,2)|[(2*m)+2,0,0])
altnod=BHP(1,1,1,p)|(RIN(2,n+1,2)|[2*m,0,0])
bot_stri=RIN(2,n,2)|{[2*m,0,-depth_1;2*m,2,-depth_1;2*m+2,2,..
    -depth_1],[2*m+2,2,-depth_1;2*m+2,0,-depth_1;2*m,0,-depth_1]}
bot_alt=RIN(2,n+1,2)|[2*m+2,0,-depth_1]
bot_nod=RIN(2,n+1,2)|[2*m,0,-depth_1]
front=LAM(2,2*n)|RIN(2,n,2)|([0,0,0;0,2,0;0,2,-depth_1]#..
[0,0,0;0,0,-depth_1;0,2,-depth_1])
side=LAM(2,2*n)|(RIN(1,m,2)|([0,0,0;2,0,0;2,0,-depth_1]#[0,0,0;0,0,..
      -depth_1;2,0,-depth_1]))
base=RINID(m,2*n,2,2)|([0,0,-depth_1;0,2,-depth_1;2,2,-depth_1]#..
[0,0,-depth_1;2,0,-depth_1;2,2,-depth_1])
supp=front#side#base
u1=width/(2*m)
u2=length/(4*n)
supp=BT(u1,u2,1)|supp
back=BT(u1,u2,1)|back
strip=BT(u1,u2,1)|strip
bot_stri=BT(u1,u2,1)|bot_stri
bot_alt=BT(u1,u2,1)|bot_alt
bot_nod=BT(u1,u2,1)|bot_nod
stripalt=BT(u1,u2,1)|stripalt
altnod=BT(u1,u2,1)|altnod
unip1=2*u1*m
unip1b=depth_2
unip1b=unip1+unip1b
unip2=2*n*u2
displ=depth_2
bot_nod=TRAN(1,displ)|bot_nod
bot_stri=LAM(2,2*u2*n)|(NOV(bot_alt,bot_nod)|bot_stri)
back=TRAN(1,displ)|back
backedge={[unip1,0,-depth_1;unip1,0,0;unip1b,0,0],[unip1b,0,0..
          ;unip1b,0,-depth_1;unip1,0,-depth_1]}
backedge=LAM(2,unip2)|backedge
altnod=TRAN(1,displ)|altnod
strip=LAM(2,2*u2*n)|NOV(stripalt,altnod)|strip
support=supp#backedge#back#strip#bot_stri
stl1=f_fin1#support
USE VH(100,50,15,0,0,-10,0,0,1),VM(2)
show stl1
stlnod=MED|stl1
stlmem=DIC(stlnod)|stl1
stl1=RED(stlnod)|stlmem
supnod=MED|support
supmem=DIC(supnod)|support
support=RED(supnod)|supmem
KEEP stl1,support]'
```

5A.3 "SCHEME2" Formian Scheme.

```
SCHEME2='[:m,n,radius,radius2,angle:
    disp=radius2+radius
    a=RINIT(m,n,2,2)|([radius2,0,0;radius2,0,2;radius2,2,2]#..
        [radius2,0,0;radius2,2,0;radius2,2,2])
    b=BC(1,angle/(2*m),1)|a
    c=TRAN(1,-disp)|VERAT(0,0,-90)|b
    u1=1
    u2=360/(2*n)
    u3=1
    surf=BC(u1,u2,u3)|c
    bound1=PEX|(RIN(3,n,2)|[radius2,0,0])
    bound2=PEX|(RIN(3,n,2)|[radius2,2*m,0])
    bound1=BC(u1,u2,u3)|TRAN(1,-disp)|VERAT(0,0,-90)..
        |BC(1,angle/(2*m),1)|bound1
    bound2=BC(u1,u2,u3)|TRAN(1,-disp)|VERAT(0,0,-90)..
        |BC(1,angle/(2*m),1)|bound2
    bound=MED|(bound1#bound2)
    interior=MED|(LUX(bound)|surf)
    totnod=bound#interior
    memb=DIC(totnod)|bound
    mem=DIC(totnod)|surf
    USE VM(2),VH(0,0,-30,0,5,0,0,5,1)
    CLEAR
    SHOW surf
    KEEP totnod,mem,memb]'
```

5A.4 "RPM2" Formian Scheme.

```
RPM2='[:m,n,radius,radius2,angle,depth:
    displ=radius+radius2
    TAKE f_fin2
    height=radius2*(SIN|angle)
    z=-(height+depth)
    mark1=200
    mark2=300
    tri1=RIN(3,n,2)|([radius2,2*m,0;radius2,2*m,2;mark1,mark1,mark1])
    tri2=RIN(3,n,2)|([radius2,2*m,0;mark2,mark2,mark2;mark1,..
    mark1,mark1])
    a=RIN(3,n,2)|([radius2,2*m,0])
    b=RIN(3,n,2)|([radius2,2*m,2])
    c=BC(1,360/(2*n),1)|TRAN(1,-displ)|VERAT(0,0,-90)..
          |BC(1,angle/(2*m),1)|b
    d=BC(1,360/(2*n),1)|TRAN(1,-displ)|VERAT(0,0,-90)..
          |BC(1,angle/(2*m),1)|a
    tri1=BC(1,360/(2*n),1)|TRAN(1,-displ)|VERAT(0,0,-90)..
          |BC(1,angle/(2*m),1)|tri1
    tri2=BC(1,360/(2*n),1)|TRAN(1,-displ)|VERAT(0,0,-90)..
          |BC(1,angle/(2*m),1)|tri2
    e=DEP(3)|c
    f=PAN(3,z)|e
    g=DEP(3)|d
    h=PAN(3,z)|g
    newmark1=RIN(3,n,2)|[mark1,mark1,mark1]
    newmark2=RIN(3,n,2)|[mark2,mark2,mark2]
    newmark1=BC(1,360/(2*n),1)|TRAN(1,-displ)|VERAT(0,0,-90)..
          |BC(1,angle/(2*m),1)|newmark1
    newmark2=BC(1,360/(2*n),1)|TRAN(1,-displ)|VERAT(0,0,-90)..
          |BC(1,angle/(2*m),1)|newmark2
    tri1a=NOV(newmark1,f)|tri1
    tri2a=NOV(newmark1,f)|tri2
    tri2a=NOV(newmark2,h)|tri2a
    side=tri1a#tri2a
    top=RIN(3,n,2)|[radius2,0,0;radius2,0,2;0,0,0]
    bot=RIN(3,n,2)|[mark1,mark1,mark1;mark2,mark2,mark2;..
          radius2,radius2,radius2]
    midbot=RIN(3,n,2)|[radius2,radius2,radius2]
    midtop=RIN(3,n,2)|[0,0,0]
    topa=BC(1,360/(2*n),1)|TRAN(1,-displ)|VERAT(0,0,-90)..
          |BC(1,angle/(2*m),1)|top
    midtop=BC(1,360/(2*n),1)|TRAN(1,-displ)|VERAT(0,0,-90)..
          |BC(1,angle/(2*m),1)|midtop
    bota=BC(1,360/(2*n),1)|TRAN(1,-displ)|VERAT(0,0,-90)..
          |BC(1,angle/(2*m),1)|bot
    midbot=BC(1,360/(2*n),1)|TRAN(1,-displ)|VERAT(0,0,-90)..
          |BC(1,angle/(2*m),1)|midbot
    value1=LIB(i=2,n)|[0,0,0]#[0,0,0]
    value2=LIB(i=2,n)|[0,0,z]#[0,0,z]
    top=NOV(midtop,value1)|topa
    botb=NOV(newmark1,f)|bota
    botc=NOV(newmark2,h)|botb
    bottom=NOV(midbot,value2)|botc
    USE VM(2), VH(0,10,0,0,5,0,0,1,0)
    CLEAR
    stl2=f_fin2#top#bottom#side
    SHOW stl2
    stlnod=MED|stl2
    stlmem=DIC(stlnod)|stl2
    tent3stl=RED(stlnod)|stlmem
    KEEP stl2,stlmem,stlnod]'
```

5A.5 "SCHEME3" Formian Scheme.

```
SCHEME3='[ :m,n,height,length,width:
    tri1=[0,0,0;2,0,-2;1,1,-1]
    tri1=RINAX(0,0,0,2,0,-2,m)|tri1
    tri2=[1,1,-1;2,0,-2;3,1,-3]
    tri2=RINAX(1,1,-1,3,1,-3,(m-1))|tri2
    tri3=[1,1,-1;3,1,-3;2,2,-2]
    tri3=RINAX(1,1,-1,3,1,-3,(m-1))|tri3
    tri4=[0,2,0;1,1,-1;2,2,-2]
    tri4=RINAX(0,2,0,2,2,-2,m)|tri4
    tri5=[0,0,0;1,1,-1;0,2,0]
    lastnode=2*m
    tri6=[(lastnode-1),1,-(lastnode-1);lastnode,0,-lastnode;..
          lastnode,2,-lastnode]
    segment=tri1#tri2#tri3#tri4#tri5#tri6
    surf=RINAX(0,0,0,0,2,0,n)|segment
    surf=LAM(1,lastnode)|surf
    u1=width/lastnode
    u2=length/(2*n)
    u3=height/lastnode
    bound1=LAM(1,2*m)|(LAM(2,n)|(RINAX(0,0,0,2,0,-2,(m+1))|[0,0,0]))
    bound2=LAM(1,2*m)|(RIN(2,n+1,2)|[0,0,0])
    bound=PEX|(bound1#bound2)
    bound=BT(u1,u2,u3)|bound
    surface=BT(u1,u2,u3)|surf
    interior=MED|(LUX(bound)|surface)
    totnod=bound#interior
    memb=DIC(totnod)|bound
    mem=DIC(totnod)|surface
    USE VM(2),VP(0,0,30)
    CLEAR
    SHOW surface
    KEEP totnod,mem,memb]'
```

5A.6 "CANOPY" Formian Scheme.

```
CANOPY='[:width,num:
TAKE f_fin3

canop=RIN(1,num,-2*width)|f_fin3

KEEP canop

]'
```

5A.7 "SCHEME4" Formian Scheme.

```
SCHEME4='{:m,n,width,length,height,num:
a1=[2*m,0,0;2*m,2,0;2*m,2,2]#[2*m,0,0;2*m,0,2;2*m,2,2]
a=LAM(2,2*m)|(RINIT(m,n,2,2)|a1)
b=VERAD(0,0,-90)|BC(1,180/(4*m),1)|a
c=RIN(2,num,4*m)|REF(1,2*m)|b
d=BS(1,360/(num*4*m),90/(2*n))|TRAN(1,2*m)|c
bound1=RINIT(2,n+1,(4*m),2)|[2*m,0,0]
bound2=RIN(2,(2*m)+1,2)|([2*m,0,2*n]#[2*m,0,2]#[2*m,0,0])
bounda=bound1#bound2
bound=MED|bounda
u1=width/(6*m*(COS|(360/(2*num))))
u2=length/(6*m*(SIN|(360/(2*num))))
u3=height/(6*m)
surf=BT(u1,u2,u3)|d
bound=VERAD(0,0,-90)|BC(1,180/(4*m),1)|bound
bound=RIN(2,num,4*m)|REF(1,2*m)|bound
bound=BS(1,360/(num*4*m),90/(2*n))|TRAN(1,2*m)|bound
bound=BT(u1,u2,u3)|bound
bound=MED|bound
interior=LUX(bound)|surf
interior=MED|interior
totnod=bound#interior
mem=DIC(totnod)|surf
memb=DIC(totnod)|bound
KEEP mem,memb,totnod
SHOW surf]'
```

5A.8 "SCHEME5" Formian Scheme.

```
SCHEME5='[:m,n,length,height,width,disp:
angle=ASIN|(height/(length+disp))
a=RINIT(m,n,2,2)|([1,0,0;1,2,0;1,0,2]#[1,0,2;1,2,2;1,2,0])
b=LAM(2,2*m)|a
c=BC(1,180/(4*m),1)|b
d=VERAS(0,0,-90)|c
u1=length/(2*n)
u2=1
u3=width/2
e=TRAN(1,disp)|(BT(u1,u2,u3)|d)
f=BC(1,angle,1)|e
surf=VERAT(0,0,90)|(TRAN(1,-disp)|f)
bound=VERAS(0,0,-90)|bound
bound=BC(1,180/(4*m),1)|bound
bound=(RIN(2,m+1,2)|([1,0,0]#[1,0,2*n]))#..
(RIN(3,n+1,2)|[1,0,0])
bound=LAM(2,2*m)|bound
bound=PEX|bound
bound=TRAN(1,disp)|(BT(u1,u2,u3)|bound)
bound=BC(1,angle,1)|bound
bound=VERAT(0,0,90)|(TRAN(1,-disp)|bound)
interior=LUX(bound)|surf
interior=MED|interior
totnod=bound#interior
mem=DIC(totnod)|surf
memb=DIC(totnod)|bound
KEEP mem,memb,totnod]'
```

5A.9 "SCHEME6" Formian Scheme.

```
SCHEME6='[:num,pitch,width,height:
length=width/2
u1=1.0
u2=1-2*(SIN|(45/2))^2
x=2*(num+1)*(COS|45)
hol_bou1=LAM(1,0)|([0,-2*num,0]#[2,-2*num,0])
hole=[0,-2*num-2,0]
add_nod1=[2*num,0,0]
bound_1=RINAD(0,-2*num-2,2*num+2,0,num+2,2*sqrt|2)|[0,-2*num-2,0]
hol_ele1=LAM(1,0)|([0,-2*num,0;2,-2*num,0;0,-2*num-2,0]#..
      [0,-2*num-2,0;2,-2*num-2,0;2,-2*num,0])
a=[0,-2,0;0,0,0;2,-2,0]#[2,-2,0;2,0,0;0,0,0]
b=GENID(num,num,2,-2,0,-1)|a
c=RINAD(0,-2*num-2,2*num+2,0,num+1,2*sqrt|2)|..
  [0,-2*num-2,0;2,-2*num,0;0,-2*num,0]
d=b#c
e=BT(u1,u2,0)|(VERAX(0,-1,0,0,1,0,45)|..
(VER(1,2,0,0,45)|d))
f=VER(1,2,0,0,-90)|e
g=BHP(1,1,1,pitch)|d
h=VER(1,2,0,0,45)|g
i=ROS(1,2,0,0,2,-90)|f
j=VERAX(0,-1,0,0,1,0,45)|h
k=BT(u1,u2,0)|j
l=ROS(1,2,0,0,2,90)|k
hole=BT(u1,u2,0)|(VERAX(0,-1,0,0,1,0,45)|..
        (VER(1,2,0,0,45)|hole))
hole=VER(1,2,0,0,-90)|hole
m=LUX(hole)|(l#i)
hol_ele2=BT(u1,u2,0)|(VERAX(0,-1,0,0,1,0,45)|..
        (VER(1,2,0,0,45)|hol_ele1))
hol_ele3=VER(1,2,0,0,45)|hol_ele2
hol_ele4=TRAN(1,-2*u2)|(VERAX(x,1,0,x,-1,0,-90)|hol_ele3)
hol_ele5=VER(1,2,0,0,-45)|hol_ele4
hol_ele6=VER(1,2,0,0,-90)|hol_ele5
n=m#hol_ele6
hol_bou2=BT(u1,u2,0)|(VERAX(0,-1,0,0,1,0,45)|..
        (VER(1,2,0,0,45)|hol_bou1))
hol_bou3=VER(1,2,0,0,45)|hol_bou2
hol_bou4=TRAN(1,-2*u2)|(VERAX(x,1,0,x,-1,0,-90)|hol_bou3)
hol_bou5=VER(1,2,0,0,-45)|hol_bou4
hol_bou6=VER(1,2,0,0,-90)|hol_bou5
bound_2=BT(u1,u2,0)|(VERAX(0,-1,0,0,1,0,45)|..
(VER(1,2,0,0,45)|(BHP(1,1,1,pitch)|bound_1)))
bound_3=ROS(1,2,0,0,2,90)|bound_2
add_nod2=BT(u1,u2,0)|(VERAX(0,-1,0,0,1,0,45)|..
(VER(1,2,0,0,45)|(BHP(1,1,1,pitch)|add_nod1)))
u1a=width/(2*(num+1)*u1)
u2a=length/(num+1)
u3a=height/(2*u2)
length=(num+1)*u2a
width=2*(num+1)*u1a
o=BT(u1a,u2a,u3a)|n
p=TRANAD(width/2,-length,0,0)|o
surf=LAM(1,0)|(LAM(2,2*length)|VER(1,2,0,0,-90)|p)
```

```
bound_4=BT(u1a,u2a,1)|bound_3
bound_5=VER(1,2,0,0,-90)|(TRANAD(width/2,-length,0,0)|bound_4)
bound_6=LAM(1,0)|(LAM(2,2*length)|bound_5)
add_nod3=BT(u1a,u2a,1)|add_nod2
add_nod4=LAM(2,-length)|add_nod3
add_nod5=VER(1,2,0,0,-90)|(TRANAD(width/2,-length,0,0)|add_nod4)
add_nod6=LAM(2,2*length)|add_nod5
add_nod=MED|add_nod6
hol_bou7=BT(u1a,u2a,u3a)|hol_bou6
hol_bou8=VER(1,2,0,0,-90)|(TRANAD(width/2,-length,0,0)|hol_bou7)
hol_bou9=LAM(1,0)|(LAM(2,2*length)|hol_bou8)
hol_boun=MED|hol_bou9
bound=(MED|bound_6)#hol_boun
int=LUX(bound)|surf
int1=MED|int
internal=int1#add_nod
internal=MED|internal
totnod=bound#internal
memb=DIC(totnod)|bound
mem=DIC(totnod)|surf
KEEP mem,memb,totnod
USE vm(2)
SHOW surf]'
```

5A.10 "SCHEME7" Formian Scheme.

```
SCHEME7 ='[:num,pitch,width:
length=width/2
u1=1.0
u2=1-2*(SIN|(45/2))^2
x=2*(num+1)*(COS|45)
add_nod1=[2*num,0,0]
bound_1=RINAD(0,-2*num-2,2*num+2,0,num+2,2*sqrt|2)|[0,-2*num-2,0]
a=[0,-2,0;0,0,0;2,-2,0]#[2,-2,0;2,0,0;0,0,0]
b=GENID(num,num,2,-2,0,-1)|a
c=RINAD(0,-2*num-2,2*num+2,0,num+1,2*sqrt|2)|..
   [0,-2*num-2,0;2,-2*num,0;0,-2*num,0]
d=b#c
e=BT(u1,u2,0)|(VERAX(0,-1,0,0,1,0,45)|..
(VER(1,2,0,0,45)|d))
f=VER(1,2,0,0,-90)|e
g=BHP(1,1,1,pitch)|d
h=VER(1,2,0,0,45)|g
i=ROS(1,2,0,0,2,-90)|f
j=VERAX(0,-1,0,0,1,0,45)|h
k=BT(u1,u2,0)|j
l=ROS(1,2,0,0,2,90)|k
m=l#i
bound_2=BT(u1,u2,0)|(VERAX(0,-1,0,0,1,0,45)|..
(VER(1,2,0,0,45)|(BHP(1,1,1,pitch)|bound_1)))
bound_3=ROS(1,2,0,0,2,90)|bound_2
add_nod2=BT(u1,u2,0)|(VERAX(0,-1,0,0,1,0,45)|..
(VER(1,2,0,0,45)|(BHP(1,1,1,pitch)|add_nod1)))
u1a=width/(2*(num+1)*u1)
u2a=length/(num+1)
length=(num+1)*u2a
width=2*(num+1)*u1a
n=BT(u1a,u2a,1)|m
o=TRANAD(width/2,-length,0,0)|n
surf=LAM(1,0)|(LAM(2,2*length)|VER(1,2,0,0,-90)|o)
bound_4=BT(u1a,u2a,1)|bound_3
bound_5=VER(1,2,0,0,-90)|(TRANAD(width/2,-length,0,0)|bound_4)
bound_6=LAM(1,0)|(LAM(2,2*length)|bound_5)
add_nod3=BT(u1a,u2a,1)|add_nod2
add_nod4=LAM(2,-LENGTH)|add_nod3
add_nod5=VER(1,2,0,0,-90)|(TRANAD(width/2,-length,0,0)|add_nod4)
add_nod6=LAM(2,2*length)|add_nod5
add_nod=MED|add_nod6
bound=(MED|bound_6)
int=LUX(bound)|surf
int1=MED|int
internal=int1#add_nod
internal=MED|internal
totnod=bound#internal
memb=DIC(totnod)|bound
mem=DIC(totnod)|surf
KEEP mem,memb,totnod
USE vm(2)
SHOW surf]'
```

REFERENCES.

5.1 J. Moore,
"Investigation of Hyperbolic Paraboloidal Roof Structures."
Meng Dissertation, Department of Civil Engineering, University of Surrey, 1994.

5.2 D. Hadker,
"Formex Configuration Processing for Space Structures."
PhD Thesis, Department of Civil Engineering, University of Surrey, 1994.

5.3 "Membrane Design in Japan 1967-1990."
Shinkenchiku-sha Co., ltd., Tokyo, Japan, pages 36-37, 1990.

CHAPTER 6

Possible Future Areas of Research.

6.1 Introduction

A discussion of some of the major applications of stable minimal surfaces in the design of both light-weight tension structures, rigid structures and mechanical components, is documented within this Section. Topics suitable for possible future research in these areas are discussed, together with the possible merits that the future work could offer.

6.2 Light-Weight Tension Structures.

It has been shown that by using the numerical form-finding algorithm presented in this thesis appropriately, it is possible to recreate accurately stable minimal surfaces, even from a very crude initial surface. However, if stable minimal surfaces are to be used in the design of light-weight membrane structures, the problems of material properties, static behaviour and determination of a suitable fabric cutting pattern will all need to be addressed.

6.2.1 Problems of Material Behaviour.

Stable minimal surfaces are the ideal shape for a pre-stressed fabric membrane made of an isotropic material and prestressed, in their unloaded state, by a constant stress in the warp and weft directions of the fabric (with zero shear stress). Isotropic materials used in the construction of light-weight tension structures have included rubbers e.g. neoprene, and plastics e.g. polyurethane. Unfortunately, the materials have a very poor strength and are only suitable for the construction of small temporary structures[6.1]. Typically, fabrics are

used which tend to be of a highly anisotropic nature, due partly to the weaving process which causes the strength and extension properties of the fabric to differ in the warp and weft directions[i]. After weaving, the fabric is usually coated with a material such as PVC or PTFE to improve the strength and reduce the permeability. (PTFE is very strong but has a low extension, whereas PVC coated fabrics tend to be of a lower strength but a higher extension - the cross-sectional view of a typical coated fabric is shown in Figure 6-1). Although the anisotropic properties of a coated fabric can be improved to some extent by the tensioning of the weft yarns before the coating of the fabric (thereby obtaining somewhat similar stress/strain characteristics for the warp and weave[1]), it has been stated that the stressing of such a coated fabric by equal amounts in the warp and weft direction can, for a low level of pre-stress, result in the negative straining of the warp yarns[6.2]. Hence, it is apparent that it is an extremely difficult proposition to manufacture a light-weight tension structure, from the coated fabrics currently available today, that resembles a stable minimal surface.

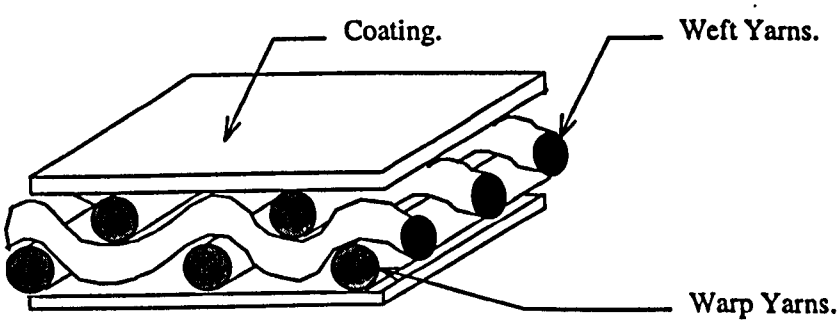

Figure 6-1 Typical Cross-Section of a Coated Fabric.

However, as the demand for structural configurations conforming to the geometry of stable minimal surfaces increases, it is likely that new fabrics/materials and manufacturing processes will be developed that aim to combat the anisotropic behaviour of fabrics. One

[i] The manufacture of a fabric involves the tensioning of the warp yarns such that they are straight, and then weaving the weft yarns backwards and forwards in a direction orthogonal to the warp. This produces a sinusoid profile for the warp yarns. [i].

type of fabric developed recently is the "précontraint" fabric by Serge Ferrari. This fabric exhibits very similar behaviour in the warp and weft directions[6.3] and is deemed to be isotropic.

Prospective research could be directed at amending the computational algorithm to take account of the material properties of a variety of fabrics, with a view to assessing the suitability of these fabrics in recreating stable minimal surfaces.

6.2.2 Static Analysis.

The scope of this thesis has been confined to the form-finding of light-weight tension structures conforming to the geometry of a stable minimal surface, and the manufacture of accurate physical models of such surfaces. The next immediate task should be the assessment of the performance of the numerically derived stable minimal surfaces under a variety of imposed load conditions such as wind, or snow. The algorithm, presented in this thesis, is capable of predicting the behaviour of stable minimal surfaces when subjected to a static loading, provided it is amended to take account of the elastic properties of the fabric material. Further work should focus on numerical modelling investigations concerning the comparison of the static behaviour of membranes possessing a stable minimal surface geometry, with those where a non-uniform pre-stress defines the shape. In addition, the effects of shear stresses[ii] should be considered in the numerical modelling, as these will be induced within the membrane fabric under the application of an imposed loading[6.2].

[ii] In areas where there is a high stress concentration, the shear stress will affect the flow of stresses and the strength of the material under tearing.

The prospective research should aim to justify further the applicability of using a stable minimal surface in the design of a light-weight tension structure and would confirm, or disprove, some of the following notions:

(A) As stated in the introduction to this thesis, Nature shows us examples of structures that have been optimised to resist the most critical load condition. This has been echoed by Isler, who has continually stressed that the most important load case that needs addressing is that which is present during the whole life span of a structure - in the case of concrete shells; the compressive forces from gravity[6.4] (Chapter 1). With regards to light-weight tension structures, the permanent load is that of the surface pre-stress under no static loading - this load is forever present, unlike those of the imposed loading conditions. A stable minimal surface, possessing a constant surface stress, would thus appear to be the optimal shape for such a structure.

(B) In practice, light-weight tension structures tend to be pre-stressed (in their unloaded state) by unequal amounts in the warp and weft direction of the fabric, to ensure an adequate resistance to the anticipated imposed load conditions. For example, if the loading from snow is considered to be a dominant load case, then the tensions in the fibres of the fabric aligned along the principal curvature in the sagging direction of the structure are increased, thereby "lifting" the fibres in the hogging direction and causing the distortion of the pre-stressed (unloaded) surface geometry[6.5]. A uniform stress field implies that a stable minimal surface will possess the same geometry irrespective of the pre-scribed stress-level (Chapter 1, Section 1.2.2, and Chapter 4, Section 4.6). A membrane structure conforming to such a geometry should be able to have its loading capacity increased, while keeping its form intact, by simply improving the unloaded

structural stiffness through the uniform increase of stresses in the warp and weft directions of the fabric (a feasible option with the use of the "précontraint" fabric for example (Section 6.2.1)). Thus, a stable minimal surface should give a geometry that is more likely to be realised in practice.

(C) Another possible advantage of adopting a stable minimal surface ideology may be derived when considering the behaviour of the surface under a static loading. If an imposed load acts perpendicular to the surface of a membrane, the fibres in the sagging direction will undergo an increase in tension while those in the hogging direction experience a reduction in tension. Although it is true that this will result in an uneven stress field for both surfaces of a non-uniform pre-stress and a uniform pre-stress (stable minimal surface), for the instance where a different pre-stress has been employed in the warp and weft directions, the fibres in these directions will possess different load displacement curves. This implies that the increase and decrease of the tensions in the sagging and hogging directions will be dissimilar, and could lead to the development of dangerous stress concentrations within the surface of the membrane which would limit the long term life span of the structure. The "précontraint" fabrics show very similar load displacement curves for the warp and weft directions when stressed equally in these directions. This observation would seem to suggest that a stable minimal surface would again be the optimum configuration for a structure constructed from such a material.

6.2.3 Cutting Pattern.

The determination of a suitable fabric cutting pattern is the area most likely to cause difficulties in recreating the geometry of a stable minimal surface. The process concerns the flattening of a segment of the three dimensional form-found surface onto a two dimensional

plane, such that the flattened segment fits within the maximum allowable width of the fabric, and the geometry of the 'sewn' structure closely approximates that of the form-found surface.

In reality, a stable minimal surface **cannot** in fact be developed onto a plane, and hence cannot be recreated exactly from a series of planar strips. Consequently, various techniques are being developed to 'unfold' or 'flatten' the surface. Commonly, the process involves a specialist surface discretisation: the seam lines of the fabric strips are defined by a series of nodes, where a single strip is formed from the triangulation of the nodes, and the width of the strip defined by a single element - from this point onwards, mesh arrangements of this type are referred to by the author as **"developable."** The triangulation is such, that the internal angles of each element remain undistorted, with no overlapping from neighbouring elements when the elements are unfolded, or flattened, on-to the same plane by rotating the elements about a common edge[6.6] (Figure 6-2). Once flattened, the unstressed dimensions of the fabric need to be determined. The last stage concerns the calculation of the distances, "offsets", of the right and left hand side seam lines from a suitable reference line. If the seam lines are of a poor definition, then the edges may be smoothed using a suitable curve approximation.

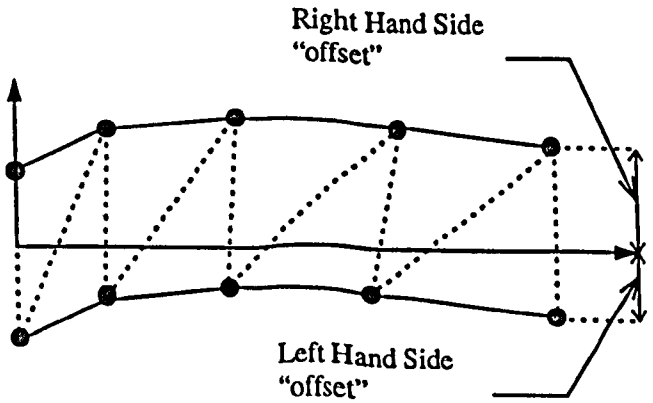

Figure 6-2 Flattening of a Fabric Strip

Employing strips that are of a width that has been maximised to ensure an economic use of material will produce an inaccurate representation of the form-found shape, unless the form-found surface is of a small curvature in comparison to the width of fabric used[6.7]. Increasing the number of strips used to define a surface will result in a more accurate approximation; however, this is often not a feasible proposition, as a large number of seam lines is an aesthetically undesirable option.

The profile of a flattened strip tends to be either curved, straight or a combination of the two. It is extremely difficult to predict the curvature of a seam line, consequently, it is possible to arrive at excessively bowed strips leading to a large wastage of material. Ideally, the seam lines should follow geodesic lines. These are defined as those lines that possess zero geodesic curvature[iii]. A simpler interpretation is that they are lines spanning the shortest possible distance, over a surface, from two given points. Using geodesic lines to define a seam line has the advantage of ensuring that the width of the fabric is minimised, and the edges of the fabric strip tend to approximate straight lines and are, hence, not excessively bowed when unfolded/flattened onto a plane.

Generally, the process of determining the triangulated "developable" strips involves one of three alternatives:

(A) In the first option, the seam lines are defined by a series of nodes lying on the form-found surface. This is only possible, if the form-found surface possesses a mesh that is not excessively distorted and is suitable for development. If the initial surface has a surface discretisation that is of a regular "developable" pattern and closely approximates

[iii] The geodesic curvature refers to the orthogonal projection of the curvature vector of a point lying on a surface (i.e. the form-found surface), onto the plane tangent to the point being considered.

the form-found surface i.e. the change in surface area is minimal during form-finding - $A_{\%}$ is low, it is easier to arrive at a suitable cutting pattern. This is illustrated for the form-found surface presented in example 5.2.1 (Chapter 5, Section 5.2) and the catenoid surface presented in Chapter 4, Section 4.3 (Examples 4.3 and 4.4). Here, the seam lines can be seen to follow a smooth "developable" pattern, whereby the fabric strips are depicted by the radial segments of the surface. The disadvantage of the method is that the designer has no control over the width of the fabric defined by the seam lines and is unable to ensure that excessive bowing will be prevented.

(B) In the second method, the deformations of the discretised elements during form-finding are dictated, in order to achieve a smooth "developable" pattern. The approach can involve neglecting the contribution of residual forces normal to the plane of the surface for those nodes joined to a seam line, and, instead, consider only the residual forces in-plane[6.8]. In this way, the seam lines restrict the in-plane nodal displacements; thereby achieving well defined seam lines. The approach is advantageous in that it produces geodesic lines but significantly, it dictates the shape of the form-found surface. A similar method is to restrict the in-plane displacements by considering only the vertical equilibrium of the nodes of the discretised surface during form-finding. The method was used by Day[6.9] in the design of a papal canopy in Dublin (Chapter 2, Section 2.5.1).

The initial surface depicted in Figure 6-3 is used to illustrate Day's technique for the form-finding of the surfaces presented in examples 6.1 and 6.2. (The form-found surfaces presented in these examples were originally published in a paper by the author & W. J. Lewisin 1994[6.10]). In both examples, the boundary of the initial surface is fixed along the lines marked AD and BC, with movement restricted only in the X and Y global

directions for the boundaries AB and CD (Figure 6-3). In addition, the surface stress, σ_S, is equivalent to $5\times10^{+6}$ kNm^{-2} and the thickness equal to 1×10^{-3} m. The initial surface has not been generated using formex algebra. (The data was originally used by the engineering firm Ove Arup in the analysis of part of the canopy for the Tête Défense Cube in Paris). The form-found surface depicted in the first example, 6.1, has been obtained by considering only the vertical equilibrium. The subscript 'V' is used to denote the convergence criteria obtained according to the maximum value of the residual force in the global Z direction (ER_V). The relevant criteria are listed in (Table 6-1). The values of the convergence criteria corresponding to the X, Y and Z components of the out-of-balance force for the form-found surface presented in example 6.1 are recorded in Table 6-2. In the second form-found surface, example 6.2, equilibrium is considered in both the X, Y and Z global directions - the convergence criteria are presented in Table 6-3.

It is apparent that where the lateral movement of the nodes has been suppressed, (example 6.1), the radial lines follow geodesic seam lines (Figure 6-4 (d)) that bound "developable" fabric strips (as illustrated in Figure 6-2). Consequently, the plan view of the initial surface (Figure 6-3 (b) and the form-found surface described in example 6.1 (Figure 6-4 (d)) are identical. In contrast, the seam lines of the surface presented in example 6.2 follow ragged lines (Figure 6-5 (d)), which would produce an unsuitable two dimensional cutting pattern for each fabric strip - the seam lines would be excessively bowed when unfolded and, hence, result in an inefficient use of material. The geometry of the form-found surfaces described in examples 6.1 and 6.2 appear identical for the side profiles illustrated in Figure 6-4 (b) and Figure 6-5 (b), whereas those profiles depicted in Figure 6-4 (c) and Figure 6-5 (c) are different.

The major discrepancy between the two form-found surfaces is apparent when comparing their respective states of equilibrium. It is noticeable, that the form-found surface presented in example 6.1 is not completely equilibrated - Table 6-2 shows that ER is equivalent to 6.37 kN for the lateral components of the residual force; a value significantly higher than that presented in Table 6-3 for the surface depicted in example 6.2. Consequently, to suppress the movements in these directions, the surface presented in example 6.1 would require a very uneven pre-stress to preserve the shape, defined by the geometry of the numerical model, in the actual constructed structure. A non-uniform pre-stress implies that the surface is no longer a stable minimal surface. It is interesting to note, that the segments forming the canopy of the Tête Défense Cube, and represented by the surface illustrated in example 6.1, were finally constructed with high tensioned cables aligned in the radial directions; this has the effect of restricting the movement of the membrane and, hence, preserving the shape of the structure while introducing a non-uniform stress field.

The form-found surfaces presented in examples 6.1 and 6.2 have a geometry almost identical to that of the Papal canopy designed by Day - the surfaces differ in that the Papal Canopy possessed only one axis of symmetry about the X global axis. As already stated in Chapter 2, Section 2.5.1, Day encountered extreme difficulties in modelling the canopy numerically when introducing fictitious tensional cables to suppress the in-plane movements during form-finding. Evidently, the approach is undesirable as it produces non-equilibrated structures that require a non-uniform stress field to preserve the geometry.

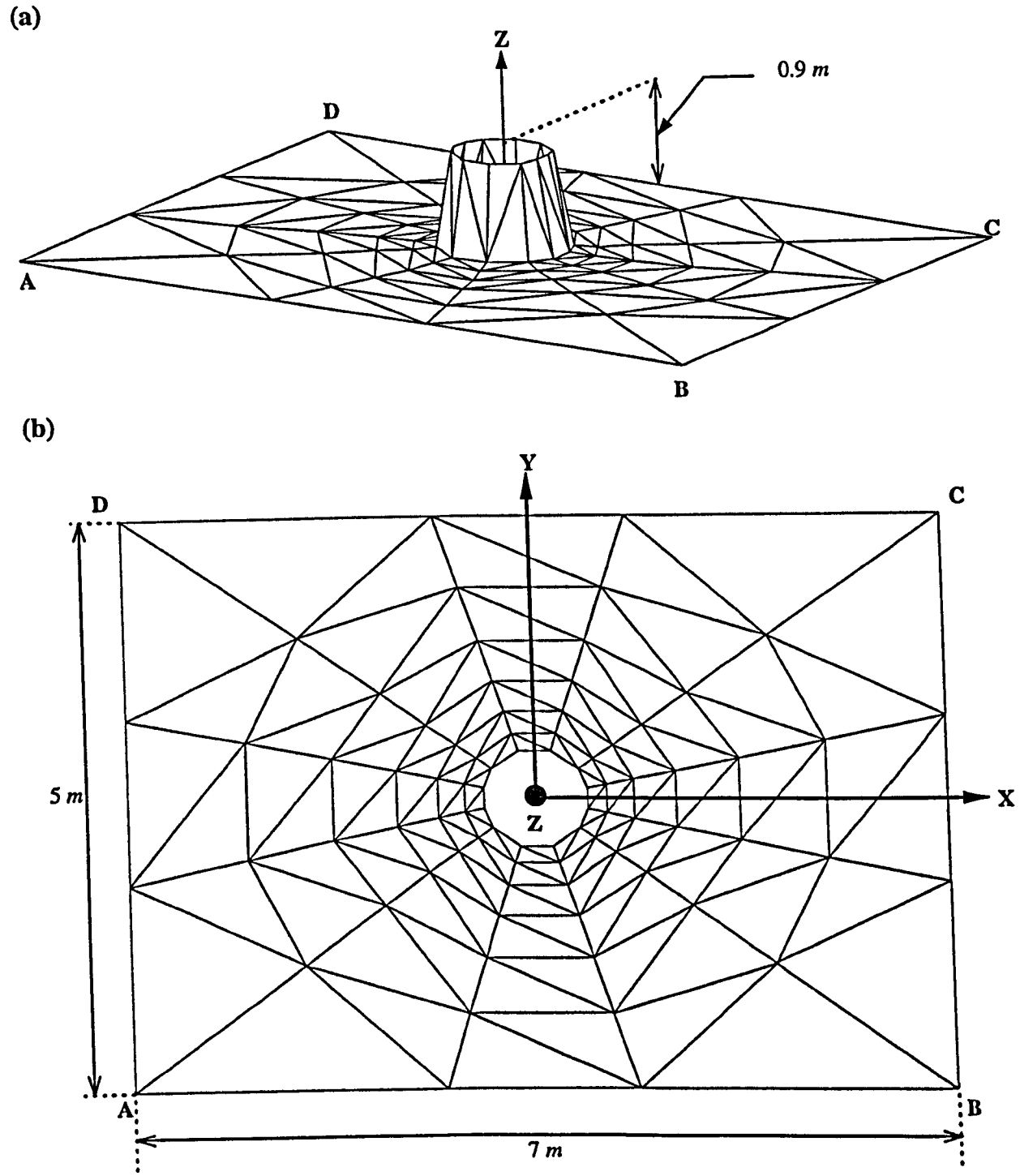

Figure 6-3 Initial Surface (Example 6.1). (a) Perspective View (b) Plan View.

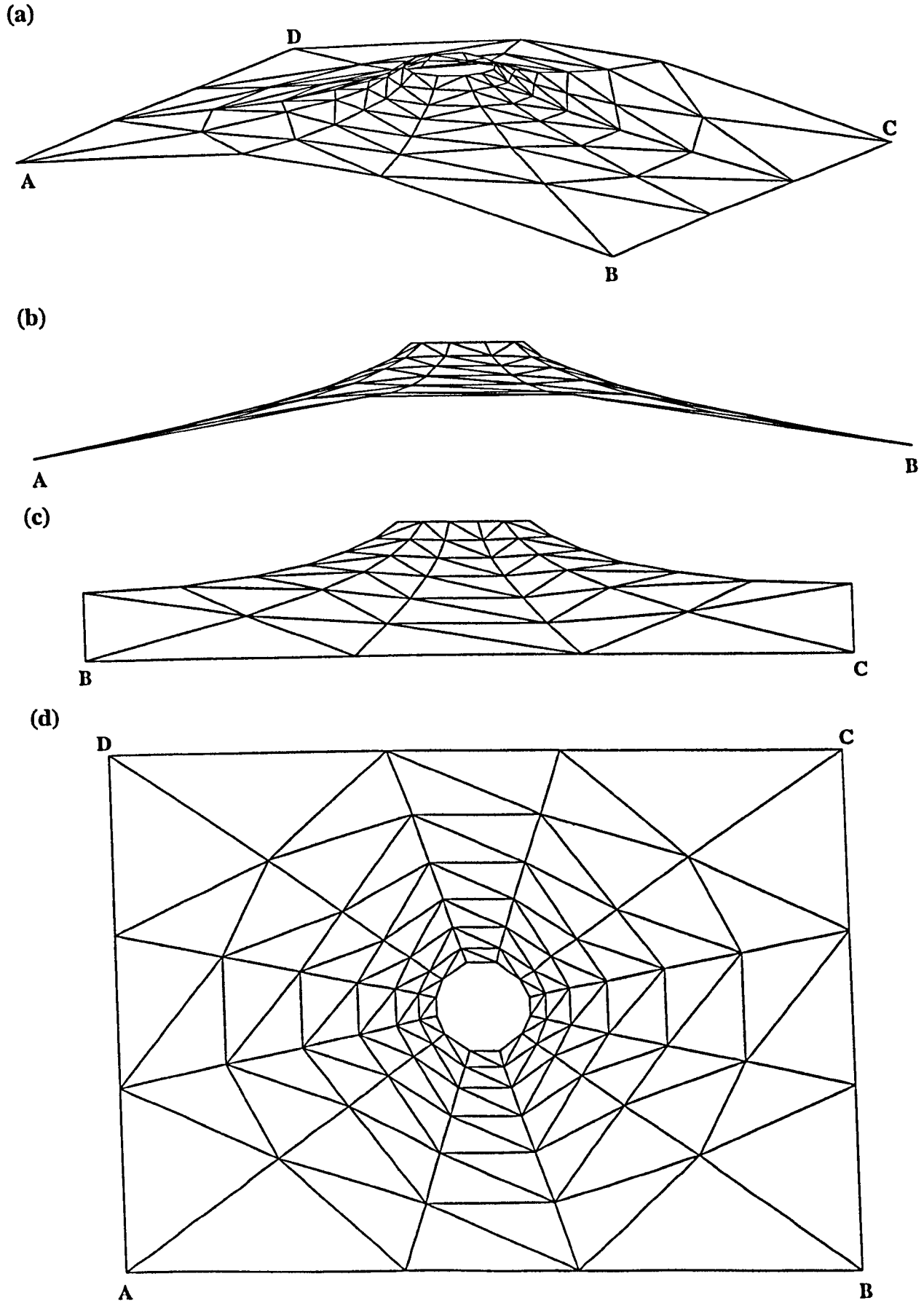

Figure 6-4 Form-Found Surface (Example 6.1 - Lateral Restriction on the Nodal Displacements). (a) Perspective View. (b) Side Elevation. (c) Front Elevation. (d) Plan View.

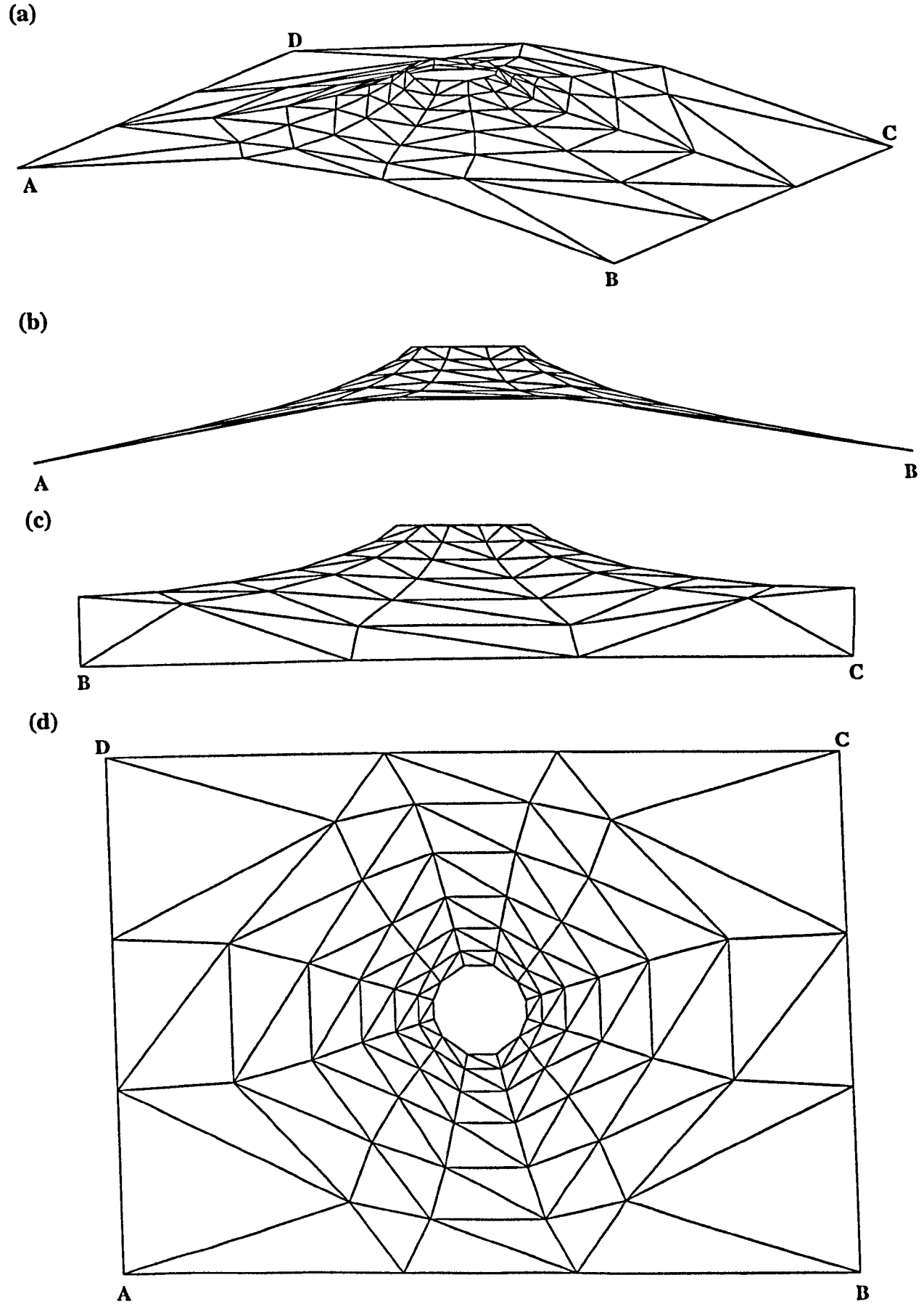

Figure 6-5 Form-Found Surface (Example 6.2 - No restriction on the Nodal displacements). (a) Perspective View. (b) Side Elevation. (c) Front Elevation. (d) Plan View.

Convergence Criterion.	Surface Area.	NIT	$A_{\%}$	ER_V	$ER_{TV\%}$	$ER_{FV\%}$
$ER_{TV\%} \leq 0.025$	35.3 m^2	378	4.3	0.75 kN	2.5×10^{-2}	1.8×10^{-2}

Table 6-1 Convergence Criteria used in Example 6.1 (Criteria Relate to the Components of the Residual Force Only in the Z Global Axis Direction).

Convergence Criterion.	Surface Area.	NIT	$A_{\%}$	ER	$ER_{T\%}$	$ER_{F\%}$
$ER_{TV\%} \leq 0.025$	35.3 m^2	378	4.3	6.37 kN	2.1×10^{-1}	1.3×10^{-1}

Table 6-2 Convergence Criteria used in Example 6.1 (Criteria Relate to Components of the Residual Force in the X, Y and Z Global Axis Directions).

Convergence Criterion.	Surface Area.	NIT	$A_{\%}$	ER	$ER_{T\%}$	$ER_{F\%}$
$ER_{T\%} \leq 0.025$	35.2 m^2	317	4.4	0.9 kN	2.5×10^{-2}	1.8×10^{-2}

Table 6-3 Convergence Criteria used in Example 6.2.

(C) In instances where no restriction is placed on the movement of the nodes during form-finding and the form-found surface is "non-developable", as it possesses an irregular mesh pattern due to excessive large scale deformations - the change in surface area during form-finding is excessive, $A_{\%}$ is large - it is difficult to produce a suitable cutting pattern (Figure 6-6 (a)). The seam lines need to be projected from a flat plane onto the surface of the three dimensional form (Figure 6-6(b)). The seam lines are then triangulated and the fabric strips unfolded. This has the disadvantage of producing bowed strips and can produce difficulties in cases where the form-found surface is of a high curvature and requires a large concentration of seam lines for accurate modelling (Figure 6-6 (b)). Also, a large number of interpolated points is required to preserve the surface curvature in the direction of the seam line. The advantage of the method is that it gives freedom to choose alternative seam line configurations, should the fabric width be exceeded. (The method adopted in the generation of the seam lines depicted in Figure 6-6 (b) and Figure 6-6 (c) is given in Appendix 6A.1 - the approach was originally suggested in a thesis written by Tan[6.7]).

(a)

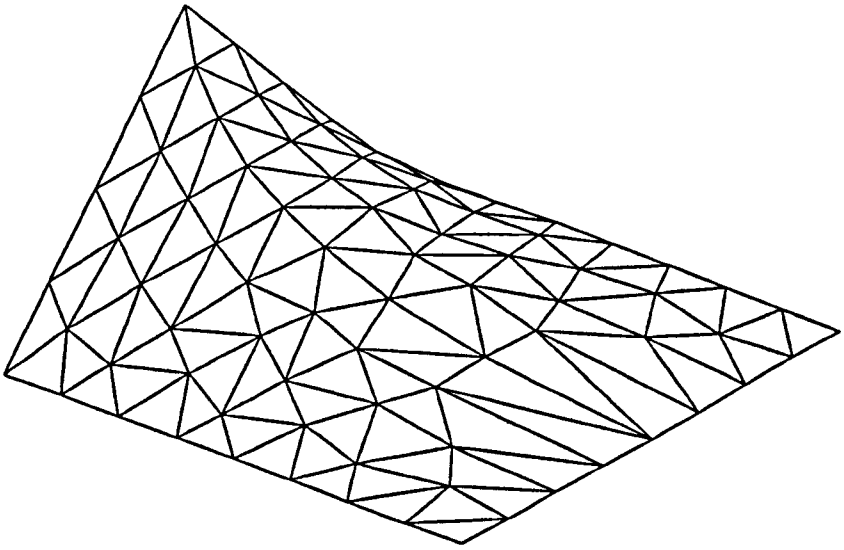

(b)

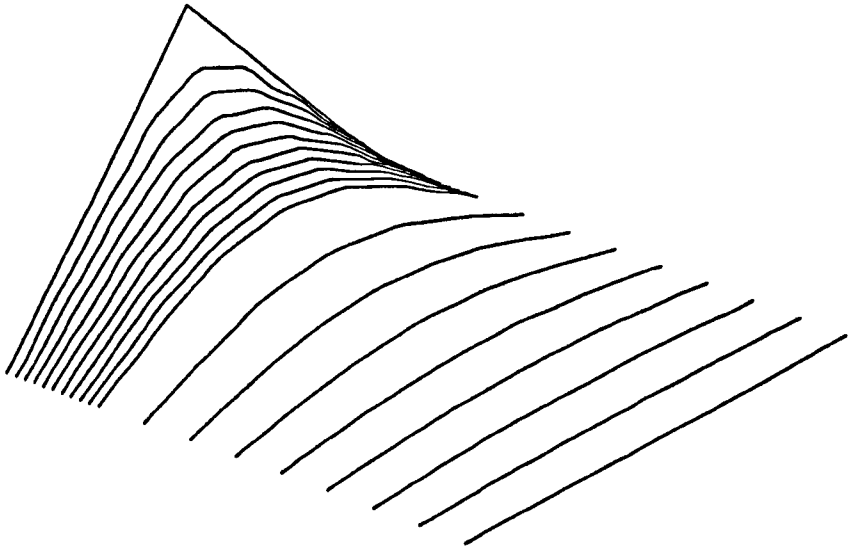

(c)

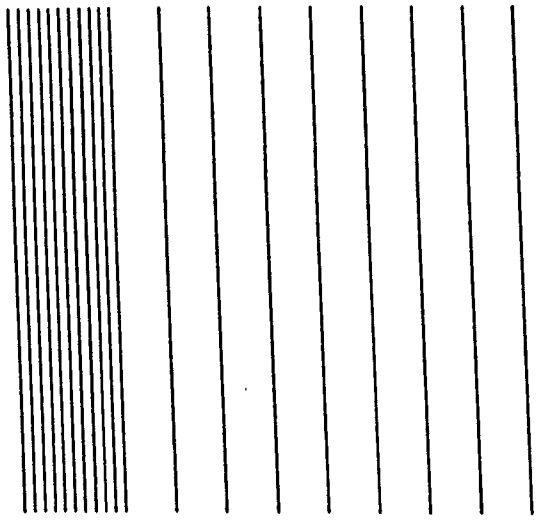

Figure 6-6 (a) Form-Found Surface (Example 5.2.1). Projection of Seam Lines. (b) Perspective View. (c) Plan View.

In all the aforementioned processes used to determine a suitable cutting pattern, the geometry of the form-found surface is compromised. The use of a single element in the defining of the fabric width ensures that the curvature of the fabric between the seam lines is incorrectly represented by a flat plane. Although this problem could be remedied by using seam lines of a smaller width, this would require a larger number of strips, which is undesirable for aesthetic reasons. Research looking at the generation of an alternative accurate cutting pattern algorithm is essential, if stable minimal surface are to make a significant contribution to the design of light-weight tension structures.

6.3 Rigid Structures.

The application of stable minimal surfaces in the design of rigid structures merits further study. This is not an unfeasible proposition, concrete tents have already been constructed in accordance with the geometry of a form-found surface that is analogous to the configuration of a light-weight tension structure[6.11]. Provided the material is of an adequate density, the dead weight of a rigid structure would provide considerable resistance to the uplift from wind, and the downward forces arising from snow loading. No cutting pattern is needed and hence no approximations to the surface geometry of the stable minimal surface are made. In the form-finding of a stable minimal surface, the weight of the soap film is neglected; this constitutes an adequate approximation for a fabric structure, but not for a rigid structure, especially if constructed from a highly dense material. Consequently, the non-uniform stress distribution of the rigid structure induced by its dead weight would have to be analysed. The erection of the formwork for the casting of a concrete minimal surface might prove difficult, thereby limiting the economic viability and feasibility of such structures. However, from as early as 1957, this problem has been addressed by Isler in the construction of his optimal concrete shells (Chapter 1, Section 1.1). Isler uses specialist

formwork, consisting of carefully manufactured laminated wooden arches, that are supported on light-weight scaffolding and timber boarding (Figure 6-7). By ensuring the formwork is standardised and re-useable, erection costs can be reduced to less than 20% of the overall cost of construction[6.12]. Although Isler's shells are **not** minimal surfaces, they are nonetheless doubly curved and, hence, support the supposition that it would be possible to construct a rigid structure of a geometry conforming to that of a stable minimal surface.

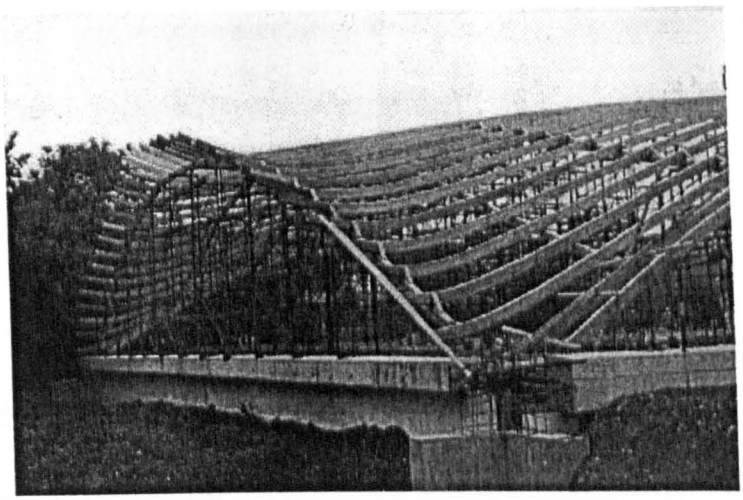

Figure 6-7 Example of Re-Usable Standardised Formwork (Photo: "Structural Art", Concrete Quarterly, Winter, 1992).

6.4 Mechanical Components

A diverse application of the form-finding of stable minimal surfaces could be in the manufacture of components for the auto-mobile, or aviation, industry where an economic use of material is an essential requirement. Components that lend themselves to a doubly curved form could have their weight reduced through adopting a geometry that possesses a minimum surface area - as exhibited by a stable minimal surface.

In addition, reducing the effects of fatigue in these components is another essential requirement in the design of a mechanical component. For instance, using the assumption

that a tree will always grow into a shape that is of a constant surface stress,[iv] Mattheck & Burkhardt showed how tree growth could be modelled numerically and used in the optimisation of mechanical components[6.13]. A numerical model, representing the initial geometry of the constant surface stress component, was subjected to an external loading. In areas where the calculated elastic Von Mises surface stresses exceeded a reference value, the component would swell volumetrically and material would be added. The procedure would continue until there was no swelling, at which time, the component would possess a constant Von Mises surface stress distribution. The conclusion was reached that components manufactured from the geometry of these numerical models benefited from an improved resistance to fatigue. Although Mattheck & Burkhardt's numerical approach deals with the three dimensional stress field induced by imposed loading, the approach has parallels with the form-finding of stable minimal surfaces through the common feature of constant surface stress. Future work could involve comparison of the behaviour of mechanical components, subjected to imposed loads, where the boundaries of the components are identical, but the surface geometry of the components differ, in that one would be designed according to a stable minimal surface ideology and the others according to a pre-defined geometry.

[iv] It is known that the growth of a tree can be traced by the examination of the growth rings of a tree's cross-section. Hence, the outermost ring is considered to be that part of the tree whose growth is susceptible to the dominant external applied loading from wind (Chapter 1).

APPENDIX 6

6A.1 Procedure for the Projection of Seam Lines onto A Form-Found Surface (Figure 6-6).

A point P (represented by a point on the seam line to be projected) will be enclosed by a element, if the sum of the internal angles subtended by point P is equal to three hundred and sixty degrees. (Only the two dimensional planar co-ordinates are considered when determining whether a node is enclosed by the element).

Consider the point P shown in Figure 6-8. The triangular element of the three dimensional form-found surface is represented by triangle ABC, which lies in the X Y plane, and has been obtained from the simple projection[v] of the 3 dimensional element of the form-found surface. The vectors aligned from point P towards each of the vertices ABC are determined, and the angle subtended at P by a side are calculated from the dot product of the two vectors associated with the side. If the node is bounded by the element, the sum of the angles will be equal to 2π (Figure 6-8 (a)), else, the sum will be equal to zero and P will lie outside the element (Figure 6-8 (b)).

(a) (b)

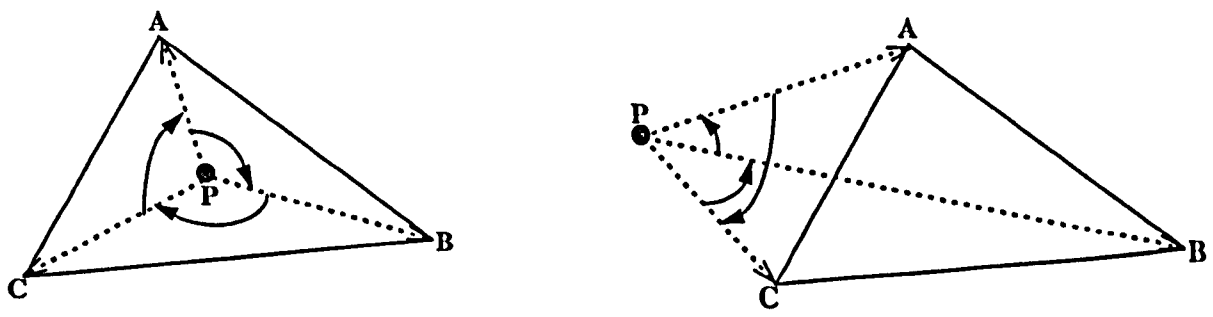

Figure 6-8 Angle Subtended by the Point 'P' Lying (a) Inside an Element (b) Outside an Element.

[v] The simple projection of a point lying on a surface is defined in Chapter 2, Section 2.2.

The positive direction of the angles is given by the direction of the angle subtended by the vectors PA and PB. Furthermore, it is necessary to check if point P lies on the edge of one of the boundaries of element ABC. It is found that this is the case for the instance where the cross product for any one of the vectors is equal to zero. Should this condition be met, it is still possible that point P lies within the element; - the criterion which describes that is the scalar dot product being negative.

Should the node lie within the element, the vertical co-ordinate of the point lying on the seam line is obtained by considering the equation of the plane continuing the three dimensional form-found element. The equation of a plane passing through three points (X_1, Y_1, Z_1,) (X_2, Y_2, Z_2) (X_3, Y_3, Z_3) - as given by the co-ordinates of the element vertices A, B, C- may be expressed in determinant form[6.14]:

$$\begin{vmatrix} x & y & z & 1 \\ X_1 & Y_1 & Z_1 & 1 \\ X_2 & Y_2 & Z_2 & 1 \\ X_3 & Y_3 & Z_3 & 1 \end{vmatrix} = 0 \qquad \textbf{(6a.1)}$$

The co-ordinates X_P and Y_P of point P are already known, hence, the vertical co-ordinate Z_P of a point on the seam line may be found by eliminating the determinant of equation (6a.1):

$$Z_P = \frac{Q_4 + Q_2 Y_P - Q_1 X_P}{Q_3} \qquad \textbf{(6a.2)}$$

where,

$$Q_1 = Y_1(Z_2 - Z_3) - Z_1(Y_2 - Y_3) + (Y_2 Z_3 - Z_2 Y_3) \qquad \textbf{(6a.3)}$$

$$Q_2 = X_1(Z_2 - Z_3) - Z_1(X_2 - X_3) + (X_2 Z_3 - Z_2 X_3) \qquad \textbf{(6a.4)}$$

$$Q_3 = X_1(Y_2 - Y_3) - Y_1(X_2 - X_3) + (X_2Y_3 - Y_2X_3) \quad \textbf{(6a.5)}$$

$$Q_4 = X_1(Y_2Z_3 - Z_2Y_3) - Y_1(X_2Z_3 - Z_2X_3) + Z_1(X_2Y_3 - Y_2X_3) \quad \textbf{(6a.6)}$$

Thus, a seam line may be generated by specifying only the planar co-ordinates for the start and end of the seam line, the number of divisions, in the direction of the seam line, and the size of each division. For each point lying on a seam line, the element of the discretised form-found surface containing the point is determined, and the vertical co-ordinate calculated using equations (6a.2-6a.6) until all points are projected, and the seam line lies on the form-found surface.

REFERENCES

6.1 T. Read and T. O' Brien,
"Coated Fabrics for Light-Weight Structures."
The Arup Journal 1980, pages 14-18.

6.2 M. R. Barnes,
"Form and Stress Engineering of Tension Structures."
Structural Engineering Review, vol. 6, no. 3-4, pages 175-202, 1994.

6.3 Serge Ferrari, 38352 La Tour Du Pin Cedex, Z.I.-B.P.54, France,
"Précontraint Technique."
Technical Specifications.

6.4 D. P. Billington,
"The Tower and the Bridge. The New Art of Structural Engineering."
Princeton University Press, New Jersey, pages 222-229, 1983.

6.5 I. Liddel,
"Tension Structures II : Membranes."
Bruro Hapold Technical Manual.

6.6 P. Kneen,
"Computer Aided Design of Tensioned Fabric Structures."
LSA 86, 1st International Conference on Light Weight Structures in Architecture, Sydney, 1986, proceedings vol. 2, pages 992-1009.

6.7 K. Y. Tan,
"The Computer Design of Tensile Membrane Structures."
PhD Thesis, Dept. of Civil Engineering, Queensland University, 1989.

6.8 M. R. Barnes,
"Form-Finding and Analysis of Pre-stressed Nets and Membranes."
Proceedings of the International Conference on Non-Conventional Structures, Volume 1, 1987, pages 327-338.

6.9 A. S. Day,
"Form-Finding Control and Modification for Tension Structures."
The Arup Journal, Ove Arup Partnership, 1980, pages 19-20.

6.10 T.S.Lewis and W. J. Lewis,
"Effectiveness of the Non-Linear Numerical Models for the Analysis of Light-weight Membranes."
SFB 230 Naturliche Konstruktionen, H9, 1994, pages 65-71.

6.11 P. Hudson and B. Topping,
"The Design and Construction of Reinforced Concrete Tents in the Middle East."
The Structural Engineer, vol. 69, no. 22, 19 November, 1991, pages 379-385.

6.12 T. Copeland,
"Structural Art"
Concrete Quarterly, Winter 1992, pages 12-15.

6.13 C. Mattheck and S. Burkhardt,
"A New Method of Structural Shape Optimization Based on Biological Growth."
International Journal Fatigue Vol. 12, no. 3, May 1990, pages 185-190.

6.14 J. Blakely,
"University Mathematics - A text book for Students of Science and Engineering."
Blackie and Son Ltd., 1967, pages354-357.

CHAPTER 7

Summary and Conclusions.

7.1 Summary

The excellent agreement shown between the geometries of stable minimal surfaces obtained through numerical, experimental and theoretical solutions (Chapter 4) provides confirmation that the numerical approach adopted by the author, is valid for the problem of form-finding of light-weight tension structures, and the generation of small scale rigid models. These forms possess a minimum surface area and a constant surface stress. It has been shown that the algorithm is particularly adept in coping with cases where the initial surface is very poorly defined, thereby negating the need to obtain an accurate approximation, based on the geometry obtained from an experimental solution, before commencing a form-finding analysis (Chapter 4, Examples 4.1, 4.2 and 4.8). The major strength of the approach lies in the novel integration of the form-finding algorithm (based on the Dynamic Relaxation method) with Formian (Chapter 3). Formian 'schemes' maximise the degree to which a diverse range of surfaces may be created (Chapter 5, Example 5.2.5), while minimising the effort necessary for the creation of an initial surface. Furthermore, schemes enhance the adaptivity of the form-finding algorithm; the surface discretisation and boundary dimensions may be conveniently altered - through the changing of a Formian scheme's parameters - in accordance with the requirements of a particular problem (Chapter 4, Examples 4.1, 4.2, 4.6 and 4.7). The provision for the optional post-processing of the results obtained from a form-finding analysis, afforded by the integration of Formian with the form-finding equation solver, allows for the construction of an exceptionally accurate physical model of a

numerical surface (Chapter 3, Section 3.4.3.3 and Chapter 5, Examples 5.2.1 and 5.2.2). Hitherto, accurate representations of stable minimal surfaces could only be obtained through the use of soap films; a tedious solution, due to the momentary existence of the soap film and the specialist equipment required to manufacture and photograph the film (Chapter 1, Section 1.2.2). The practicality of adopting a geometry conforming to that of a stable minimal surface for use in the design of a light-weight tension structure is, at present, limited, due to the need to obtain an accurate cutting pattern for the fabric material (Chapter 6, Section 6.2.3), and the general anisotropic behaviour of the fabric materials currently available (Chapter 6, Section 6.2.1). The general consensus of today that the surface geometry must be dictated in order to meet anticipated loading conditions (Chapter 1, Section 1.4, Chapter 2, Section 2.5.1 and Chapter 6, Section 6.2.2) adds to the controversy of what constitutes an optimal shape of a light-weight tension structure.

7.2 Conclusions.

The following, is a list concerning the detailed conclusions reached from the work presented in this thesis:

(A) The form-finding algorithm was shown to produce comparable solutions to those obtained using alternative computational programmes, irrespective of the accuracy of the initial surface and significantly, without violating the condition of a uniform surface stress (Chapter 4).

(B) The pseudo cable forces, and hence residual forces, are dependent on the magnitude of the applied pre-stress, membrane thickness, and the mesh size, which in turn is related

to the dimensions of the boundaries (Chapter 4). Consequently, the maximum admissible value for the components of the residual nodal force, ER, is not an all-encompassing criterion for assessing the accuracy of a solution. It is suggested that ER should be expressed as a percentage of the maximum "pseudo cable" force - $ER_{T\%}$ - the value being no greater than 0.025% for a convergent solution. Although, the criterion $ER_{T\%}$ is a non-dimensional measurement of the stability and convergence of the numerical solution to a stable minimal surface, it is, however, dependent on the value of $A_{\%}$ (Chapter 4, Section 4.6) - a low value of $A_{\%}$ indicates that $ER_{T\%}$ can be satisfied to a value lower than 0.025% for an increased number of iterations. A plot of the maximum nodal displacement over a number of iterations can also be used to give some measure of the stability of the solution (Chapter 3, Section 3.3.7 and Chapter 4, Section 4.3).

(C) The accuracy and rate of convergence of the numerical solution is related to the decrease in surface area from the initial state to the stable form-found state; as given by the value of $A_{\%}$. For a high percentage change of $A_{\%}$, the elements deform significantly, resulting in elements possessing excessively high 'pseudo cable' forces as a consequence of the poor aspect ratio of the elements (Chapter 4, Section 4.3). Highly deformed elements of this type can also produce a non-smooth geometry (Chapter 4, Example 4.1). A dense surface discretisation is only advisable in cases where the change in area is minimal - $A_{\%}$ is small.

(D) Formex algebra provides a conceptual means of expressing the geometry and the data corresponding to a surface. A general procedure for the generation of form-finding data using formex algebra has been suggested (Chapter 3, Section 3.2.3). The procedure was successfully implemented in Formian schemes responsible for the generation of

numerous initial surfaces (Appendices 4 and 5). Provided the user has a working knowledge of the concepts and syntax of formex algebra, an examination of the text of a scheme provides an understanding of how the data relating to a surface has been created. This replaces the need for deciphering unintelligible data files. Furthermore, an exact representation of an initial surface may be recreated, at a later date, using the formex algebra expressions contained within the relevant scheme (Chapter 4 and Chapter 5).

(E) The potential for the integration of formex algebra with the form-finding algorithm is constrained, to some extent, by the intellectual process involved in the creation of a scheme and the necessity to adhere to the rules and syntax of formex algebra. The process could be seen as overwrought, or 'intellectually demanding', in the generation of apparently simple geometrical configurations (Appendix 5, Section 5A.9 - Formian "SCHEME6"), and too complex when considering difficult geometrical arrangements such as the tessellated models used in the manufacture of rapid prototype models (Chapter 3, Table 3-4, Section 3.4.3).

(F) Formex algebra requires the configuration pattern of a surface to be considered as a whole; there is no provision to alter individual parts of an initial surface, should divergence or ill-conditioning be experienced in a local area of the surface during form-finding. Formian would be further enhanced by a 'hands on' approach, using an interactive graphical environment. This would simplify the construction of an initial surface and provide a greater degree of flexibility in altering the surface geometry, particularly in cases where a non regular or non-symmetrical geometry is desirable (Chapter 5,examples 5.2.6, 5.2.7.1 and 5.2.7.2).